5

B S

COLUMBIA UNIVERSITY

DEPARTMENT OF PHYSICS

PROGRESS REPORT No. 27

JULY 1, 1976 THROUGH MARCH 31, 1977

CONTRACT DAAB07-74-C-0341

To:

THE JOINT SERVICES TECHNICAL ADVISORY COMMITTEE

REPRESENTING: THE U.S. ARMY ELECTRONICS COMMAND
THE U.S. ARMY RESEARCH OFFICE
THE OFFICE OF NAVAL RESEARCH
THE AIR FORCE OFFICE OF SCIENTIFIC RESEARCH

COLUMBIA RADIATION LABORATORY NEW YORK, NEW YORK 10027

March 31, 1977

(5)

COLUMBIA RADIATION LABORATORY

RESEARCH INVESTIGATION DIRECTED TOWARD EXTENDING THE USEFUL RANGE OF THE ELECTROMAGNETIC SPECTRUM

Progress Report No. 27

July 1, 1976 through March 31, 1977

Contract DAAB07-74-C-0341

Object of the research:

Submitted by: W. Happer, Director

Coordinated by: Mrs. H. M. Ghobadi, Administrative Assistant

COLUMBIA UNIVERSITY

Division of Government-Aided Research

New York, New York 10027

March 31, 1977

The research reported in this document was made possible through support extended the Columbia Radiation Laboratory, Columbia University, by the Joint Services Electronics Program (U. S. Army Electronics Command and U. S. Army Research Office, Office of Naval Research, and the Air Force Office of Scientific Research) under Contract DAAB07-74-C-0341.

Portions of this work were also supported by:

Air Force Office of Scientific Research

Grant AFOSR-74-2685

National Aeronautics and Space Administration

Grant NGR-33-009-181 Scope T

National Science Foundation

Grant NSF-DMR73-07600 A02

Grant NSF-MPS75-13383

Grant NSF-ENG76-16424

Grant NSF-MPS75-04118

Grant NSF-ENG75-09325

Army Research Office

DAAG29-77-G-0015

The support of these agencies is acknowledged in footnotes in the text.

Unclassified

SECURITY CLASSIFICATION OF THIS PAGE *(When Data Entered)*

REPORT DOCUMENTATION PAGE

READ INSTRUCTIONS BEFORE COMPLETING FORM

1. REPORT NUMBER: Progress Report No. 27

2. GOVT ACCESSION NO.

3. RECIPIENT'S CATALOG NUMBER

4. TITLE *(and Subtitle)*: RESEARCH INVESTIGATION DIRECTED TOWARD EXTENDING THE USEFUL RANGE OF THE ELECTROMAGNETIC SPECTRUM.

5. TYPE OF REPORT & PERIOD COVERED: Progress rept. no. 25 (Final), 1 July 76 - 31 March 77

6. PERFORMING ORG. REPORT NUMBER

7. AUTHOR(s): William Happer

8. CONTRACT OR GRANT NUMBER(s): DAABØ7-74-C-Ø341, AFOSR-74-2685

9. PERFORMING ORGANIZATION NAME AND ADDRESS:
Columbia Radiation Laboratory
Columbia University
New York, New York 10027

10. PROGRAM ELEMENT, PROJECT, TASK AREA & WORK UNIT NUMBERS: 1T161102BØØR00 / ØØ

11. CONTROLLING OFFICE NAME AND ADDRESS:
Department of the Army
U. S. Army Electronics Command
Fort Monmouth, New Jersey 07703

12. REPORT DATE: 31 MARCH 1977

13. NUMBER OF PAGES: 213

14. MONITORING AGENCY NAME & ADDRESS *(if different from Controlling Office)*

15. SECURITY CLASS. *(of this report)*: Unclassified

15a. DECLASSIFICATION/DOWNGRADING SCHEDULE

16. DISTRIBUTION STATEMENT *(of this Report)*

Approved for public release; Distribution unlimited.

17. DISTRIBUTION STATEMENT *(of the abstract entered in Block 20, if different from Report)*

Portions of this work were supported by the Air Force Office of Scientific Research, the National Aeronautics and Space Administration, the National Science Foundation, and the Army Research Office

18. SUPPLEMENTARY NOTES

19. KEY WORDS *(Continue on reverse side if necessary and identify by block number)*

High density optical pumping
Laser optical pumping
Interactions between laser beams
Magnetometric displays

continued on page iv

20. ABSTRACT *(Continue on reverse side if necessary and identify by block number)*

A theoretical limit, ω^2/ω_{hfs}, has been deduced for the exchange narrowed linewidth of magnetic resonance transitions in alkali vapors. Here ω is the Larmor frequency and ω_{hfs} is the hyperfine frequency of the atomic ground state. Experimentally measured linewidths do not approach this limit. The reason for the discrepancy is under investigation.

DD FORM 1 JAN 73 1473 EDITION OF 1 NOV 65 IS OBSOLETE

Unclassified

SECURITY CLASSIFICATION OF THIS PAGE *(When Data Entered)*

Ø88 6ØØ

Long range interactions were found to exist between self focused, spatially separated laser beams in alkali vapors. These forces were shown to be due to the exchange of spin-polarized atoms.

A simple optically pumped device has been developed for visual, real-time display of contours of constant magnetic field in a region of inhomogeneous magnetic field. The same device can be used as an unconventional frequency spectrum analyzer for the radio frequency or microwave range.

Both Cs_2 and Rb_2 molecules, when excited by certain lines of an Ar^+ laser, lead to the formation of alkali hydride crystals when hydrogen is mixed with the alkali vapor. No isotopic selectivity could be demonstrated in the case of laser excitation of Rb_2.

Plasmas in cesium vapor have been produced with a 0.1 watt dye laser at 6010.5 Å. The resonant laser wavelength corresponds to the transition $6P_{1/2} \rightarrow 8D_{3/2}$ in atomic cesium. The same laser wavelength produces dramatic oscillating clouds of cesium hydride crystals when deuterium is added to the cesium vapor.

A very curious reversal of the polarization of Rayleigh scattered light has been observed for frequencies between the D_1 and D_2 resonance lines. These observations are in good agreement with theoretical predictions of Placzek.

Precise measurements of P and D state fine structure intervals of helium have been completed.

Certain narrow absorption bands of Cs_2 molecules have been shown to originate from unusually large internuclear separations. These bands may be the first known examples of absorption in the triplet system of Cs_2.

Precise measurements of the hyperfine structures of highly excited S and P states of cesium atoms have been completed. The first precise radio frequency spectroscopic measurements of fine structure intervals in the F states of rubidium were also completed.

Spectroscopic studies of the visible absorption bands of alkali-noble gas excimers have been completed, and potential curves for the higher lying excimer states have been obtained by analysis of the data.

A theoretical analysis of the interchange of angular momentum between light and an anisotropic transparent medium has been completed. Both the spin and the orbital angular momentum of the light are exchanged with the spin angular momentum of the medium.

Block 20 Continued

A CO_2 laser has been used to stimulate the isomerization of fluorinated dewar benzene to normal fluorinated benzene. Both progressive and chain-reaction conversion were observed under appropriate conditions.

Radiation from a CO_2 laser has been used to sensitize the decomposition of tetramethyl-1-2-dioxetane. Methyl fluoride and SF_6 are excellent sensitizers. The decomposition products include electronically excited states of acetone, which fluoresce in the blue region of the spectrum.

Rate constants for vibrational energy transfer between the various modes of methyl fluoride and oxygen molecules have been deduced from transient experiments with a CO_2 laser. Substantial heating and cooling of the translational degrees of freedom occurs in the CH_3F/O_2 system.

Strong localization of CO_2 laser pump energy in a single vibrational mode has been observed in methyl fluoride. Calculations show that in striking contrast to heating by a bunsen burner, heating by a CO_2 laser decreases the mean translational energy, and greatly enhances the vibrational energy of a few selected modes.

Transfer of energy from electronically excited bromine atoms Br* ($4^2P_{1/2}$) into vibrational energy of carbonyl sulfide OCS has been observed. Mode specific energy transfer and heating were observed.

A comprehensive review article on electronic to vibrational energy transfer has been completed and will be published in the Annual Review of Physical Chemistry, Volume 28.

Strong pumping of carbonyl fluoride, COF_2, by CO_2 laser light has been observed. Two markedly different pumping processes are observed, depending on the excitation wavelength. Hot band pumping leads to a very rapid buildup and decay of certain vibrational modes, while ground state pumping leads to much slower equilibration of vibrational modes.

Vibrational energy exchange rates between various modes of pure methyl fluoride gas have been determined by using thermal lensing techniques, laser induced fluorescence and laser-laser double resonance in concert. An almost complete vibrational energy flow map has been obtained for this system.

Photon echo modulation for various transitions of Pr^{3+} in LaF_3 has been used to deduce the spin hamiltonian for several states of Pr^{3+} A nitrogen pumped dye laser was used for excitation.

Block 20 Continued

Improved values for the parameters of the spin hamiltonian of Cr^{3+} in ruby have been obtained.

Work on Raman echoes has led to some very fruitful studies of three-wave mixing in atomic vapors. Remarkably strong coherent radiation due to E2 or M1 transitions is observed with proper preparation of a coherent initial state. Under some conditions a transverse magnetic field must be applied to the atomic vapor to allow conservation of angular momentum in the mixing process. For sum frequency generation in sodium vapor, interference between the noncollinear direct amplitude and the magnetically induced amplitude leads to a strong dependence of the sum frequency intensity on the sign of the transverse field.

Dicke superradiance has been observed in atomic vapors of thallium, cesium, rubidium, and sodium. In the case of sodium Dicke superradiance was observed at 8133 Å ($3P_{1/2}$ - 3D) and 8195 Å ($3P_{3/2}$ - 3D) which is "visible" to many photomultiplier tubes. The accessibility of this superradiance to photomultiplier detection will make it possible to explore fluorescence phenomena all the way from conventional weak fluorescence to strong Dicke superradiance.

A microwave spectrometer for ions has been constructed and successfully tested. A clever modulation scheme makes it possible to discriminate against spurious signals, so that the spectrometer is sensitive to a molecular ion absorption of 10^{-8} cm^{-1} in the presence of a glow discharge.

An improved torsion pendulum has been constructed to measure, for the first time, the pressure dependence of the viscosity of liquid helium. At the highest frequency of operation this apparatus will give direct information about the boundary layer between the bulk liquid and the wall.

A precise measurement of the superfluid fraction of liquid helium has been made near the lambda point with a temperature precision of 2×10^{-6}°K and a superfluid fraction precision of 3×10^{-5}.

By varying the excitation pulse amplitude we have demonstrated that instantaneous diffusion plays no role in the behavior of electron spin echoes of Mn^{+2} and Er^{+3} in $CaWO_4$. However, the experimental data is consistent with the sudden jump model of spectral diffusion. The two parameters of the model were determined as a function of temperature.

Block 19 continued - Key Words

RF spectrum displays
Laser-excited alkali vapors
Laser-produced plasma
Oscillating laser-particulation
Unusual Rayleigh scattering
Hyperfine structure
Fine structure
Dye laser spectroscopy
Absorption studies of diatomic alkali molecules
Laser fluorescence
Excimer Molecules
High Pressure discharge
Dissociative lasers
Carbonyl Fluoride
Carbonyl sulfide
Perflouro Dewar Benzene
Methyl Fluoride
Vibrational temperatures
Trapped modes
Tetramethyl dioxetane
Infrared lasers
Infrared detection
Electronic-to-vibrational energy transfer
Raman echoes
Two-photon superradiance
Photon-echo resonance
Magnetically induced three-wave mixing
Sum-frequency generation
Difference-frequency generation
Dicke superradiance
Second-order hyperfine interaction
Instantaneous spectral diffusion
Sudden jump model of spectral diffusion
Superfluidity
Healing length
Molecular rotational spectroscopy
Photon counting
Nonlinear heterodyne detection
Infrared sensing
Optical communications
Optical radar
Multiphoton heterodyne detection

TABLE OF CONTENTS

The names of the authors are arranged alphabetically.

PUBLICATIONS AND REPORTS

Publications

A. Tam and W. Happer, "Polarization of Laser-Excited Fluorescent Lines from $^{85}Rb_2$ and $^{87}Rb_2$ Molecules," J. Chem. Phys. 64, 4337, (1976).

P. Tsekeris[1], K. Liao, and R. Gupta, "Radiofrequency Spectroscopy of the $5^2S_{1/2}$ State of ^{23}Na: Hyperfine-Structure Measurement," Phys. Rev. A. 13, 2309 (1976).

R. Guernsey, Jr., R. J. McCoy[2], M. Steinback, and J. K. Lyden, "Reduced Viscosity of Superfluid ^3He A and B Near T_c," Phys. Letters 58A, 26 (1976).

Richard C. Slater[3] and George W. Flynn, "Mode Specific Excitation of SO_2 by Resonant Energy Transfer from Laser Excited CH_3F," J. Chem. Phys. 65, 425 (1976).

G. Moe, A. Tam, and W. Happer, "Absorption Studies of Excimer Transitions in Cs-Noble-Gas and Rb-Noble-Gas Molecules," Phys. Rev. A. 14, 349 (1976).

A. Tam and George Moe, "Emission Bands From Discharge-Excited Alkali-Noble-Gas Systems," Phys. Rev. A. 14 528 (1976).

Y. C. Chen and S. R. Hartmann, "Photon Echo Modulation Effects in $LaF_3:Pr^{3+}$," Phys. Letters 58A, 201 (1976).

A. Flusberg and S. R. Hartmann, "Probing Adiabatic States," Phys. Rev. A. 14, 813 (1976).

S. Meth and S. R. Hartmann, "The Effect of Instantaneous Diffusion on the Relaxation of Photon Echoes in Ruby," Phys. Letters 58A, 192 (1976).

A. Flusberg, T. Mossberg, and S. R. Hartmann, "Observation of Dicke Superradiance at 1.30 μm in Atomic Tl vapor," Phys. Letters 58A, 373 (1976).

---

[1] Present Address: University of Ioannina, Ioannina Greece

[2] Present Address: Bell Telephone Laboratories, Murray Hill, New Jersey.

[3] Present Address: Avco Everett Research Laboratories, Everett, Massachusetts.

William E. Farneth, George Flynn, Richard Slater and Nicholas J. Turro, "Time Resolved Infrared Laser Photochemistry and Spectroscopy: The Methyl Fluoride Sensitized Decomposition of Tetramethyl-1,2-dioxetane.An example of Infrared Laser Induced Electronic Excitation," J. Am. Chem. Soc. 98, 7877 (1976).

A. C. Tam and C. K. Au[4], "Polarization Reversal of Rayleigh Scattering Near a $^2P_{3/2, 1/2} - {}^2S_{1/2}$ Resonance Doublet," Optics Comm. 19, 265 (1976).

A. C. Tam, "Fine-structure Intervals in the 3^3P and n^3D States of ^4He," J. Phys. B:Atom. Molec. Phys. 9, L559 (1976).

A. Flusberg, T. Mossberg and S. R. Hartmann, "Hyperfine Structure, Isotopic Level Shifts and Pressure Self-Broadening of the 7^2P States of Natural Thallium by Doppler-free Two-photon Absorption," Phys. Rev. A. 14, 2146 (1976).

A. C. Tam and W. Happer, "Long Range Interactions Between CW Self-Focused Laser Beams in an Atomic Vapor," Phys. Rev. Letters 38, 278 (1977).

J. Farley[5], P. Tsekeris, and R. Gupta, "Hyperfine Structure Measurements in the Rydburg S and P States of Rubidium and Cesium," Phys. Rev. A 15, 1530 (1977).

A. Flusberg, T. Mossberg, and S. R. Hartmann, "Optical Sum-Frequency-Generation Interference in Atomic Sodium Vapor," Phys. Rev. Letters 38, 694 (1977).

J. Farley and R. Gupta, "Fine-Structure Measurements in the 6^2F and 7^2F States of Rubidium by Radio-Frequency Spectroscopy," Phys. Rev. A. 15, 1952 (1977).

A. C. Tam and W. Happer, "Optically Pumped Cell for Novel Visible Display of Inhomogeneous Magnetic Field or of rf Frequency Spectrum," Applied Phys. Letters, 30, 580 (1977).

Irwin Shamah and George Flynn, "Trapped Metastable Vibrational Energy Distributions in Laser Pumped Molecules," J. Am. Chem. Soc., 99, 3191 (1977).

---

[4] Present Address: Department of Physics and Astronomy, University of South Carolina, Columbia, South Carolina.

[5] Present Address: Physics Department, University of Arizona, Tucson, Arizona.

S. Lemont, R. Giniger and G. W. Flynn, "Radiative Lifetime and Quenching Cross Section of the $B^1\pi_u$ State of K_2 by Time Correlated Single Photon Counting Using a Mode-Locked He-Ne Laser," J. Chem. Phys. 66, 4509 (1977).

R. Novick, G. Sprott and T. Lucatorto, "Identification of the Lowest Metastable Autoionizing Level in Rb from rf spectroscopic Studies,"[6] Phys. Rev. A. 14, 273 (1976).

A. Flusberg, T. Mossberg, and S. R. Hartmann, "Optical Difference-Frequency Generation in Atomic Thallium Vapor," Phys. Rev. Lett., 38, 59 (1977).

---

[6] This work was completed in 1967, but was not published until 1976.

Papers by CRL Staff Members Presented at Scientific Meetings

G. W. Flynn, "Laser Studies of Molecular Energy Transfer," E. I. DuPont De Nemours Lecture Series on Energy Related Topics, Furman University, Greensville, South Carolina, July 1, 1976.

G. W. Flynn, "Energy Transfer and Laser Initiated Chemical Reactions," Gordon Conference on Molecular Collisions, Holderness School, Plymouth, New Hampshire, July 27, 1976.

G. W. Flynn, "Vibrational Energy Exchange in Molecular Collisions," Gordon Conference on Atomic and Molecular Interactions, Brewster Academy, Wolfboro, New Hampshire, August 11, 1976.

G. W. Flynn, "Laser Studies of Intermode Energy Transfer in Small Molecules," Harvard-MIT Joint Physical Chemistry Symposium, Cambridge, Massachusetts, November 4, 1976.

G. W. Flynn, "Lasers, Energy Transfer, and Vibrational Photochemistry," American Chemical Society Symposium on State-to-State Chemistry, New Orleans, Louisianna, March 21, 1977.

G. W. Flynn "Lasers, Energy Transfer, and Vibrational Photochemistry: Is Chemical Nirvana Near?" Illinois Institute of Technology, Symposium on Laser Chemistry, May 19, 1977.

G. W. Flynn, "A Review of Laser Studies of Molecular Energy Transfer: Ramifications for Laser Chemistry," Symposium in Honor of E. Bright Wilson, Georgia Institute of Technology, Atlanta, Georgia, May 25, 1977.

S. R. Hartmann, "Two-Photon Coherent Hanle Effect," Fourth Rochester Conference on Coherence and Quantum Optics, Rochester, New York, June 10, 1977.

R. Gupta, "Hyperfine Structures in the Excited States of Alkali-Metal Atoms," Fourth International Conference on Hyperfine Interactions, Madison, New Jersey, June 13, 1977.

W. Happer, "Long Range Interactions Between CW Laser Beams," Third International Conference on Laser Spectroscopy, Jackson, Wyoming, July 8, 1977.

Lectures

K. Casleton, "Mode to Mode Energy Transfer in Carbonyl Fluoride," Seminar, Vanderbilt University, Nashville, Tennessee, February 23, 1977; Seminar S.V.N.Y. at Albany, Albany, New York, March 2, 1977; Seminar, University of Nebraska, Lincoln, Nebraska, April 22, 1977; Seminar, Southern Illinois University, Carbondale, Illinois, April 28, 1977.

W. Farneth, "Infrared Photochemistry," Seminar, State University of New York, Stony Brook, New York, December 13, 1976; Seminar, University of Minnesota, Minneapolis, Minnesota, January 10, 1977; Seminar, Amherst College, Amherst, Massachusetts, February 2, 1977.

A. Flusberg, "Hyperfine Structure of the 7^2P States of Thallium: The Anomalous n^2P Series," Seminar, Bell Laboratories, Holmdel, New Jersey, May 12, 1976; "Three-Wave Mixing in Atomic Media," Seminar, Bell Laboratories, Murray Hill, New Jersey, January 27, 1977; "Coherent Hanle Effect," Seminar, New York University, New York, New York, February 10, 1977.

G. W. Flynn, "Vibrational Energy Transfer in Small Molecules," Seminar, University of Wisconsin, Madison, Wisconsin, September 21, 1976; "Laser Studies of Intermode Energy Transfer in Small Molecules," Seminar, Yale University, New Haven, Connecticut, October 8, 1976; "Lasers, Energy Transfer, and Vibrational Photochemistry," Seminar, University of Maryland, College Park, Maryland, October 28, 1976; "Intermode Energy Transfer in Small Molecules," Seminar, State University of New York, Stony Brook, New York, February 25, 1977; "Lasers, Energy Transfer, and Vibrational Photochemistry: Is Chemical Nirvana Near," Seminar, Exxon Corporate Research Laboratory, Linden, New Jersey, March 16, 1977; "Vibrational Energy Transfer in Small Molecules," Seminar, Pennsylvania State University, University Park, Pennsylvania, April 6, 1977; "Lasers, Energy Transfers, and Vibrational Photochemistry," Seminar, Allied Chemical Co., Moorestown, New Jersey, June 6, 1977.

R. W. Guernsey, "Superfluid ^3He: New Measurements of Viscosity and Superfluid Fraction," University of Michigan, Department of Physics, Ann Arbor, Michigan, February 8, 1977; IBM Watson Labs, Physical Sciences, Yorktown Heights, New York, March 3, 1977; University of Notre Dame, Department of Physics, Notre Dame, Indiana, May 3, 1977.

R. Gupta, "Excited States of Alkali Atoms," Colloquium, Wesleyan University, Middletown, Connecticut, October 28, 1976; Colloquium, Kansas State University, Manhattan, Kansas, February 22, 1977; Colloquium, Air Force Institute of Technology, Wright-Patterson Air Force Base, Ohio, May 13, 1977.

S. R. Hartmann, "Two-Photon Doppler-Free Spectroscopy," The New York Academy of Sciences, New York, New York, October 15, 1976; "Sum and Difference Frequency Generation in Atomic Vapors," Seminar, Bell Laboratories, Holmdel, New Jersey, February, 1977.

R. Slater, "Vibrational Energy Transfer and Infrared Photochemistry," Seminar, Allied Chemical, Morristown, New Jersey, August 16, 1977; "Energy Transfer in Small Polyatomic Molecules and the Scattering of Low Energy Electrons by Polar Molecules," Seminars, AVCO, Everett, Massachusetts, August 26, 1977.

A. C. Tam, "Interaction of Laser-beam with Dense Alkali Vapors - Recent Development," Colloquium, University of South Carolina at Columbia, Columbia, South Carolina, November 23, 1976; "Bouncing Laser Beams and Laser-Snow," Seminar, Brookhaven National Laboratory, Upton, New York, March 31, 1977; "Bouncing Laser Beams and Glowing Laser-produced Plasma," Seminar, Bell Laboratories, Murray Hill, New Jersey, April 14, 1977.

W. Happer, "Laser Snow," University of California at Santa Barbara, February 16, 1977; Allied Chemical Research Labs, Morristown, New Jersey, March 14, 1977; Wesleyan University, April 7, 1977; Harvard University, Cambridge, Massachusetts, May 23, 1977. "Highly Excited Alkali Inert Gas Excimers," Aussois France, June 15, 1977; Paris Observatory, June 10, 1977.

Resonance Seminars

Meetings are held weekly at Columbia University, New York, New York, during the academic year and are open to all members of the Physics Department. Guest speakers are invited to discuss work in the general area of the research in the Columbia Radiation Laboratory.

H. Schlossberg, A. F. Cambridge Research Laboratories, "Optically Pumped Infrared Lasers," June 11, 1976.

J. C. Lehmann, Labortoire de Spectroscopie Hertzienne de L'E.N.S., Paris, "The Effect of the Hyperfine Interaction on the Predissociation of Diatomic Molecules," August 5, 1976.

J. Gary Eden, Naval Research Laboratory, "Progress in the Development of the Rare Gas Halide Lasers," September 17, 1976.

Henri Dubost, Massachusetts Institute of Technology, "Strong Vibrational Excitation by V-V Energy Transfer Following Weak Laser Pumping in Low Temperature Molecular Solids," October 1, 1976.

Robert Melcher, Watson Laboratories, "Polarization Echoes in Powders," October 8, 1976.

A. Winnacker, Universitat Heidelberg, "Optical Pumping in a Solid State System: F-Centers," October 15, 1976.

W. C. Stwalley, University of Iowa, "Long Range Atomic Interactions," October 18, 1976.

Guenter Adler, Bell Laboratories, "Experimental Investigation of Critical Phenomenon," October 22, 1976.

B. Sayer, Centre d'Etudes Nucleaire de Saclay, "Departure From Thermodynamic Equilibrium in Ionized Cesium Vapor," October 29, 1976.

Walter Faust, Naval Research Laboratory, "Experimental Studies of Solid State Systems with Laser Sources," November 5, 1976.

Harold Jacobs, Rudolf Buser and Edward H. Poindexter, U. S. Army Electronics Command -"Electronics Research at Fort Monmouth," November 12, 1976.

Rogers H. Stolen, Bell Laboratories, "Non Linear Optics in Fibers," December 3, 1976.

Robert Kennedy, Massachusetts Institute of Technology, "Quantum Information Theory: Unanswered Questions," January 28, 1977.

Patrick Hu, Bell Laboratories, "Spin-Flip Raman Echoes," February 4, 1977.

Charles Bowden, Redstone Arsenal, "Effects of Chemical Reaction in Laser-Induced Molecular Excitation and Molecular Internal Relaxation," February 11, 1977.

Thomas Karras, G. E. Space Science Laboratory, "Probed Metal-Vapor Lasers; High Efficiency, High Gain Superfluorescent Emission," February 11, 1977.

L. Kravitz, AFOSR, "Civics for Scientists," February 25, 1977.

T. Venkatesan, Bell Laboratories and Brooklyn College. "Optical Bistability and Differential Gain Using a Nonlinear Medium," March 4, 1977.

Hermann Robl , U. S. Army Research Center, "Coherent Excitation of Atoms by Charged Particles," March 11, 1977.

Jon Hon, Rocketdyne Division, Rockwell Inc., "High Energy Lasers," March 25, 1977.

Curt Wittig, "Experimental Unimolecular and Bimolecular Kinetic Studies: E-V Energy Transfer and Muliphoton Dissociation," March 28, 1977.

Avigdor Ronn, Brooklyn College, "Laser-Induced Particulate Formation," April 15, 1977.

Howard Card, Columbia University, "Physics and Applications of MOS Devices with Ultra-Thin (Tunnelable) Oxides," June 8, 1977.

I. ATOMIC PHYSICS

A. PHYSICS OF OPTICALLY-PUMPED ATOMIC VAPORS*

(W. Happer, A. C. Tam)

The progress in this project during the past interval is described in the following subsections: 1. Magnetic resonance in dense alkali vapors;[1] 2. Interactions between laser beams in an alkali vapor due to optical pumping;[2] 3. Utilization of optical pumping for novel visible displays of an inhomogeneous magnetic field or of an RF frequency spectrum.[3]

1. Magnetic resonance in dense alkali vapors

For the past several years[4][5][6][7] we have been investigating optical pumping in very dense alkali vapors with the hope that we would eventually be able to use these systems to develop miniature, inexpensive optically pumped devices like magnetometers and gyroscopes. We have published experimental observations[1] in Rb and Cs that for increasing alkali density, magnetic resonance linewidth first broadens with higher alkali density, reaches a maximum broadening, and then shrinks with higher alkali density. Preliminary theoretical explanations for this behavior of spin-exchange narrowing, with an associated spin-exchange shifting of the position of the magnetic resonance line-center, have also been given.[1] This theory predicts that in spin-exchange narrowing, the linewidth decreases as the reciprocal of the alkali density, and this is substantiated in our observation for alkali density $< 10^{16}$ cm^{-3}. However, the question

arises as to whether there is any ultimate limit to exchange narrowing at very high alkali density. In this report, we describe some preliminary theoretical and experimental efforts to study this problem.

Exchange narrowing occurs because the spin exchange collisions cause an alkali atom to jump rapidly between the atomic ground-state Zeeman multiplets of total angular momentum F = a = I + 1/2 and F = b = I - 1/2. In essence it is the existence of a nuclear spin I which leads to spin exchange narrowing in the alkali atoms, because the two different Zeeman multiplets have Larmor frequencies ω_a and ω_b which are very nearly equal and opposite. The mechanism for spin exchange broadening and narrowing is illustrated in Figure 1. The atoms precess freely between spin exchange collisions in either the upper Zeeman multiplet, the intervals labelled A, or the lower Zeemen multiplet, the intervals labeled B. The transverse magnetization of the atoms is proportional to the sine of the phase angle φ.

Every time a spin exchange collision occurs the atoms reverse their sense of precession and a break occurs in the sine wave. For slow spin exchange (i) of Figure 1, the exchange collisions occur infrequently and a Fourier analysis of the precessing magnetization would reveal sharp resonances at the Larmor frequencies ω_a and ω_b of the upper and lower Zeeman multiplets. The widths of the peaks in case (i) are proportional to 1/T, the spin exchange rate. When the spin exchange rate 1/T is comparable to the Larmor precession rates ω_a and ω_b, the precessing magnetization will exhibit no sharp resonance frequencies, as shown in (ii) of Figure 1. However, when the spin exchange

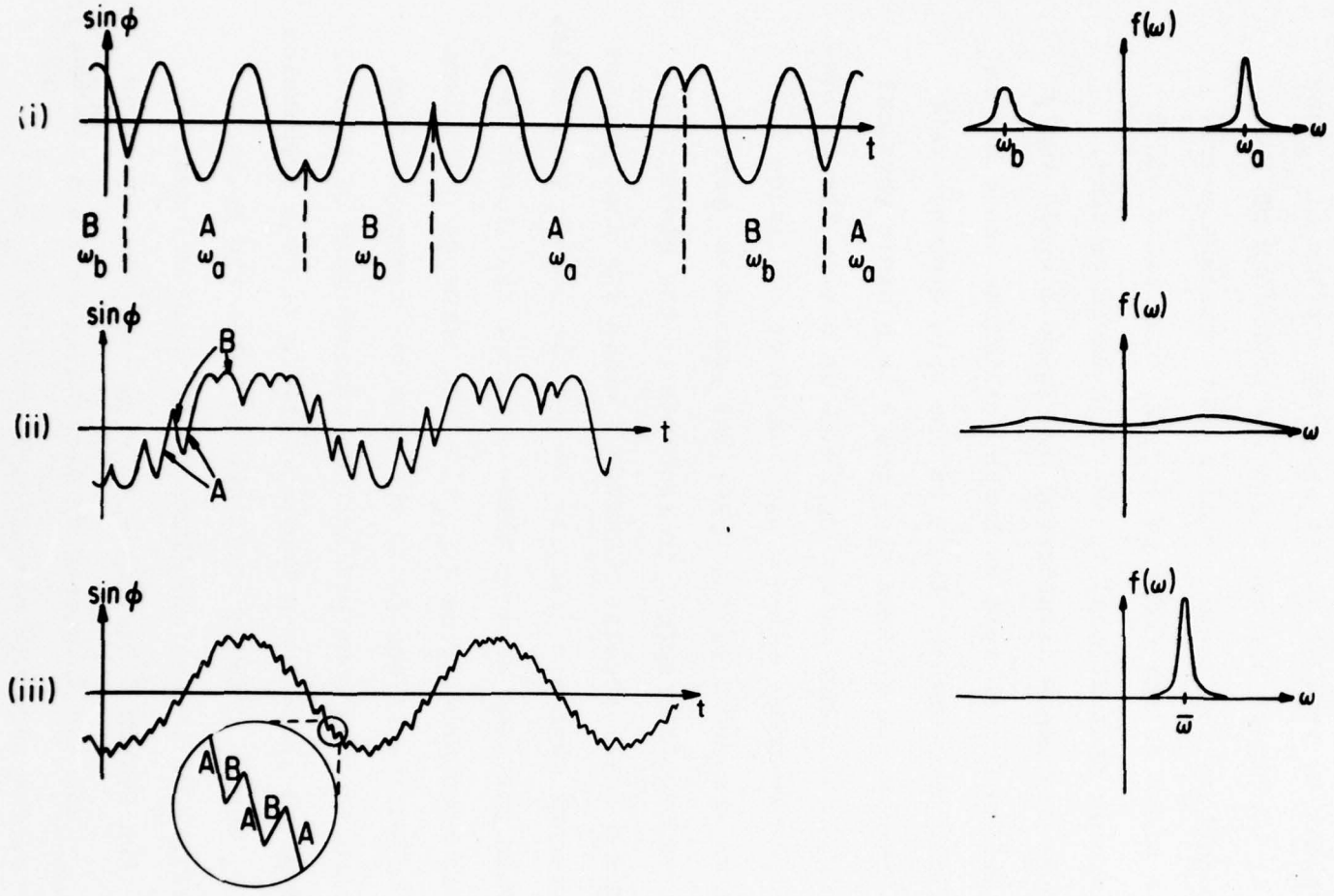

Figure 1: Qualitative graph of the sine of the precession angle φ versus time t, and the corresponding Fourier analysis $f(\omega)$ versus ω, for various alkali density: (i) Low density, i.e. spin exchange rate << Larmor precession; (ii) Intermediate density; (iii) High density, i.e. spin exchange rate >> Larmor precession.

rate is very much faster than the Larmor precession rate, the atoms will appear to precess at the weighted average of ω_a and ω_b (case (iii) of Figure 1), and a Fourier transform of the precessing magnetization would reveal a sharp resonance frequency with a width on the order of $|\omega_a|^2 T$, that is, a width which is inversely proportional to the spin exchange rate.

The simple arguments illustrated by Figure 1 would imply that the linewidth due to spin exchange collisions would become narrower and narrower without limit as the spin exchange rate increased. However, we believe that there is a basic physical limit to the spin exchange narrowing which is due to the following physical phenomenon: after a spin exchange collision it takes a time on the order of one hyperfine precession period $(\omega_{hfs})^{-1}$ for the nuclear spin I to recouple to the electronic spin S to form a total angular momentum F which can then precess about the external magnetic field at one of the Larmor frequencies ω_a or ω_b. When the time between these exchange collisions is less than this recoupling time $(\omega_{hfs})^{-1}$, the exchange collisions become less effective in narrowing the magnetic resonance line. We have carried through some preliminary calculations of this effect and typical results are shown in Figure 2. The precession frequencies ω_+ and ω_- undergo rapid changes when the spin exchange rate $1/T$ is in the neighborhood of three critical frequencies, the Larmor frequency $(\omega_o \approx \omega_a \approx -\omega_b)$, the hyperfine frequency (ω_{hfs}), and the frequency of decoupling of I and S $(\frac{\omega_{hfs}^2}{\omega_o})$. The behavior of the magnetic resonance linewidths Γ_+ and Γ_-, also exhibits sharp changes at these critical frequencies. Some computed values of $\omega_{\pm}$ and $\Gamma_{\pm}$ for Cs^{133} are given in Table I. Thus

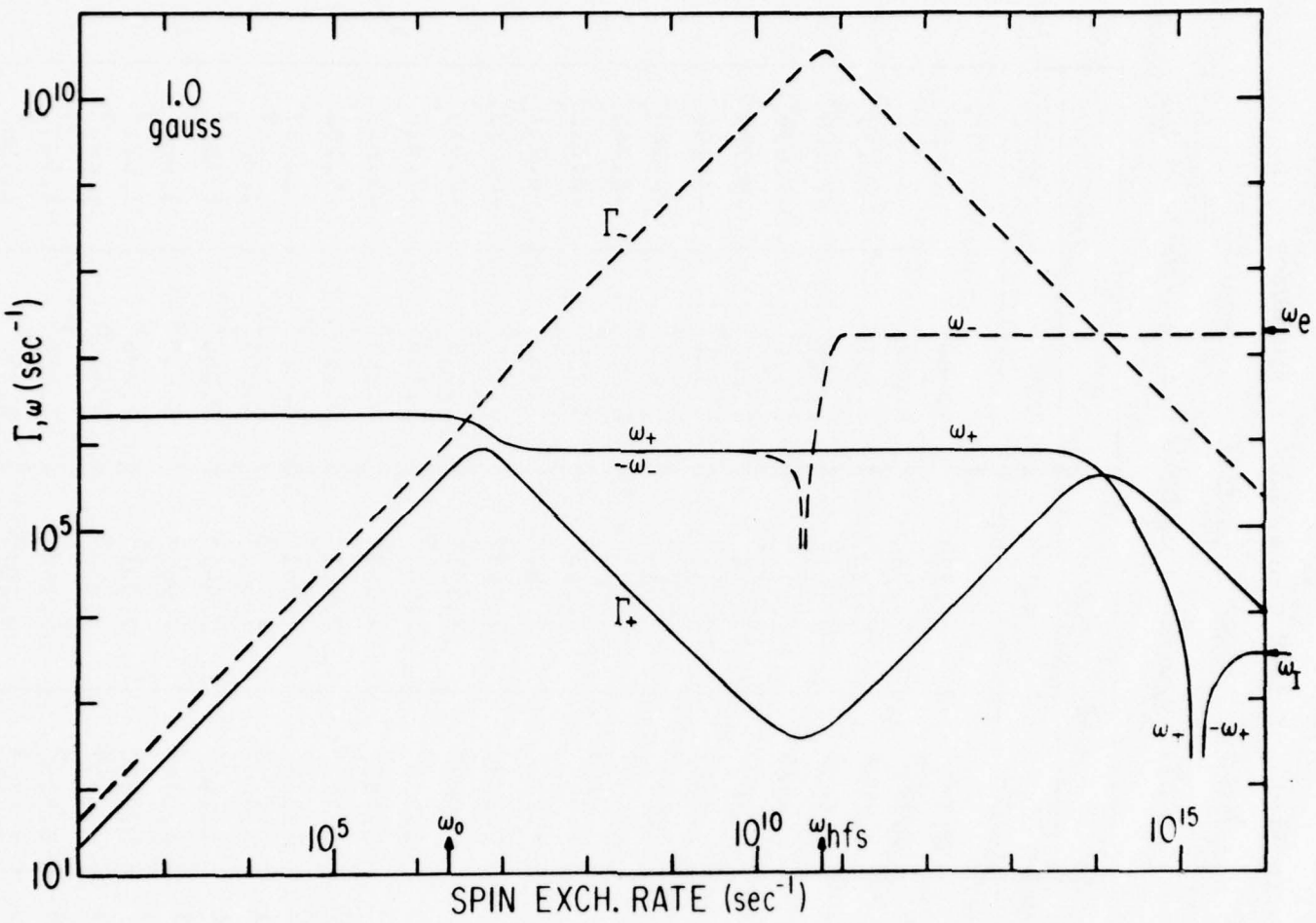

Figure 2: Computed magnetic resonance linewidths Γ_+, Γ_-, and frequencies ω_+, ω_- versus spin exchange rate in Cs for an applied field of 1.00 Gauss. The Larmor frequencies of a Cs atom, a free electron, and a bare Cs nucleus are denoted by ω_o, ω_e and ω_I respectively. ω_{hfs} is the hyperfine frequency of a Cs atom.

TABLE I

Computed values in sec^{-1} of $\Gamma_{\pm}$ and ω_I for Cs^{133} ($I = \frac{7}{2}$) for magnetic field of 1.00 Gauss. Larmor frequency ω_o/H is 2.198^6 sec^{-1} $Gauss^{-1}$ and hyperfine frequency ω_{hfs} is 5.776^{10} sec^{-1}. All upper-case numbers denote powers of 10.

Spin exchange rate (sec^{-1})	$\lambda_+ = -\Gamma_+ - i\omega_+$		$\lambda_- = -\Gamma_- - i\omega_-$	
	Γ_+	ω_+	Γ_-	ω_-
10^4	2.188^3	2.195^6	4.688^3	-2.202^6
10^5	2.187^3	2.195^6	4.688^4	-2.202^6
10^6	2.174^5	2.172^6	4.701^5	-2.179^6
2×10^6	4.263^5	2.101^6	9.486^5	-2.108^6
5×10^6	8.674^5	1.611^6	2.570^6	-1.618^6
10^7	6.209^5	9.724^5	6.254^6	-9.794^5
2×10^7	3.076^5	8.335^5	1.344^7	-8.406^5
5×10^7	1.222^5	8.018^5	3.425^7	-8.088^5
10^8	6.105^4	7.975^5	6.869^7	-8.045^5
2×10^8	3.052^4	7.965^5	1.375^8	-8.035^5
5×10^8	1.221^4	7.962^5	3.437^8	-8.031^5
10^9	6.109^3	7.961^5	6.875^8	-8.027^5
2×10^9	3.063^3	7.961^5	1.375^9	-8.015^5
5×10^9	1.250^3	7.961^5	3.435^9	-7.928^5
10^{10}	6.689^2	7.961^5	6.855^9	-7.609^5
2×10^{10}	4.222^2	7.961^5	1.358^{10}	-6.204^5
5×10^{10}	4.148^2	7.961^5	3.103^{10}	1.337^6
10^{11}	6.464^2	7.961^5	2.605^{10}	1.800^7
2×10^{11}	1.201^3	7.961^5	1.184^{10}	1.726^7
5×10^{11}	2.939^3	7.961^5	4.610^9	1.686^7
10^{12}	5.8603	7.961^5	2.296^9	1.681^7
10^{13}	5.827^4	7.920^5	2.293^8	1.679^7
10^{14}	3.915^5	5.134^5	2.254^7	1.707^7
10^{15}	1.027^5	9.294^3	2.191^6	1.758^7
10^{16}	1.042^4	-3.380^3	2.189^5	1.759^7
10^{17}	1.038^3	-3.508^3	2.189^4	1.759^7

our theory predicts that there is a limit to spin-exchange narrowing, when the spin exchange rate equals ω_{hfs}. For Cs, this means a density $\sim 10^{19}$ atoms/cc.

We would like to experimentally observe the effect of spin-exchange narrowing at very high alkali density, and to establish the predicted limit of spin-exchange narrowing. Most of our work is done for Cs, which has the highest vapor pressure and corrodes glass vessels least compared to other alkali metals. At a Cs density $> 10^{15}$ atoms/cc, it becomes impossible to pass the first resonance D_1-line (8943Å) through the Cs vapor, even for a thin cell with high density buffer gas. It seems that the best way to optically pump the high density Cs-buffer-gas system is to use a tunable CW dye laser, tuned onto or near the second D_1-line (4593Å) or perhaps the third D_1-line (3889Å). Such dye lasers must be pumped by large UV Argon or Krypton ion lasers, which we plan to acquire in mid-1977. These higher resonance lines are absorbed more weakly than the first-resonance line (the oscillator strengths are down by two orders of magnitude or more) so that the optical thickness is less of a problem. However, before such light sources become available (in the coming interval), we did some experiments using an indirect mixture pumping[6][7] of Cs atoms via a slight admixture ($\sim 10^3$:1) of Na atoms. The experimental arrangement is shown schematically in Figure 3. A circularly polarized dye laser beam at 5896Å is used to pump the Na atoms, whose spin polarization is tightly coupled to the much more abundant Cs atoms by spin-exchange collisions. Magnetic resonance in the Cs atoms is

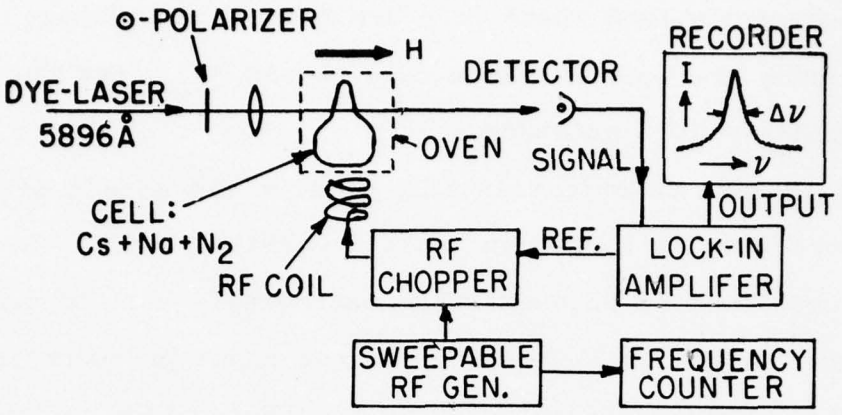

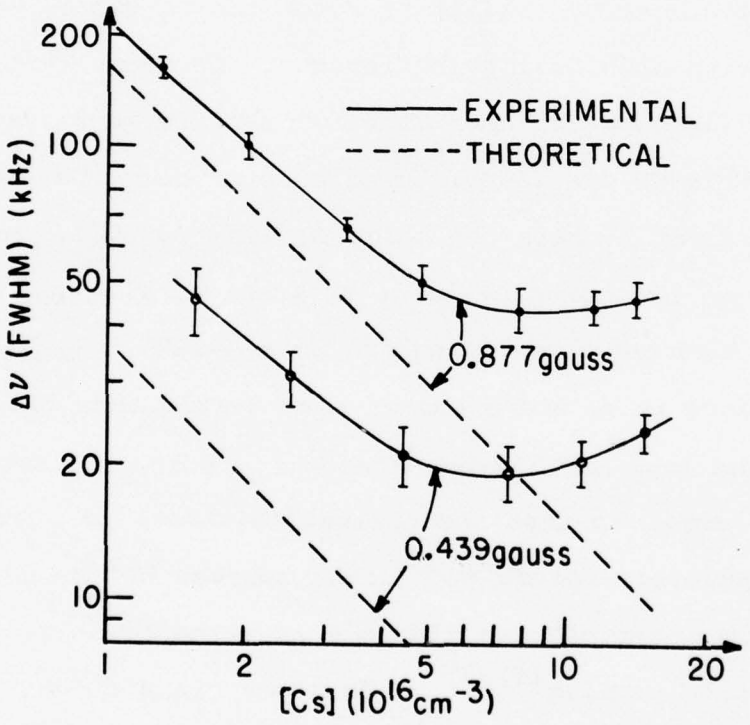

Figure 3: Top: Sketch of the experimental arrangement to use "mixture pumping" to observe magnetic resonance of Cs at densities $\sim 10^{17}$ cm^{-3}.
Bottom: Observed full width $\Delta\nu$ compared to the theoretical full width $2\Gamma_+/(2\pi)$ for fast spin exchange (see Eq. 18 of Ref. 1).

detected for a Cs density in the range of 10^{16}-10^{17} atoms/c.c. The experimentally observed magnetic resonance linewidth $\Delta\nu$ is plotted in Figure 3 together with the theoretically expected linewidth. We notice that at lower Cs densities, the observed $\Delta\nu$ follows roughly the predicted $(\text{density})^{-1}$ dependence. It reaches a minimum linewidth of some tens of kHz (dependent on the applied H) at a Cs density $\sim 5 \times 10^{16}$ atoms/c.c., beyond which the observed $\Delta\nu$ does not decrease further, but seems to increase again with Cs density. For this mixture-pumping experiment, exchange narrowing limit seems to occur at a Cs density that is two orders of magnitude lower than the predicted limit of 10^{19} atoms/c.c. So we are faced with two important questions concerning exchange-narrowing:

(a) What is the mechanism that overwhelms exchange-narrowing in the mixture-pumping experiment at a Cs density $\sim 10^{17}$ atoms/c.c.? Can it be due to impurity atoms like H_2 [8] (The severe corrosion of the glass envelope by Na atoms may cause the release of a variety of impurities, particularly H_2) or could it be due to Cs/Na collisions?

(b) If the above unknown mechanism can be removed or greatly reduced, can we then experimentally observe the predicted exchange-narrowing limit at 10^{19} atoms/c.c. of Cs?

We hope to be able to give some answers to these important questions in the next interval. Our work will be facilitated by a

CW dye laser which can operate at or near 4593Å, so that a pure Cs-buffer-gas system can be optically pumped. The glass we use to fabricate the experimental cells is Corning-1720 aluminosilicate glass, which was verified by us to have excellent resistance to Cs-corrosion (but not to Na-corrosion) if it is initially outgassed at 650°C in high vacuum (10^{-6} Torr) for about a day. We would expect that the pure Cs-buffer-gas cells will be much less contaminated with impurities than the Cs-Na-buffer-gas cells, and hopefully we can then determine experimentally when and why the exchange-narrowing limit is reached.

2. Interactions between laser beams due to optical pumping

While we tried to optically pump a pure Na vapor ($\sim 10^{13}$ atoms/c.c.) without buffer gas with a dye laser beam on the high-frequency wing of the Na D_1-line, we discovered the following interesting new phenomena: (a) If the beam is circularly polarized, it undergoes strong self-focusing, and can be observed as a single, constant-diameter ($\sim$ tens of μm) filament (or a self-trapped filament) in the cell; (b) If the beam is linearly polarized, then it will break up into two coherent circularly polarized filaments of opposite circular polarization after traversing a few cm in the Na vapor; (c) If the laser beam is first decomposed into two circularly polarized beams, which are then fed into the cell, then the two beams are observed to repel each other in the vapor if they are of opposite circular polarization, and they attract each other if they are of equal circular polarization--in other words, unlike beams repel and

like beams attract. In this report, we shall present simple qualitative explanations of these new effects. More details can be found in a recent publication.[2] There is sufficient general interest in these beam-interaction effects that a popular write-up recently appeared in the New Scientist.[9]

We can explain the strong self-focusing behavior of circularly polarized laser beams on the high frequency wing of the D_1 absorption line by the combined effects of optical pumping and anomalous dispersion. The spin polarization due to optical pumping by the σ_+ laser beam in the Na vapor is represented schematically in Figure 4(a). The σ_+ beam can drastically lower its own ground state density N_g (i.e. density of spin-down atoms inside the beam) by "dumping" many atoms into a non-interacting state (spin-up atoms, of density N_{dump}). Thus N_g inside the laser beam is smaller than the spin-down density outside the laser beam. The indices of refraction inside, n_{in}, and outside, n, the beam are:

$$n_{in} = 1 + 2\pi N_g \alpha(\nu) \tag{1}$$

$$n_{out} = 1 + 2\pi \frac{N}{2} \alpha(\nu) \tag{2}$$

where $\alpha(\nu)$ is the atomic polarizability (real part) depending on the laser frequency ν, and N is the total sodium atomic density, and the excited-state density inside the beam is neglected. Thus the refractive index excess inside the beam is

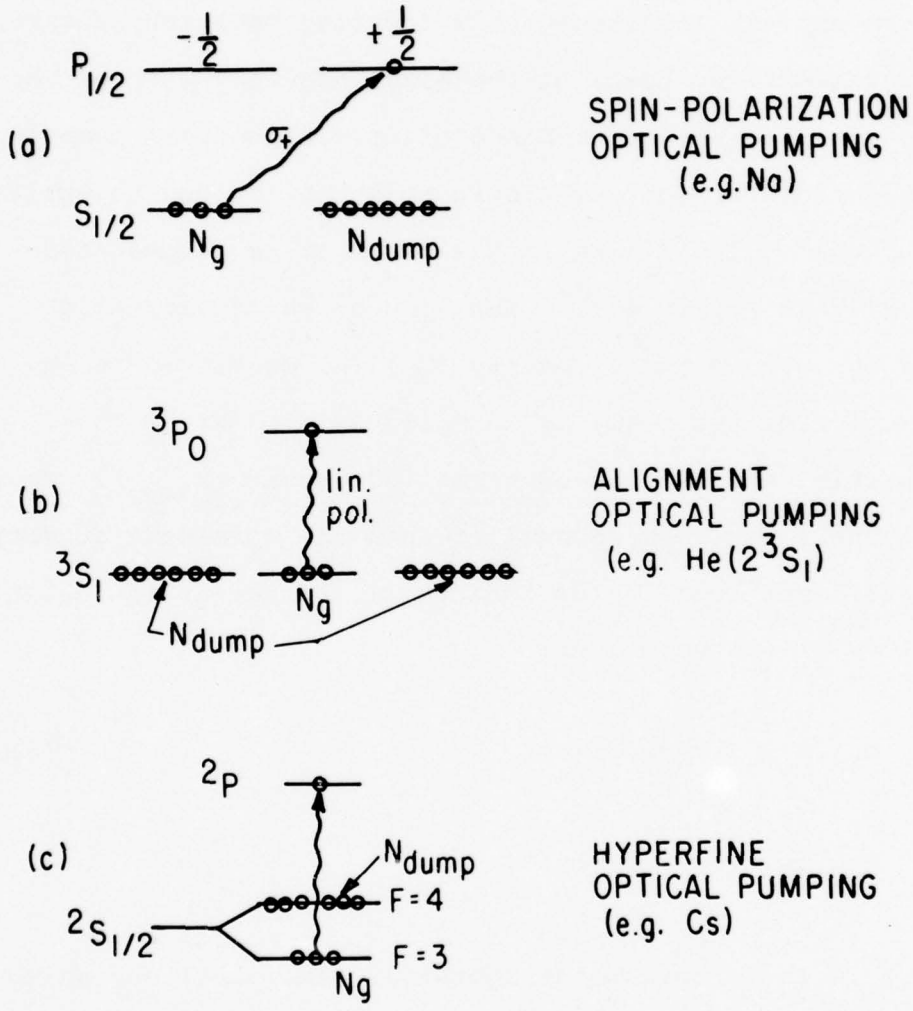

Figure 4: Various cases for self-focusing of laser beams due to optical pumping when the laser frequency is on the high frequency wing of the absorption line indicated.

$$\delta n = n_{in} - n_{out} = -2\pi \left(\frac{N}{2} - N_g\right) \alpha(\nu) \qquad (3)$$

For strong optical pumping, $N_g << N/2$ and then $\delta n = -\pi\, \alpha(\nu) N$. Now for ν larger than the center frequency of the D_1 transition, $\alpha(\nu)$ is negative and so δn is positive and self-focusing can occur. (For ν smaller than the center frequency, $\alpha(\nu)$ is positive and self-defocusing occurs.) Of course, the self-focusing is counteracted by diffraction effects, so the beam narrows down to a stable, self-trapped filament which propagates with no further change in radius. This self-focusing on the high frequency wing due to spin-polarization optical pumping can be extended to other cases of optical pumping. For example, we believe that self-focusing on the high frequency wing also occurs for alignment optical pumping (e.g. a linearly polarized laser beam exciting the $2^3S_1 \rightarrow 2^3P_o$ transition in He, as shown in Figure 4(b)), and for hyperfine optical pumping (e.g. a laser beam exciting a 6^2S (F=3) $\rightarrow 6^2P$ transition in Cs as shown in Figure 4(c)).

The self-focusing in sodium due to spin-polarization optical pumping can also be understood in an atomic model (Figure 5(a)) which is equivalent to the refractive index model discussed above. The interaction energy U between spin-down atoms and the σ_+ laser beam (Figure 5(a)) is

$$U(\nu) = -\frac{1}{2}\, \alpha(\nu)\, E^2 \qquad (4)$$

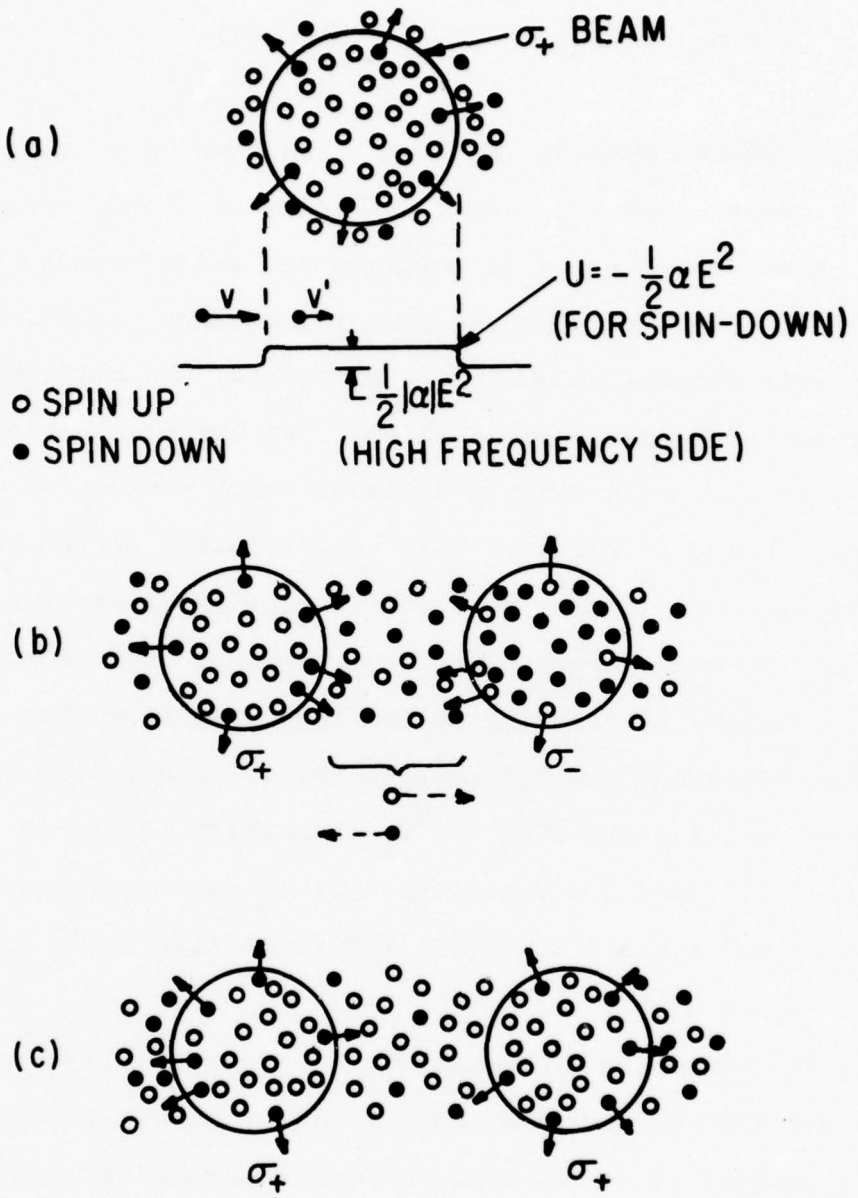

Figure 5: (a) Explanation of self focusing due to spin-polarization optical pumping on the high frequency wing of the D_1 line. The full arrow indicates force on a spin down atom, which sees the laser beam as a potential hill (potential U) and slows down from velocity V to V' on entry. (b) Explanation of the repulsion between σ_+ and σ_- beams due to exchange of spin-polarized atoms. The broken arrows indicate preferred velocities in-between the beams. (c) Explanation of the attraction between two σ_+ beams.

where E is the rms field intensity. For ν being on the high frequency wing of the D_1 line, $U(\nu)$ is positive, and so the spin-down atoms "see" the laser beam as a potential hill. Thus the atoms experience a radially outward force when they enter the laser beam. By action and reaction, the laser beam experiences radially inward forces due to the entry of spin-down atoms, and these inward forces cause self focusing of the beam.

We can extend the above atomic picture for the case of two parallel laser beams, one σ_+-polarized and one σ_--polarized, in the sodium vapor (Figure 5(b)). Due to optical pumping, the σ_+ beam is predominantly filled with spin-up atoms which do not interact with the σ_+ beam. These spin-up atoms move freely (when the mean free path is very long) at thermal velocities, and so the σ_- beam will experience more influx of spin-up atoms from the side of the σ_+ beam than from the opposite side. Since the σ_- beam exerts a radially outward force on the spin-up atoms only (for ν on the high frequency wing), the σ_- beam experiences a net force away from the σ_+ beam due to the asymmetric influx of spin-up atoms, and so the two beams repel. An alternative equivalent description is that the σ_+ beam is creating a graded refractive index for the σ_- beam, which sees a higher refractive index away from the σ_+ beam. Our qualitative theory predicts that self-focused σ_+ and σ_- beams will repel each other due to their exchange of spin-polarized atoms. This is indeed experimentally verified [2] and, in fact, we found that the repulsive force is big enough so that we can "bounce" σ_+ and σ_- beams against each other, i.e., the two beams are observed to undergo an "anticrossing" inside the Na cell.

If the repulsion is mediated by spin- polarized atoms, then the repulsion can be decreased by depolarizing the atoms by a transverse magnetic field (~ a few Gauss). This is also experimentally verified. (2)

Figure 5(c) explains the case of beam-attraction: two self-focused beams of equal circular polarization attract each other for ν on the high frequency wing of the D_1 line. Consider two σ_+ beams parallel to each other. The beams experience less influx of spin-down atoms on their near sides than on their far sides, and so they are deflected towards each other. This attractive behavior is also experimentally verified.(2)

The repulsion between σ_+ and σ_- beams is also manifested in the break-up of a linearly polarized laser beam into two coherent beams of opposite circular polarization (Figures 6 and 7). The linearly-polarized parent beam is a superposition of a σ_+ and a σ_- beam on top of each other. This is really an unstable situation (like a pencil standing on its tip on a table) because the two components repel each other if they are ever slightly displaced, i.e. any small distortions of the wave-front of the parent beam will cause the decomposition of the parent beam into two repelling σ_+ and σ_- beams. The asymptotic splitting half-angle between the two daughter beams can be estimated theoretically as

$$\theta \sim \sqrt{-\pi\, \alpha(\nu)\, N} \qquad (5)$$

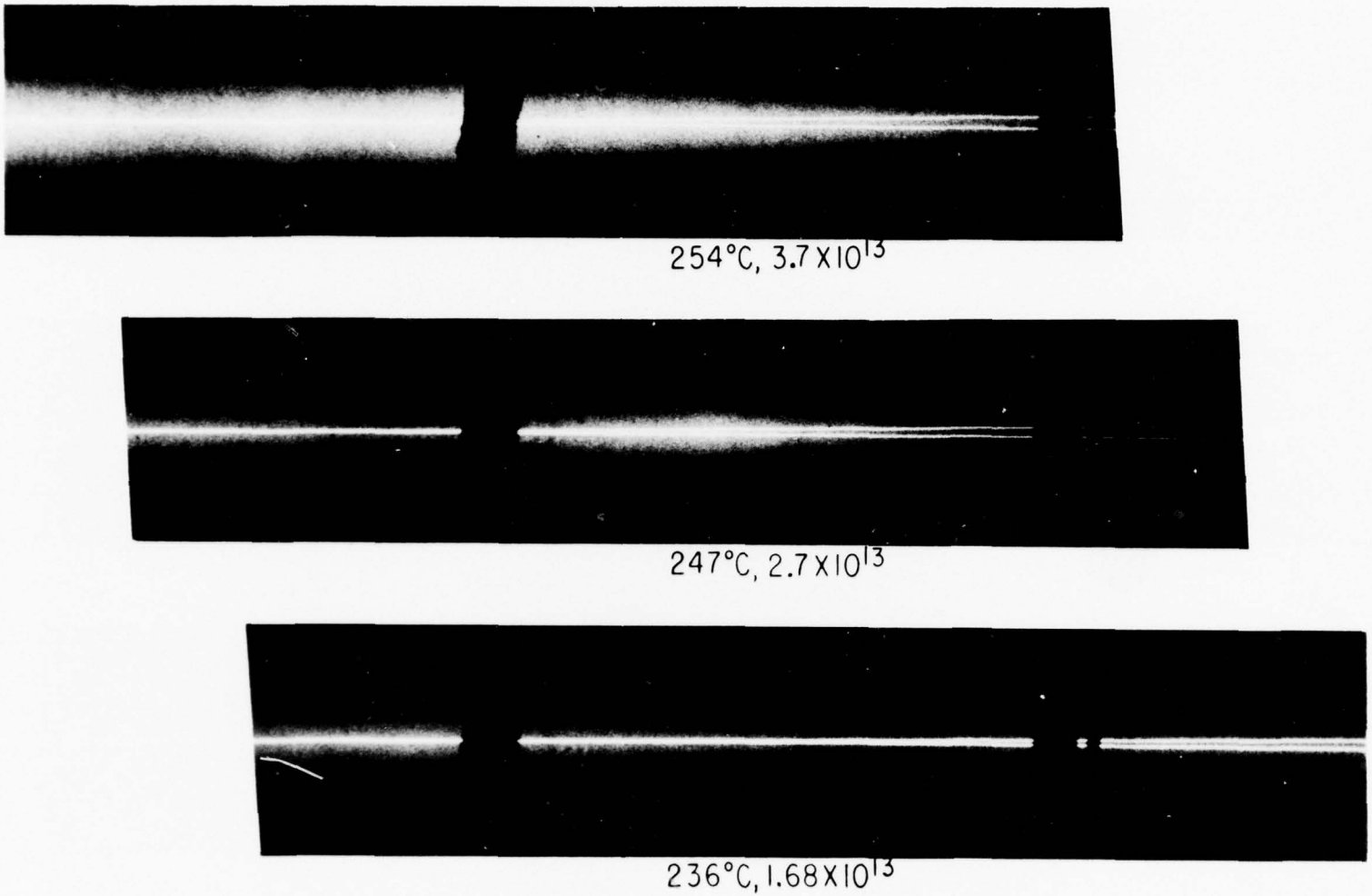

Figure 6: Observed break-up of a parent linearly polarized beam, incident on the Na vapor from the left, into two coherent daughter beams of opposite circular polarization, equal intensity, and symmetrical deviation from the parent direction. The splitting angle increases as cell temperature and sodium density increases.

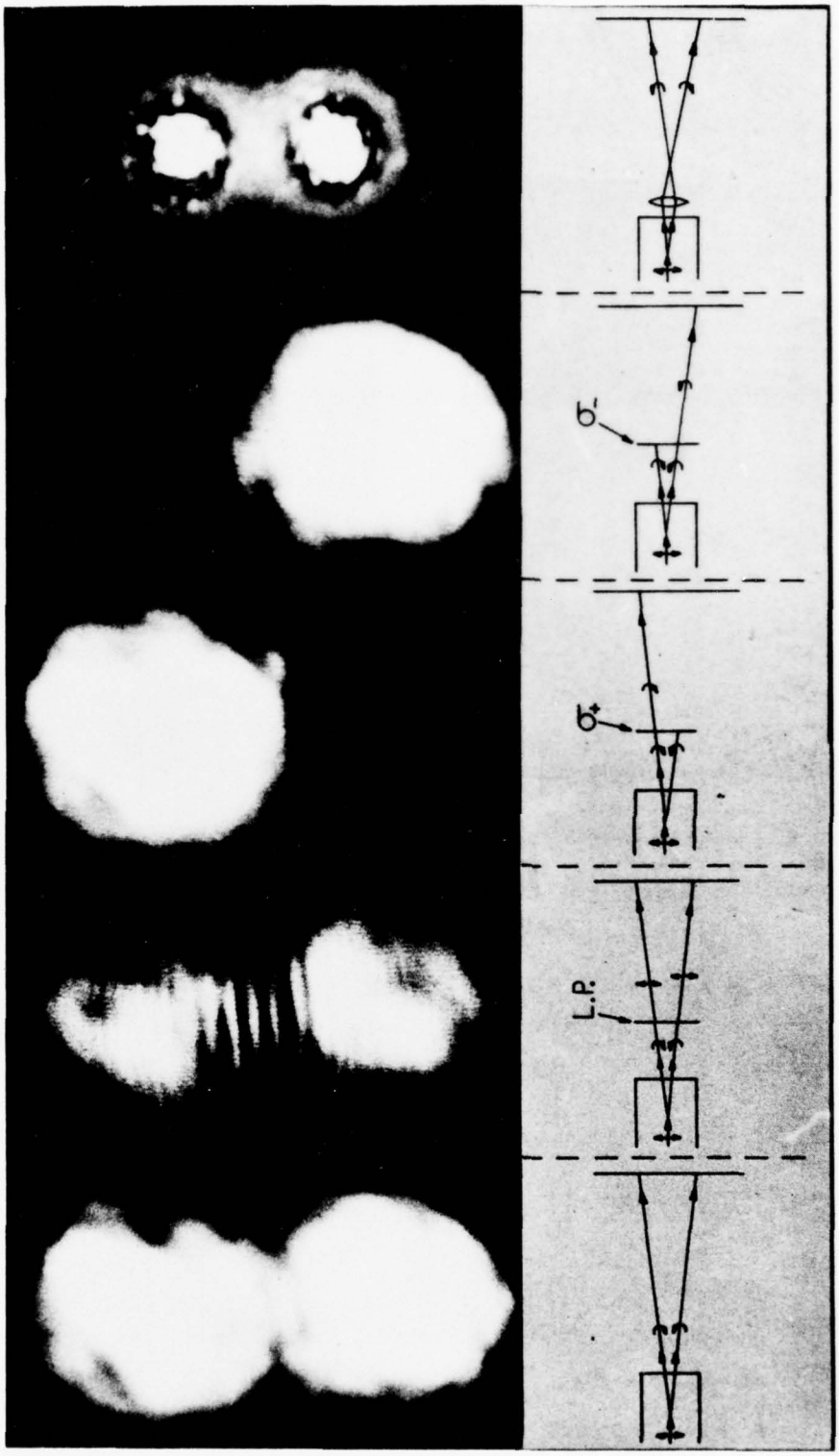

Figure 7: Observed patterns when the daughter beams hit the screen about 175 cm from the Na cell. From left to right: no polarizer, linear polarizer, σ_+-polarizer, σ_--polarizer, and when a convex lens (of f = 2" and placed about 2" from the exit window) is inserted between the Na cell and the screen.

which agrees well with experimental observations.[2] If the parent beam is perfectly linearly polarized, then the daughter beams are observed to be of equal intensity, and they deviate symmetrically from the parent direction. If the parent is slightly elliptically polarized (say with ellipticity σ_+), then the σ_+ daughter beam is more intense than the σ_- daughter beam, and the former deviates less than the latter from the parent direction.

To summarize, we have discovered previously unknown long-range forces between CW self-focused, circularly polarized laser beams on the high frequency wing of the D_1 line in a sodium vapor. These forces have the following features: (a) Like beams attract; unlike beams repel; (b) The forces are mediated by spin-polarized ground state atoms, so they are long-range and they are attenuated by transverse magnetic fields; (c) The forces are large enough to be readily observable near the D_1-resonance; (d) The forces are negligible if the light is too far off resonance. Theorists have long been interested in calculating the scattering cross-section of two light beams from each other in vacuum. This effect of photon-photon scattering turns out to be far too small to be observable in the present-day laboratory. What we found is that the scattering between two light beams is greatly enhanced when mediated by suitable atoms.

We believe that suitable laser-beams in other atomic systems that can be readily optically pumped should also exhibit forces on each other, and we believe that beam interactions due to alignment optical pumping (Figure 4(b)) or hyperfine optical

pumping (Figure 4 (c)) are also possible. For example, two linearly polarized laser beams on the higher frequency side of the He ($2^3S_1 \rightarrow 2^3P_o$) transition should repel or attract each other in a He (2^3S) atomic system if the laser polarizations are perpendicular or parallel to each other respectively. Thus, we believe that the long-range forces we observed in sodium should be a rather general effect. Such forces are potentially useful for micro-manipulations of a laser beam, controlled by another spatially-resolved laser beam.

The quantitative understanding of the scattering between two laser beams in an atomic vapor and the generalization of the scattering to various other atomic systems besides sodium will be goals during the next interval. An exact analysis would entail the consideration of population hole-burning, detailed laser-frequency dependence, hyperfine structure, effects of buffer gases, etc.

3. Utilization of optical pumping for novel visible display of magnetic field or rf spectrum

We have recently constructed[3] a novel optically pumped device for a sensitive, real-time and visible display of the quantitative variation of a magnetic field with high spatial variation. Photographs of typical displays in the form of "contour maps" of the magnetic field being studied are reproduced in Figure 8. The field contours give quantitative magnitude of the field component in a specified direction, and they are spaced 5 mG apart in Figure 8. These first contour photographs of a

Figure 8: Photographs of the field contour lines (spaced 5 mG apart). (a) δH_z is produced by a pair of single-turn Helmholtz coils separated by 3.1 cm (at positions indicated by arrows) carrying 0.2 A current. The central bright region indicates a field δH_z of 57 mG uniform within $\pm$ 1 mG, and field decreases from center outwards. (b) δH_z is now due to a screwdriver tip placed about 10 cm from the upper left corner of the cell. (c) Display of the superimposed fields in (a) and (b). (d) Same as in (a) except now the currents through the two coils are in opposite sense.

(a)

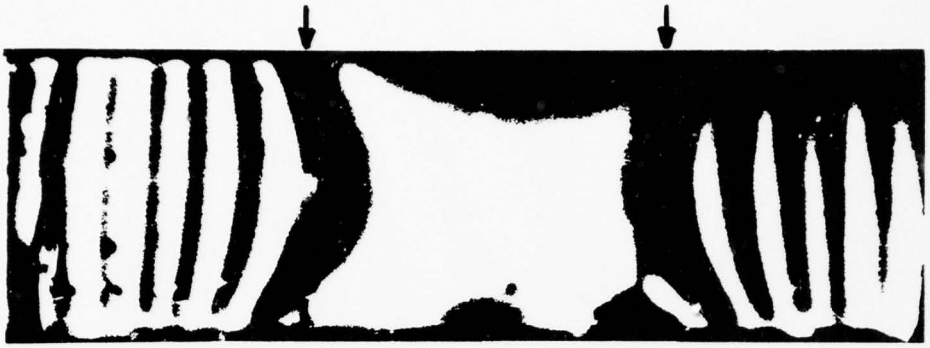

HELMHOLTZ COILS

(b)

SCREWDRIVER

(c)

SCREWDRIVER + HELMHOLTZ COILS

(d)

ANTI-HELMHOLTZ COILS

Figure 8

magnetic field demonstrate that our display device is a powerful new tool to study an extended irregular magnetic field that may vary rapidly in space and time.

The description of our device is given in a recent communication.[3] Briefly, it consists of an aluminosilicate glass cell containing sodium atoms ($\sim 10^{12}$ atoms/c.c.) mixed with 640 Torr He and 130 Torr N_2, optically pumped by a circularly-polarized dye-laser beam at 5896Å in the z-direction. The beam, of power $\sim$ 10 mW, has a cross-sectional area about 0.4 cm $\times$ 2.5 cm (i.e. ribbon-shaped beam). The cell is situated in the inhomogeneous field $\delta\vec{H}$ to be studied (say varying from 0 to tens of mG) and a homogeneous field $\vec{H}_o$ (in the z direction, of magnitude $\sim$ 1 G) is superimposed on $\delta\vec{H}$. Under these conditions, the Na atoms are highly spin-polarized by optical pumping, and so the whole cell looks dark from the side. A comb of equally spaced rf frequencies ν_i (i=1, . . . , K) is then applied to the cell. We discovered that a localized glow inside the cell can be observed at position $\vec{r}$ if

$$\nu_i = \gamma \, (H_o + \delta H_z \, (\vec{r})) \tag{6}$$

where γ is the gyromagnetic ratio of Na, and is 700 kHz/G at low field. Thus for the comb of rf frequencies applied, a corresponding set of nested glowing surfaces of constant δH_z separated by dark layers is observable inside the cell. We use a ribbon-shaped laser beam to "cut a planar section" out of the field contours so that the display can be readily photographed, as given in Figure 8.

Our device can also be used as a novel rf spectrum analyzer (no reference local oscillator is needed). To display an rf spectrum, a known magnetic field gradient in the z direction is applied to the cell. The rf wave, containing unknown frequencies f_i with unknown intensities $I(f_i)$, is applied to the cell. We can then observe a glowing planar surface at position z_i when

$$f_i = \gamma H(z_i)$$

with a glow intensity proportional to $I(f_i)$. Thus our frequency spectrum display is quite similar to the optical spectrum given by a grating monochromator. Photographs of the rf frequency spectrum display for various FM waves are given in Figure 9(a), and the recorded intensities of the RF components in the photographs are quite consistent with the theoretical intensities of the components, as plotted in Figure 9(b).

During the next interval, we plan to do more theoretical and experimental work on the optimization and real limits of the above display device for magnetic field or RF spectrum. We also would like to investigate the possible use of the device for microwave frequency analysis (near the hyperfine frequency of the alkali atom).

*This research was mainly supported by the Air Force Office of Scientific Research under Grant AFOSR-74-2685. The present project title includes work under the previous title of "Spin-exchange shift and narrowing of magnetic resonance lines in alkali vapors" in previous Progress Reports.

(1) W. Happer and H. Tang, Phys. Rev. Lett. 31, 273 (1973).

(2) A. C. Tam and W. Happer, Phys. Rev. Lett. 38, 278 (1977).

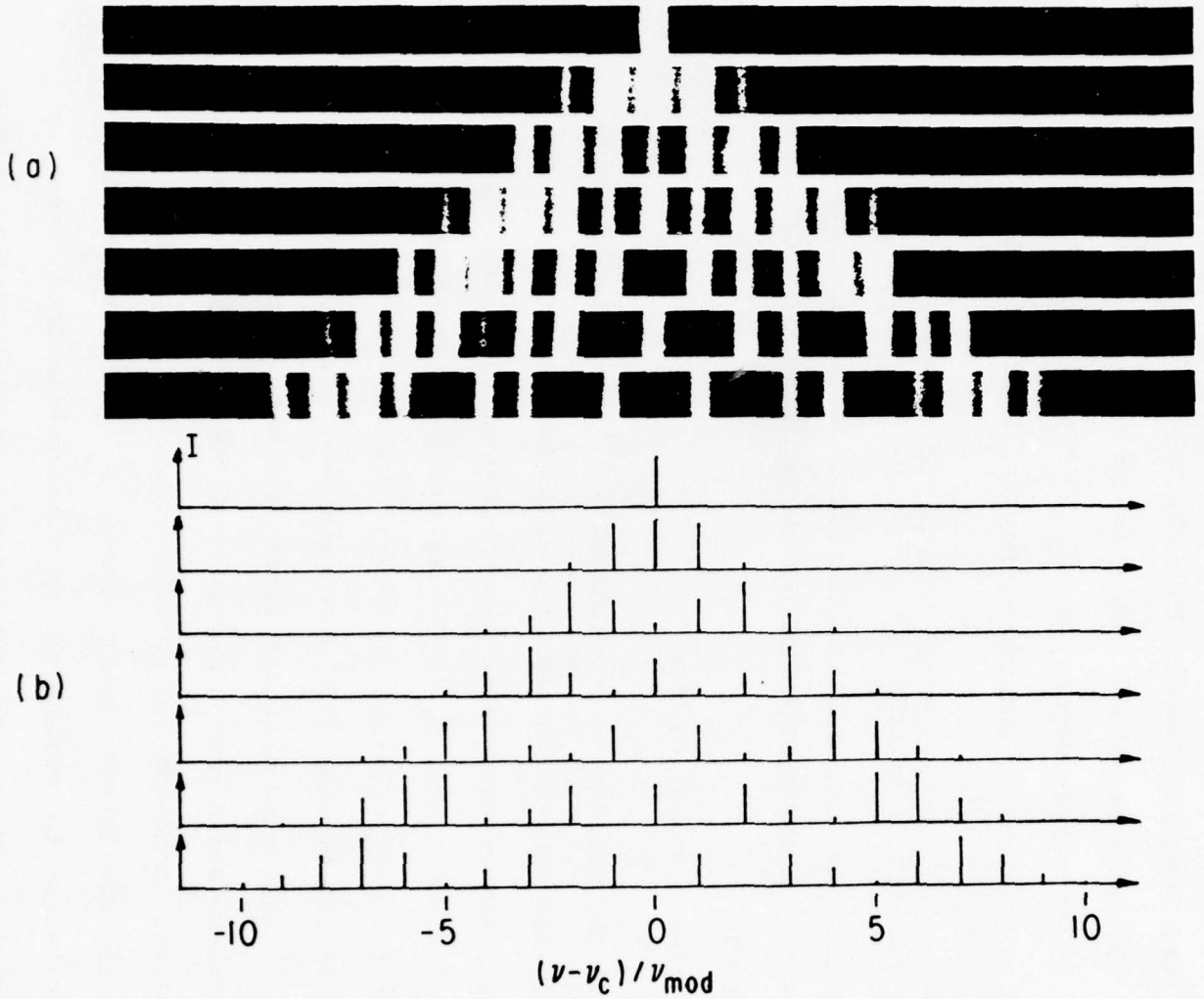

Figure 9: (a) Photograph of the rf spectrum display for FM waves of carrier frequency 455 kHz, sinusoidally modulated at 3.50 kHz with increasing amplitude of modulation (or frequency deviations) from top to bottom.
(b) The theoretical rf spectrum of the FM waves in (a).

(3) A. C. Tam and W. Happer, App. Phys. Lett. 30, 580 (1977).

(4) CRL Progress Report, June 30, 1973, p. 44.

(5) CRL Progress Report, June 30, 1974, p. 59.

(6) CRL Progress Report, June 30, 1975, p. 28.

(7) CRL Progress Report, June 30, 1976, p. 21.

(8) A. C. Tam, G. Moe, and W. Happer, Phys. Rev. Lett. 35, 1630 (1975).

(9) "Like light attracts, unlike light repels" in New Scientist, February 24, 1977, p. 455.

B. SELECTIVE LASER EXCITATIONS AND CHEMICAL PHYSICS OF SIMPLE SYSTEMS*

(W. Happer and A. C. Tam)

About two years ago, we reported[1][2] the first observation of particulate-formation in a metallic vapor (cesium or rubidium) under resonant laser excitation of the alkali atoms or molecules. A little H_2 or D_2 gas must be present in the vapor for the particulation to occur. For the case of a Cs/H_2 mixture excited by the 4579Å argon ion laser line, spectroscopic analysis[3] indicates that the laser beam manufactures many CsH molecules, which then dimerize and condense into CsH solid particulates. Condensation readily occurs because CsH solid has very low equilibrium vapor pressure.[1] This resonant laser excitation to produce micron-sized particulates seems to be a promising new way for laser-isotope-separation, and this phenomenon has stirred world-wide interest.[4][5][6] During the past interval, we have tried to gain more understanding of

this phenomenon, and have discovered some related phenomena. We have studied the molecular excitation of cesium or rubidium[7] by certain argon ion laser lines. We also discovered that stepwise excitation of Cs atoms to the $8D_{3/2}$ state causes the formation of particulates very efficiently when D_2 is present;[8] however, in the absence of foreign gas, a laser-produced plasma is formed near the laser focus.[9] Our progress in the past interval is reviewed briefly in the following; more details are given in the publications cited.

1. Laser excitation of a cesium vapor system

As reported previously,[1][2] two blue argon ion laser lines, 4545Å and 4579Å, are found to form particulates very efficiently in a vapor mixture of Cs (> 1 Torr) and H_2 (> 50 Torr) in the absence of helium (so that the Cs atomic absorption lines at 4555Å and 4593Å are sharp). Under these circumstances, the laser can only be absorbed by Cs_2 molecules. As indicated in Figure 10, there is a broad Cs_2 absorption band in the region 4500-5100Å, which matches quite well the blue argon ion lines. However, we found that the argon ion lines other than the above two will hardly form any particulates. In particular, the 4880Å line forms no particulates, although it is one of the brightest argon ion lines, and is very strongly absorbed by Cs_2 (see Figure 10). Hence we conclude that only special Cs_2^* molecules (produced by the 4545Å or the 4579Å lines) can form particulates, probably through the production of Cs*(7P) atoms by excitation transfer collisions:

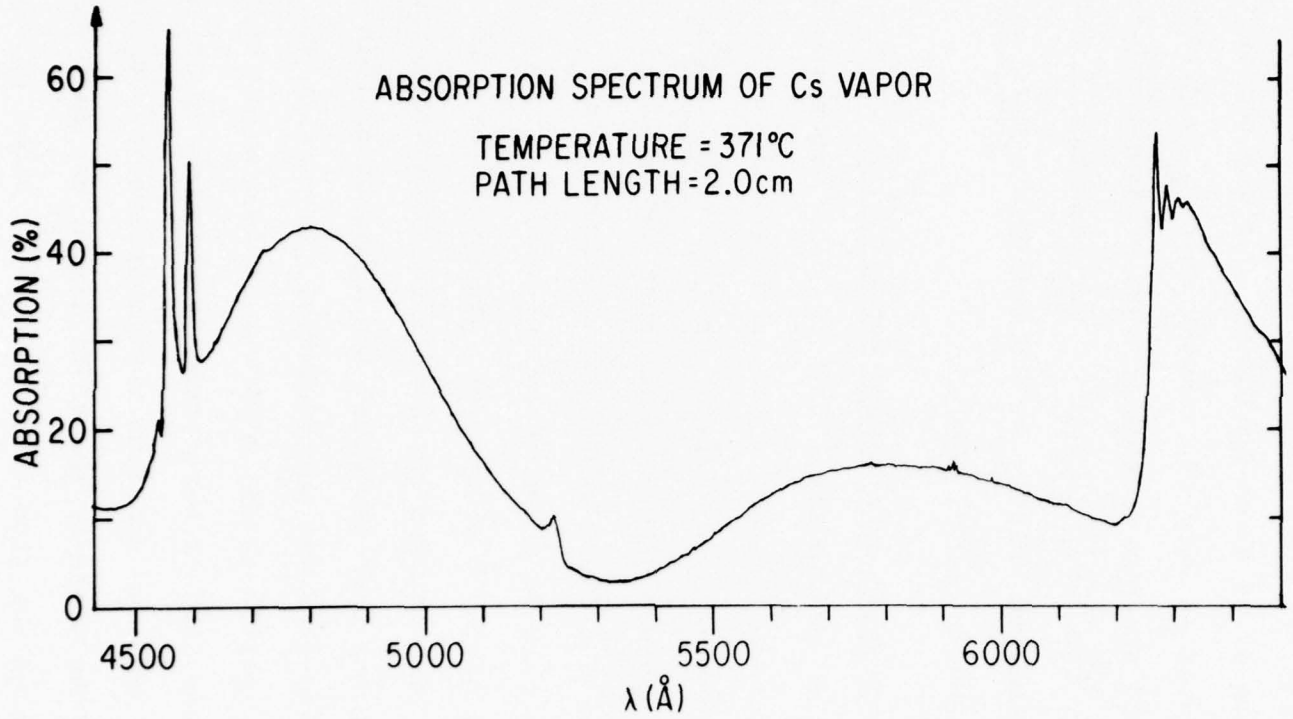

Figure 10: Absorption spectrum of a pure Cs vapor obtained from a Cary-14 dual-beam spectrophotometer.

$$Cs_2(X^1\Sigma_g^+) \xrightarrow{4545\text{Å},\ 4579\text{Å}} Cs_2^* \qquad (1)$$

$$Cs_2^* + Cs(6S) \rightarrow Cs_2(X^1\Sigma_g^+) + Cs^*(7P) \qquad (2)$$

For the Cs_2^* produced by the 4545Å or 4579Å lines (but not the other argon ion lines), the excitation transfer reaction (2) is nearly resonant, and large excitation transfer rates are expected, as for a similar case in Na/Na_2 excitation transfer investigated by Lam et al.[10] Our assertion of rapid excitation transfer is supported by the spectroscopic observation shown in Figure 11: a pure Cs vapor (~ 3 Torr) is excited by a focused argon ion laser beam at 4579Å, and intense atomic fluorescence at 4555Å and 4593Å (marked A in Figure 11) corresponding to $Cs^*(7P_{3/2,1/2}) \rightarrow Cs(6S)$ transitions, is observed together with molecular fluorescence lines (marked M in Figure 11) spaced about $40.5 \pm 2\ cm^{-1}$ apart (which is close to ω_e'' of the $Cs(X^1\Sigma_g^+)$ state, $42.0\ cm^{-1}$). However, little Cs*(7P) atomic fluorescence is observed for argon ion laser lines to the red side of the 4579Å line. Thus we believe that only the 4545Å and 4579Å lines can form the Cs*(7P) states efficiently by excitation transfer, and these Cs*(7P) atoms react readily with H_2 or D_2 through the reaction

$$Cs^*(7P) + H_2 \rightarrow CsH + H\ , \qquad (3)$$

and the CsH rapidly condenses into the solid phase, forming the observed particulates. These particulates remain suspended

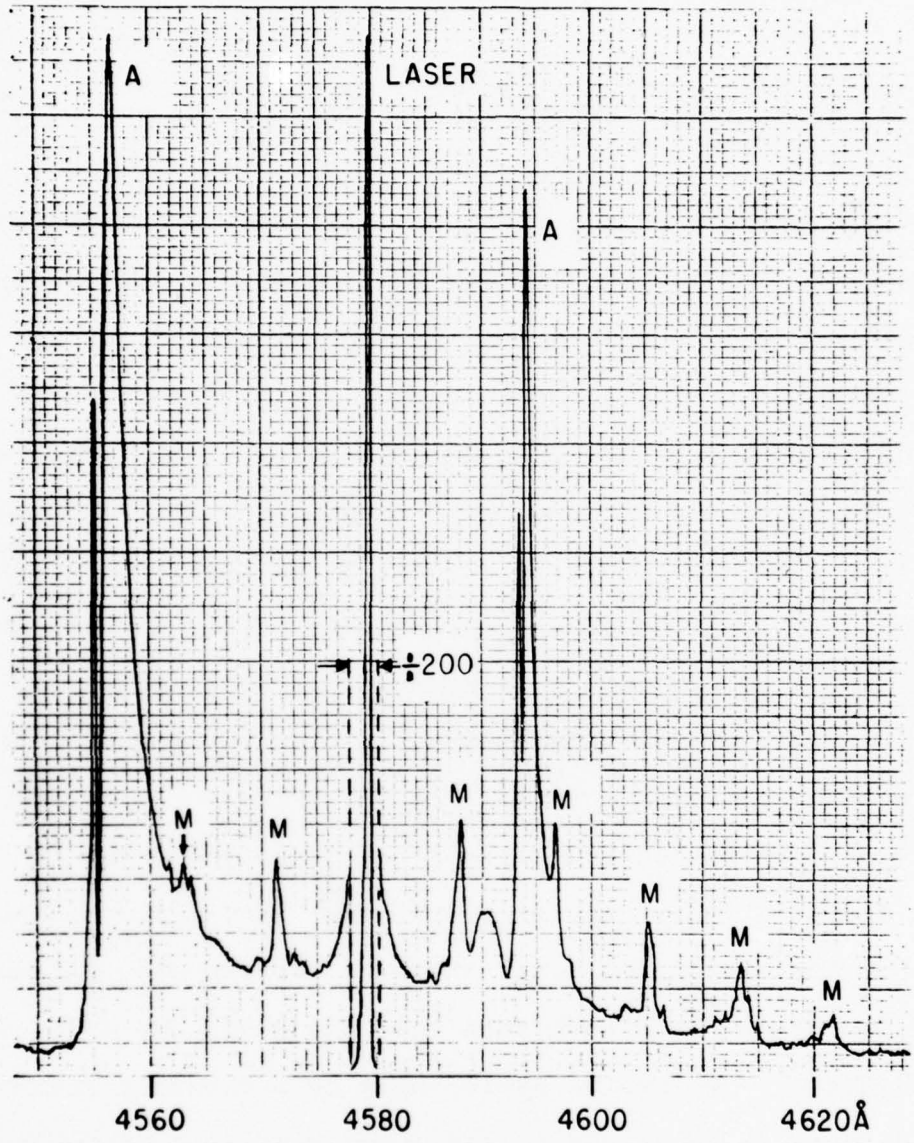

Figure 11: Fluorescence spectrum from a pure Cs vapor (~ 3 Torr) excited by a focused 4579Å Argon ion laser beam of power ~ 300 mW. A = atomic fluorescence lines (7P → 6S). M = molecular fluorescence lines ($Cs_2^*(v', J') \rightarrow Cs_2(v'', J'')$).

inside the cell for many seconds before they fall onto the cell surface and are decomposed by the hot cell surface (although they occasionally form a white deposit on the cell surface). However, these CsH solid particulates should be thermodynamically unstable, and should decompose rapidly into Cs vapor and H_2 gas. The fact that these particulates are stable or at least "metastable" may mean that they are probably highly deficient in H^-, i.e. there may be many vacant sites where there should be H^- atoms. In the next interval, we plan to try to understand how the CsH particulates could be metastable.

2. Laser excitation of a rubidium vapor system

The phenomenon of laser-particulation is more interesting in a rubidium system than a cesium system in one respect: Rb has two naturally occurring isotopes (72% Rb^{85} and 28% Rb^{87}) while Cs has only one naturally occurring isotope. We have reported[1] that RbH-particulates are observed when a system of Rb (~ 1 Torr) and H_2 (~ 150 Torr) is irradiated by two and only two argon ion lines: 4765Å and 4880Å. These two lines excite the molecular transition $Rb_2(X^1\Sigma_g^+) \rightarrow Rb_2^*(C)$. The C state is assumed to be of symmetry $^1\pi_u$ by Brom and Broida,[11] although the classification of this state is uncertain.[7][12] Our observed particulation effect indicates that $Rb_2^*(C)$ reacts readily with H_2, producing RbH molecules, which we have identified spectroscopically in a way very similar to CsH molecules,[3] i.e. the 4765Å is found to produce the $RbH(A^1\Sigma^+)$ excited state

with v' = 12 and J' = 4, and this excited level decays radiatively to the RbH($X^1\Sigma^+$) state with various v'', producing a progression of fluorescence doublets. We become quite interested in the possibility that the 4765Å or 4880Å lines may selectively excite $^{85}Rb_2$ or $^{85}Rb^{87}Rb$ or $^{87}Rb_2$ molecules, thus making the RbH-particulates isotopically enriched. This stimulates us to attempt more understanding of the laser-excited transitions in isotopic Rb_2 molecules.

A few known molecular states in Rb_2 are indicated in Figure 12(a). The 4765Å or 4880Å laser lines can excite the Rb_2 molecules to the C state, and possible transitions for the 4765Å case are indicated in Figure 12(b). Because many rotational-vibrational levels in the C state can be populated, the laser-excited fluorescence is rather complicated, consisting of many partially overlapping progressions of fluorescent lines. These lines are quite different for the $^{85}Rb_2$ and the $^{87}Rb_2$ cases, as illustrated in the observed emission spectra shown in Figure 12(c) and (d). Brom and Broida[11] claimed that these lines are all Q-lines, but we later verified by polarization spectroscopy[7] that the fluorescent lines are made up of Q-lines and R-, P- lines in roughly equal numbers. The fact that quite different emission spectra are obtained for $^{85}Rb_2$ and $^{87}Rb_2$ indicates that selective laser excitation is possible. So we tried to single-mode the 4765Å laser, and we also tried to use an extra-cavity absorption cell of only one Rb isotope to make the emerging beam be isotopically selective. However, in both cases, we still found that the

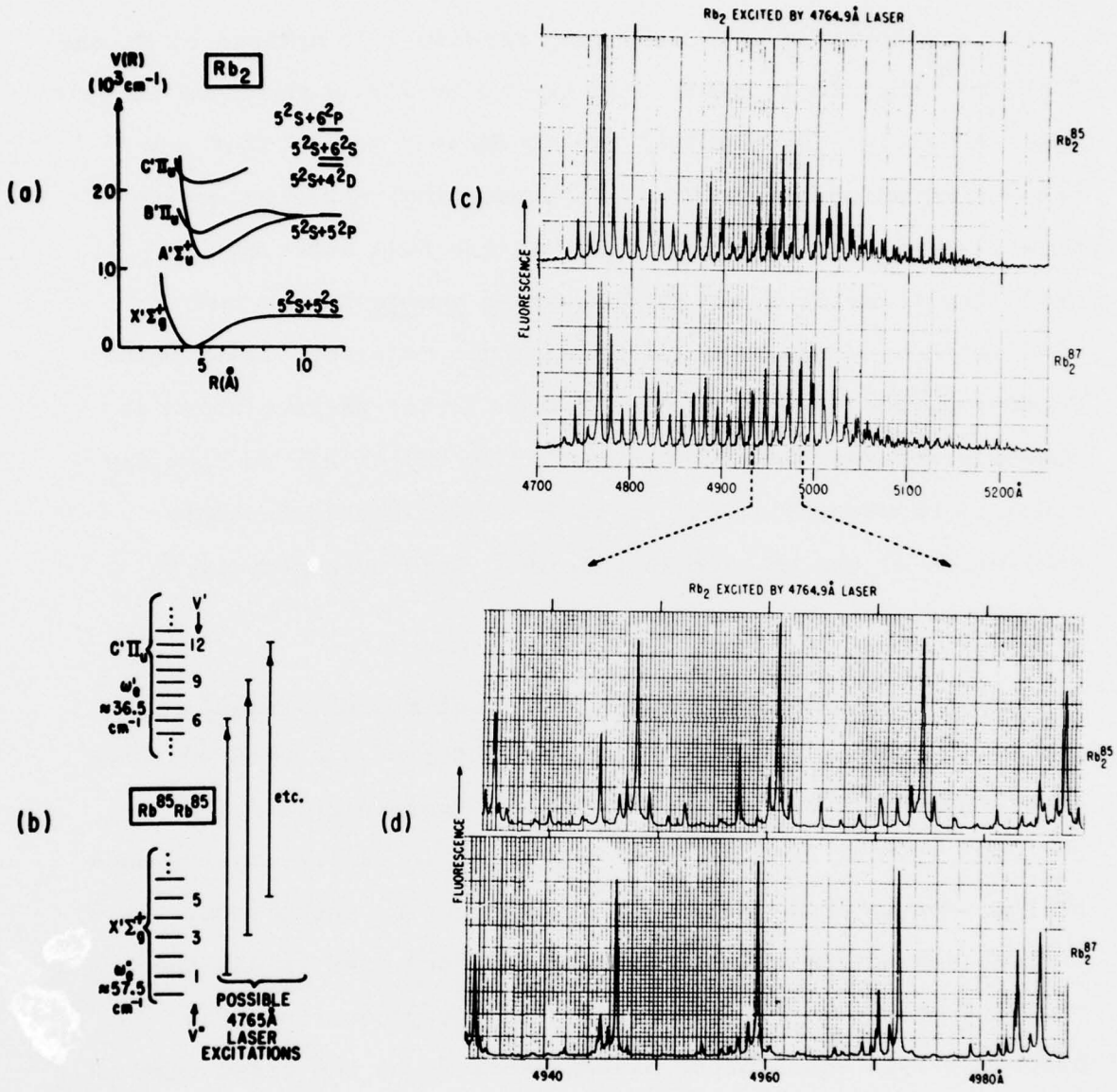

Figure 12: (a) Known molecular states of Rb_2. (b) Possible excitation transitions caused by the incident 4765Å Argon ion laser in $^{85}Rb_2$. (c) Observed fluorescence from $^{85}Rb_2$ or $^{87}Rb_2$ caused by a focused 4765Å multimode beam of power ~ 0.5W. Rb cell temperature ≈ 350°C. (d) A magnified portion of (c) showing clearly the drastic difference between the $^{85}Rb_2$ fluorescence and the $^{87}Rb_2$ fluorescence.

laser beam forms particulates very readily in a mixture of H_2 and ^{85}Rb or ^{87}Rb. So it seems that the molecular transitions in this spectral region (4700-4950Å) are so densely packed that any broadening effect (e.g. pressure broadening) makes selective molecular excitation impossible. In the next interval, we shall try to selectively excite the Rb atomic system near 4200Å with a narrow-band (perhaps single mode) dye laser beam. Hopefully, for this atomic excitation, laser-particulation is possible for much lower pressures of Rb and of H_2, so that any pressure broadening effect is small and selective isotopic excitation of the Rb atom is possible, leading, hopefully, to isotopically enriched particulates.

3. Laser-produced plasmas due to the production of Cs*(8D)

We recently reported[9] the discovery of plasma production in a pure Cs vapor ($\sim 10^{17}$ atoms/c.c.) excited by a 0.1 W cw laser beam at 6010.5Å. Our discovery is surprising, because while laser-produced plasma is a widely known phenomenon, intense pulsed laser beams (power $\gtrsim$ MW) are used in all the cases we know of. Our observation of the production of a discharge-type equilibrium plasma seems to be the first case of plasma production by a weak beam (0.1 W).

As shown in Figure 13, if a Cs cell is slowly heated up, it absorbs a focused 6010.5Å beam more and more, for a cell temperature less than 350°C. The 6010.5Å light excites the $Cs(6P_{1/2}) \rightarrow Cs(8D_{3/2})$ transition, and so it may seem surprising that the laser beam should ever be absorbed because there are

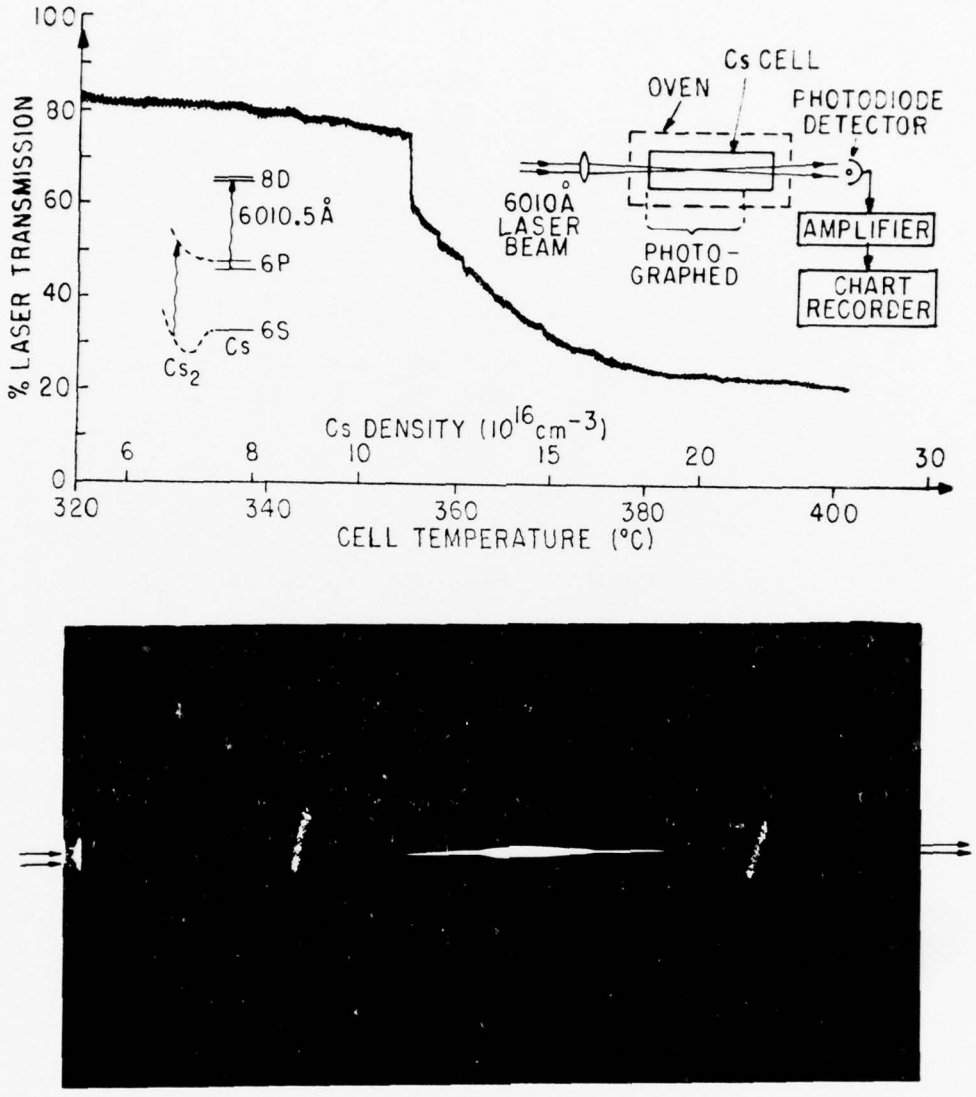

Figure 13: Top: Observed transmission of a focused 6010.5Å laser beam through a 6 cm long Cs cell as the cell temperature is slowly raised. At about 355°C, a localized glowing plasma suddenly appears near the laser focus, and the transmission drops sharply. The left insert indicates the laser excitations and the right insert indicates the experimental arrangements.
Bottom: Photograph of the localized plasma (about 5 mm long) at center of photograph. The laser beam is indicated by arrows. Two heater coils outside the cell separated by 2.1 cm are seen.

almost no $6P_{1/2}$ atoms present in equilibrium in the cell to do the absorption. The answer to this puzzle is that Cs_2 molecules are also present in the cell (~ a few % at 350°C), and Cs_2 has an absorption band in the yellow-orange region (see Figure 10). There is evidence[9] that the 6010.5Å laser beam causes dissociative excitations of Cs_2, producing Cs(6P) atoms, which then absorb the laser in a second step excitation (as shown in the left insert in Figure 13).

At a cell temperature of around 355°C, there is a sudden drop in transmission, and simultaneously a localized white glow appears near the laser focus, as shown in the photograph at the bottom of Figure 13. The emission spectrum of this white glow reveals many atomic emission lines (similar to a discharge) and also recombination continua (in particular, the recombination continuum onto the Cs(6P) state, i.e. $Cs^+ + e \rightarrow Cs(6P) + h\nu$). The emission lines from the F states are observed to be greatly plasma-broadened (linewidth typically ~ 10Å), and by the method of Stone and Agnew,[13] we can derive the electron density to be typically 3×10^{14} cm^{-3}. Also by the method described by Agnew and Reichelt,[14] we can derive from the shape of the recombination continuum the electron temperature, which is found to be typically 0.2 eV. The derived electron density and electron temperature are found to satisfy the Saha equation; hence our plasma is in local thermodynamic equilibrium. We have also used internal electrodes to verify that we can draw a current when the white glow is on. This glowing plasma also exhibits the common hysterisis property of a discharge, i.e. if

the incident laser intensity is gradually decreased, it disappears at intensity I_{off}, and if the laser intensity is increased again, it appears at I_{on}, and $I_{on} > I_{off}$. More details of these observed properties of the localized plasma produced by the 6010Å beam are given in a recent publication.[9]

The question may now arise as to why the 6010Å laser should ever produce a discharge-type plasma. We believe that the most reasonable explanation is the following. At a low Cs density, the laser-excited Cs(8D) states decay mainly radiatively. However, at a sufficiently high Cs density ($\gtrsim 10^{17}$ atoms/c.c.), radiative decay becomes less frequent than decay by associative ionizations:[15]

$$Cs(8D) + Cs(6S) \rightarrow Cs_2^+ + e + 0.2 \text{ eV} \qquad (4)$$

The electron thus produced can be heated up by superelastic collisions with Cs(8D) if the laser is sufficiently intense:

$$Cs(8D) \overset{e}{\rightleftarrows} Cs(n\ell) \overset{e}{\rightleftarrows} Cs(n'\ell') \overset{e}{\rightleftarrows} \ldots \qquad (5)$$

For rapid electron collisions(5), a local thermodynamic equilibrium (LTE) can be established, and a large population of Cs(6P) is maintained by collisions, and so strong absorption of the 6010Å laser is possible. We believe that our observed localized white glow is due to the production of this LTE plasma. The fact that there is a threshold Cs density ($\sim 10^{17}$ cm^{-3}) and a correlated threshold laser power ($\sim$ 80 mW) is consistent with the above picture of the production of the LTE plasma.

We have mentioned the property of hysterisis in a preceding paragraph. For intermediate laser intensity (between I_{off} and I_{on}), the laser beam can form either a strongly-ionized plasma (i.e. the localized white glow), or a very weakly-ionized plasma (which looks orange and dim), depending on the history of the laser intensity (i.e. depending on which branch of the hysterisis curve corresponds to the current situation). Could we view this dual-state behavior for the same laser power as a phase transition? Is it conceivable that the localized white glow is a "plasma droplet" analogous to an electron-hole droplet recently discovered in semiconductors? After-all, the radiative recombination time in our plasma is long ($\sim$ msec), so a plasma droplet seems to be a possibility. We hope to be able to answer some of these intriguing questions in the next interval.

4. Oscillating laser-production of particulates in a Cs/D_2 vapor

In the last section, we have described that a focused 6010.5Å laser beam produces a plasma in a pure Cs vapor. However if 10-150 Torr of D_2 or H_2 is mixed with the Cs vapor, no plasma is produced, but instead dense clouds of micron-sized particulates are produced near the laser focus. Optimum production occurs for medium D_2 or H_2 densities (about 20 to 40 Torr), and particulate productions seem to be more efficient in D_2 than in H_2 (Mie-scattering of the laser is much more intense in D_2). We have verified[8] that the full width at half maximum for this laser-particulation to occur is only about 4.6 GHz, and hence it is a highly resonant effect, and selective

production of isotopically enriched particulates seems quite possible.

Perhaps the most fascinating feature of the above laser-particulation phenomena is that the particulates are produced in a perfectly periodic fashion, with the period τ decreasing as the Cs density increases or the D_2 density increases. In the range of period (0.1 to 10 sec) we studied,[8] we observed that $\tau \sim [Cs]^{-2}[D_2]^{-1}$, where the square bracket indicates number density. This oscillating production of particulates which fall down from the laser causes "ripples" of particulates to be observable below the laser beam, as seen from the photographs in Figure 14.

We note that oscillating reactions and periodic precipitations[16] have interested chemical physicists and biophysicists for many years, and we need only to mention the strong general interest in "Liesegang Rings", "Zhabotinsky's Reaction" etc. Scientists are fascinated by these periodic chemical reactions because so many biological processes in nature are periodic (heart-beat, breathing rythm, etc.). Of the periodic reactions reported up to date, we think that our observation of periodic particulation in Cs/D_2 vapor-mixture is perhaps the simplest, involving only Cs atoms, D_2 molecules and light. No quantitative understanding of any one periodic reaction seems to have been reported. Perhaps our system of Cs, D_2, and resonant light is simple enough that a detailed quantitative understanding of the periodicity is possible in the near future.

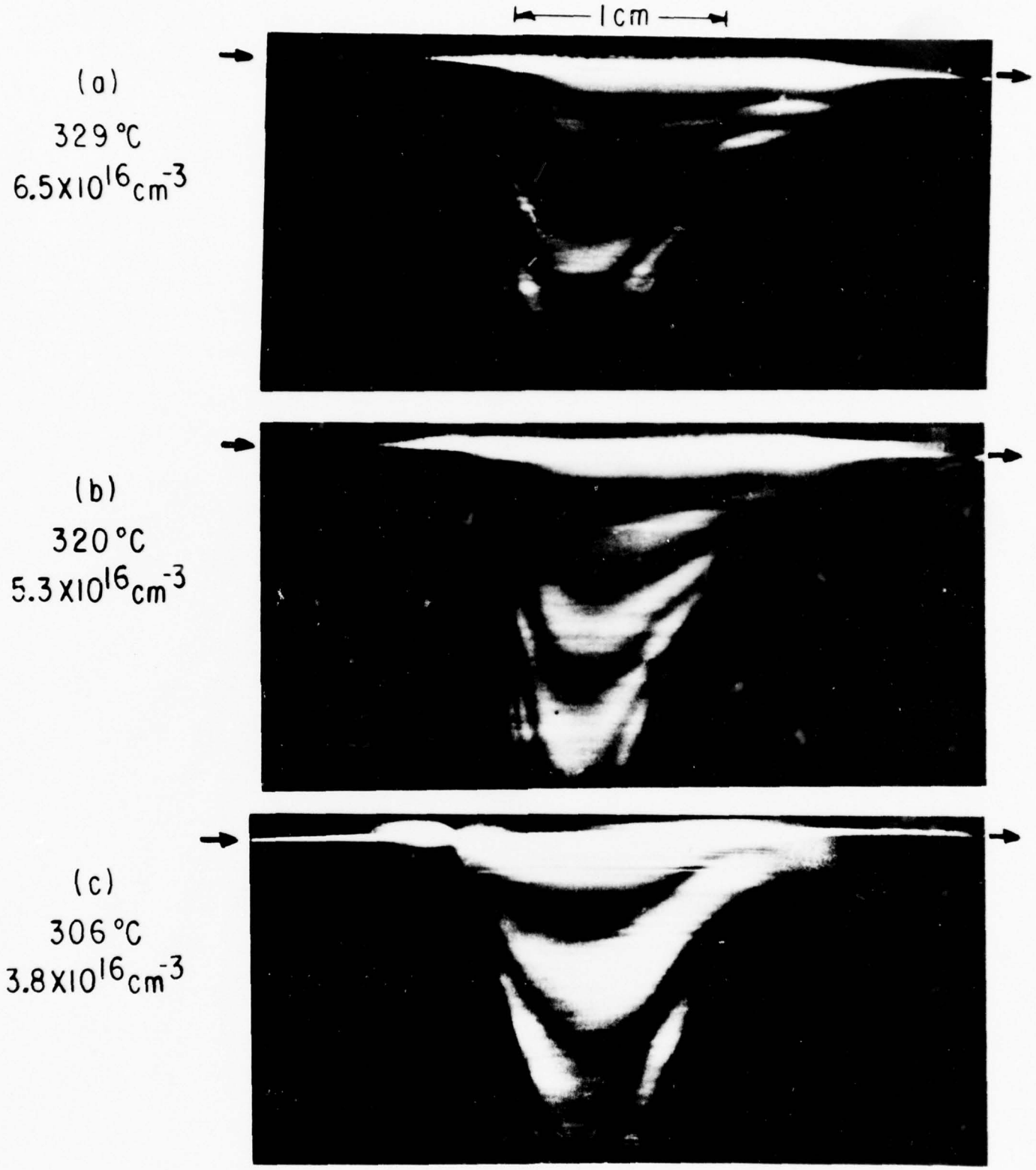

Figure 14: Oscillating production of micron-sized particulates in a mixture of Cs (of number density indicated) and D_2 (20 Torr) by a focused dye laser beam (indicated by arrows) at 6010.5Å. To take these photographs, the laser beam coming out of the cell is defocused and reflected back into the cell to illuminate the "ripples" of particulates below the focused laser beam.

In the next interval, we would like to attempt a quantitative understanding of the time development of our nucleation processes, leading to oscillations under suitable conditions. The time development of the particulate size-distributions can perhaps be studied by the Brownian motions of the particulates. The "quantum efficiency" of the laser-particulation process (i.e. mass of CsD-particulates produced per photon) can perhaps be obtained by detecting the density drop in D_2 or in Cs after particulation begins. We would also like to understand why particulates form more easily in D_2 than in H_2.

5. Polarization reversal of Rayleigh scattering near a resonance doublet

We have observed[17] that the polarization of the Rayleigh-scattered light from a single-mode linearly polarized dye laser beam incident on a Na vapor varies drastically (Figure 15), as the laser frequency is tuned near the resonance-doublet. In particular, the Rayleigh polarization is 100% "flipped" near 5894Å. This phenomenon of polarization reversal of Rayleigh scattering near a resonance doublet was predicted about 40 years ago by Placzek[18] and discussed by Penney,[19] but our observation seems to be the first experimental verification of the prediction. Vriens[20] has reported similar observations in a Na vapor and a Na plasma over a more limited spectral region, and he proposed that such variations in the Rayleigh polarization may find important applications in plasma diagnostics.

*This research was also supported by the National Science Foundation under Grant NSF-ENG76-16424.

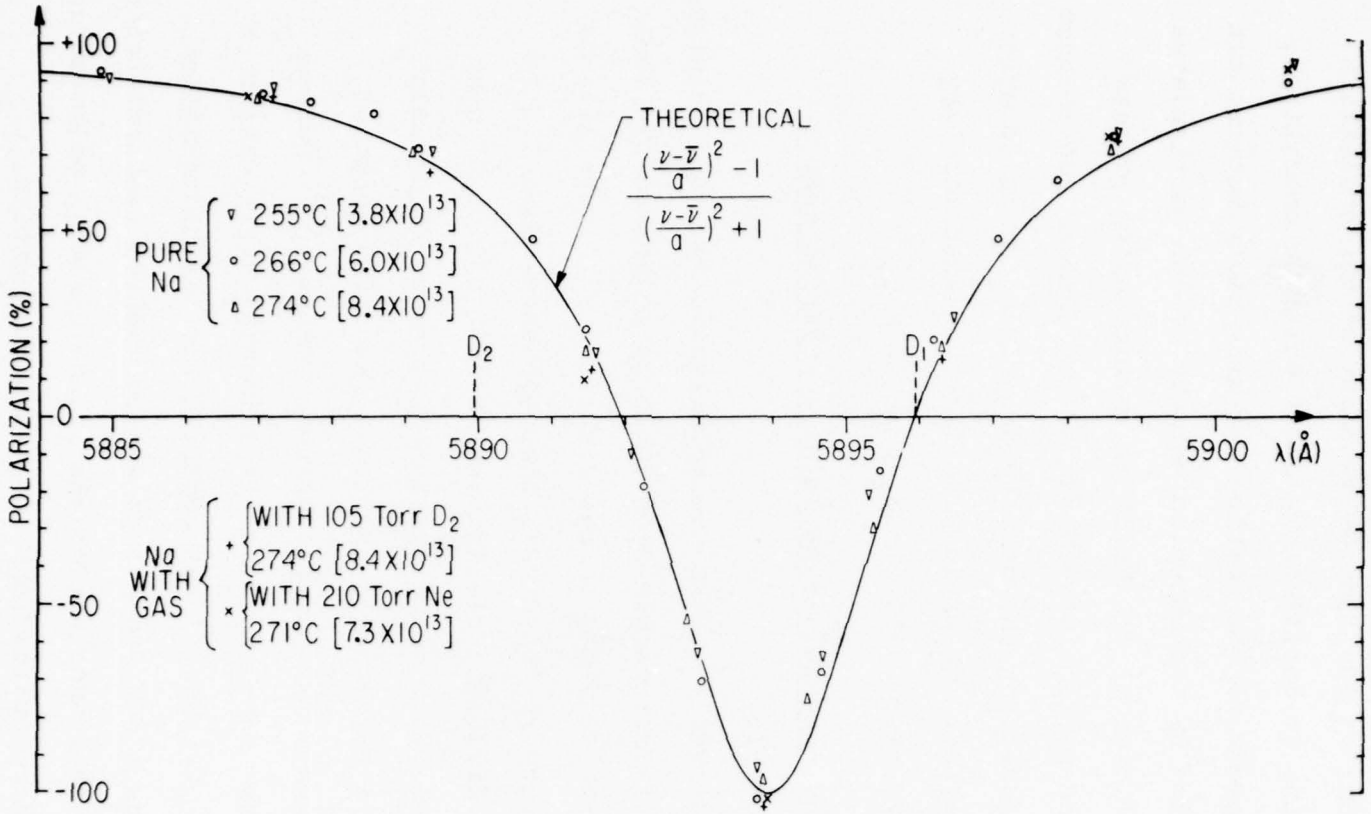

Figure 15: Variation of the polarization of the sideward Rayleigh Scattering of a linearly polarized single mode dye laser beam incident into a sodium vapor.

(1) A. C. Tam, G. Moe, and W. Happer, Phys. Rev. Lett. 35, 1630 (1975).

(2) CRL Progress Report, June 30, 1976, p. 27.

(3) A. C. Tam and W. Happer, J. Chem. Phys. 64, 2456 (1976).

(4) "Motes in the Laser's Eye", Science News 109, 25 (1976).

(5) "Laser-snow to separate heavy isotopes?", New Scientist, November 25, 1976, p. 450.

(6) W. Happer, "Laser Snow: Particle Formation by Resonant Light," presented in the IXth International Conference on Quantum Electronics, Amsterdam, The Netherlands, June 15, 1976. See.W. Happer, Optics Communications, 18, 93 (1976).

(7) A. C. Tam and W. Happer, J. Chem. Phys. 64, 4337 (1976).

(8) A. C. Tam, W. Happer and D. Siano, "Oscillating laser-production of particulates in a Cs/D_2 vapor," Chem. Phys. Lett, in the press.

(9) A. C. Tam and W. Happer, "Plasma-production in Cs vapor by a weak CW laser beam at 6010Å," Optics Comm., in the press.

(10) L. Lam, T. Fujimoto, and A. C. Gallagher, Bull. Am. Phys. Soc. 22, 193 (1977); L.K. Lam, A. Gallagher and M. M. Hessel, J. Chem. Phys. 66 , 3550 (1977)

(11) J. M. Brom and H. P. Broida, J. Chem. Phys. 61, 982 (1974).

(12) B. Rosen, Spectroscopic Data Relative to Diatomic Molecules, International Table of Selected Constants (Pergamon, New York, 1970).

(13) P. M. Stone and L. Agnew, Phys. Rev. 127, 1157 (1962).

(14) L. Agnew and W. H. Reichelt, J. App. Phys. 39, 3149 (1968).

(15) B. V. Dobrolezh, A. N. Klyucharev, and V. Yu. Sepman, Opt. Spectrosc. 38, 630 (1975).

(16) See for example a review of oscillating reactions by H. Degn, J. Chem. Educ. 49, 302 (1972).

(17) A. C. Tam and C. K. Au, Optics Comm. 19, 265 (1976).

(18) G. Placzek, Handbuch der Radiologie VI (Leipzig, 1934) Vol. 2, P. 205.

(19) C. M. Penney, J. Opt. Soc. Am. 59, 34 (1969).

(20) L. Vriens, J. App. Phys. 48, 653 (1977) and references therein.

C. ATOMIC SPECTROSCOPY: STEPWISE EXCITATION AND LEVEL-CROSSING SPECTROSCOPY OF THE TRIPLET STATES OF HELIUM-4*

(W. Happer and A. C. Tam)

This project has been completed, and the experimentally determined 3^3D and 4^3D fine structure intervals have been reported.[1][2] The calculations of numerous ^3D intervals, and the experimental determination of a 3^3P interval, are given in a more recent paper.[3] Our calculated ^3D intervals are summarized in Table II, together with our calculated singlet-triplet mixing coefficients. Our calculated ^3D intervals and those of Chang and Poe[4] seem to be the most accurate calculations reported so far.

We have also reported[3] a precision measurement of the $3^3P_1 - 3^3P_2$ interval obtained by stepwise excitation level-crossing spectroscopy.[2] The value we obtained is

$$3^3P_1 - 3^3P_2 = 658.76 \pm 0.13 \text{ MHz} \qquad (1)$$

in fair agreement with the only previous determination (658.55 ± 0.15 MHz) by Wieder and Lamb,[5] who also determined the larger interval:

$$3^3P_o - 3^3P_1 = 8113.78 \pm 0.22 \text{ MHz} \qquad (2)$$

TABLE II

Fine Structure Intervals and Singlet-Triplet Mixing Coefficients in the ^3D States of Helium-4

n	$n^3D_1 - n^3D_2$ (MHz)		$n^3D_2 - n^3D_3$ (MHz)		Singlet-Triplet Mixing Coefficients (P.C.[a])
	P.C.[a]	Experimental[b]	P.C.[a]	Experimental[b]	
3	1328	1324.7 ± 0.3	85.8	75.97 ± 0.23	0.0155
4	558.3	555.1 ± 0.2	41.8	36.15 ± 0.24	0.0113
5	285.6	284.1 ± 0.6	22.5	20.3 ± 0.3	0.01003
6	165.3	165.3 ± 1.0	13.35	12.3 ± 0.3	0.00946
7	104.0	101.6 ± 1.1	8.62	7.3 ± 0.3	0.00913
8	69.7	69 ± 3	5.77		0.00896
9	48.9		4.08		0.00883
10	35.7		2.99		0.00875

[a] Present Calculations. For details, see Ref. 3.

[b] Best experimental determinations from various sources. For details, see Ref. 1-3.

Recently, Lhuillier et al.[6] reported the precision neutral-impact level-crossing spectroscopy of He at high field, and obtained

$$3^3P_o - 3^3P_2 = 8772.565 \pm 0.062 \text{ MHz} \qquad (3)$$

It is very satisfactory to note that equation (1) to (3) are fully consistent.

*This research was also supported by the Air Force Office of Scientific Research under Grant AFOSR-74-2685.

(1) CRL Progress Report, June 30, 1975, p. 41.

(2) A. C. Tam, Phys. Rev. A 12, 539 (1975).

(3) A. C. Tam, J. Phys. B. Atom. Molec. Phys. 9, L559 (1976).

(4) T. N. Chang and R. T. Poe, Phys. Rev. A 14, 11 (1976).

(5) I. Wieder and W. E. Lamb, Phys. Rev. 107, 125 (1957).

(6) C. Lhuillier, J. P. Faroux, and N. Billy, J de Physique 37, 335 (1976).

D. ABSORPTION STUDIES OF Cs_2 BANDS

(R. Gupta and W. Happer)

Alkali-metal dimer bands are of interest in connection with tuneable lasers. Na_2 has already been shown to lase on several transitions.[1] However, not very much is known about the Cs dimer bands. It is not even known, for example, whether some of these bands originate from the singlet or the triplet ground states. We have started an experiment to measure the absorption in Cs_2 bands as function of the temperature of the vapor, with the vapor pressure held constant. Results of this experiment will determine whether and

which of these bands originate from the singlet states or triplet states. We should also be able to determine the internuclear separations that correspond to various transitions. Results of this investigation are also of interest in connection with the alkali-noble gas excimer systems which are being studied in our laboratory. Moreover, these studies may also be useful in solar energy research. Alkali vapors have been suggested as an absorbing medium of solar radiation in Brayton cycles.[2]

Our experimental setup is shown in Fig. 16. Cs is contained in a 1720 glass cell with a long stem. The main body of the cell is contained in an oven at temperature T_2 while the stem is placed in another oven at temperature T_1. T_1 is held lower than T_2. Therefore, the vapor pressure of Cs is determined by T_1 while the temperature of the vapor is determined by T_2. The absorption of light by Cs_2 is measured as a function of the wave length of light. The absorption spectrum is taken for various values of T_2, while T_1 is held constant. Part of the light is taken through a dummy cell and is used to normalize the spectral response of the photomultiplier tube, any fluctuations in the lamp intensity,etc. Our preliminary data are shown in Fig. 17. Since the temperature T_2 determines the distribution of molecules at various internuclear separations, and since this distribution is different for singlet and triplet states, an analysis of this data will give us the desired information. The data shown in Fig. 17 is preliminary and we have not analyzed it yet. In the next interval, we will take more careful data and analyze it.

(1) H. Itoh, H. Uchiki, and M. Matsuoka, Optics Comm. 18, 271 (1976); M. Henesian, R. L. Herbst, and R. L. Byer, 1975 IEEE/OSA Conference on Laser Engineering and Applications.

(2) A. Hertzberg, private communication.

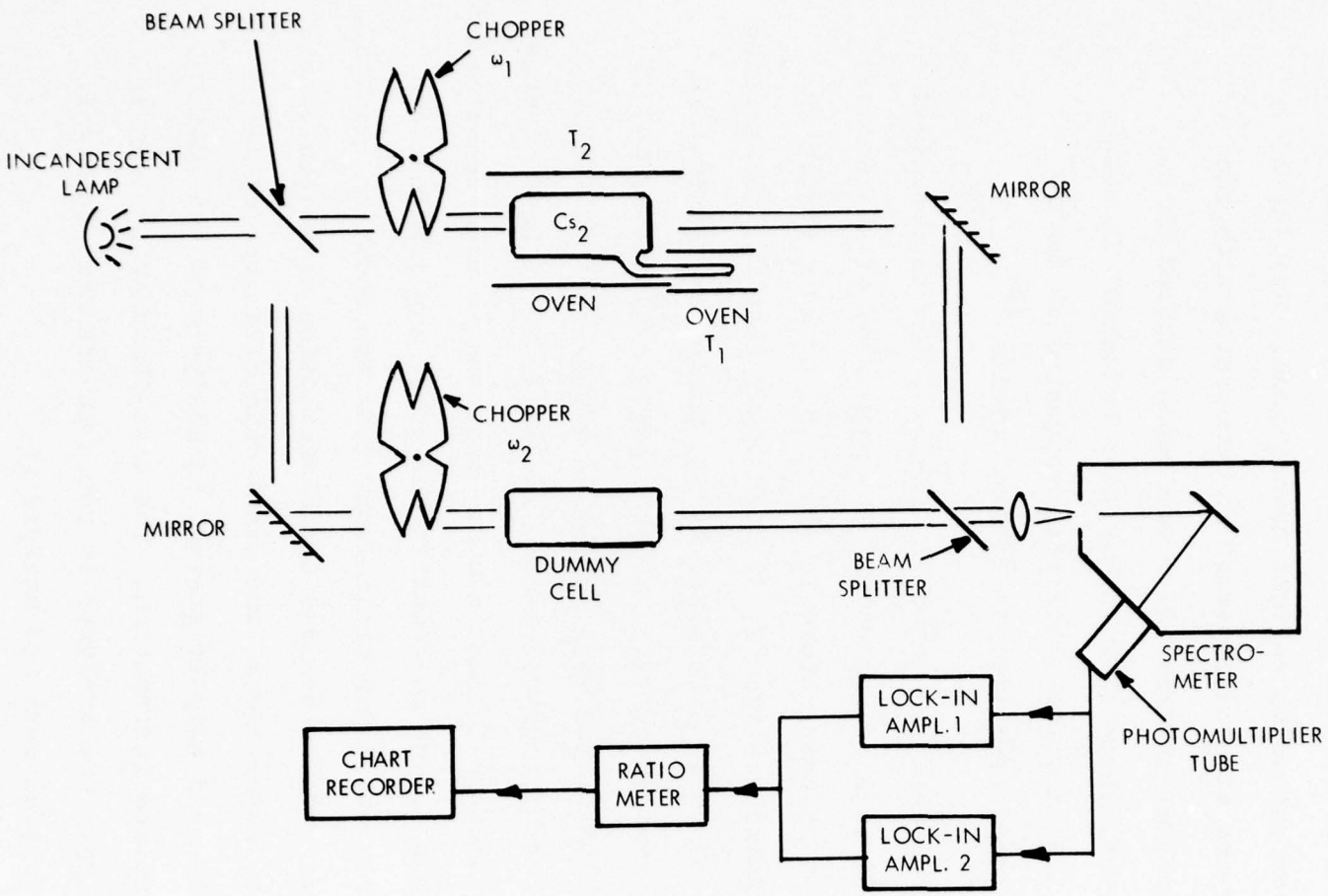

Figure 16: Schematic illustration of experimental arrangement used to study the absorption by Cs_2 vapor.

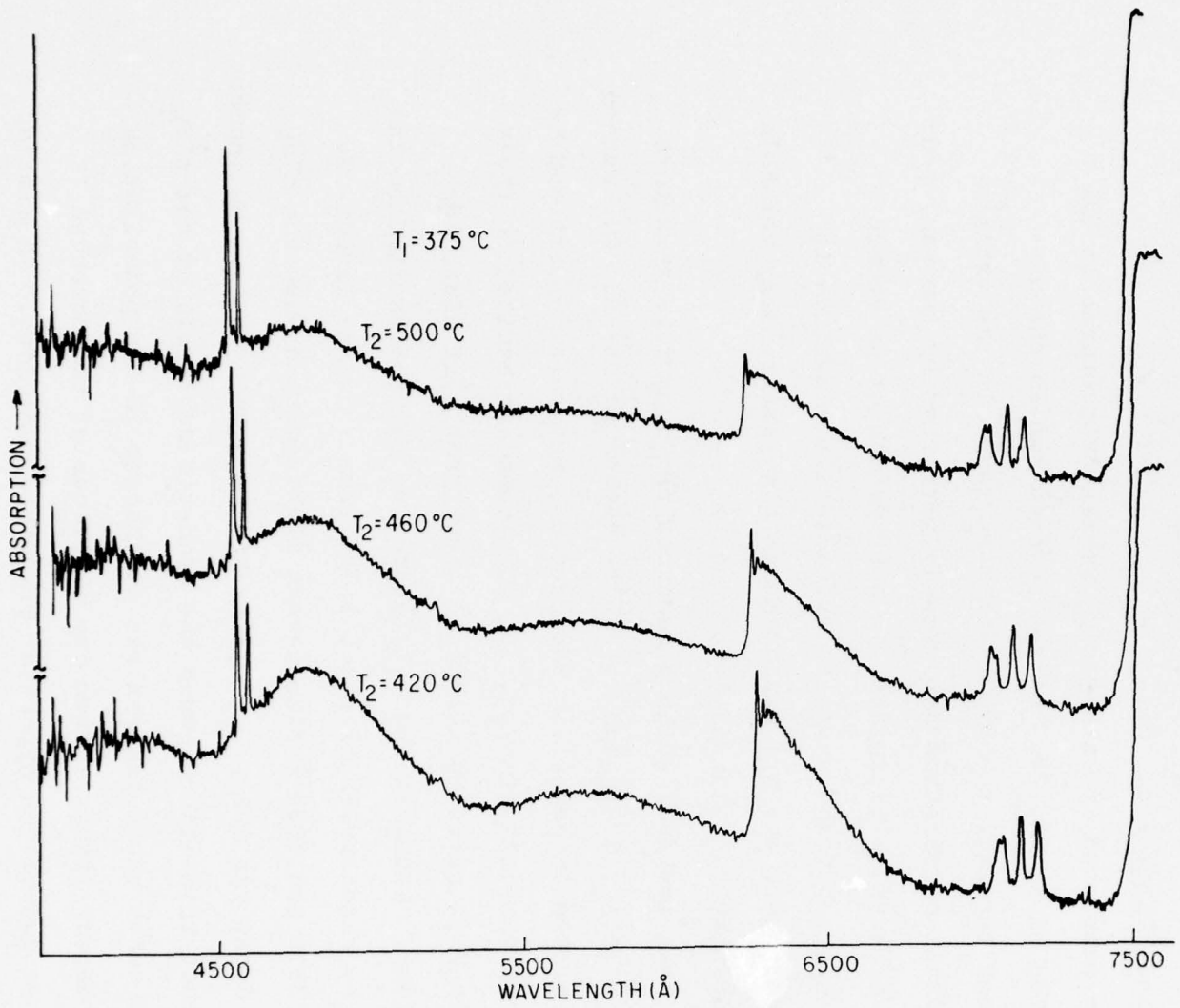

Figure 17: Cs_2 absorption spectrum for various temperatures of the Cs_2 vapor. These curves are sitting on sloping baselines (not shown).

E. TUNABLE DYE LASER SPECTOSCOPY OF HIGHLY EXCITED STATES IN ALKALI ATOMS.

(J. Farley, R. Gupta, and W. Happer)

1. Hyperfine Structure Measurements in the Highly Excited S and P States of Cs

We have completed the study of hyperfine structures in the excited states of Rb and Cs. As was pointed out in the previous progress reports, the hyperfine structures in the excited states of alkali-metal atoms are grossly perturbed by the many-body correlation effects. Therefore, in contrast to other atomic properties, e.g., binding energies or radiative lifetimes for allowed transitions, the hfs measurements are particularly valuable tests of many-body calculational techniques.

In the last interval we have measured the hyperfine structure in the $15^2S_{1/2}$, $16^2S_{1/2}$, $17^2S_{1/2}$ and the $10^2P_{1/2}$ states of Cs^{133}. Our method has been described in detail in the previous progress reports and is also shown schematically in Fig. 18. Cs atoms are excited to their first excited $P_{3/2}$ state by resonance light from a rf discharge excited Cs lamp. Atoms in the $P_{3/2}$ state are further excited to the $n^2S_{1/2}$ states by circularly polarized light from a cw dye laser. We observe the 3876 and 3888 Å fluorescent light emitted when the $n^2S_{1/2}$ state atoms decay via $8^2P_{1/2,\ 3/2}$ states to the ground state. We induce radio-frequency transitions among the magnetic sublevels of the $n^2S_{1/2}$ state, and observe these transitions as changes in the polarization of the fluorescent light. From the positions of the observed transitions we deduce the hyperfine structure constants. A similar scheme is used for the $10^2P_{1/2}$ state, as shown in Figure 18.

These experiments turned out to be rather difficult due to a number of experimental problems. For example, highly excited

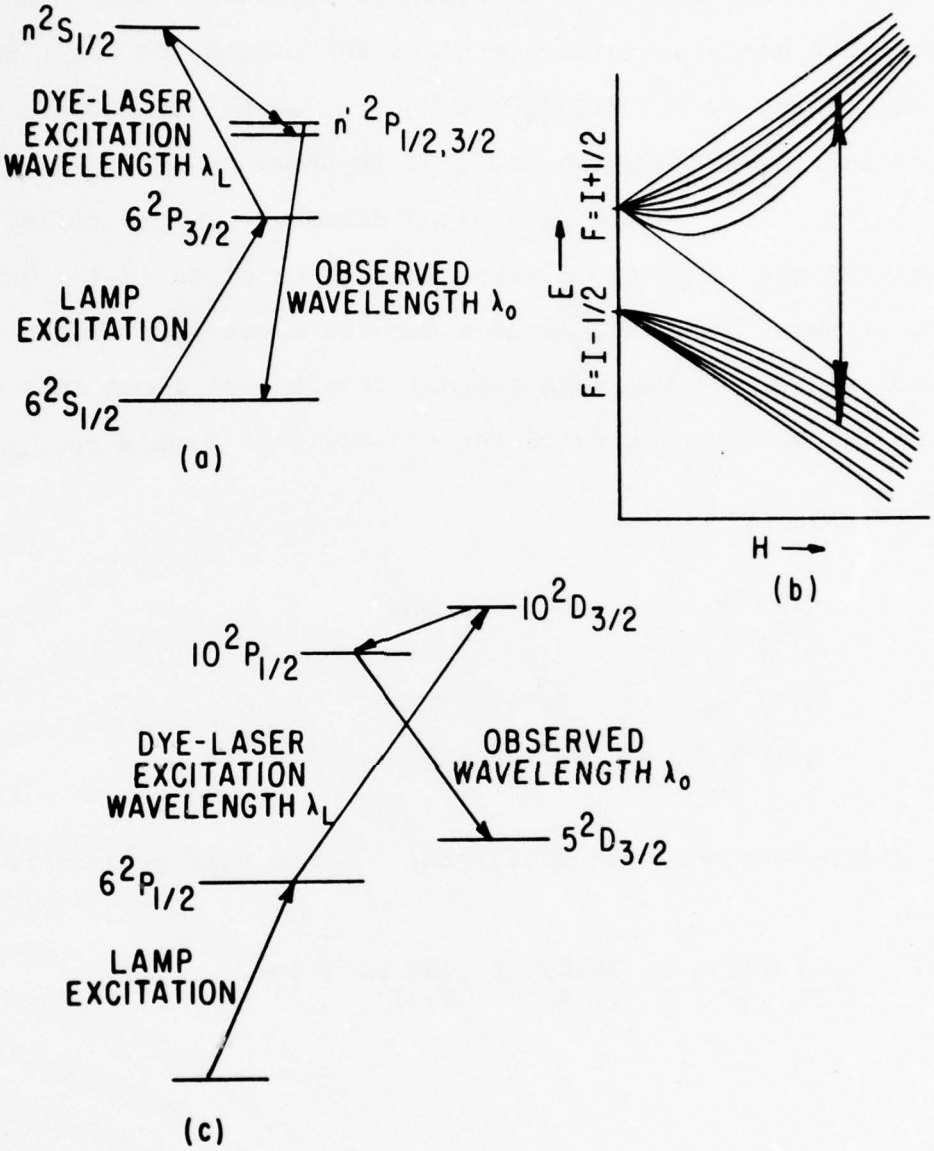

Figure 18: Excitation and detection scheme for rf spectroscopy in the $n^2S_{\frac{1}{2}}$ and $10^2P_{\frac{1}{2}}$ states of Cs.

atoms are very susceptible to collisional depolarization. We found that pyrex was not a satisfactory glass for making Cs cells because of the outgassing by the cell walls. Also, we had to operate at very low vapor density of Cs which made the experiments difficult. It was very difficult to avoid rf induced discharge in the cells, presumably triggered by associative ionization of Cs ($Cs^* + Cs \rightarrow Cs_2^+ + e$). In spite of these problems, we have carried these experiments to a successful conclusion and some typical results are shown in Fig. 19. We obtain the following results for the magnetic dipole coupling constant A:

$$A(15^2S_{1/2}) = 10.1\ (1)\ \text{MHz}$$
$$A(16^2S_{1/2}) = 7.73(5)\ \text{MHz}$$
$$A(17^2S_{1/2}) = 6.06(10)\ \text{MHz}$$
$$A(10^2S_{1/2}) = 13.9\ (2)\ \text{MHz}$$

These results have now been published, [1] and this project is now complete.

(1) J. Farley, P. Tsekeris, and R. Gupta. Phys. Rev. A 15, 1530 (1977)

2. Fine structure measurements in the F-states of Rb

We have measured the fine structure intervals in the 6^2F and 7^2F states of Rb. When we started our work, fine structure intervals in the F states of Rb and Cs were known to be inverted from conventional spectroscopic measurements. However, their magnitudes were very poorly known. Therefore, it was very interesting to make an accurate measurement of these fine structure intervals.

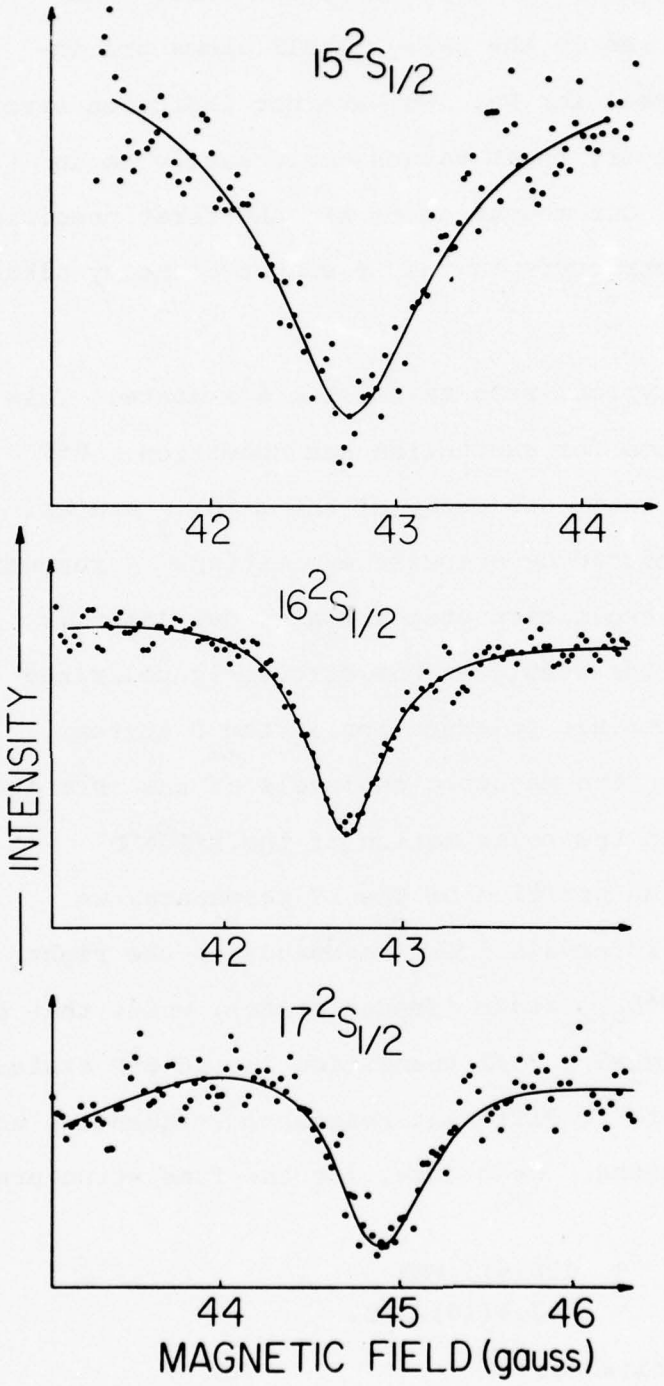

Figure 19: Typical rf resonance curves for the $15^2S_{\frac{1}{2}}$, and the $17^2S_{\frac{1}{2}}$ states of Cs^{133}.

Fig. 20 shows the state of our knowledge of the fine structure intervals in F states of alkali atoms prior to our work. We note that the fine structures in the heavy alkali atoms are inverted, while they are normal for Na. We have not indicated error bars for Rb and Cs. However, these values could easily be in error by as much as 100%. Our measurements are the first precision measurements of the fine structure in the F states of heavy alkali metal atoms.

Figure 21 shows our typical results for the 6^2F state. This figure also shows our scheme for excitation and detection. n^2F states are populated by spontaneous decay of the $n'^2D_{5/2}$ states. The $n'^2D_{5/2}$ states are produced by stepwise excitation. A resonance lamp is used in the first excitation step and a cw dye laser is used in the second excitation step. We use circularly polarized laser light to create electronic polarization in the F states. Rf resonances induced among the magnetic sublevels of the F states are detected as a change in the polarization of the n^2F-4^2D fluorescent light. From the position of the rf resonance, we deduce the fine structure intervals. The resonance on the right in Fig. 21 is due to the $8^2D_{5/2}$ state (feeder state), while that on the left is due to J=7/2, M_J=7/2 ↔5/2 transition in the 6^2F state. We have taken extensive data at different resonance frequencies and observed different transitions. We deduce, for the fine structure intervals,

$$\delta W\ (6^2F) = 486(4)\ \text{MHZ}$$
$$\delta W\ (7^2F) = 347.6(10)\ \text{MHZ}.$$

These results have been published.[2]

(2) J. Farley and R. Gupta, Phys. Rev. A 15, 1952 (1977)

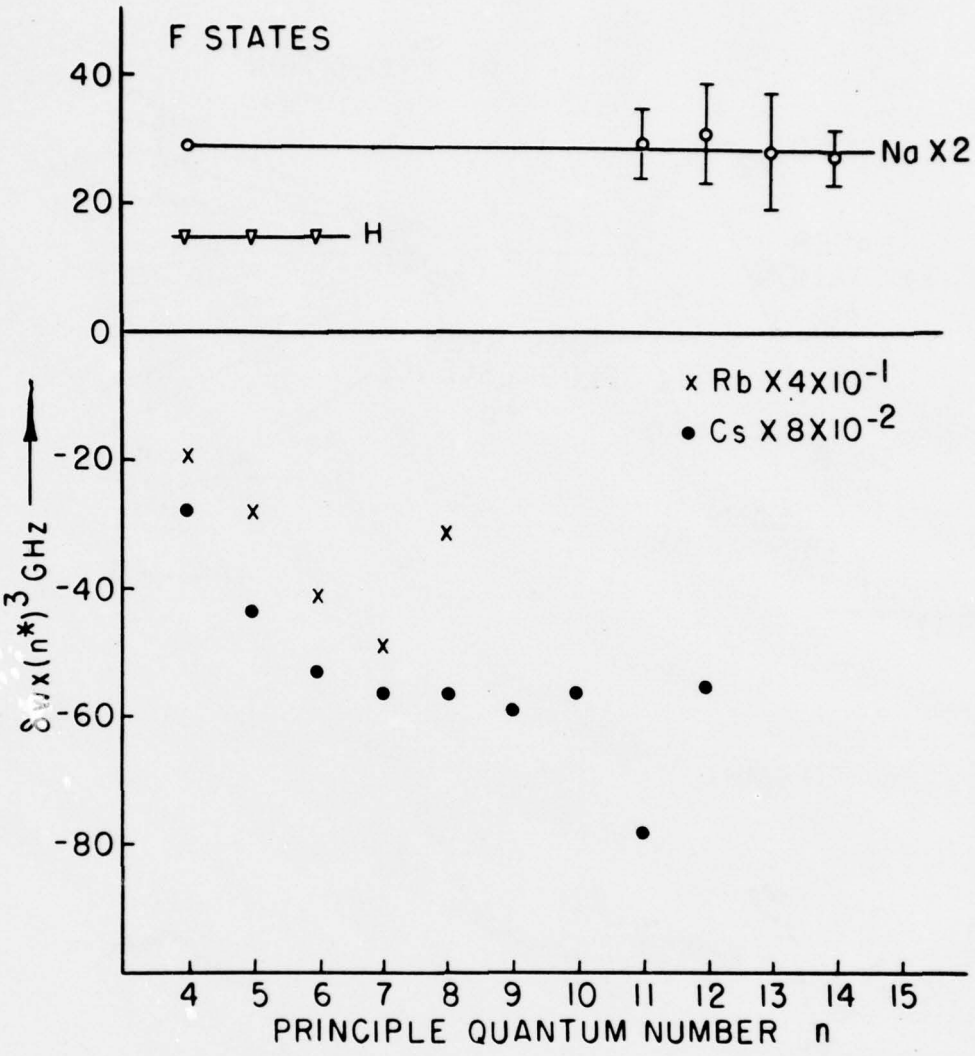

Figure 20: A plot of $\delta Wx\ (n^*)^3$ against principal quantum number n for the F states of H, Na, Rb and Cs. Here $\delta Wx(n^*)^3$ should be a positive constant according to Lande' formula.

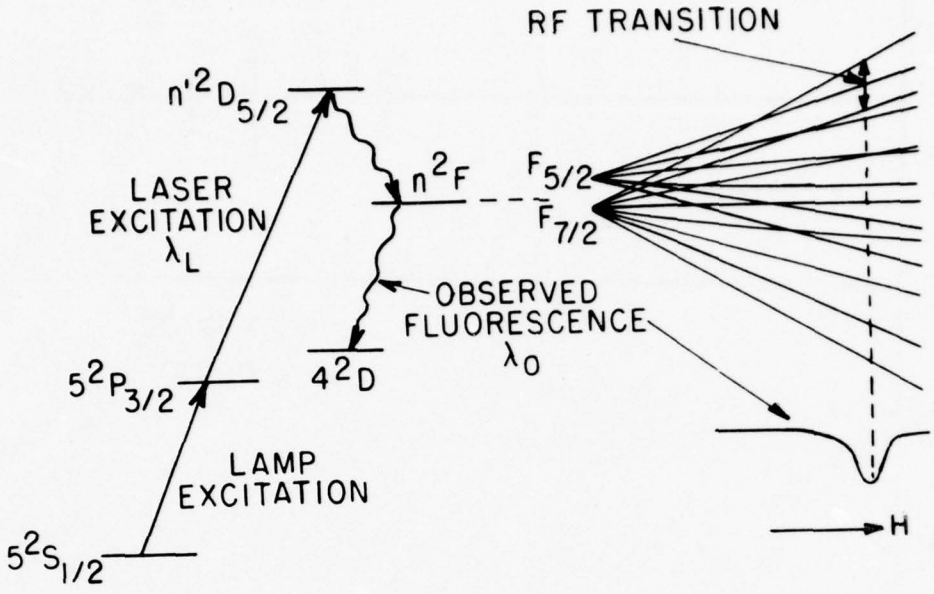

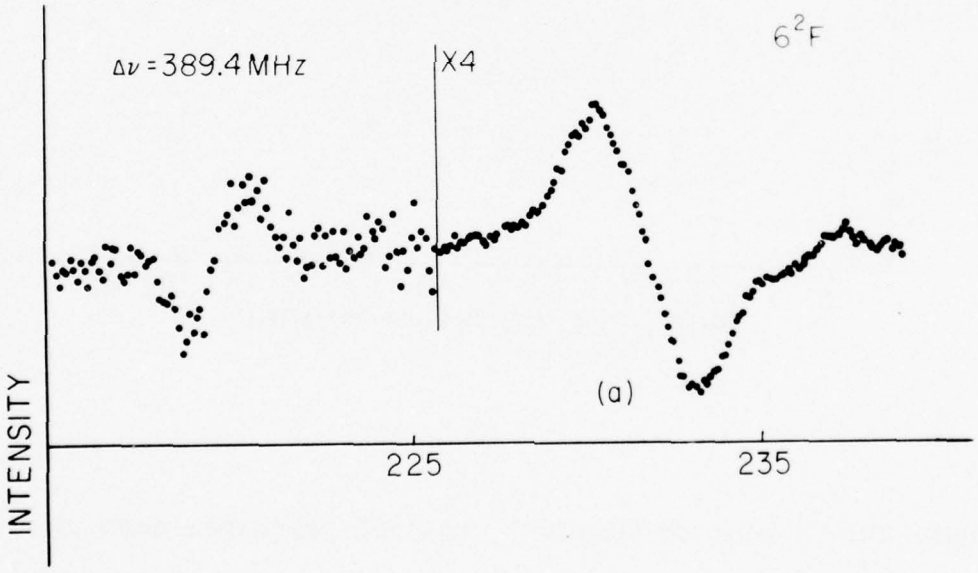

Figure 21: Our excitation and detection scheme for rf spectroscopy of the $n\,^2F$ states and some typical data for the 6^2F states.

F. EXCIMER BANDS IN ALKALI-NOBLE GAS MOLECULES

(W. Happer, G. Moe, R. Gupta and A. C. Tam)

In the preceeding progress report, we discussed our discovery of a new class of emission and absorption bands in high density alkali-metal-noble-gas vapor mixtures. We interpreted these bands as excimer transitions in alkali-noble-gas diatomic molecules which would correspond to forbidden transitions in isolated alkali atoms. We have been able to confirm this interpretation through a series of emission (laser and discharge-excited) and absorption experiments, most of which are described in the last progress report. At the time that report was written we were in the process of completing a systematic study of the absorption spectra of Cs and Rb in all the noble gases. That study has since been completed and published.[1] It includes the quantitative reduced absorption coefficients as a function of wavelength for the red bands associated with the 5D state in atomic Cs (Fig. 22) (which are visible in the raw spectra shown in Fig. 18 of the previous report) as well as a discussion of the accuracy of the only theoretical calculation[2] of the potential curves correlated with the first excited S and D states in Cs and Rb. These theoretical potential curves would give absorption and emission spectra substantially different from our experimental spectra. Figure 23 shows the theoretical potential curves and difference potentials together with difference potentials (dotted lines) compatible with our measured spectra for the case of CsXe.

Our interest in the study of these excimer transitions was stimulated by our realization that these transitions, together with those in the A-X bands proposed by Phelps[3] and by York and Gallagher[4] make the high density alkali-noble-gas systems (particularly NaXe)

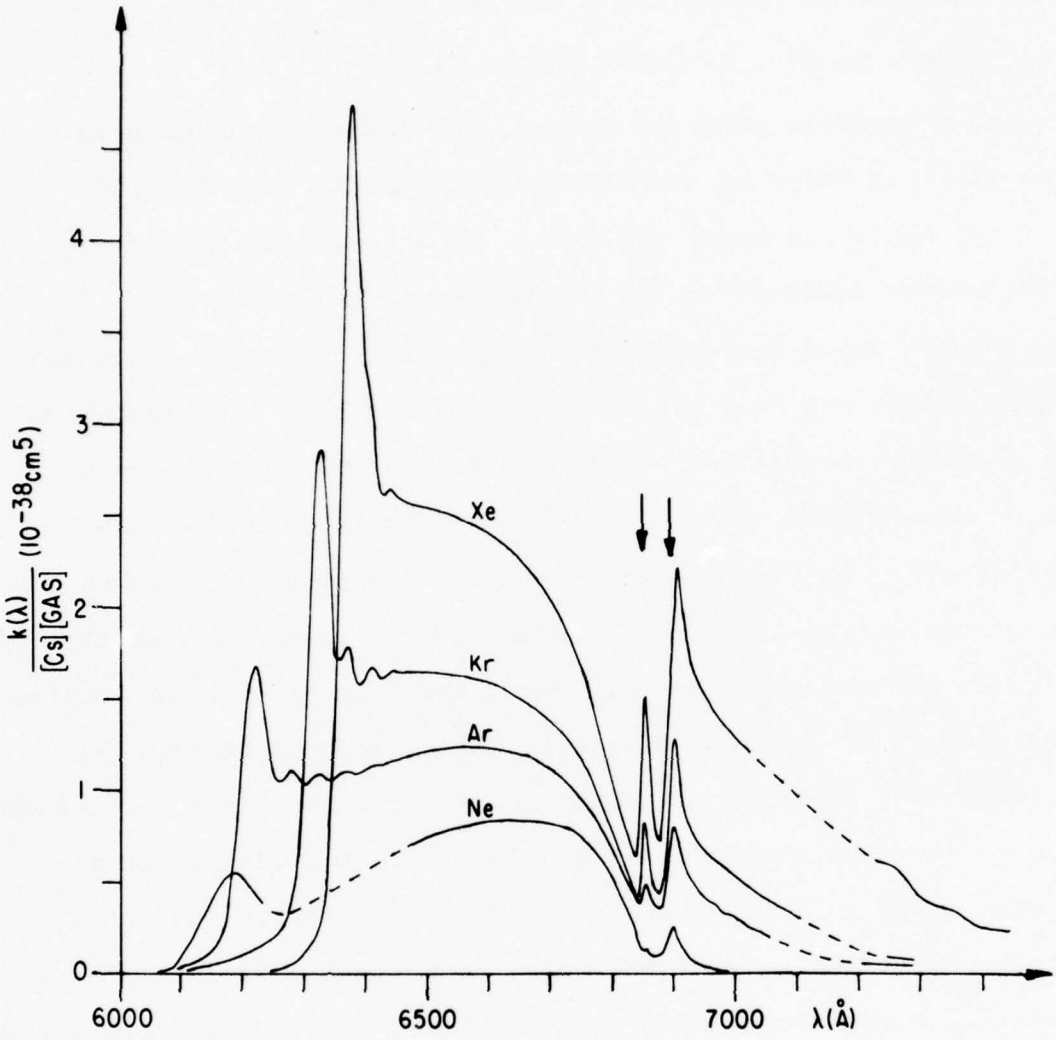

Figure 22:

Reduced absorption coefficients for the Cs-noble-gas red bands. The noble gas densities are 4.5, 5.0, 7.9, and 3.0 amagats for Xe, Kr, Ar, and Ne, respectively. The arrows indicate the wavelengths of the forbidden Cs atomic $6S_{1/2}$-$5D_{5/2,3/2}$ transitions at 6849Å and 6895Å.

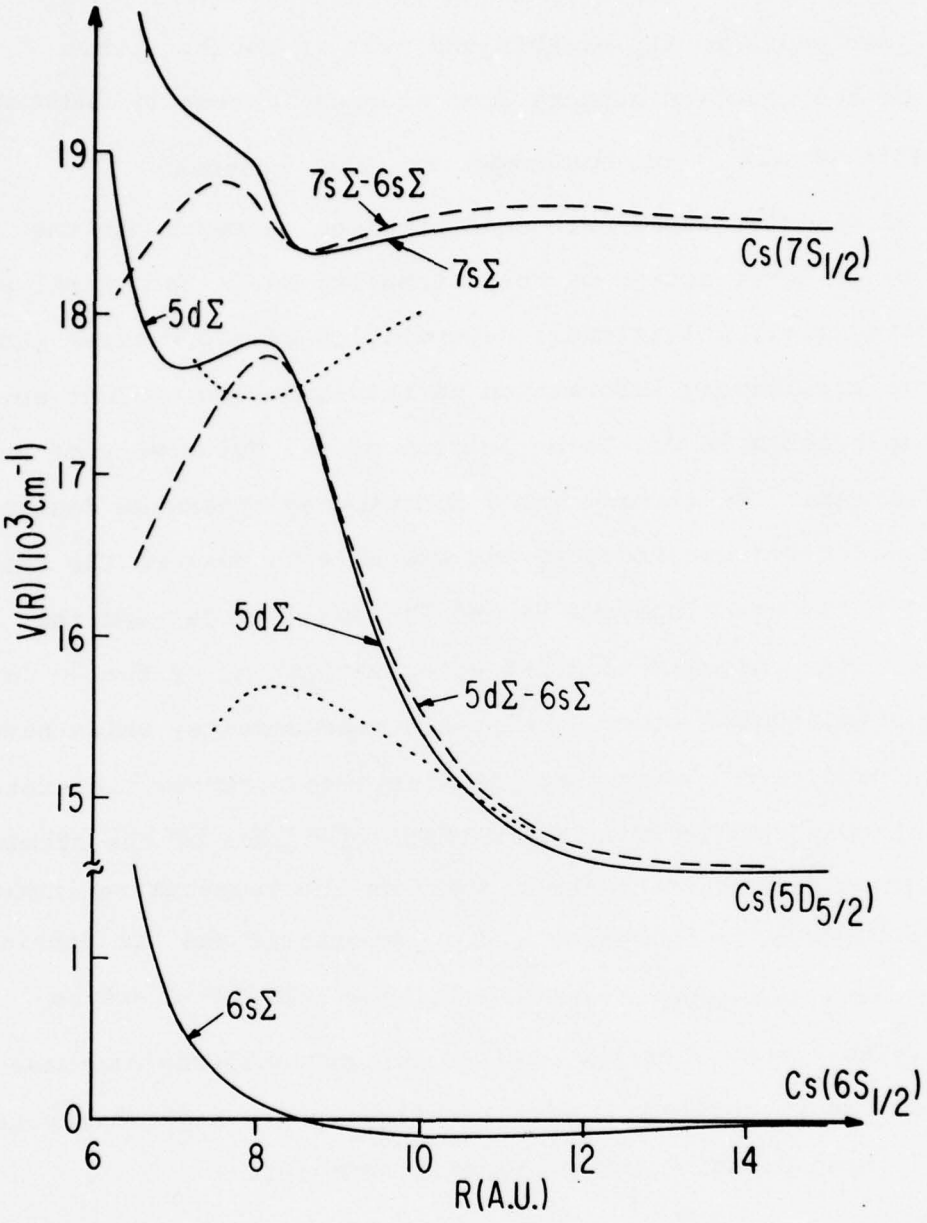

Figure 23:

Theoretical adiabatic potential curves (solid lines) for CsXe from Ref. 2, with the corresponding difference potentials (dashed lines). The dotted lines show difference potentials compatible with our spectra.

promising candidates for powerful, efficient electron-pumped tunable laser media in the visible and near infrared. This expectation has received support from studies (currently underway by Gallagher et al)[5] of discharges in these systems.

One of the most important considerations in regard to the possibility of laser action on these transitions is the extent of nonradiative (i.e., collisional) depopulation of the excited state. To get some preliminary information on this question we lent several of our sample cells to Dr. Jean Delpech of the University of Paris at Orsay, France. He already had a functioning apparatus designed to do time-resolved spectroscopy and was able to measure the rate of decay of fluorescence from the 7P and 7S levels of Cs (and the associated CsXe molecular levels) after excitation of the 7P level in Cs by a pulsed dye laser. Delpech's measurements, which have since been published[6] show that the lifetimes of these two states are considerably shorter than the natural lifetimes of the atomic states. The lifetimes decrease rapidly as the temperature increases and as the Xe density increases. The temperature and Xe density were high under his experimental conditions (250-375°C and Xe pressure .9 to 7 atmospheres). Delpech interpreted the decrease in lifetime as due to collisions with Xe atoms in the high energy tail of the Boltzmann distribution of kinetic energies.

Marek and Niemax[7] in a similar recent study conducted at lower Xe densities (a few torr to 600 torr) and at low temperatures (below 100°C) found no such temperature dependence, although they did see nearly complete mixing of the populations of nearby levels (e.g. 7P and 6D) at pressures of only a few torr of Xe, so that the lifetime of 7P, for example, would be a statistically weighted average of the lifetimes of 7P and 6D. Marek and Niemax did comment that above a certain temperature (70°C for 7P and 100°C for 8P and 9P) the

lifetime began to decrease very rapidly with temperature, but this also happened when no noble gas was present. Normally one would expect the apparent lifetime of atoms in a pure atomic vapor to increase, if anything, as the temperature (and therefore density) increases due to radiation trapping. The reason for the decrease in lifetime in the pure vapor is not clear. It could be due to collisions with other Cs atoms or to stimulated emission. It is certainly not due to collisions with Xe atoms, since none were present.

In the temperature range between 100°C and 250°C no similar lifetime measurements have been reported for high noble gas densities. The mechanisms involved in the collisional shortening of the lifetimes of these states are not at all understood. Since the possibility of quenching and excitation transfer are important in laser considerations, we determined to undertake a study of these lifetimes and excitation transfer processes ourselves.

This type of experiment, involving the direct measurement of transient processes on a nanosecond time scale,has not been done before in our laboratory, so it was necessary to construct a completely new apparatus. This task is nearly complete, but it has occupied much of our time during the last interval. We have constructed a 300 kw peak power pulsed nitrogen laser which is extremely well shielded to prevent RF noise from the discharge from interfering with the measurement of low-level signals. We also constructed a Hansch-type tunable N_2 - laser pumped dye laser which provides ~6 nsec pulses. Fluorescence is measured by using a fast photodiode or photomultiplier tube,and by measuring the output with a sampling oscilloscope. This sampling oscilloscope has been interfaced to a PDP 8/E mini computer-based data acquisition system and it functions as

a very fast sample-and-hold and as a timing device with subnanosecond resolution. The sampling scope, triggered by the laser pulse via a fast photodiode, takes a single sample per laser shot. By measuring its vertical and horizontal deflection output voltages, respectively, the computer determines the intensity at the time the sample was taken and the time interval between the trigger and the sample time. The computer stores the intensity in memory as a function of time delay after the laser pulse and accumulates an average of all samples taken, sorted into time delay intervals - i.e., it functions as a signal averager. In addition, if the computer is provided with a measurement of the integrated intensity of each laser shot, it is programmed to divide the signal by this integrated intensity shot-by-shot. We hope by this means to eliminate the problem of noise due to shot-to-shot fluctuations in the laser intensity, a problem which is inherent in this type of (sampling) approach.

In the next interval we plan to use this new apparatus, which is now functional, to study collisional relaxation and excitation transfer processes in dense alkali-noble-gas vapors, as well as to continue our investigation of the absorption and emission spectroscopy of these systems.

(1) G. Moe, A. C. Tam & W. Happer, Phys. Rev. A14, 349 (1976).

(2) J. Pascale and J. Vandeplanque, J. Chem, Phys. 60, 2278 (1974).

(3) A. V. Phelps, "Tunable Gas Lasers Utilizing Ground State Dissociation," Joint Institute for Laboratory Astrophysics, University of Colorado, Report No. 110, 1972 (Unpublished).

(4) G. York and A. Gallagher, "High Power Gas Lasers Based on Alkali-Dimer A-X Band Radiation," Joint Institute for Laboratory Astrophysics, University of Colorado, Report No. 114, 1974 (Unpublished).

(5) A.Gallagher, private communication.

(6) J. C. Gauthier, F. Devos and J. F. Delpech. Phys. Rev. A14, 2346 (1976).

(7) J. Marek and K. Niemax, J. Phys. B: Atom, Molec. Phys. 9, L483 (1976).

G. CONSERVATION OF ANGULAR MOMENTUM FOR LIGHT PROPAGATING IN A TRANSPARENT ANISOTROPIC MEDIUM.

(G. Moe and W. Happer)

A light beam propagating inside a transparent spatially uniform medium exerts no forces on the medium, even if the medium is anisotropic, because the light propagates in a straight line without any change of momentum. Although the light beam exerts no bulk forces on the medium it may exert bulk torques. As a simple and well-known example, consider a light beam propagating at right angles to the optic axis of a uniaxial crystal (Fig.24). If the light beam is initially linearly polarized at 45° to the optic axis, it will become circularly polarized after the optical path difference of the ordinary and extraordinary waves is $\lambda/4$, one quarter of an optical wavelength. Since the linearly polarized light wave carries no net spin angular momentum while the circularly polarized light wave carries an angular momentum of $\hbar$ per photon we see that a torque must have been exerted by the crystal on the light wave to account for the change in angular momentum. Naturally, the light wave will exert an equal and opposite torque on the crystal. This torque on the crystal has been detected experimentally.(1)

The type of interchange of angular momentum illustrated in Fig. 24 occurs only when the polarization of the light is the superposition of the polarization of two eigenwaves (ordinary and extraordinary in Fig.24). A characteristic feature of this type of torque is the fact that it alternates in direction as the light beam propagates through the medium.

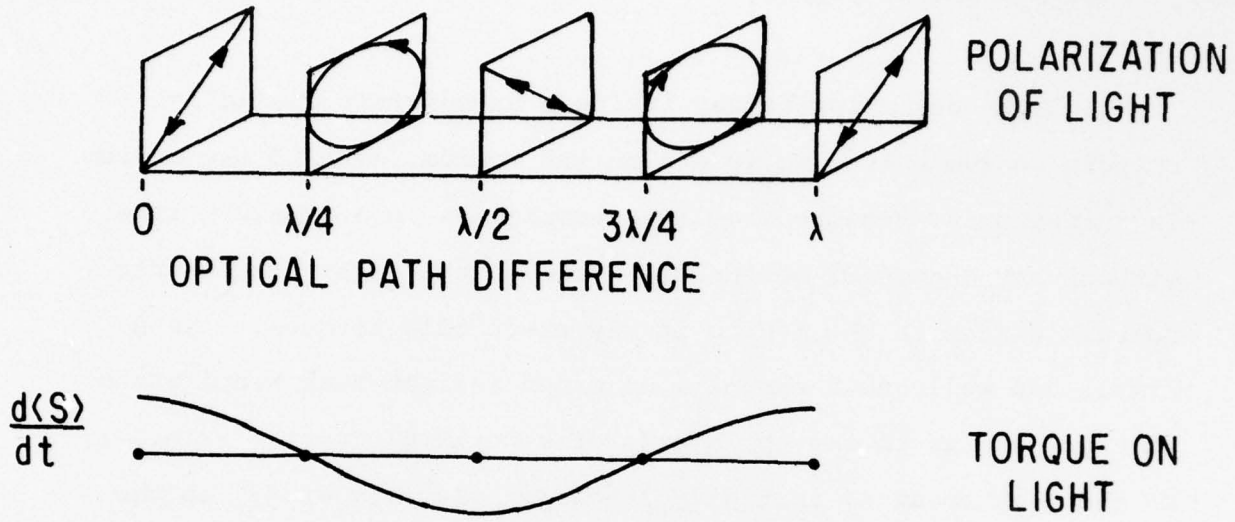

Figure 24:

The spin angular momentum of a light wave alternates in direction when the polarization of the light is a superposition of two eigenpolarizations. Here we have sketched the polarization of a beam of light which was originally linearly polarized at 45° to the optic axis of a uniaxial crystal.

There is another, less widely known way for a light beam to exchange angular momentum with a transparent medium, even when the light wave is an eigenstate of polarization. This is illustrated in Fig. 25. Suppose that a uniaxial birefringent crystal is cut at an oblique angle to the optic axis, and suppose that a light beam with the polarization of the extraordinary ray enters the crystal and propagates obliquely through the crystal in accordance with Huyghens' construction. Then the momentum of the photons is $\hbar\vec{k}$ and the "orbital" angular momentum of the photons is

$$\vec{L} = \vec{R} \times \hbar\vec{k}$$

Since the photon momentum is constant within the crystal while the photon position $\vec{R}$ changes at a rate equal to the group velocity $\vec{v}_g = \frac{d\vec{R}}{dt}$ we see that the torque on the photon is simply

$$\frac{d}{dt}\vec{L} = \vec{v}_g \times \hbar\vec{k}$$

Thus, any light wave which propagates in a different direction from the direction of $\vec{k}$ will experience a constant torque which is given by the preceeding very simple expression. Of course we expect this torque on the light to be balanced by an equal and opposite torque on the medium.

Perhaps the simplest conceivable anisotropic medium is a vapor of spin-polarized atoms. Happer and Mathur [2] suggested, without giving a general proof, that in such a vapor the angular momentum of the light is transferred directly to the atomic spins. It is not immediately apparent that one can ignore any angular momentum associated with the recoil of the atoms after the virtual absorption and reemission of the light. One might also feel uneasy about the naive discussion of the orbital angular momentum of the light in terms of linear momenta and lever arms instead of vector spherical harmonics.

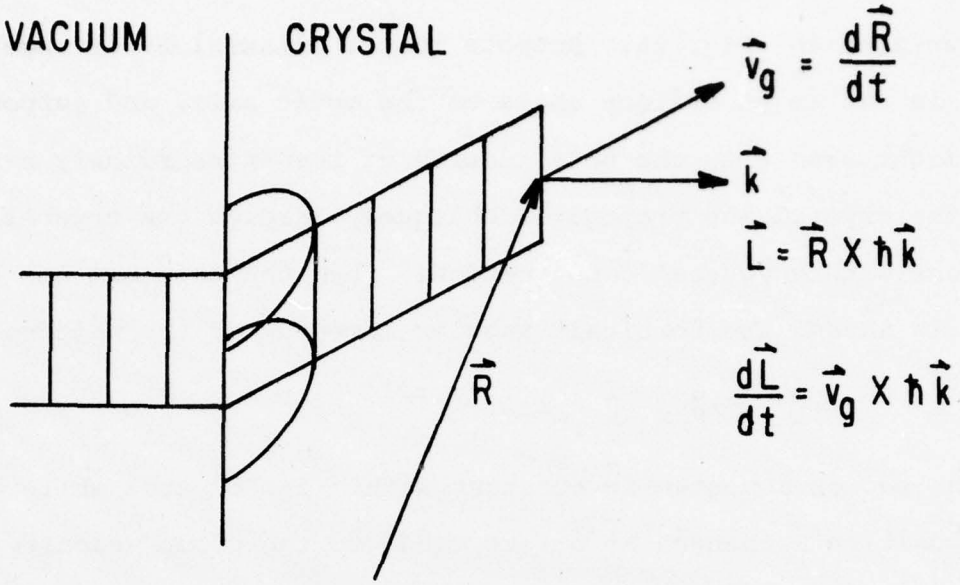

Figure 25:

The orbital angular momentum of a light wave in an eigenstate of polarization can change at a constant rate (the light beam may experience a constant torque). A "point" $\vec{R}$ of a ray of light moves with a group velocity $\vec{v}_g$ so that the angular momentum $\vec{L} = \vec{R} \times \hbar\vec{k}$ of a photon changes at a rate $\vec{v}_g \times \hbar\vec{k}$. The linear momentum $\hbar\vec{k}$ of the photon is constant.

Since there seems to be no analysis of this problem in the literature, and since we have had quite a few informal discussions of the problem with interested colleagues, we thought it would be worthwhile to present a more rigorous discussion of the interchange of angular momentum between a spin polarized vapor and a beam of off-resonant light.

We have completed a detailed study of this problem and the results will be published in J. Phys. B: Atom and Mol. Phys. (Great Britain) 10 (1977). In this paper we treated the light as a classical electromagnetic field and we showed that the classical angular momentum can be expressed very naturally as the sum of an orbital part $\langle \vec{L} \rangle$ and a spin part $\langle \vec{S} \rangle$, i.e.

$$\int d^3r \, \vec{r} \times \frac{(\vec{D} \times \vec{H})}{4\pi c} = \langle \vec{L} \rangle + \langle \vec{S} \rangle$$

Here $\vec{D}$ and $\vec{H}$ are the classical displacement vector and magnetic field of Maxwell's equations (we assume that $\vec{B} = \vec{H}$). The physical meaning of $\langle \vec{S} \rangle$ and $\langle \vec{L} \rangle$ is consistent with the naive concepts of spin and orbital angular momentum which were illustrated in Fig. 24 and 25.

Furthermore we showed that

$$\frac{d}{dt} \int d^3r \left\{ N\hbar \langle \vec{J} \rangle + \vec{r} \times \frac{(\vec{D} \times \vec{H})}{4\pi c} \right\} = 0$$

Where $\langle \vec{J} \rangle$ is the mean angular momentum per atom and n is the atomic number density of the vapor.

This analysis of the conservation of angular momentum involved some points of contention in quantum electrodynamics. For example, it is often claimed that there is no unique way to define the spin and orbital components of the photon angular momentum. We have shown how both can be defined in a physically meaningful way.

This project has been completed and no further work is contemplated in the next interval.

(1) R. A. Beth, Phys. Rev. 50, 115 (1936)

(2) W. Happer and B. S. Mathur, Phys. Rev. 163 12 (1967)

II. CHEMICAL REACTIONS IN NON-EQUILIBRIUM SYSTEMS PUMPED BY INFRARED LASERS.

A. LASER TRIGGERED RELEASE OF CHEMICALLY STORED ENERGY*

1. The infrared laser driven Isomerization of Perflouro-Dewar Benzene

(William E. Farneth, George Flynn, and Nicholas J. Turro)

Perfluoro-Dewar benzene (D-C_6F_6) is a metastable form of normal perfluoro-benzene C_6F_6. This compound is sufficiently stable to be stored in decaline (an inert solvent) for long periods of time but can undergo spontaneous decomposition as the neat liquid. D-C_6F_6 has sufficient vapor pressure that it can be easily studied at several torr pressure in the gas phase where it is quite stable. The isomerization reaction is simply

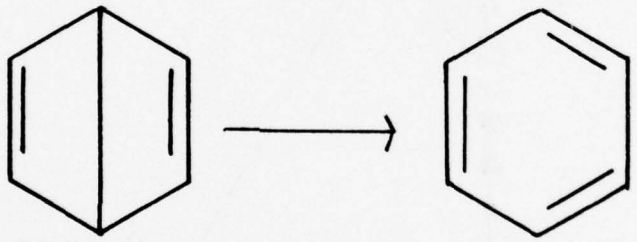

D-C_6F_6 C_6F_6

A diagram of the relevant energy considerations for the D-C_6F_6/C_6F_6 chemical system is shown in Fig. 26. The activation energy (E_a) required to convert the Dewar form to the normal form is approximately 28 Kcal/mole (10,000 cm^{-1}/molecule) while the overall reaction is exothermic by 52 Kcal/mole (19,000 cm^{-1}/molecule) or about twice E_a.

Figure: 26

LASER DRIVEN UNIMOLECULAR DECOMPOSITION FLUORINATED DEWAR BENZENE

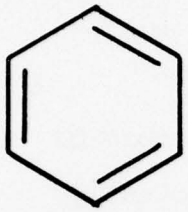

BENZENE

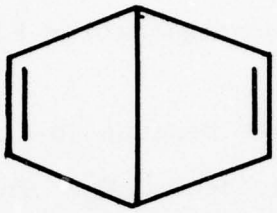

DEWAR BENZENE

2 CO_2 ABSORPTIONS 9.6 AND 10.6μ

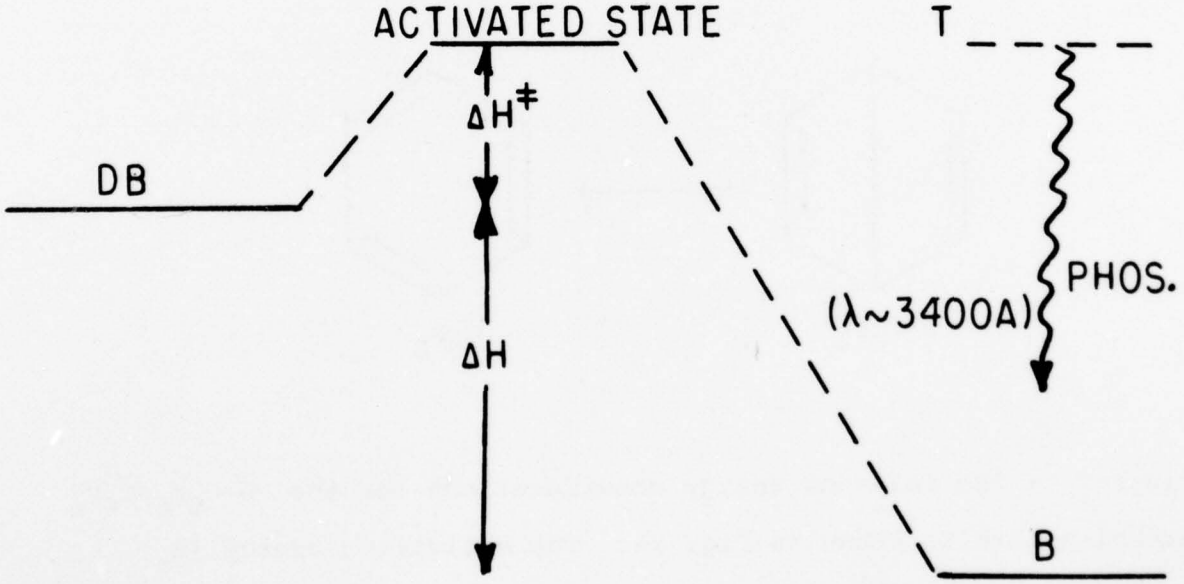

$\Delta H^{\ddagger}$	~	28	Kcal/mole	(10,400 cm^{-1}/molecule)
ΔH	~	52	Kcal/mole	(19,300 cm^{-1}/molecule)

The Dewar form strongly absorbs radiation from both the 9.6μ and 10.6μ CO_2 laser bands. We have made a preliminary study of the effects of laser pumping on perfluoro-Dewar benzene using both Q-switch and TEA type lasers. Infrared fluorescence from D-C_6F_6 and isomeric transformation of D-C_6F_6 to C_6F_6 have both been observed. This system offers several extremely interesting possibilities for laser triggered release of chemically stored energy, possible production of excited electronic states by IR laser pumping, and IR laser photochemistry. A summary of the characteristics of this system, noted in our initial experiments, is given below.

a) Unfocused TEA CO_2 Laser Pumping

Complete decomposition of D-C_6F_6 to C_6F_6 occurs with a <u>single</u> laser shot (~500mJ, 0.5 MW/cm^2) for pure D-C_6F_6 at pressures above approximately 2 Torr. All material in the cell is converted suggesting a laser initiated chain reaction mechanism. Quenching can be achieved by adding Argon gas and the chain reaction shows a laser power threshold of ~0.2 Mw/cm^2 which may only reflect limitations of the TEA laser. Both 9.6μ and 10.6μ laser pumping leads to isomerization to C_6F_6.

b) Focused Q-Switch CO_2 Laser Pumping

The TEA laser experiments suggested a rather low threshold for isomeric conversion. We then used a rather weakly focused (43 cm lens) Q-switch laser to initiate decomposition of D-C_6F_6. The improved beam quality and shot-to-shot reproducibility of this laser make threshold measurements much easier and more accurate. The pulse energy and width were 4.8 mJ and 1 μsec respectively. Focused power densities were about 50-100 times larger than unfocused densities.

Complete conversion of all D-C_6F_6 in the cell occurs in less than 100 laser shots at a power density of ~0.1MW/cm^2. Most likely this actually occurs in a single laser shot. We are purchasing a single pulse selector to test this point. The pressure threshold for complete decomposition is 1.2 Torr in pure D-C_6F_6.

Progressive (non-chain reaction) conversion of D-C_6F_6 to C_6F_6 can be achieved by the addition of a rare gas heat bath such as argon. For example, at a pressure of 1.7 Torr D-C_6F_6 and 8.0 Torr argon about 10% isomerization occurs in 6000 laser shots at an average laser pumping power of 85mw.

c) Unfocused Q-Switch CO_2 Laser Pumping

No chemical reaction (isomerization) is observed with an unfocused Q-switch laser. Infrared fluorescence in the 7μ region can be readily detected, however, and this should be very useful in maping the flow of vibrational energy in perfluoro-Dewar benzene.

Many questions remain to be answered for this extremely interesting laser triggered isomerization. We plan to search for phosphorescence emission from the triplet states of C_6F_6 which lie close in energy to the "activated state" for isomeric D-C_6F_6/C_6F_6 conversion. If intersystem crossing occurs efficiently, the production of electronically excited states may be significant. On the other hand, if conversion from the Dewar to the normal form takes place solely on the singlet ground state potential surface, the product perfluorobenzene molecules are almost certain to be very hot vibrationally. Fortunately, the infrared emission from the two isomeric forms is readily distinguishable, and we expect to be able to monitor IR chemiluminescence from C_6F_6. We also plan to monitor the time resolved rate of formation of C_6F_6 and the rate of thermal equilibration. Finally, the parameters (laser line and power, bath

gas pressure, etc.) which control the laser driven explosion of perflouoro-Dewar benzene will be investigated.

2. Time Resolved Infrared Laser Photochemistry and Spectroscopy: The Methyl Fluoride Sensitized Decomposition of Tetramethyl-1, 2-Dioxetane. An Example of Infrared Laser Induced Electronic Excitation

(William E. Farneth, George Flynn, Richard Slater, and Nicholas J. Turro)

The enhancement of chemical reactivity by infrared light absorption has been demonstrated in a variety of systems.(1) Efforts to date have fallen characteristically into one of two domains: (1) bimolecular reactions involving selectively excited small molecules (2, 3 atoms) in which the goal was to obtain detailed information on the dynamic course of the reaction,(2) (2) bulk reaction studies in which product identities and yields have been used to demonstrate the potential of IR laser excitation for production of unusual, or at least enhanced, chemical reactivity.(3) The competition between collisional energy transfer processes and chemical reaction, which plays a crucial role in determining the mechanism of a laser initiated chemical reaction, can be probed using pulsed infrared excitation followed by time resolved detection of the reaction and energy transfer coordinates. We have studied a system that is capable of yielding this type of information, the pulsed CO_2 laser-enhanced decomposition of gas phase tetramethyl-1,2-dexetane 1 in a methyl fluoride bath. Methyl fluoride is a "sensitizer" for the CO_2 laser induced decomposition of tetramethyl-1, 2-dioxetane 1 (eq.1). Some unique features of this system are: (1) the observed

infrared photochemistry is extremely clean, acetone being formed quantitatively; (2) their laser induced decomposition of 1 is accompanied by the emission of blue light ($\lambda_{max} \simeq 410$nm.); (3) the

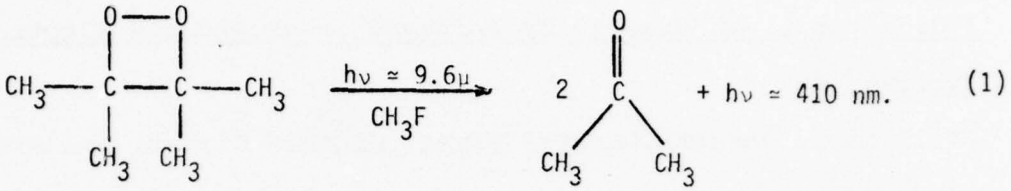

(1)

1

thermochemistry of reaction 1 is well established and is such that acetone may be produced in an electronically excited state;[4] (4) the reaction dynamics can be probed after excitation by monitoring time resolved visible emission from acetone, time resolved spontaneous infrared emission from CH_3F, and time resolved translational temperature changes (probed by the thermal lensing opto-acoustic technique);[5,6] (5) energy transfer processes in CH_3F are well understood[7,8] and serve as a benchmark for rate measurements in the mixture.

Irradiation of mixtures of CH_3F (2 to 30 torr) and 1 (vapor pressure $\simeq$ 1 torr at 25°C) with an unfocused CO_2 TEA laser (1 μsec pulse duration; 300 mjoules per pulse) operating on the P_{20} (9.6μ) line is accompanied by blue luminescence from the reaction cell and results in a smooth conversion of 1 to acetone. Laser radiation at this frequency excites only CH_3F although the luminescence is observed only when both CH_3F and 1 are present in the cell. Thus, CH_3F is a true photosensitizer of reaction 1. The thermochemistry of this "up-conversion" of photon energy is displayed in Figure 27. Typical blue luminescence is displayed in Figure 27a. Attempts to

Figure 27:

A partial energy level diagram for CH_3F. $\underline{1}$ and acetone up to about 32,000 cm^{-1}. Energy scale referenced to CH_3F and acetone both in ground vibrational state. $1^{\mp}$ denotes the transition state for the decomposition of $\underline{1}$. Also displayed are:

(a) Time resolved visible luminescence ($\lambda_{max} \simeq 410nm.$). Signal is inverted with respect to (b) and (c). The small spike at short time is an instantaneous spark reflected off of the front of the reaction cell. Zero on the abscissa represents the initiation of the laser pulse. Zero on the ordinate represents the ambient signal level.

(b) Time resolved 3μ infrared fluorescence. Zero on the abscissa represents the initiation of the laser pulse.

(c) Time resolved translation heating. Zero on the abscissa represents the inititation of the laser pulse.

Time base is 5 μsec per major division along the abscissa in (a), (b) and (c) measured with $P_{CH_3F} = P_{C_6H_{12}O_2} \simeq 1$ torr.

Figure 27

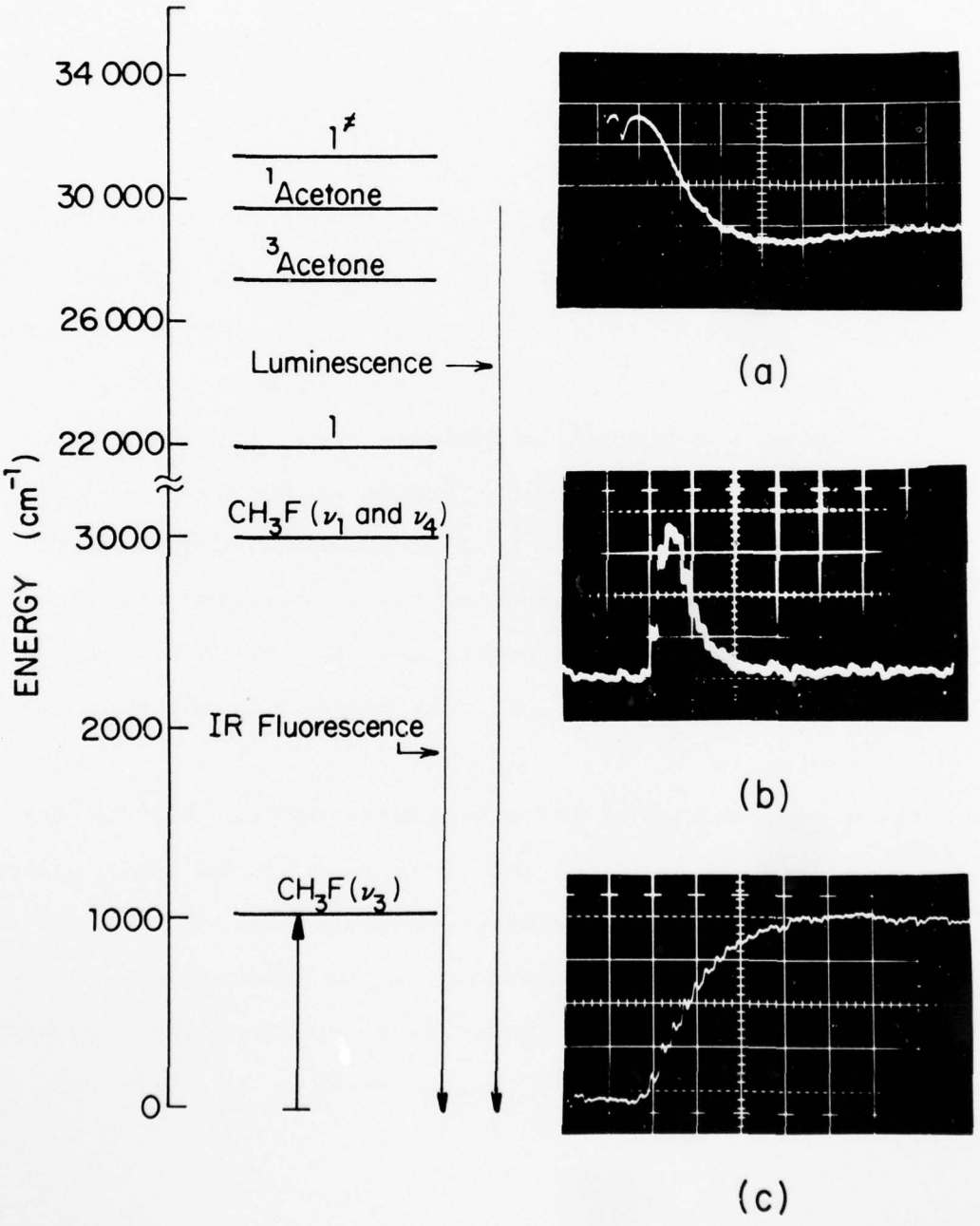
34 000
30 000
26 000
22 000
3000
2000
1000
0
ENERGY (cm⁻¹)
1*
¹Acetone
³Acetone
Luminescence
1
CH₃F (ν₁ and ν₄)
IR Fluorescence
CH₃F (ν₃)
(a)
(b)
(c)

generate luminescence using other CO_2 absorbers as sensitizing agents (SF_6, CO_2, OCS, COF_2) failed in every case except SF_6, which generates luminescence at least as effectively as CH_3F.

In two other experiments using different experimental configurations the 3μ infrared emission emanating from the C-H stretches in CH_3F was monitored using the laser induced fluorescence technique,[9,10] and the translational temperature rise was monitored using the thermal lensing technique.[5,6] Typical results performed under conditions identical to those of the luminescence experiment are also displayed in Figures 27b and 27c, respectively. These results show clearly that reaction is initiated by IR absorption into CH_3F and that the visible light generated by decomposition of $\underline{1}$ is produced on an energy transfer timescale. The following mechanism serves as a model to explain these observations.

(2)	$CH_3F + h\nu(IR) \longrightarrow CH_3F^{\dagger}$	ABSORPTION OF INFRARED LIGHT
(3)	$CH_3F^{\dagger} + \underline{1} \rightleftharpoons CH_3F + \underline{1}^{\dagger}$	VIBRATIONAL (V-V) ENERGY TRANSFER
(4)	$CH_3F^{\dagger} + \underline{1} \longrightarrow \underline{1}(T') + CH_3F(T')$	VIBRATION TO TRANSLATION (V-T) ENERGY TRANSFER
(5)	$\underline{1}^{\dagger} + CH_3F \rightleftharpoons \underline{1}(T') + CH_3F(T')$	
(6)	$\underline{1}^{\dagger} + \underline{1} \longrightarrow 2\,\underline{1}(T')$	
(7)	$\underline{1}^{\dagger}$ and/or $1(T') \longrightarrow A^* + A$	CHEMIELECTRONIC EXCITATIONS
(8)	$A^* \longrightarrow A + h\nu(vis)$	EMISSION OF VISIBLE LIGHT
(9)	HEAT DIFFUSION	

In this mechanism, daggers refer to vibrationally hot, translationally cold molecules and asterisks refer to electronically excited acetone, while T' refers to species whose translational temperature T' is above the ambient equilibrium temperature of the gas mixture. The thermal decomposition of $\underline{1}$ is known to be

chemiluminescent due to the efficient formation of A*. According to our mechanism, the blue luminescence should therefore correspond to electronic emission of acetone. Indeed, the blue emission produced in reaction 1 was shown to be experimentally identical to acetone fluorescence.[11]

The rapid rate of deactivation of vibrationally excited CH_3F (Figure 27b) is probably due to a combination of processes (3), (4), (5) and (6). Process (4) should not significantly contribute to the overall rate of decay based upon vibrational deactivation studies in CH_3F-rare gas mixtures[7b] and in pure CH_3F.[7a] In the latter case the overall deactivation rate is two orders of magnitude slower than the rate observed here. On the other hand, vibrational energy transfer processes like (3) are known to be rapid in many cases,[12] and (5) and (6) should also be efficient based upon the number and level spacing of states in 1. In support of these assumptions we note that the rapid fall to the baseline in Figure 27b and the observation of greatly diminished 3μ fluorescence intensity upon addition of 1 to pure CH_3F indicate negligible back coupling in (3) implying (5) and (6) compete effectively with rapid V-V processes in pure CH_3F.[8]

Thermal lensing data in pure CH_3F[5] and CH_3F/O_2 mixtures [13] conclusively show that rapid V-V processes in pure CH_3F ($\simeq$2μsec. at 5 torr) are overall endothermic (translations cool), and that laser energy is stored in CH_3F vibrations on this V-V timescale. In contrast to this, the rapid rise in translational temperature (Figure 27c) in CH_3F - 1 mixtures indicates that on this same timescale, energy transfer is overall highly exothermic (translations heat). These results are consistent with and support the idea that (3), (5), and (6) rapidly drain laser energy into heat. The buildup rate of acetone luminescence should be governed both by these processes and

(8). Based on figures 27a and 27c, which show comparable risetimes for visible luminescence and translational heating, the rate of production of acetone is apparently limited only by the translational heating rate. This observation is indicative of a "laser temperature jump" mechanism; the rate of product formation occurs on a timescale comparable to (or slower than) the rate of ambient temperature rise.[14]

In summary, reaction 1 is the first example of an infrared photo-sensitized chemiluminescent organic reaction. A combination of measurements of infrared flourescence from the photosensitizer, of visible luminescence from the primary product and of the translational temperature reequilibration are consistent with a predominant "temperature jump" mechanism (eqs. 2-7) wherein any contribution from $\underline{1}^{\dagger}$ in (7) is dominated by the contribution from 1(T'). These studies are being extended to 1,2-dioxetanes which directly absorb the laser pulse and to other systems in which a high energy content reaction possesses the potential of infrared laser induced electronic excitation.

We have completed our study of the sensitized decomposition of tetramethyl-1,2-dioxetane by unfocused TEA laser light. Further work remains to be done on the direct decomposition of the deuterated species by both focused and unfocused CO_2 lasers. The deuterated compound absorbs laser radiation quite strongly and there is good reason to believe that focused pumping may lead to direct multiphoton absorption with efficient visible light production.

*This work was also supported by the Air Force Office of Scientific Research (Grant AFOSR-74-2589), by the National Science Foundation (Grants NSF-MPS70-02165 and NSF-MPS73-04672 and NSF-MPS75-04118), and in part by the Advanced Research Projects Agency of the Department of Defense monitored by the Office of Naval Research under Grant N00014-75-C-1106.

(1) M.J. Berry, Ann. Rev. Phys. Chem., 26 259 (1975) and references cited therein.

(2) See, for example, T. J. Odiorne, P.R. Brooks and J.V.V. Kasper, J. Chem. Phys., 55 1980 (1971); D. Arnoldi, K. Kaufmann and J. Wolfrum, Phys. Rev. Lett., 35, 100 (1975).

(3) See, for example, H. R. Bachmann, H. North, R. Rinck and K. L. Kompa, Chem. Phys. Lett., 29 627 (1974); S. D. Rockwood and J. W. Hudson, Chem. Phys. Lett., 34, 542 (1975).

(4) N. J. Turro, P. Lechtken, N. E. Shore, G. Schuster, H. C. Steinmetzer and A. Yekta, Acc. Chem. Res., 7, 97 (1974).

(5) F. R. Grabiner, D. R. Siebert and G. W. Flynn, Chem. Phys. Lett., 17, 189 (1972).

(6) D. R. Siebert, F. R. Grabiner and G. W. Flynn, J. Chem. Phys., 60, 1564 (1974).

(7) (a) E. Weitz, G. W. Flynn and A. M. Ronn, J. Chem. Phys., 56, 6060, (1972);

(b) E. Weitz and G. W. Flynn, J. Chem. Phys., 58, 2679 (1973).

(8) F. R. Brabiner and G. W. Flynn, J. Chem. Phys., 59, 2330 (1973); E. Weitz and G. W. Flynn, J. Chem. Phys., 58 2781 (1973).

(9) L. O. Hocker, M. A. Kovacs, C. K. Rhodes, G. W. Flynn and A. Javan, Phys. Rev. Lett., 17, 233 (1966).

(10) R. D. Bates, Jr., G. W. Flynn, J. T. Knudtson and A. M. Ronn, J. Chem. Phys., 53, 3621 (1970).

(11) CO_2 Laser excited emission spectrum of reaction (1) was compared to an emission spectrum of a gas mixture of acetone, 1 and CH_3F excited at 300 nm with a Xenon lamp using the identical detection system in both cases. Approximately 10^6 CO_2 photons must be absorbed per visible photon emitted in the CO_2 laser initiated reaction.

(12) P. F. Zittel and C. B. Moore, J. Chem. Phys., 58, 2004 (1973); B. M. Hopkins, A. Baronavski and H. L. Chen, J. Chem. Phsy., 59, 836 (1973); R. C. Slater and G. W. Flynn, J. Chem. Phys., 65, 425 (1976).

(13) I. Shamah and G. W. Flynn, submitted for publication in J. Chem. Phys.

(14) Similar processes can be found in W. M. Shaub and S. H. Bauer, Internat. J. Chem. Kin., 7, 509 (1975).

(15) R. C. L. Yuan and G. W. Flynn, J. Chem. Phys., 56, 1316 (1972).

B. METASTABLE VIBRATIONAL ENERGY DISTRIBUTIONS INDUCED BY VIBRATIONAL RELAXATION OF LASER PUMPED POLYATOMIC MOLECULES.*

1. Laser Fluorescence Study of Vibrational Energy Equilibration in CH_3F:O_2 Mixtures: "Impurity" Molecules as Probes of Mode To Mode Energy Flow Pathways*

(J. M. Preses, G. W. Flynn, E. Weitz)

Laser induced fluorescence studies of vibrational energy transfer have been most useful in elucidating some of the parameters which are responsible for the relative efficiencies of various relaxation processes.[1-7] Considerable information is now available concerning the vibration-vibration (V-V) and vibration-translation/rotation (V-T/R) behavior of many small molecules, particularly CH_3F.[4-7] The present work describes laser fluorescence studies of the equilibration of CH_3F with O_2. This investigation serves three distinct purposes. First, it provides data for comparison of energy transfer processes in CH_3F/O_2 with those in CH_4/O_2 which

were investigated in a classic early laser fluorescence study employing the phase shift technique.[8] Second, it shows clearly that, at least in CH_3F/O_2 mixtures, all the modes in CH_3F are tightly coupled by collision processes in the absence of infrared radiation which might lead to multiple photon or multiple excitation effects. Finally, by a careful consideration of vibrational and translational energy balance during the equilibration of CH_3F and O_2, it can be shown that the observed fluorescence decay characteristics are consistent only with a limited number of vibrational energy transfer pathways in CH_3F. This effect, which can be referred to as "vibrational quanta conservation", appears to have been overlooked as a powerful diagnostic tool for determining energy flow pathways, at least in small polyatomic molecules.

All experiments were performed on a standard CO_2 laser induced fluorescence apparatus which is described in detail elsewhere.[4] A series of experiments designed to elucidate V-V processes in CH_3F-O_2 mixtures, was performed. An energy level diagram for the CH_3F-O_2 system is shown in Fig. 28. Fluorescence was studied which emanated from the C-H bending modes (ν_2, ν_5) at $\lambda = 6.8\mu$, from the overtone of the C-F stretch ($2\nu_3$) at $\lambda = 5\mu$, and from the C-H stretches (ν_1, ν_4) at $\lambda = 3.3\mu$. Following laser excitation by the P(20), 9.6μ CO_2 laser pulse of the 0-ν_3 CH_3F transition, fluorescence at all three wavelengths rises rapidly to a peak value. At typical pressures used in these experiments ($\sim$ 35:1, O_2:CH_3F, total pressure $\sim$ 30-40 torr) the risetimes were too fast to measure ($<$ 2 μ sec) with any of our available detectors. This risetime corres-

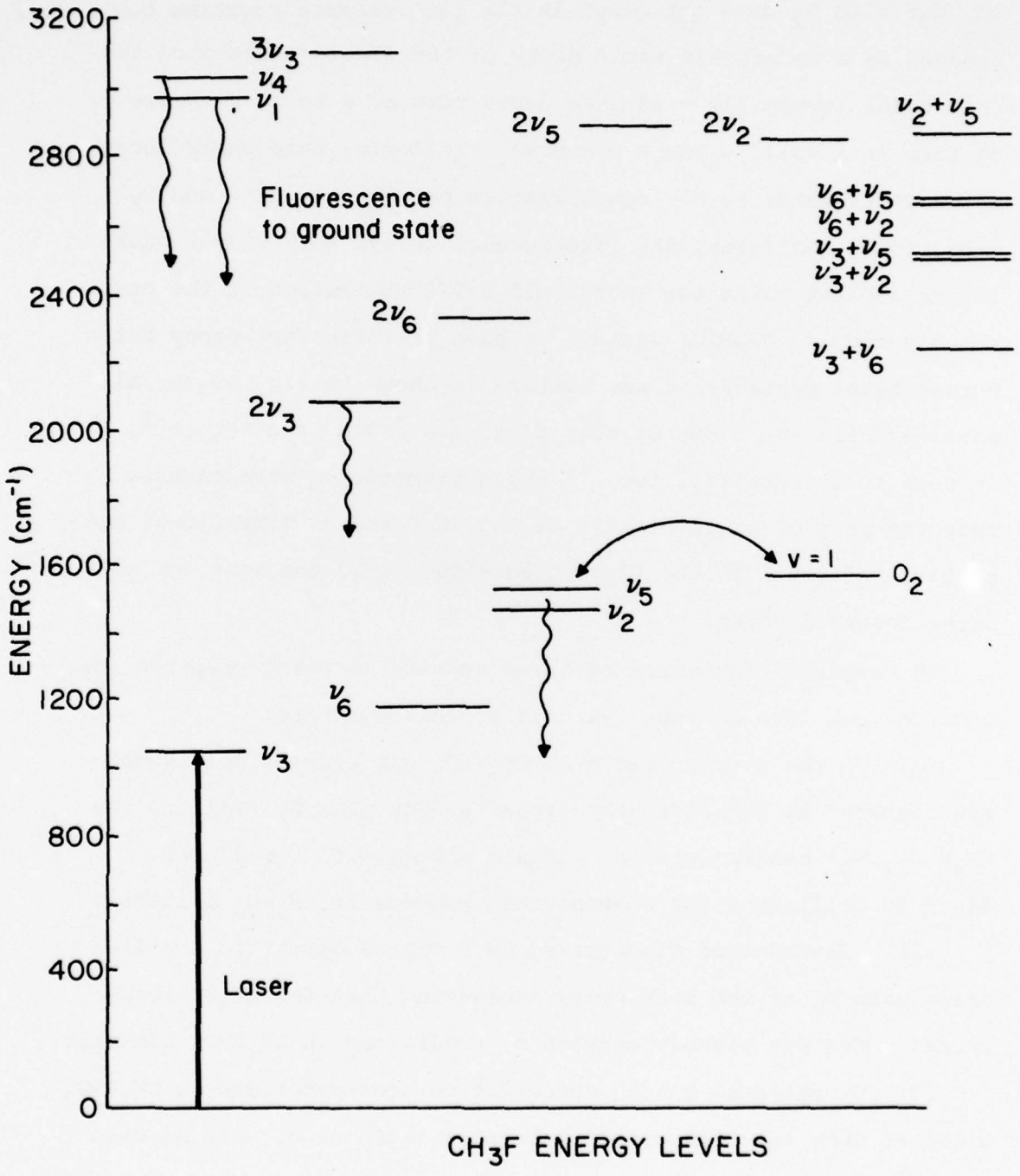
3200
2800
2400
2000
1600
1200
800
400
0
ENERGY (cm⁻¹)
3ν3
ν4
ν1
Fluorescence
to ground state
2ν5
2ν2
ν2+ν5
ν6+ν5
ν6+ν2
ν3+ν5
ν3+ν2
2ν6
ν3+ν6
2ν3
v = 1
O2
ν5
ν2
ν6
ν3
Laser
CH3F ENERGY LEVELS

Figure 28

ponds physically to the redistribution of energy among only the CH_3F vibrational modes due to CH_3F-CH_3F and CH_3F-O_2 collisions. Equilibration of CH_3F with O_2 does not occur in the fluorescence risetime but rather appears as a relatively rapid decay of the fluorescence from its peak value (typically ~ 10 μsec decay time at a total pressure of 35 torr in a 35:1, O_2:CH_3F mixture). Following this rapid decay, which corresponds to V-V equilibration between the CH_3F and O_2 vibrational manifolds, the fluorescence decays very slowly back to its ambient value due to overall V-T/R relaxation of the now tightly coupled CH_3F/O_2 system. A plot of these fast decay rates versus total pressure in the mixture is shown in Fig. 29 for all wavelengths. The slope of this plot, 4.0 ± 0.8 $msec^{-1}$ $torr^{-1}$, is seen to be identical for all three fluorescing wavelengths. Thus the rate of equilibration of the CH_3F and O_2 vibrational manifolds, reflected in the fluorescence decay, is the same for all three observed modes.

A complete discussion of these results is being prepared for publication. The salient features of this work are:

(1) On the average 140 ± 28 CH_3F-O_2 gas kinetic collisions are required to transfer vibrational energy from O_2 (v=1) to the CH_3F (ν_2,ν_5) bending states. This compares with a value of 440 ± 40 collisions for a comparable process in CH_4-O_2 mixtures.

(2) All observed fluorescing CH_3F states appear to equilibrate with O_2 at the same rate, suggesting that the CH_3F vibrational modes are tightly coupled by collisions in CH_3F-O_2 mixtures.

(3) Vibrational quanta conservation considerations in CH_3F-O_2 mixtures show that "impurity" molecules (such as O_2) can be used

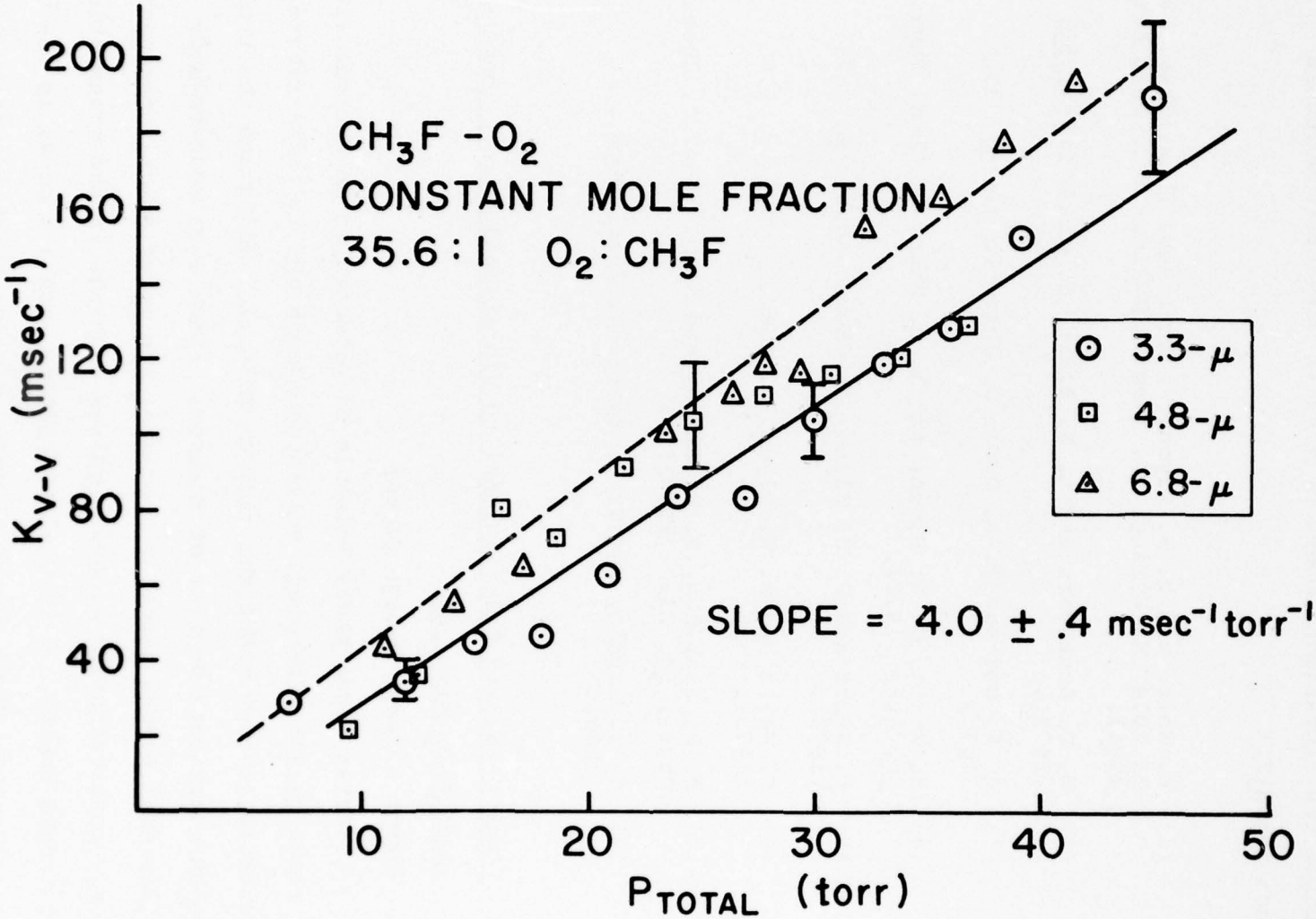
200
160
120
80
40
K_{V-V} (msec^{-1})
$CH_3F - O_2$
CONSTANT MOLE FRACTION
35.6 : 1 $O_2 : CH_3F$
3.3-μ
4.8-μ
6.8-μ
SLOPE = 4.0 ± .4 msec^{-1} torr^{-1}
10
20
30
40
50
P_{TOTAL} (torr)

Figure 29

to place a limit on the possible energy transfer paths which couple the vibrational modes of a small polyatomic molecule such as CH_3F.

(1) E. Weitz and G. W. Flynn, Ann. Rev. Phys. Chem., Vol 25 1974, H. Eyring. ed. (Annual Reviews In., Palo Alto, 1974).

(2) W. D. Breshears and L. S. Blair, J. Chem. Phys., 59, 5824 (1973).

(3) K. K. Hui and T. A. Cool, J. Chem. Phys., 65, 3536 (1976).

(4) E. Weitz, G. W. Flynn, and A. M. Ronn, J. Chem. Phys., 56, 6060 (1972).

(5) E. Weitz and G. W. Flynn, J. Chem. Phys., 58, 2679 (1973).

(6) E. Weitz and G. W. Flynn, J. Chem. Phys., 58, 2781 (1973).

(7) F. R. Grabiner, G. W. Flynn, and A. M. Ronn, J. Chem. Phys., 59, 2330 (1973).

(8) J. T. Yardley and C. B. Moore, J. Chem. Phys., 48, 14 (1968).

2. Laser Catalyzed Translational to Vibrational Energy Conversion in CH_3F-O_2 Mixtures

(Irwin Shamah, George Flynn)

Whenever a gas phase molecule is promoted to an excited vibrational state by laser pumping, collision events act to redistribute the excitation energy among the various molecular modes and the translational/rotational degrees of freedom. Since even mode-to-mode collisional energy transfer processes are never exactly resonant, this energy redistribution always requires a change in the translational/rotational energy. A typical example of such a process is the vibration-vibration (V-V) energy transfer process which occurs in SO_2 after laser pumping of the ν_1 (1151 cm^{-1}) symmetric stretching mode.[1,2]

$$SO_2(\nu_1) + SO_2 \rightleftharpoons SO_2(\nu_3) + SO_2 - 210\ cm^{-1} \qquad (1)$$

Every ν_1 molecule which undergoes the above process gains 210 cm^{-1} of vibrational energy at the expense of the translational/rotational degrees of freedom. In general such V-V energy transfer events can be either endo- or exothermic with respect to the translational/rotational degrees of freedom. In addition, these processes, whether endothermic or exothermic usually occur quite rapidly. For example, reaction (1) above reaches "equilibrium" in approximately 135 gas kinetic collisions.[1,2]

Laser induced fluorescence and double resonance techniques, which probe the time dependent populations of excited vibrational states, can be used to obtain accurate values for energy transfer rates;[3-10] nevertheless, neither of these techniques is a priori sensitive to the translational energy changes which accompany a given relaxation event. As has been pointed out recently and generally recognized for some time, the spectrophone or other techniques which employ the acousto-optic effect are sensitive to both the rates and magnitude (including sign) of translational energy changes which accompany vibrational relaxation processes.[11,12]

The time resolved thermal lensing method, which also employs the acousto-optic effect, displays the complete time dependence of the translational energy changes in a gas following laser excitation.[13,14] This technique is also sensitive to the magnitude and sign, as well as the rate, of translational energy fluctuations. The magnitude and sign of these translational energy changes act as a fingerprint which can be used to identify a particular vibration-vibration (V-V) or vibration-translation/rotation (V-T/R) energy transfer event. In the present work we have utilized the thermal

lens method to study translational energy changes in mixtures of CH_3F and O_2 following laser excitation of the CH_3F (ν_3) C-F stretching mode. In such mixtures an enormous enhancement in translational cooling is observed during V-V equilibration compared to that measured for pure CH_3F. The magnitude and variation of this cooling with O_2 mole fraction provides evidence which defines the V-V energy transfer pathways in CH_3F unambiguously.

To date complete energy transfer maps have not been determined for molecules more complicated than triatomics. Such maps define the vibrational temperatures of each state in a gaseous molecule which has reached a vibrational steady state after laser pumping.[15,16] A knowledge of such temperatures bears directly on the interpretation and prediction of laser induced "infrared photochemistry" effects and on the development of new polyatomic infrared laser devices.

As illustrated above for SO_2 in reaction (1), an endothermic V-V process can act to raise the vibrational energy of a gas at the expense of the translational energy. In CH_3F/O_2 mixtures which contain a large excess of O_2, this effect can be exaggerated to the extent that the incident laser excitation energy is converted to a vibrational excitation energy one and a half times its initial value. In essence this enhancement of the vibrational energy occurs by forcing translational energy into the vibrational degrees of freedom. At first glance this increase in the separation of vibrational and translational energies would not be expected to occur spontaneously; however rapid redistribution of vibrational energy is known to occur following laser excitation. The present experiments demonstrate that such an <u>energetically</u> unfavorable process can occur by permitting the system to increase its overall

randomness. This leads to a storage of excess vibrational energy in a translationally cold gas at least for short periods of time. The apparatus used in these experiments has been described in detail elsewhere.[13,14] The signals obtained were unusually large. Figure 30a shows a signal obtained for 80.0 torr of a 1/267 mixture of CH_3F/O_2. This corresponds to a partial pressure of CH_3F of only 300 mtorr. Excellent signals were obtained for this mixture at total pressures of 40 torr or less. In pure CH_3F essentially noise free signals were obtained for pressures as low as 500 torr.

A hypothetical thermal lensing signal is illustrated in figure 30b. The curve traces out the time dependence of the translational energy of a gas following laser excitation. A rising curve represents an increasing translational energy or heating, while a falling curve indicates the gas is cooling. For the curve shown in figure 30 the gas initially cools as it undergoes V-V equilibrium and then heats as the necessarily exothermic V-T processes take over. The minimum indicates that a V-V steady state has been reached. The rising portion of the curve below the initial baseline represents the return of the heat E_{VV}, which was lost to the vibrational degrees of freedom during the endothermic V-V process, to the translational and rotational degrees of freedom. The remaining portion of the rise above the baseline is the net translational heating E_{NET} resulting from the absorption of the laser radiation by the gas. On a longer time scale this net heating will decay back to the baseline as thermal conduction and mass diffusion to the walls cause the hot gas to cool back to ambient conditions. The magnitude of the net energy increase above the baseline is simply the product of the laser pump energy per photon times the number of photons absorbed by the gas. This quantity is always the same for a given power absorbed and is not dependent on the

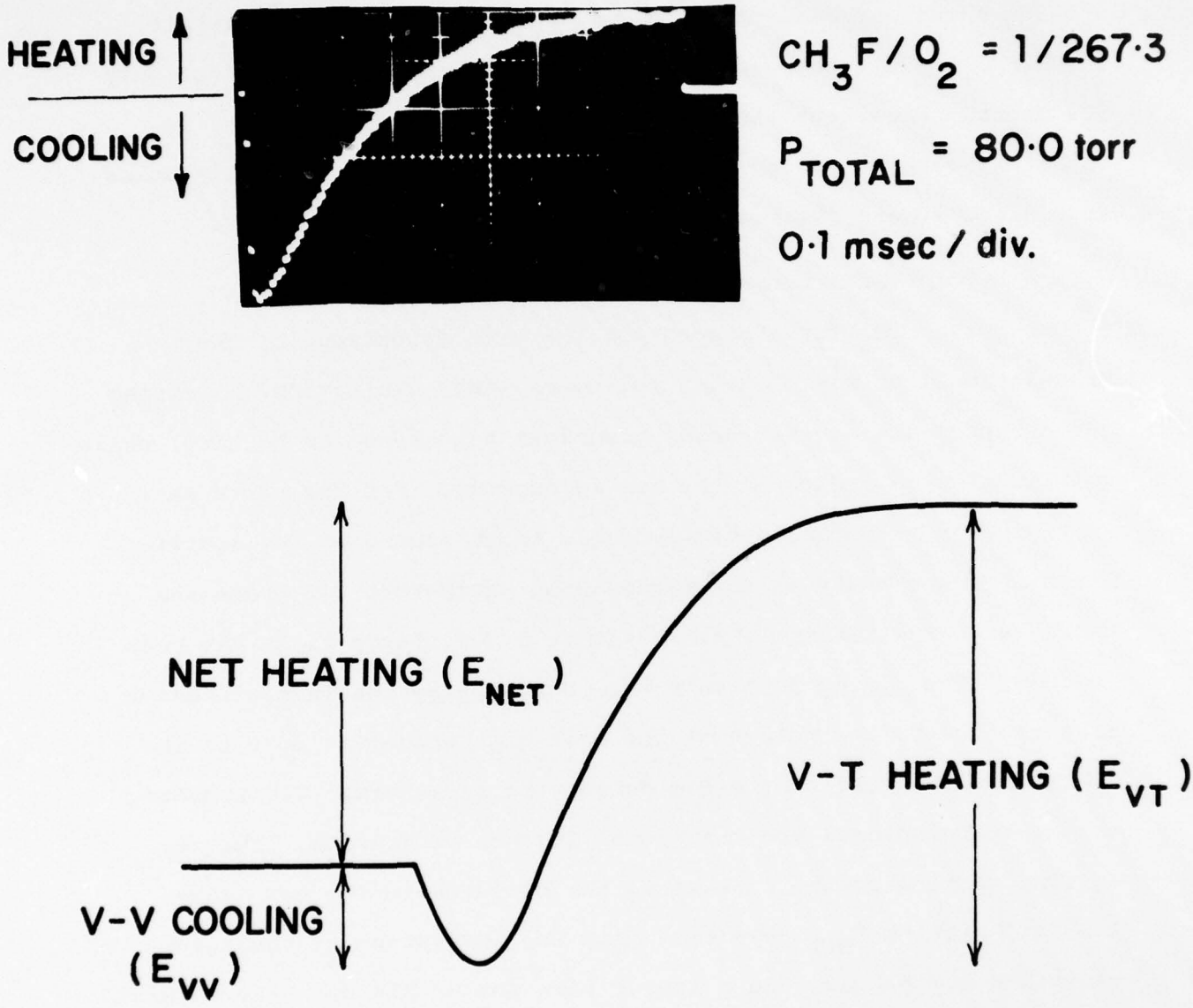

Figure 30:
a) (Upper) Sample experimental thermal lensing signal obtained for CH_3F/O_2 1/267 mixture. b) (Lower) Hypothetical thermal lensing curve showing translational energy changes during V-V and V-T equilibrations. For the signal shown the amplitude below the baseline represents translational cooling at V-V steady state (E_{VV}), peak-to-peak amplitude represents V-T heating (E_{VT}), and their difference represents net heating due to the laser (E_{net}).

specific collisional pathway followed in equilibration. On the other hand the cooling amplitude which reflects the total translational energy loss resulting from V-V equilibrium is entirely path dependent.

Cooling amplitudes have been examined for various mole fraction mixtures of CH_3F/O_2. An enhanced cooling has been observed over equivalent mixtures of pure CH_3F, and CH_3F/Ar. Figure 31 shows thermal lensing signals for equivalent pressures of the mixtures CH_3F/Ar (1:31.1), CH_3F/O_2 (1:10.1), CH_3F/O_2 (1:31.3), and CH_3F/O_2 (1:269.3). The cooling in the CH_3F/Ar mixture is very close to the cooling in pure CH_3F, while the O_2 mixtures show a large increase in cooling relative to heating.

A complete discussion of these results is being prepared for publication. The major conclusions which follow from the experiments and discussion are described below.

CH_3F/O_2 mixtures have been found to exhibit an enhanced translational cooling over pure CH_3F. The amplitude of this cooling increases with increasing O_2 mole fraction. Equivalent mixtures of CH_3F/Ar show a cooling amplitude which is similar to that of pure CH_3F and independent of the mole fraction of Ar. Since the cooling amplitude is sensitive to the particular V-V equilibration pathway in CH_3F, these results support the presence of the following endothermic vibrational energy transfer channel in pure CH_3F:

$$CH_3F\ (\nu_3) + CH_3F \rightleftharpoons CH_3F\ (\nu_6) + CH_3F - 133\ cm^{-1}$$

$$CH_3F\ (\nu_6) + CH_3F \rightleftharpoons CH_3F\ (\nu_2,\nu_5) + CH_3F - 284\ cm^{-1}$$

A knowledge of the energy transfer pathway yields an unambiguous description of the V-V steady state thermodynamic parameters, and, along with the energy transfer cross sections, determines the complete kinetic behavior of the system. In par-

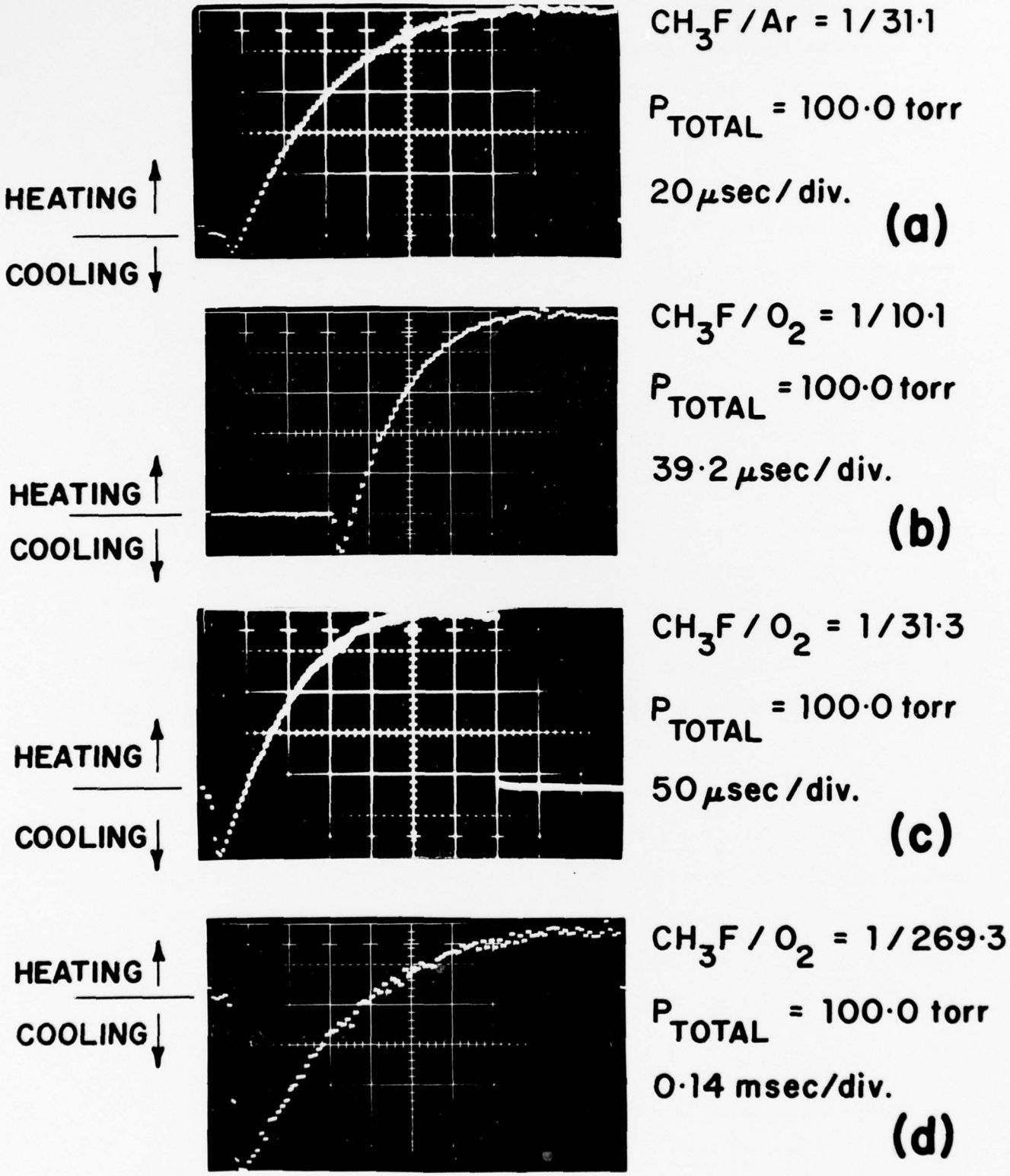

Figure 31: Equal pressure thermal lensing signals for various CH_3F/X mixture showing a marked increase in cooling amplitude with increasing mole fraction of oxygen.

ticular the pathway defines the various vibrational and translational/rotational temperatures which alone are sufficient to quantitatively describe the V-V steady state. Because of the endothermic steps in the pathway for CH_3F V-V equilibration, vibrational mode 3, the C-F stretch, has a higher vibrational temperature and contains more energy than the remaining modes at V-V equilibrium. This fact suggests that future laser chemistry efforts in CH_3F should concentrate on cleaving the C-F bond.

V-V equilibration in CH_3F is a spontaneous process leading to a steady state separation of vibrational and translational/rotational temperatures. A simple argument using a three level model demonstrates that the iso-energetic separation of temperatures is accompanied by an increase in entropy. It is this increase in overall randomness that provides the driving force which enables CH_3F to take the energetically unfavorable endothermic pathway.

At very high O_2 concentrations in CH_3F-O_2 mixtures, the endothermic V-V processes act to convert each absorbed laser photon of 1049 cm^{-1} energy to a vibrational energy content of 1556 cm^{-1}. The difference between the absorbed and steady state vibrational energies is, of course, supplied by the translational/rotational degrees of freedom.

The vibrational temperatures, which are controlled by the energy transfer pathway in CH_3F, can lead to population inversion between modes for an optically pumped gas at vibrational steady state.

(1) D. R. Siebert and G. W. Flynn, J. Chem. Phys., 62, 1212 (1975).

(2) B. L. Earl, A. M. Ronn, and G. W. Flynn, Chem. Phys., 9, 307 (1975).

(3) L. O. Hocker, M. A. Kovacs, C. K. Rhodes, G. W. Flynn, and A. Javan, Phys. Rev. Lett., 17, 233 (1966).

(4) J. T. Yardley and C. B. Moore, J. Chem. Phys., 45, 1066 (1966).

(5) J. C. Stephenson and C. B. Moore, J. Chem. Phys., 56, 1295 (1972).

(6) E. Weitz, G. W. Glynn and A. M. Ronn, J. Chem. Phys., 56, 6060 (1972).

(7) C. K. Rhodes, M. J. Kelly and A. Javan, J. Chem. Phys., 48, 5730 (1968).

(8) J. I. Steinfeld, I. Burak, D. G. Sutton, and A. V. Nowak, J. Chem. Phys., 51, 2275 (1969).

(9) J. I. Steinfeld, I. Burak, D. G. Sutton, and A. V. Nowak, J. Chem. Phys., 52, 5241 (1970).

(10) J. M. Preses and G. W. Flynn, "Infrared Laser Double Resonance Study of Vibrational Energy Exchange Between $^{12}CH_3F$ and $^{13}CH_3F$", to be published.

(11) M. Huetz-Aubert and F. Lepoutre, Physica., 78, 435 (1974); M. Huetz-Aubert, P. Chevalier and C. Klapisz, Compt. Rend., B268, 748 (1969).

(12) R. Tripodi, J. Chem. Phys., 52, 3298 (1970).

(13) F. R. Grabiner, D. R. Siebert, and G. W. Flynn, Chem. Phys. Lett., 17, 189 (1972).

(14) D. R. Siebert, F. R. Grabiner, and G. W. Flynn, J. Chem. Phys., 60, 1564 (1974).

(15) W. D. Breshears and L. S. Blair, J. Chem. Phys., 59, 5824 (1973).

(16) W. D. Breshears, Chem. Phys. Lett., 20, 429 (1973).

3. Trapped Metastable Vibrational Energy Distributions in Laser Pumped Molecules*

(Irwin Shamah, George Flynn)

Laser assisted unimolecular decompositions have been recently reported which suggest that for some molecules absorbed laser energy is highly localized in at most a small number of vibrational modes.[1,2] Although certain molecules[3] (e.g. CO_2, N_2O, and SO_2) are known to require many thousands of collisions to transfer energy between vibrational modes, such an occurrence is in fact a rarity. Indeed, for the kinds of molecules and pressure regimes used in the laser decomposition experiments, complete intermode energy equilibration involving the entire vibrational manifold is expected to occur within a laser pulse-width.[3,4] Thus the observation of highly localized energy distributions under such conditions is startling.[5] Nevertheless, for at least some laser pumped molecules, intermode relaxation processes involving all modes can occur and still lead naturally to localization of energy in a small number of vibrational modes. Such distributions require thousands of collisions to reach equilibrium with the translational and rotational degrees of freedom. Thus the normal energy distribution characterized by a single temperature, that is expected for a gas heated by a Bunsen burner, does not necessarily apply to a laser pumped gas. Pulsed laser heating leads automatically to a substantial separation of vibrational and translational temperatures which lasts for a time of the order of the overall vibration-translation/rotation (V-T/R) relaxation time. In addition the intermode energy equilibration processes which occur either during or shortly after the laser pulse almost always require the exchange of a small amount of energy with the translational degrees of freedom. Under such conditions the energy distribution in the

vibrational modes cannot be described by a single temperature.[6,7] Nevertheless, once the dominant kinetic processes which couple the various vibrational modes are known, the vibrational temperatures of all the modes are well defined in the harmonic oscillator limit.[8] These features can lead to a highly localized metastable vibrational energy distribution as illustrated below for CH_3F.

The laser excitation and subsequent dominant vibrational equilibration pathways coupling the fundamental modes of CH_3F are as follows:[9-14]

Characteristic Time	Reaction	
τ_p	$CH_3F(0) + h\nu_3 \rightarrow CH_3F(\nu_3)$	(1)
τ_{VV}	$CH_3F(\nu_3) + CH_3F \rightleftarrows CH_3F(\nu_6) + CH_3F - 133\ cm^{-1}$	(2)
	$CH_3F(\nu_6) + CH_3F \rightleftarrows CH_3F(\nu_2,\nu_5) + CH_3F - 284\ cm^{-1}$	(3)
	$2\ CH_3F(\nu_2,\nu_5) \rightleftarrows CH_3F(2\nu_2,2\nu_5) + CH_3F(0)$	(4)
	$CH_3F(2\nu,2\nu_5) + CH_3F \rightleftarrows CH_3F(\nu_1,\nu_4) + CH_3F - 60\ cm^{-1}$	(5)
τ_{VT}	$CH_3F(\nu_3) + CH_3F \rightarrow CH_3F(0) + CH_3F + 1049\ cm^{-1}$	(6)

The typical laser pulse width τ_p is about 10^{-6} sec while the four vibration-vibration (V-V) intermode equilibration processes ((2) - (5)) can be considered to reach steady-state in about 75 gas kinetic collisions (7×10^{-6} sec at one torr).[10,14] However, the V-T/R process (6), which restores an energy distribution characteristic of Bunsen burner heating, typically takes 15,000 gas kinetic collisions (1.4×10^{-3} sec at one torr) under low level laser excitation conditions.[11] Thus the highly specialized conditions which exist in laser pumped CH_3F at vibrational steady-state after a time τ_{VV} persist for a time τ_{VT} which is at least three orders of magnitude longer than τ_{VV}.

The steady-state equilibrium constant for process (2) in the time domain $\tau_{VV} < t < \tau_{VT}$ leads to the following relationship[6,7,12]

$$K_{eq} = 2e^{-133/kT'} = \left(2e^{-E_{\nu_6}/kT_{\nu_6}}\right) / \left(e^{-E_{\nu_3}/kT_{\nu_3}}\right), \tag{7}$$

with T_{ν_i} defined by

$$N_{\nu_i} = N_o \, g_{\nu_i} \, e^{-E_{\nu_i}/kT_{\nu_i}} \, . \tag{8}$$

E_{ν_i}, T_{ν_i}, g_{ν_i}, N_{ν_i} are the energy, vibrational temperature, degeneracy and population of level ν_i, respectively; N_o is the ground state population, and k is Boltzmann's constant (cm^{-1}/K). T' is the steady-state translational/rotational temperature which is less than the ambient temperature T since the intermode equilibration pathway for CH_3F requires a loss of translational energy.[15] Equation (7) merely illustrates that the equilibrium constant at steady-state is defined by the bath temperature T' whereas the vibrational state populations are defined by their respective vibrational temperatures or energies. Equation (7) gives immediately the result:

$$\left(E_{\nu_3}/T_{\nu_3}\right) - \left(E_{\nu_6}/T_{\nu_6}\right) = (-133/T'). \tag{9}$$

This analysis can easily be performed on the remaining V-V processes to yield equations relating all of the six mode fundamental temperatures with each other and the translational temperature. The remaining vibrational state temperatures are linear combinations of the mode fundamental temperatures in the harmonic oscillator approximation. In addition the requirement of conservation of particles and total energy at steady state leads to a

relation between the fundamental temperatures and the initial experimental conditions. The distribution of fundamental temperatures can thus be obtained in terms of the input laser energy by combining the temperature and conservation equations and solving iteratively on a computer.[16] Since the steady-state vibrational energy expressions are functions of the vibrational temperatures and the translational/rotational energy is 3kT', the entire steady-state energy distribution can be calculated.[17]

Figure 32 presents a comparison of the Boltzmann equilibrium energy distribution in CH_3F with the laser induced steady-state distribution for the input energy range equivalent to 0-9 kcal/mole (0-3 photons absorbed per molecule). The upper plot represents the case where the added energy is divided among the various degrees of freedom according to the equilibrium equipartition, Boltzmann description. The lower plot representing the pulsed laser heating V-V equilibrated case differs substantially from the Bunsen burner-like expectations. Here the translational/rotational energy is slowly decreasing with increasing input energy reflecting the fact that the relaxation pathway is translationally endothermic. The C-H stretches ν_1, ν_4 receive practically no excitation while the C-F stretch ν_3 is overwhelmingly enhanced compared to the remaining vibrational modes, particularly at excitation levels greater than 4.5 kcal/mole (1.5 photons per molecule). Therefore CH_3F in this high excitation regime will trap most of the input laser energy in the ν_3 mode for a period lasting for thousands of gas kinetic collisions. The overall features of the distinctive laser induced energy distribution of Fig. 32 have also been observed experimentally.[18] Similar results have been obtained independently for

Figure 32:

(Upper) Plot of the average energy in the translational, rotational and vibrational degrees of freedom of CH_3F vs. added energy. A Boltzmann equilibrium at a single temperature and harmonic oscillator states is assumed. E_{TRANS} is the sum of the translational and rotational energies, E_{VIB} is the total average vibrational energy and E_i is the mean vibrational energy of mode i.

(Lower) Plot of the average energy distribution in CH_3F vs. laser input energy for a system at vibration-vibration equilibrium obeying the energy transfer mechanism of Eqs. (1) - (5). 3 kcal per mole is equivalent to 1 laser photon absorbed per molecule. The calculated curves neglect vibration-translation/rotation relaxation.

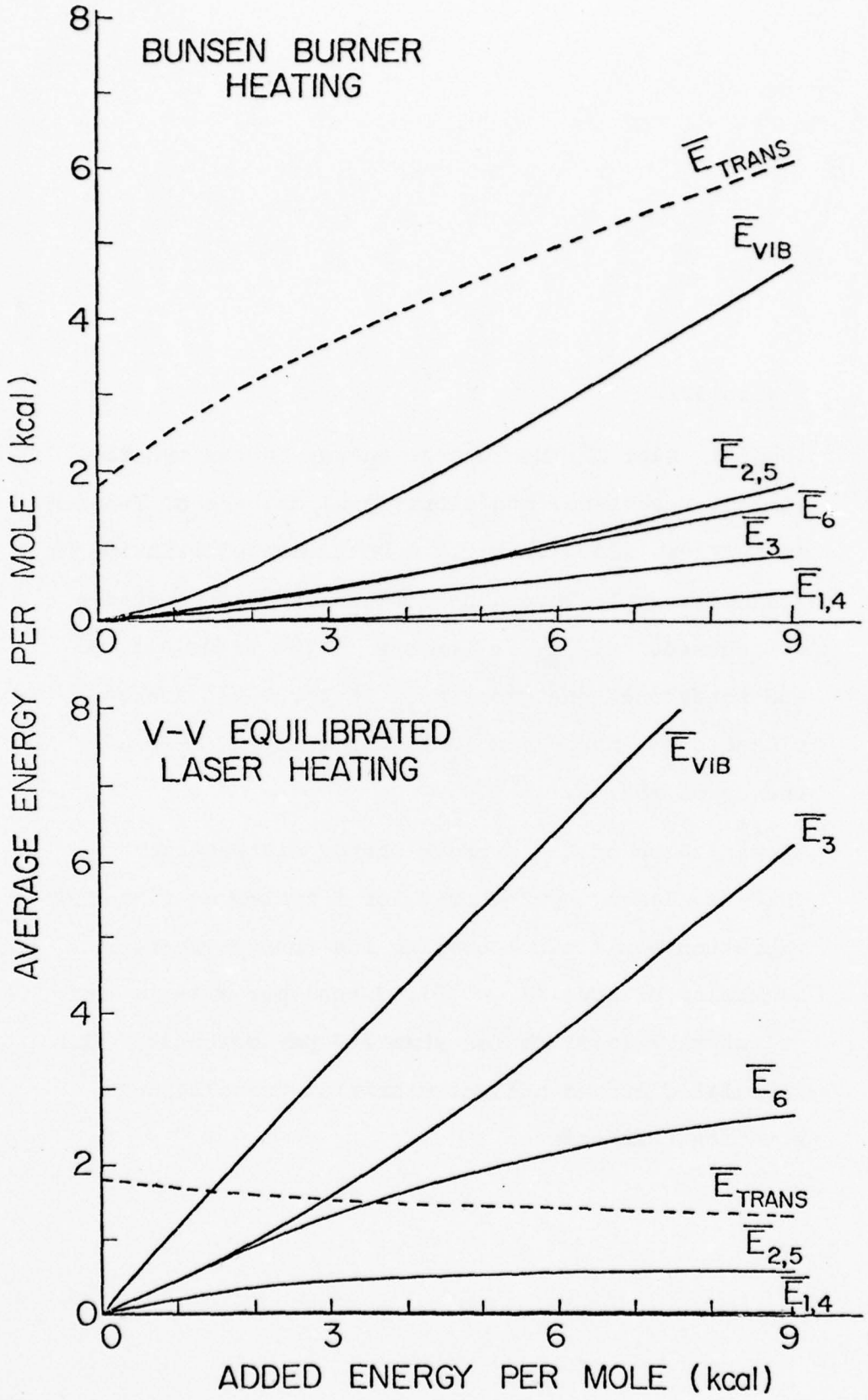
BUNSEN BURNER
HEATING
$\overline{E}_{TRANS}$
$\overline{E}_{VIB}$
$\overline{E}_{2,5}$
$\overline{E}_6$
$\overline{E}_3$
$\overline{E}_{1,4}$
V-V EQUILIBRATED
LASER HEATING
$\overline{E}_{VIB}$
$\overline{E}_3$
$\overline{E}_6$
$\overline{E}_{TRANS}$
$\overline{E}_{2,5}$
$\overline{E}_{1,4}$
AVERAGE ENERGY PER MOLE (kcal)
ADDED ENERGY PER MOLE (kcal)
0
2
4
6
8
0
3
6
9

Figure 32

laser pumped CCl_3F [19] using the CH_3F model [18] and an assumed energy transfer path with constant translational temperature.

The assumption of a vibrational steady-state in which the molecular modes are equilibrated with each other but not with the translational and rotational degrees of freedom is not the only model nor the only effect which can lead to vibrational energy localization.[5,20] Nevertheless, the effects which are described here for CH_3F are quite general. Any laser pumped polyatomic molecule which undergoes nonresonant mode-to-mode equilibration processes much faster than the overall V-T/R relaxation can exhibit highly localized metastable vibrational energy distributions.

*Work also supported by the National Science Foundation under grant number MPS75-04118.

(1) D. F. Dever and E. Grunwald, J. Am. Chem. Soc., 98, 5055 (1976).

(2) J. M. Preses, R. E. Weston, and G. W. Flynn, "Unimolecular Decomposition of Cyclo-C_4F_8 Induced by a CO_2 TEA Laser," to be published, Chem. Phys. Lett.

(3) E. Weitz and G. W. Flynn, Ann. Rev. Phys. Chem., 25, 275 (1974).

(4) F. R. Grabiner and G. W. Flynn, J. Chem. Phys., 60, 398 (1974).

(5) S. A. Rice and J. Jortner, "Reactions Induced by Incoherent Multiphoton Absorption," private communication.

(6) W. D. Breshears and L. S. Blair, J. Chem. Phys., 59, 5824 (1973).

(7) W. D. Breshears, Chem, Phys. Lett., 20, 429 (1973).

(8) D. R. Siebert and G. W. Flynn, J. Chem. Phys., 62, 1212 (1975).

(9) E. Weitz and G. W. Flynn, J. Chem. Phys., 58, 2781 (1973).

(10) F. R. Grabiner, G. W. Flynn, and A. M. Ronn, J. Chem. Phys., 59, 2330 (1973).

(11) E. Weitz, G. W. Flynn, and A. M. Ronn, J. Chem. Phys., 56, 6060 (1972).

(12) I Shamah and G. W. Flynn, "Laser Catalyzed Translational to Vibrational Energy Conversion in CH_3F-O_2 Mixtures," submitted for publication, J. Chem. Phys.

(13) J. M. Preses, Ph.D. Thesis, Department of Chemistry, Columbia University, New York, New York, 1975. This reference is available from University Microfilms, Ann Arbor MI.

(14) J. M. Preses, R. Sheorey, R. C. Slater, E. Weitz, and G. W. Flynn, work in progress.

(15) F. R. Grabiner, D. R. Siebert, and G. W. Flynn, Chem. Phys. Lett., 17, 189 (1972).

(16) I. Shamah and G. W. Flynn, to be published.

(17) Radiative cooling via spontaneous emission was not included in these calculations. We are indebted to Ramesh Sharma for pointing out the importance of this effect.

(18) R. E. McNair, B. J. Feldman, M. S. Feld, and G. W. Flynn, "Vibrational Temperature Distribution in Laser Pumped CH_3F," submitted for publication.

(19) S. Mukamel and J. Ross, "Comment on Non-Statistical Behavior in Laser Chemistry and Chemical Activation", private communication.

(20) R. V. Ambartsumyan, Yu. A. Gorokhov, V. S. Letokhov, and G. N. Makarov, JETP LETT., 21, 171 (1975); JETP LETT., 22, 43 (1975).

III. LASER STUDIES OF MOLECULAR ENERGY TRANSFER

A. ELECTRONIC-TO-VIBRATIONAL ENERGY TRANSFER*

1. Dye Laser Excited Electronic-to-Vibrational Energy Transfer: $Br^*(4^2P_{\frac{1}{2}}) \rightarrow OCS$

(S. Lemont, G. W. Flynn)

Over the past several years, a great many studies have been made concerning the quenching of fluorescence from excited electronic energy levels.[1] Lasers have played an important role in many of these experiments since they are powerful light sources which can be used to selectively excite a significant fraction of molecules into specific vibration-rotation levels of an upper electronic state. However, most of the quenching experiments performed to date have given us little information concerning the states into which electronic energy is channelled. Comprehensive studies of the transfer of energy from excited vibrational states of the ground electronic state to other vibrations, and to the translational and rotational degrees of freedom have been made.[2] The information obtained from these experiments is fairly well understood. On the other hand, relatively few experiments have been performed which have proved the existence of energy transfer between excited electronic levels and molecular vibrations, rotations and translations.

We have made a detailed kinetic analysis of electronic-to-vibrational energy transfer from Br $(4^2P_{\frac{1}{2}})$ to the polyatomic molecule, OCS. Following dye laser photodissociation of Br_2 in bromine-carbonyl sulfide mixtures, infrared fluorescence from the ν_3 (C-O stretch) mode of OCS was observed at 4.8μ. (See Fig. 33) A schematic diagram of the apparatus used in the study of electronic-to-vibrational energy transfer is shown in Fig. 34. A nitrogen-pumped laser was used to dissociate bromine molecules. Using the

Figure: 33

A partial vibrational energy level diagram for OCS. All levels up to an energy of approximately 4250 cm^{-1} are included. The position of the Br ($4^2P_{\frac{1}{2}}$) state is shown by the dashed line.

Figure 33:

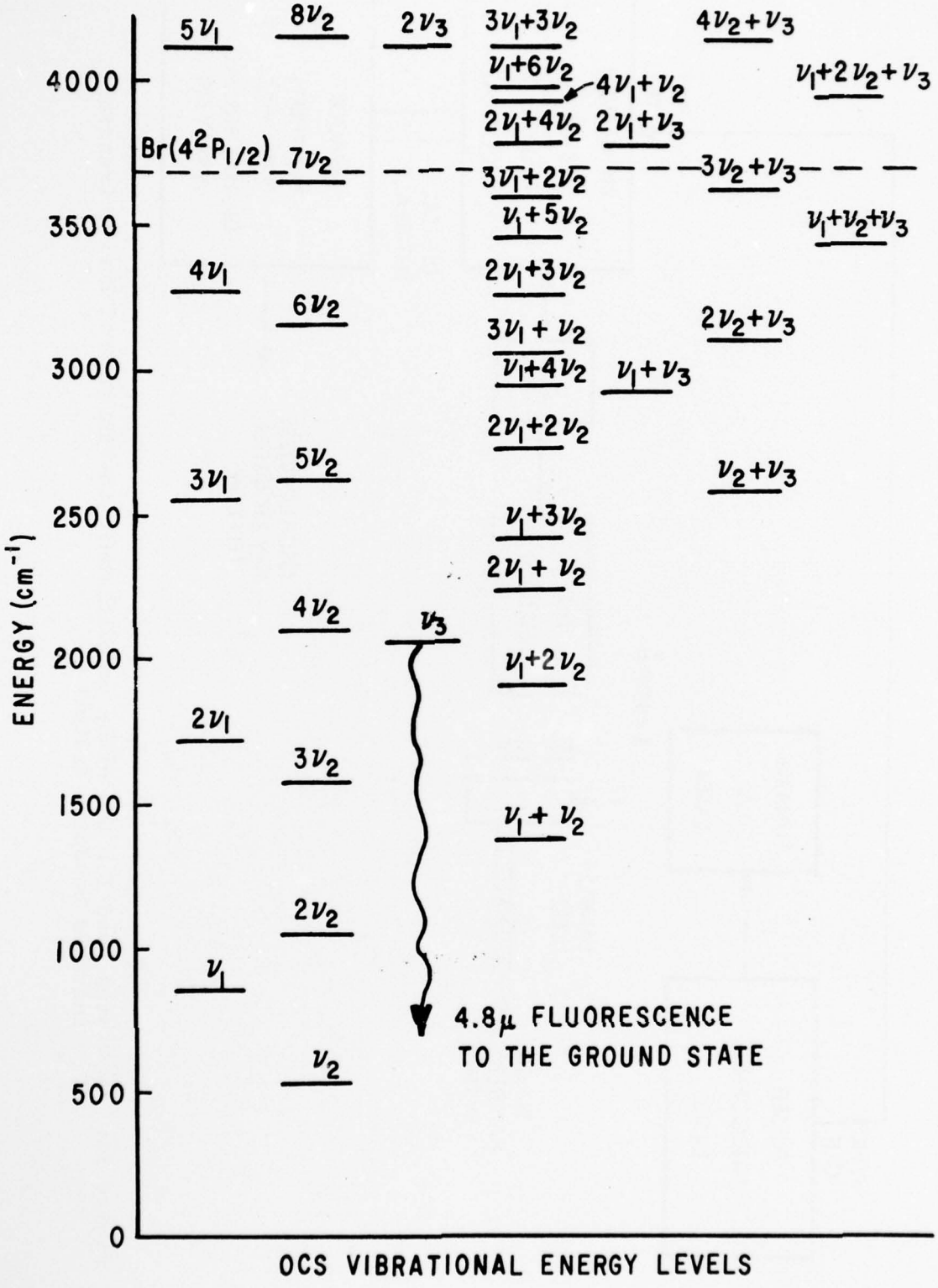
ENERGY (cm⁻¹)
4000
3500
3000
2500
2000
1500
1000
500
0
Br(4²P1/2)
5ν1
8ν2
2ν3
3ν1+3ν2
4ν2+ν3
ν1+6ν2
4ν1+ν2
ν1+2ν2+ν3
2ν1+4ν2
2ν1+ν3
7ν2
3ν1+2ν2
3ν2+ν3
ν1+5ν2
ν1+ν2+ν3
4ν1
2ν1+3ν2
6ν2
3ν1+ν2
2ν2+ν3
ν1+4ν2
ν1+ν3
2ν1+2ν2
5ν2
3ν1
ν2+ν3
ν1+3ν2
2ν1+ν2
4ν2
ν3
ν1+2ν2
2ν1
3ν2
ν1+ν2
2ν2
ν1
4.8μ FLUORESCENCE
TO THE GROUND STATE
ν2
OCS VIBRATIONAL ENERGY LEVELS

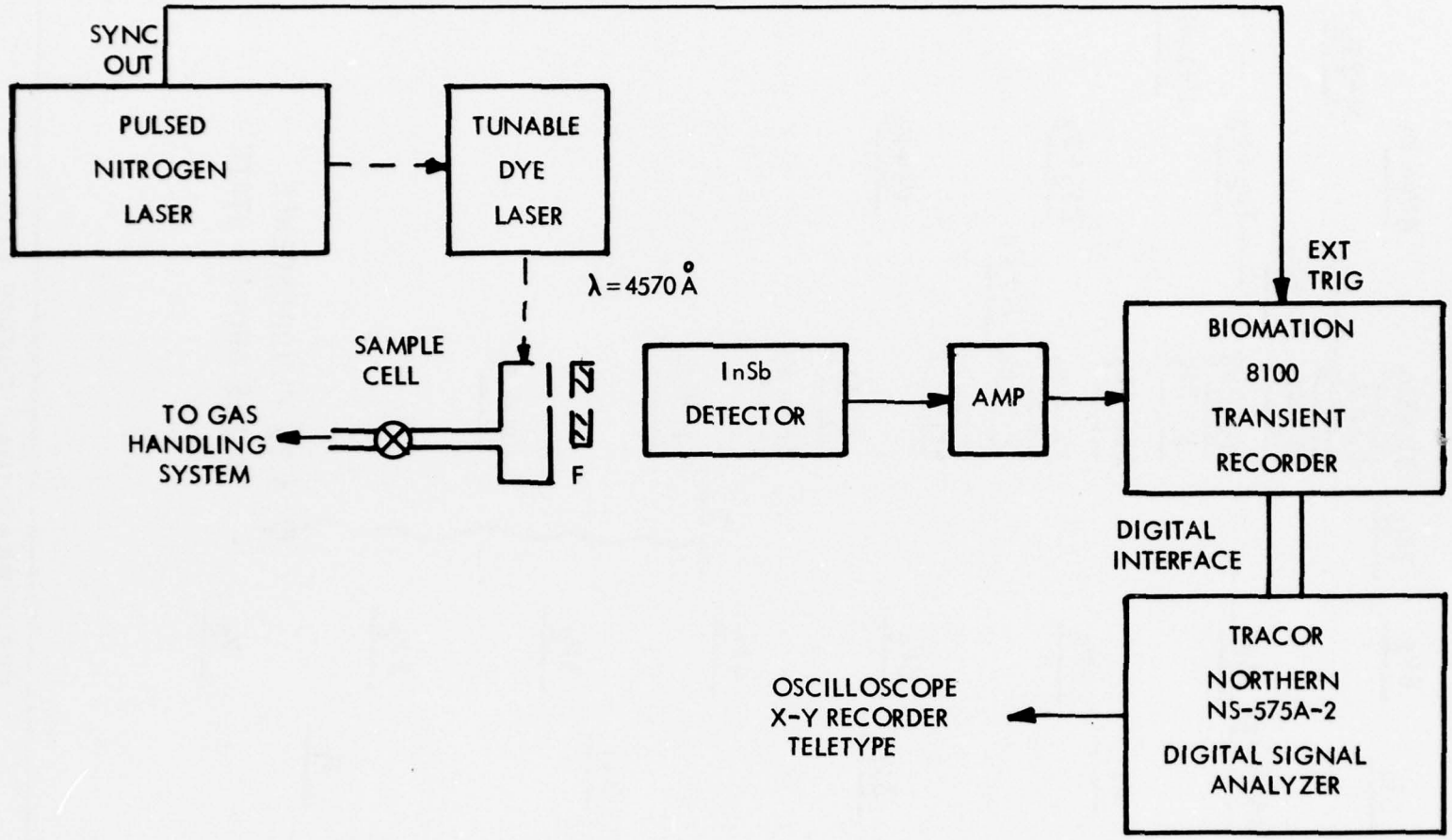

Figure 34: Apparatus used for the study of electronic-to-vibrational energy transfer. (F = infrared bandpass filter)

dye 7-diethylamino-4-methylcoumarin at its wavelength of maximum power, 4570 Å, the dye laser produced approximately 75 kW and a laser pulse energy of 450μj. Under these conditions, the partial pressure of Br at the instant of laser excitation was about 1% that of Br_2 at a bromine pressure of 1 torr. The laser had a pulse width of about 6 nsec (FWHM) and operated at a repetition rate of 10 Hz.

The gas mixtures were contained in a sample cell made of square Pyrex tubing (4 cm x 4 cm) with circular O-ring end joints which were large enough so that the laser beam could pass as close to the cell wall as possible. A germanium fluorescence window was used on the sample cell to block scattered laser light to which the infrared detector was sensitive.

Following Br_2 photodissociation by a dye laser pulse, the subsequent infrared emission was viewed normal to the excitation axis by a photovoltaic InSb detector (77°K) with a matched amplifier. These components were enclosed in an aluminum chassis box to shield against most of the RF noise from the pulsed nitrogen laser. A 4.812-μ, 0.16-μ bandwidth, narrow bandpass filter (see F in Fig. 34) was used when observing OCS fluorescence from the ν_3 fundamental at 4.8μ. For experiments where fluorescence from Br ($4^2P_{\frac{1}{2}}$) at 2.7μ was observed, a 3-μ bandpass filter with a 1-μ bandwidth (2.5-3.5μ) was used to discriminate against the much stronger OCS fluorescence.

The signals from the InSb detector were further amplified with a wide bandwidth (1MHz) amplifier and averaged by a wide bandwidth (25 MHz) digital signal averaging system consisting of a Biomation 8100 transient recorder connected through a digital interface to a Tracor Northern NS-575A-2 Digital Signal Analyzer. The signal averager

was triggered by a timing pulse from the N_2 laser trigger generator. With the detector loaded to 50 ohms, the risetime of the data acquisition system was about 1μsec.

RESULTS AND DISCUSSION

a) Quenching of Br ($4^2P_{\frac{1}{2}}$)

Although extremely weak, fluorescence at 2.7μ from Br ($4^2P_{\frac{1}{2}}$), henceforth called Br, could be observed after considerable signal averaging. Br was significantly deactivated by the two major components of all the gas mixtures studied, Br_2 and OCS. From observations of the decay of 2.7μ Br fluorescence in this pressure range as a function of Br_2 pressure, a rate of 26 ± 6 $msec^{-1}$ $torr^{-1}$ was found for the deactivation of Br by Br_2.

The rate of deactivation of Br by OCS was found to be 47 ± 11 $msec^{-1}$ $torr^{-1}$. In addition to electronic-to-vibrational energy transfer, this rate includes small contributions from electronic-to-translational and rotational (E-T/R) energy transfer in Br-OCS collisions, as well as quenching effects by impurities in the OCS sample. The major impurity, CO_2, which, at equilibrium, is present at about 1.7% of the total OCS pressure because of disproportionation has been found to quench Br fluorescence at a rate of approximately 490 ± 30 $msec^{-1}$ $torr^{-1}$. Subtraction of this contribution from the present Br-OCS quenching rate leaves 39 ± 11 $msec^{-1}$ $torr^{-1}$.

b) Br-OCS E-V and Subsequent OCS-OCS V-V processes

Following dye laser photodecomposition of bromine, weak infrared fluorescence was observed from OCS at 4.8μ. About 95% of this fluorescence was absorbed by 50 torr of OCS placed in a

2-cm path length cold gas filter cell between the sample cell and the InSb detector, indicating that the infrared emission from OCS results primarily from a transition from ν_3 to the ground state.

The usual way of analyzing the experimental fluorescence signals is as follows: First, the decay rate is determined by fitting the semilog plot of the exponential decay to a straight line. Next, the decaying exponential is extrapolated to short time. This provides a baseline for a semilog plot of the fluorescence rise. If this is done, and the rates of rise and decay of OCS fluorescence for each signal are plotted vs. OCS pressure, then the rate constants obtained from the slopes of these straight line plots are 99 ± 5 msec^{-1} torr^{-1} and 32 ± 1 msec^{-1} torr^{-1} for the rates of rise and decay, respectively. Note that these rise and decay rates differ by only a factor of three, and, since they are so close in magnitude, analysis of the data by the method described above does not yield accurate results.

The problem under consideration is thus to recover from experimental data the rate constants K_a and K_b in an expression of the form

$$\left[OCS(\nu_3)\right] \sim [\exp(-K_b t) - \exp(-K_a t)] \qquad (1)$$

Where K_a and K_b are the actual rates of filling and emptying of ν_3, respectively. Furthermore, $K_a \approx K_b$, and, since this is the case, a natural parameter of smallness for this system is $K_a - K_b$. Rewriting

$$K_a = (K_a + K_b)/2 + (K_a - K_b)/2 \qquad (2a)$$

and

$$K_b = (K_a + K_b)/2 - (K_a - K_b)/2 \qquad (2b)$$

gives

$$[OCS\ (\nu_3)] \sim \exp\left[-\left(\frac{K_a + K_b}{2}\right) t\right]\left\{\exp\left[\left(\frac{K_a - K_b}{2}\right) t\right] - \exp\left[-\left(\frac{K_a - K_b}{2}\right) t\right]\right\} \tag{3}$$

$\exp\left[\pm \frac{K_a - K_b}{2}\ t \right]$ can be expressed in terms of a power series; and, since K_a and K_b are close in magnitude, at short times we can neglect second and higher order terms. Equation (3) may now be rewritten as

$$[OCS\ (\nu_3)]_{rise} \sim (K_a - K_b)\ t \exp -\left[\left(\frac{K_a + K_b}{2}\right) t\right] \tag{4}$$

$[OCS\ (\nu_3)]_{rise}$ represents points on the rising part of the fluorescence signal where t is small. Dividing through by t and taking the logarithm of both sides of Equation (8), we obtain

$$\ln \frac{[OCS\ (\nu_3)]_{rise}}{t} = -\left(\frac{K_a + K_b}{2}\right) t + C \tag{5}$$

The constant C is a combination of K_a, K_b and the amplitude of the fluorescence signal. Thus, a plot of the factor $\ln \{[OCS\ (\nu_3)]_{rise}/t\}$ vs. t should be a straight line with a slope which is the average of the two rate constants.

The rate of deactivation of Br by OCS, 39 ± 11 msec^{-1} torr^{-1}, is the limiting rate of filling, K_a, of the ν_3 state of OCS. Since a plot of $\ln \{[OCS\ (\nu_3)]_{rise}/t\}$ vs. t would give us $K_a + K_b$ (see Equation (5)), we can find K_b from

$$K_b = K_a + K_b - 39 \tag{6}$$

After application of the above deconvolution procedure, the corrected rate constant, K_b, for the emptying of the ν_3 state of OCS was found to be 47 ± 14 msec^{-1} torr^{-1}.

The final vibrational temperatures of the OCS fundamentals were calculated based on the supposition that states $\ell\nu_1+m\nu_2+n\nu_3$ (ℓ, m, n = 0, 1, 2, . . .) near Br ($4^2P_{\frac{1}{2}}$) are excited and then rapidly decompose to give $\underline{\ell}\ \nu_1$, $\underline{m}\ \nu_2$ and $\underline{n}\ \nu_3$ quanta. The results of these calculations, shown in Table III, illustrate that any state having at least one quantum of ν_3 will eventually end up giving $T_{\nu_3} > T_{\nu_1}, T_{\nu_2}$, where T_{ν_i} is the vibrational temperature of the mode ν_i. Only those states with n = 0 end up giving $T_{\nu_3} < T_{\nu_1}, T_{\nu_2}$. Since the filling of ν_3 is at the E-V rate, 39 $\pm$ 11 $msec^{-1}$ $torr^{-1}$, the E-V transfer cannot populate exclusively a mode or state of the type $\ell\nu_1 + m\nu_2$ (e.g., $7\nu_2$, $3\nu_1 + 2\nu_2$, $2\nu_1 + 4\nu_2$, etc.), but must also excite at least one state of the type $\ell\nu_1 + m\nu_2 + n\nu_3$ with $n \geq 1$ in processes such as

$$Br + OCS(0)$$

$$\longrightarrow Br + OCS(2\nu_3) - 416\ cm^{-1} \quad (7)$$

$$\longrightarrow Br + OCS(2\nu_1 + \nu_3) - 84\ cm^{-1} \quad (8)$$

$$\longrightarrow Br + OCS(3\nu_2 + \nu_3) + 70\ cm^{-1} \quad (9)$$

$$\longrightarrow Br + OCS(\nu_1 + \nu_2 + \nu_3) + 261\ cm^{-1} \quad (10)$$

$$\longrightarrow Br + OCS(\nu_1 + 2\nu_2 + \nu_3) - 252\ cm^{-1} \quad (11)$$

The filling of such overtones or combination states is not unlikely since it has been demonstrated that in the transfer of energy from Br to CO_2, the ($10^0 1$) state and perhaps the ($02^0 1$) state receive a large fraction of the Br excitation energy, enough for these to be the upper states of lasing transitions in the E-V pumped Br -CO_2 laser.[3] Transfer of energy to $2\nu_3$ and $2\nu_1 + \nu_3$ involve the smallest changes in the number of quanta, and these, as well as other combination states, will rapidly populate the ν_3 state after collision with a ground state OCS molecule by the extremely efficient, near-resonant processes

TABLE III

Vibrational Temperatures[a] of OCS Fundamentals After E-V Excitation by Br

OCS Energy Level	T_{ν_1}(°K)[b]	T_{ν_2}(°K)	T_{ν_3}(°K)
$4\nu_1$	496	298	298
$5\nu_1$	536	298	298
$7\nu_2$	298	463	298
$2\nu_3$	298	298	873
$\nu_1+5\nu_2$	362	416	298
$\nu_1+6\nu_2$	362	440	298
$2\nu_1+3\nu_2$	411	369	298
$2\nu_1+4\nu_2$	411	393	298
$3\nu_1+2\nu_2$	455	347	298
$3\nu_1+3\nu_2$	455	369	298
$4\nu_1+\nu_2$	496	323	298
$2\nu_1+\nu_3$	411	298	726
$2\nu_2+\nu_3$	298	347	726
$3\nu_2+\nu_3$	298	369	726
$4\nu_2+\nu_3$	298	393	726
$\nu_1+\nu_2+\nu_3$	362	323	726
$\nu_1+2\nu_2+\nu_3$	362	347	726

[a]Calculated based on the assumption that states $\ell\nu_1+m\nu_2+n\nu_3$ (ℓ, m, n = 0, 1, 2, . . .) near Br ($4^2P_{\frac{1}{2}}$) are excited with 100% efficiency and then rapidly decompose to give $\underline{\ell}\ \nu_1$, $\underline{m}\ \nu_2$ and $\underline{n}\ \nu_3$ quanta. We assume that 1.7% of the total number of OCS molecules are excited.

[b]T_{ν_i} is the vibrational temperature of state ν_i.

$$OCS(2\nu_3) + OCS(0) \longrightarrow 2OCS(\nu_3) \quad (12)$$

and

$$OCS(2\nu_1+\nu_3) + OCS(0) \longrightarrow OCS(2\nu_1) + OCS(\nu_3) \quad (13)$$

SUMMARY

Electronic-to-vibrational energy transfer has been observed to occur in mixtures of electronically excited bromine atoms in the $4^2P_{\frac{1}{2}}$ state and OCS following formation of the Br atoms by dye laser photodissociation of Br_2. Infrared fluorescence was observed from the ν_3 fundamental of OCS. The measured rates of fluorescence rise and decay had to be corrected to obtain the true kinetic rate constants. An approximate deconvolution technique has been derived. Available experimental evidence indicates that energy is transferred from Br to OCS overtone or combination states with a ν_3 component, although there is no evidence which would indicate the exact state or states to which energy is transferred. The corrected rate of emptying of the ν_3 state was shown to correspond to the rate of ν_2-ν_3 V-V equilibration in OCS. This is borne out by the fact that ν_2 is vibrationally cold with respect to ν_3 following E-V energy transfer and acts as a sink for vibrational energy from ν_3. The ν_2-ν_3 equilibration was also studied in OCS-rare gas mixtures. The results of these studies are consistent with a rate limiting filling of $4\nu_2$ from the ν_3 state.

In this study, fluorescence was only observed from the ν_3 state of OCS. If a more powerful laser were to be used such that a larger initial concentration of Br could be produced, a greater num-

ber of OCS molecules could be excited. Fluorescence might then be observed from other OCS vibrational levels, giving greater insight into the exact energy states involved in electronic-to-vibrational energy transfer.

(1) (a) J. I. Steinfeld, Accts. Chem. Res., 9, 313 (1970);
(b) J. T. Yardley, Chemical and Biochemical Applications of Lasers., (C. B. Moore, ed.), Academic Press, New York (1974), p. 231;
(c) R. J. Donovan and D. Husain, Chem. Revs., 70, 489 (1970);
(d) D. Husain and R. J. Donovan, Adv. Photochem., 8, 1 (1971);
(e) L. Krause, Appl. Opt., 5, 1375 (1966).
These works contain several references concerning the quenching of fluorescence from excited electronic states of atoms and molecules.

(2) E. Weitz and G. W. Flynn, Ann. Rev. Phys. Chem., 25, 275 (1974). Additional references may be found in this review article.

(3) A. B. Petersen, C. Wittig, and S. R. Leone, J. Appl. Phys., 47, 1051 (1976).

2. Vibrational State Analysis of Electronic-To-Vibrational Energy Transfer Processes*

(Stephen Lemont, George W. Flynn)

This work is a review of the field of Electronic-to-Vibrational energy transfer over the past 18 years (111 references). Since the entire article will appear in Volume 28 of Annual Review of Physical Chemistry, we include here only the Table of Contents and the Summary.

Table of Contents

SUMMARY

Significant progress has been made over the past few years in the study of electronic-to-vibrational energy transfer processes employing vibrational state detection methods. Two laser techniques appear to be exceptionally promising in their ability to yield large quantities of detailed information regarding such events, and molecular beam studies can be expected to grow significantly in importance over the next few years. Nevertheless, the field itself is, at this stage, relatively unexplored and offers rich opportunities for future work. The area of vibrational-to-electronic energy transfer appears to be even less explored. Studies in this field, which are certainly related to E-V work, can be expected to expand rapidly, particularly as laser techniques capable of producing high vibrational temperatures are improved and developed.

*This work was also supported by the National Science Foundation under Grant MPS 75-04118.

B. VIBRATION-VIBRATION ENERGY TRANSFER

1. Equilibration of the ν_1 and ν_2 Modes of Laser Pumped COF_2.

(Kent Casleton, George Flynn)

The molecule COF_2 is a particularly convenient one in which to study vibrational energy transfer processes. The C-F symmetric stretch mode, ν_2, strongly absorbs pulsed CO_2 laser radiation while the C=O stretch mode, ν_1, exhibits intense infrared emission at $\lambda \simeq 5\mu$. In addition the C-F overtone $2\nu_2$ is coupled to ν_1 by Fermi resonance [1] suggesting the possibility of efficient collisional energy transfer between these states.[2,3,4] On the other hand, the remaining vibrational modes are rather widely separated in frequency from ν_1, ν_2 and are not significantly mixed with these modes by mechanical anharmonicities. Thus loss of vibrational excitation from the coupled C-F and C=O stretches due to collisions is expected to be slow leading to localization of energy in a small number of vibrational modes. Such metastable energy distributions, which are rare in polyatomic molecules, are of considerable interest in laser chemistry, laser development, and contribute significantly to an understanding of intermode energy transfer processes.

We have investigated laser induced fluorescence in COF_2 which gives detailed information regarding the time scale required for the ν_1, ν_2 modes to reach vibrational steady-state and to lose excitation to the remaining modes. The general approach used to analyze and unravel the energy transfer kinetics is expected to be useful for other poly-atomic molecules.

A detailed description of the apparatus employed in the laser induced infrared fluorescence experiment has been given previously. In brief, a Q-switched CO_2 laser operating in either the P or R branch of the 10.6μ band excites the COF_2 ν_2 symmetric C-F stretch as shown in the energy level diagram in Figure 36. The carbonyl fluoride sample was specially prepared by Synthatron Corporation (Edgewater, NJ) with total impurities less than 200 ppm.

Fluorescence near 5μ was observed through a MgF_2 side window with a photovoltaic InSb detector (77°K). The detector was sensitive to fluorescence over a region established by a 4.6μ long pass interference filter and the detector cutoff. Signals were preamplified with a matched amplifier having a pulse response of 0.7μsec, and averaged using a Biomation 8100 transient recorder interfaced to a Tracor Northern NS- 575A-2 digital signal analyzer.

In order to identify the molecular states responsible for the observed 5μ fluorescence, several experiments were conducted using a variety of infrared filters. The fluorescence wavelength was found to be consistent with that expected for emission from the ν_1, $2\nu_2$ vibrational states (see Fig. 35). These levels, which are mixed by Fermi resonance, are respectively, the C-O stretch fundamental at 1944 cm^{-1} and the first overtone of the (pumped) C-F stretch at 1910 cm^{-1}.

Upon excitation of the COF_2 by a CO_2 laser operating near 10.6μ, very strong fluorescence from the ν_1, $2\nu_2$ states was observed near 5μ. Over 30 CO_2 laser lines in the P and R branches of the 10.6μ band were found to produce fluorescence at 5μ, and the observed fluorescence could be classified as one of two distinctive types.

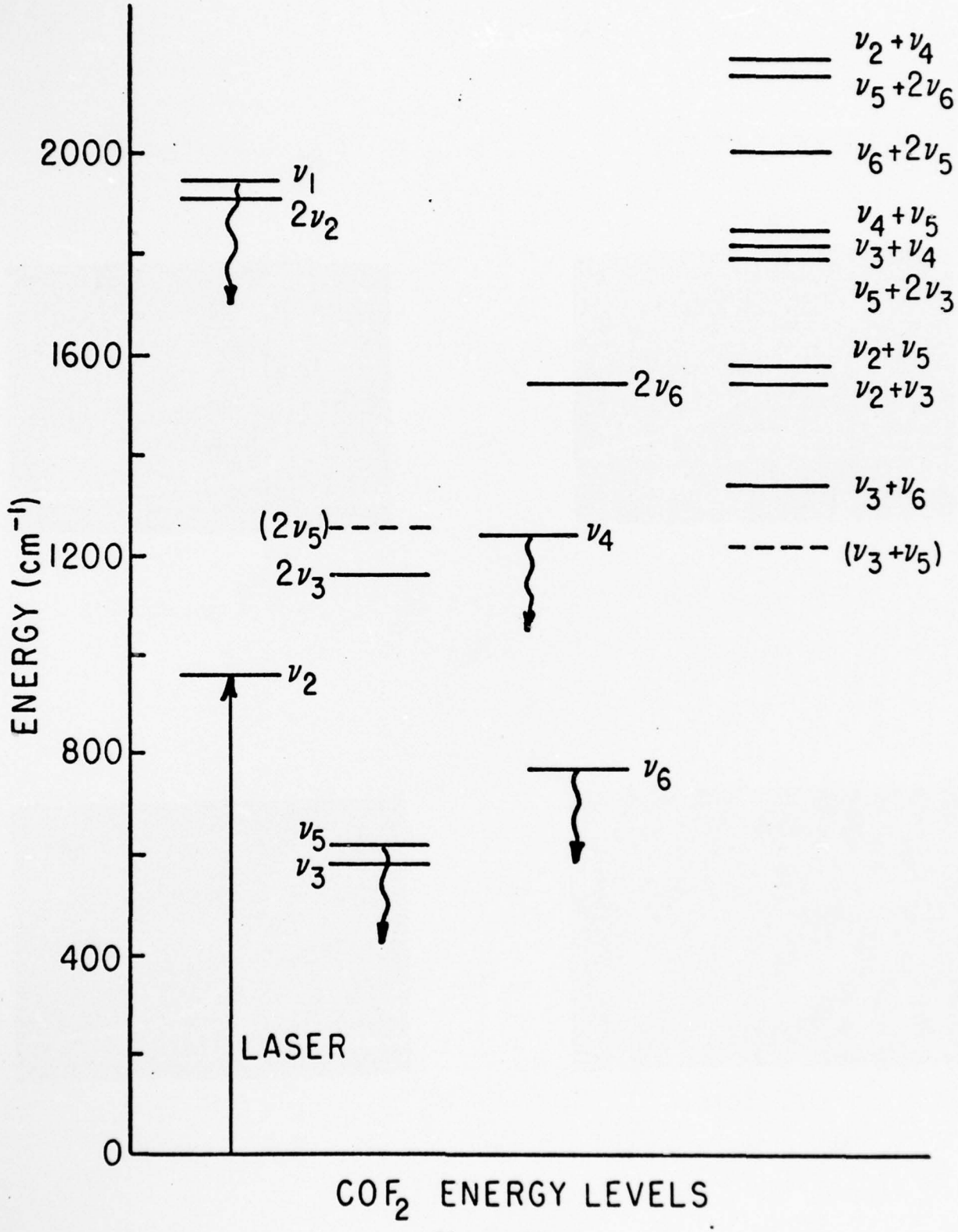
ENERGY (cm⁻¹)
2000
1600
1200
800
400
0
ν_1
$2\nu_2$
$2\nu_6$
$(2\nu_5)$
$2\nu_3$
ν_4
ν_2
ν_6
ν_5
ν_3
LASER
$\nu_2+\nu_4$
$\nu_5+2\nu_6$
$\nu_6+2\nu_5$
$\nu_4+\nu_5$
$\nu_3+\nu_4$
$\nu_5+2\nu_3$
$\nu_2+\nu_5$
$\nu_2+\nu_3$
$\nu_3+\nu_6$
$(\nu_3+\nu_5)$
COF_2 ENERGY LEVELS

Figure 35

COF_2 FLUORESCENCE

$\lambda = 5\mu$

P_{22} EXCITATION

(a)

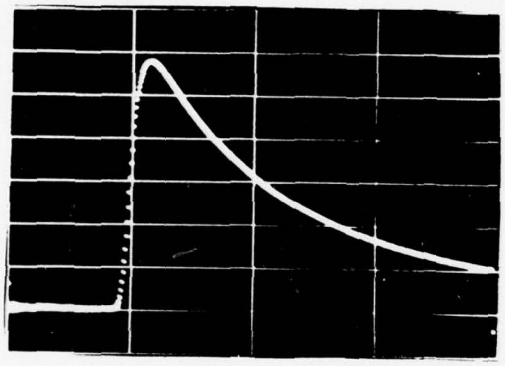

p = 1 Torr

25.6 μsec/div

P_{30} EXCITATION

(b)

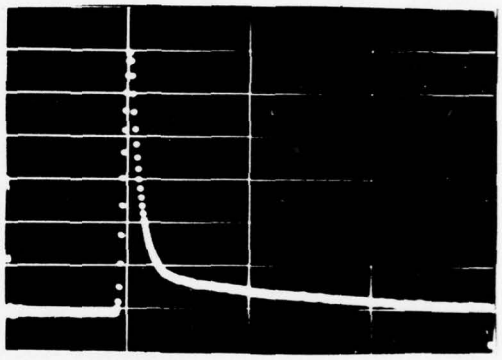

p = 1 Torr

25.6 μsec/div

(c)

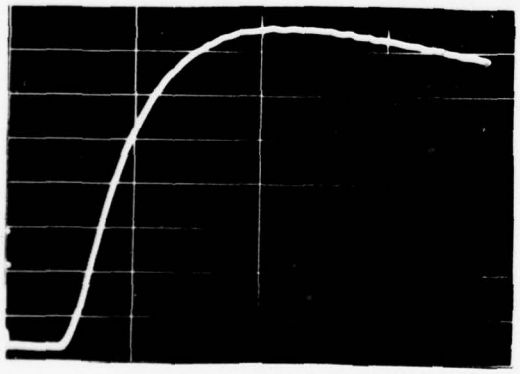

p = 0.5 Torr

6.4 μsec/div

(d)

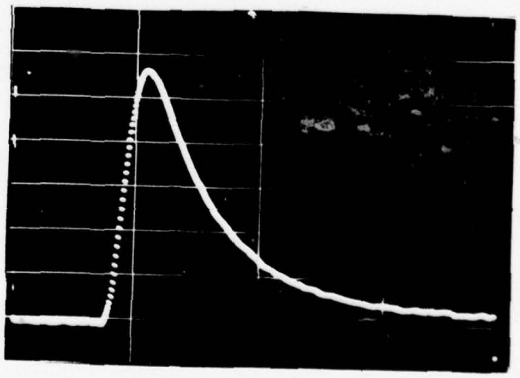

p = 0.5 Torr

6.4 μsec/div

Figure 36

Figure 36 shows fluorescence oscillograms representative of the two types observed. Only the laser pumping line was changed to produce the two different types of fluorescence. The majority of laser pumping lines produced fluorescence, denoted Type I, similar to that shown in Fig. 36a. This is characterized by a rapid fluorescence rise and a considerably slower decay. Laser lines which produced very strong Type I fluorescence included P_{22}, R_{22}, and R_{14}. In contrast, a radically different fluorescence shape was observed when laser lines such as P_{30}, P_{14}, and R_{10} pumped the COF_2. Clear examples of this behavior were seen for eight CO_2 laser pumping transitions, and Figure 36b shows a typical trace, which we call Type II. The rise of this Type II fluorescence is extremely rapid. Over the pressure region examined (1.7 torr to 0.14 torr) the rise is apparently limited by the radiative pumping rate (laser pulse width). The decay rate is also rapid and, in fact, is similar to the risetime of the Type I fluorescence. As can be seen in Figure 36b, the amplitude of this fast Type II decay is 90-95% of the maximum fluorescence amplitude and is followed by a much slower decay to the baseline of the last 5-10% of the signal.

Rates for Type I rise and fall and Type II fast fall were obtained by fitting semilog plots of fluorescence intensity versus time. These rates were then measured as a function of COF_2 pressure, typically over a range from 0.15 to 1.5 torr, and a linear least squares fit of the slope of the rate versus pressure plot produced the appropriate rate constants. A rate constant plot for the decay of Type I fluorescence is shown in Figure 37, and Table IV lists the fitted rate constants in units of $msec^{-1}$ $torr^{-1}$ and in numbers of gas kinetic collisions for these processes. Both the Type I rise and

Figure 37

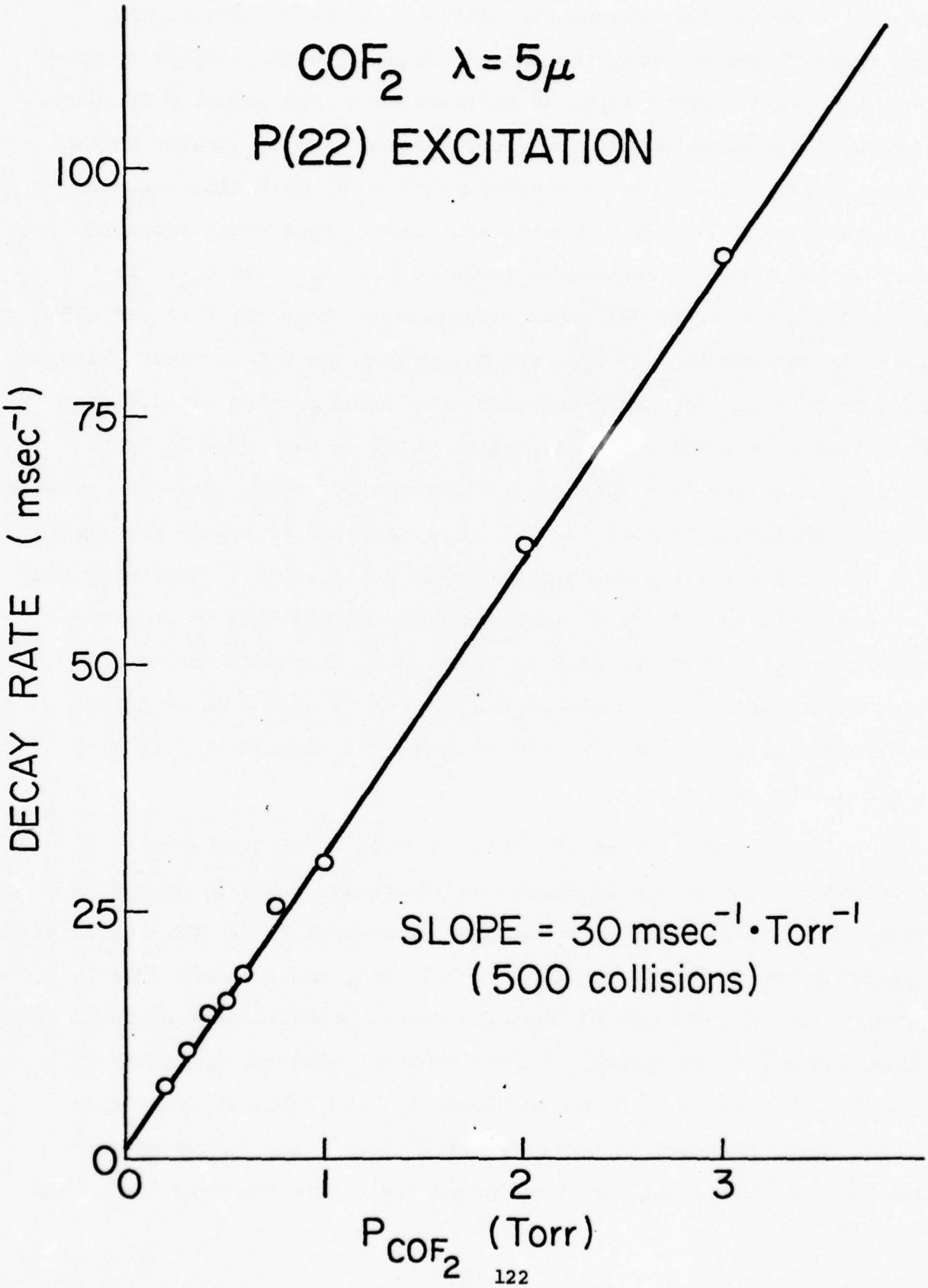
COF2 λ = 5μ
P(22) EXCITATION
DECAY RATE (msec-1)
100
75
50
25
0
0
1
2
3
PCOF2 (Torr)
SLOPE = 30 msec-1 • Torr-1
(500 collisions)

Table IV

Experimental 5μ Fluorescence Data

Process	Observed Rate[a] ($msec^{-1} \cdot torr^{-1}$)	Number of Collisions (Z)[b]	Probability (1/Z)
P_{30} Excitation			
Fall	561 ± 30	29	0.034
P_{22} Excitation			
Rise	608 ± 25	27	0.037
Fall	30 ± 1	540	1.8×10^{-3}

[a] Slope of best least squares fit of rate versus COF_2 pressure. Uncertainty is two standard deviations. Individual fluorescence rates were assumed to be single exponential.

[b] The collision number is obtained by dividing the gas kinetic collision frequency by the observed rate.

Type II fast fall were single exponential to within experimental error, indicating the presence of only one resolvable kinetic process for the pressure ranges studied. Using spectroscopic data from matrix isolated COF_2[1] and a first order perturbation approach, [5] we estimate that, due to Fermi resonance, the two observed vibrational states are nearly 50:50 mixtures of the unperturbed ν_1 and $2\nu_2$ states. Because of this tight coupling between ν_1 and $2\nu_2$, it is unlikely that the kinetic crossover process between these two levels could be observed. As a check, experiments were performed at sample pressures of 50 mtorr or less but no evidence for additional processes was observed.

A careful examination of the general qualitative features of the Type I and Type II fluorescence near $\lambda = 5\mu$ as shown in Fig. 36 provides a great deal of information about the detailed kinetic processes involved. With this information we can suggest plausible mechanisms to be considered further. First, the rise of Type II fluorescence is extremely rapid, limited apparently by the laser pulse width or the bandwidth of the detection electronics to pressures as low as 0.15 torr. This strongly suggests that this fluorescence is coming from a state directly filled by the laser rather than one filled via collisional processes. Second, the amplitude of the fast Type II decay, which falls to within a few percent of the baseline, indicates that the fluorescing state is losing population to a state much lower in energy than itself. Loss of 90% of the population of a state requires equilibration of two states separated by 500 cm^{-1} or more. This obviously rules out the equilibration of $2\nu_2$ with ν_1 as the primary contribution to the fast Type II fall. Since the two states are very close in energy, their

Boltzmann factors are nearly equal, and $2\nu_2$ will lose only about 50% of its population to ν_1 in such a process. Third, the similarity of rates for the Type I rise and Type II fall is clearly evident in comparing Figures 36c and 36d. In fact, the rate constants listed in Table IV, obtained from the pressure dependence of rates for these two processes, are identical to within experimental error. The rate versus pressure data for both Type I rise (P_{22} excitation) and Type II fall (P_{30} excitation) are plotted together in Figure 38. The close correspondence of these rates strongly suggests that the kinetic process controlling the Type II fall is also the primary step contributing to the Type I rise. In addition, the large cross section for energy transfer, corresponding to about 30 gas kinetic collisions, is indicative of a process that is near resonant.[8,9] Finally, the Type I decay rate is much slower than rates of the other processes observed. The rate constant (~500 gas kinetic collisions) is about a factor of 20 slower than that for the Type II fast fall. Whereas a rate constant of 30 collisons suggests an efficient near-resonant process, the rate constant for the Type I decay is indicative of an intermode crossover process and probably reflects the equilibration of the ν_2 pumped mode with other nearby modes.

A complete discussion of these results has been submitted for publication. The main experimental points and the conclusions are as follows:

(a) Strong laser-induced fluorescence has been observed emanating from the $2\nu_2$, ν_1 states ($\lambda = 5\mu$) of COF_2. An unusually large number of laser lines from the 10.6μ band (over 30) have been found to efficiently produce this fluorescence in contrast to the 1-3 coincidences typical of many other polyatomic molecules.

(b) The fluorescence curves consist of two very distinct

Figure 38

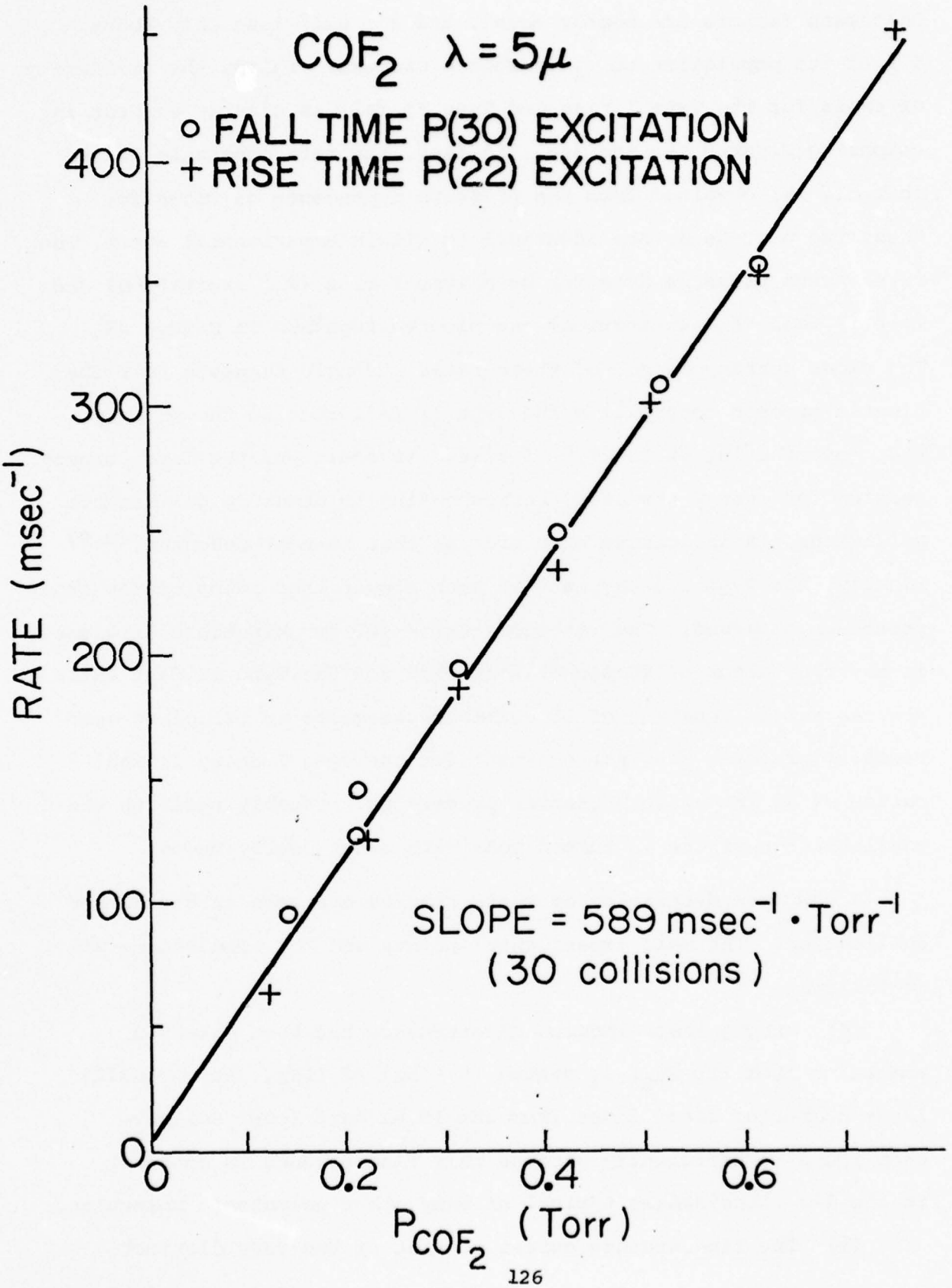
COF2 λ = 5μ
o FALL TIME P(30) EXCITATION
+ RISE TIME P(22) EXCITATION
RATE (msec-1)
400
300
200
100
0
0
0.2
0.4
0.6
PCOF2 (Torr)
SLOPE = 589 msec-1 • Torr-1
(30 collisions)

types. The first displays a fast (~30 gas kinetic collisions) rise followed by a relatively slow (~500 collisions) decay. The second rises in a time that is limited by the laser pulsewidth and falls with a rate constant corresponding to 30 gas kinetic collisions, indicating that the same kinetic process is rate limiting for the rise of Type I and fall of Type II fluorescence. A simple kinetic analysis in conjunction with a comparison of absorption coefficients and examination of decay rates under varying levels of laser excitation indicate that the first type is due to the pumping of molecules into the ν_2 state from the ground state followed by excited state-excited state collisions to fill $2\nu_2$ and ν_1. The second, faster process results from direct filling of $2\nu_2$, ν_1 via hot band pumping of the $\nu_2 \rightarrow 2\nu_2$ transition, followed by a rapid collisional equilibration with ν_2. The rapid V-V up the ladder energy transfer process in COF_2 is identified as the step controlling the rise of the first type and fall of the second.

(c) An examination of the energy transfer data and Fermi resonance effects indicate that $2\nu_2$ and ν_1 are very strongly mixed, providing a very efficient means for collisionally exciting the C=O stretch very low in the ν_1 manifold.

(d) The slow decay (~500 collisions) of energy out of the tightly coupled ν_2, ν_1 manifold is most likely due to intermode V-V energy transfer into the remaining vibrational modes. Thus the C=O and C-F stretches are expected to remain vibrationally hot relative to the other modes for periods of tens of microseconds at a few torr. Such a molecule offers several possibilities for the study of laser driven chemical reactions, the development of new optically pumped infrared laser transitions, and the investigation of many different types of energy transfer processes.

2. Vibrational Energy Exchange Between the ν_3, ν_6 and ν_2, ν_5 Modes of CH_3F in the Pure Gas

(Rekha Sapre Sheorey, Richard Slater, George Flynn)

A great deal of information concerning vibration to vibration (V-V) and vibration to translation/rotation (V-T/R) energy transfer processes in CH_3F has been obtained using laser induced fluorescence, laser-laser double resonance and time resolved thermal lensing experiments. Fluorescence and double resonance techniques measure the time dependence of excited vibrational state populations whereas thermal lensing measures both the time dependence of, and the net change in, the energy of the translational states. When used in concert, all these methods represent a very powerful tool for elucidating the vibrational energy flow in polyatomic systems.

In the CH_3F fluorescence experiments, signals were obtained from the pairs of states (ν_1, ν_4) at 3.3μ and (ν_2, ν_5) at 6.8μ, from $2\nu_3$ at 4.8μ and from ν_6 at 8.6μ. (Fig. 39) During the past year, by working with an improved detection system and at lower CH_3F pressures, multiple exponential rises and decays of CH_3F laser induced fluorescence have been observed and analyzed. These multiple exponential functions have been identified with some of the eigenvalues of the CH_3F V-V energy transfer rate matrix. In particular two internal V-V rate constants relating 3 vibrational modes of CH_3F to each other have been calculated from measured exponential rates. This constitutes an extremely significant link between energy transfer theory and experiment.

A Q-switched CO_2 laser operating essentially on the P_{20} line

Figure 39

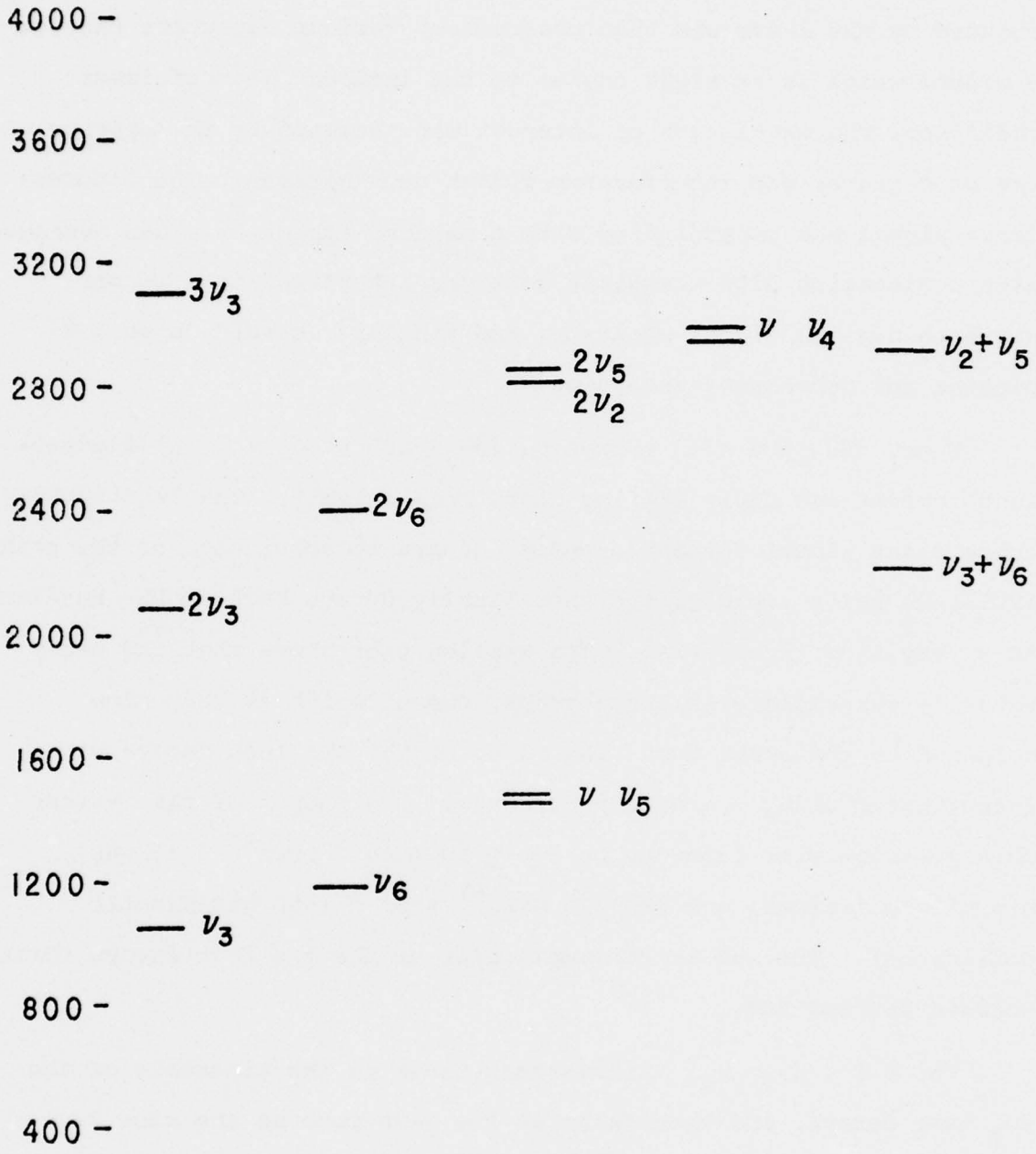
4000
3600
3200
$3\nu_3$
$\nu\ \nu_4$
$\nu_2+\nu_5$
$2\nu_5$
$2\nu_2$
2800
2400
$2\nu_6$
$\nu_3+\nu_6$
$2\nu_3$
2000
1600
$\nu\ \nu_5$
1200
ν_6
ν_3
800
400

of the 9.6μ band was used to vibrationally excite the ν_3 mode of CH_3F contained in a 1" diameter stainless steel cell. Fluorescence induced by the laser was then observed by various detectors through a window which is at right angles to the incident beam of laser radiation. The wavelength of interest was isolated by the appropriate use of detector and interference filter combinations. The fluorescence signal was preamplified with a matched amplifier, then averaged with a Biomation 8100 transient recorder interfaced to a Tracor Northern digital signal analyzer, and finally recorded on an X-Y plotter for subsequent analysis.

Figs. (40) and (41) show 4.8μ ($2\nu_3$) and 6.8μ (ν_2, ν_5) fluorescence curves and their semilog plots respectively. The $2\nu_3$ fluorescence rises almost instantaneously, decays to about half of the peak amplitude quite rapidly, and then finally decays back to the baseline as a very slow exponential. Its semilog plot shows that the decay actually takes place in three steps, one of which is very slow compared to the other two. The rates of the two fast decays were deconvoluted using standard procedures. The slopes of rate versus CH_3F pressure were found to be 600 ± 50 $msec^{-1}$ $torr^{-1}$ (~15 gas kinetic collisions) and 190 ± 20 $msec^{-1}$ $torr^{-1}$ (~50 gas kinetic collisions). The sum of the amplitudes of the two fast decays varied between 45% and 50%.

The 6.8 μ (ν_2, ν_5) fluorescence rises on the timescale of the $2\nu_3$ fast decays, and then falls at the same rate as the slow $2\nu_3$ third exponential decay. As can be seen in Fig.41 the ν_2, ν_5 fluorescence rises in two steps. Deconvolution of the two rates shows that the apparently fast rise (later in time) is actually the smaller eigenvalue (rate) and vice versa.

Figure 40

CH_3F 4.8μ FLUORESCENCE ($2\nu_3$)

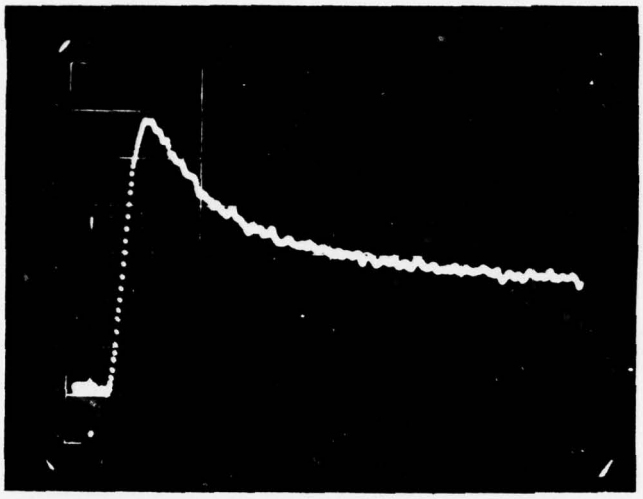

0.500 Torr CH_3F

51.2 μsec Full Scale

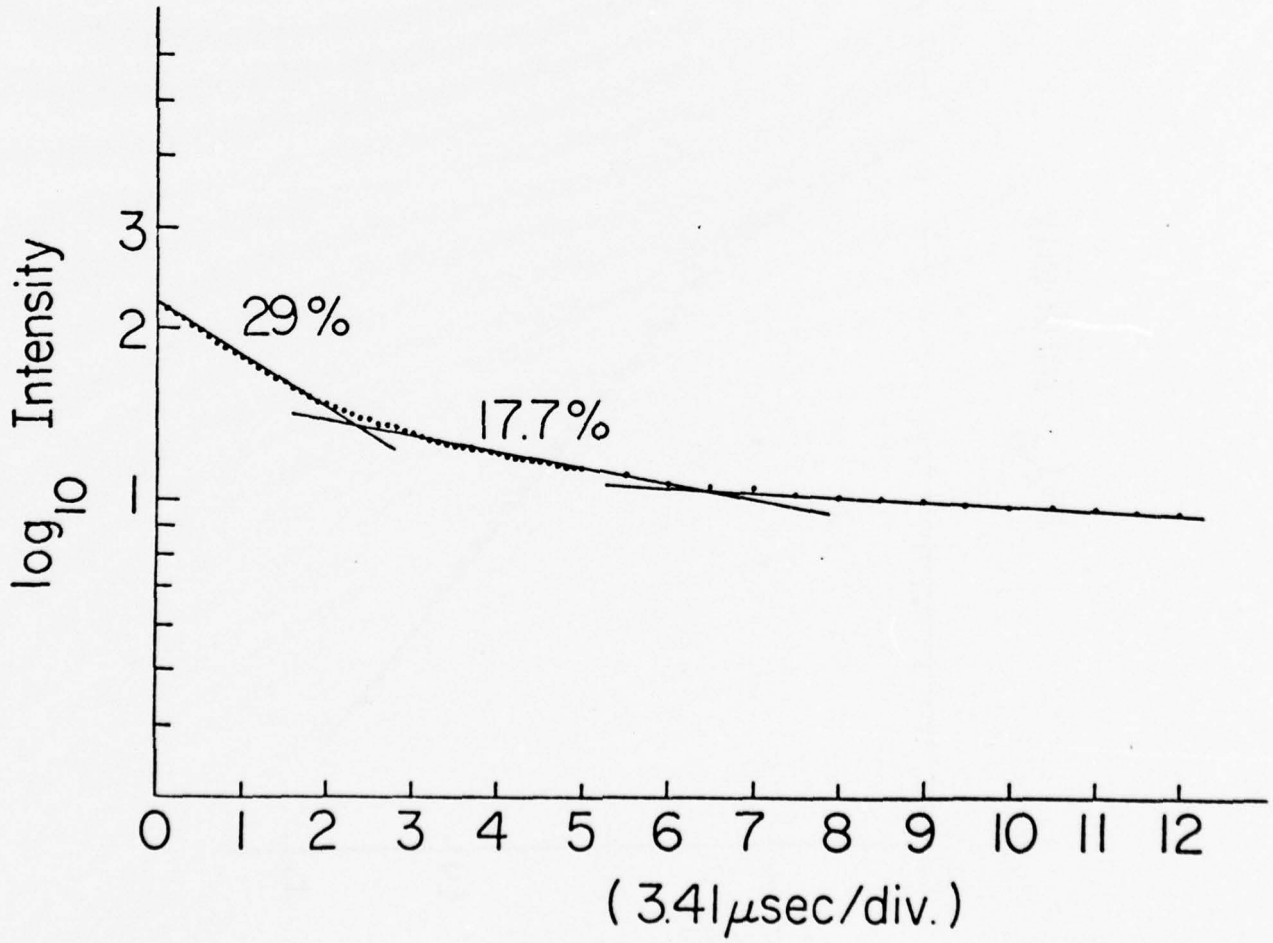

Fig. 41 CH_3F 6.8μ FLUORESCENCE RISE (ν_2 ν_5)

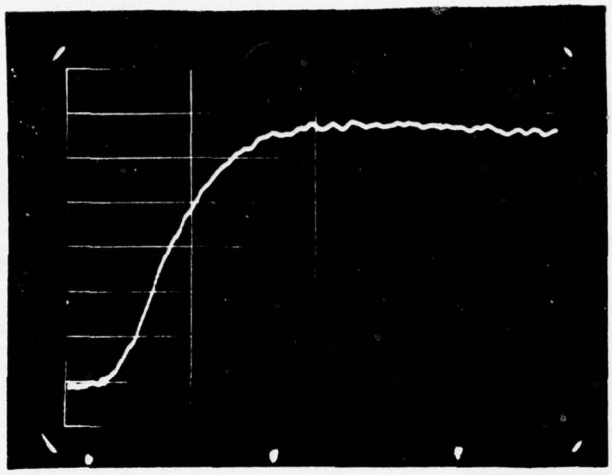

1.00 Torr CH_3F

51.2μsec Full Scale

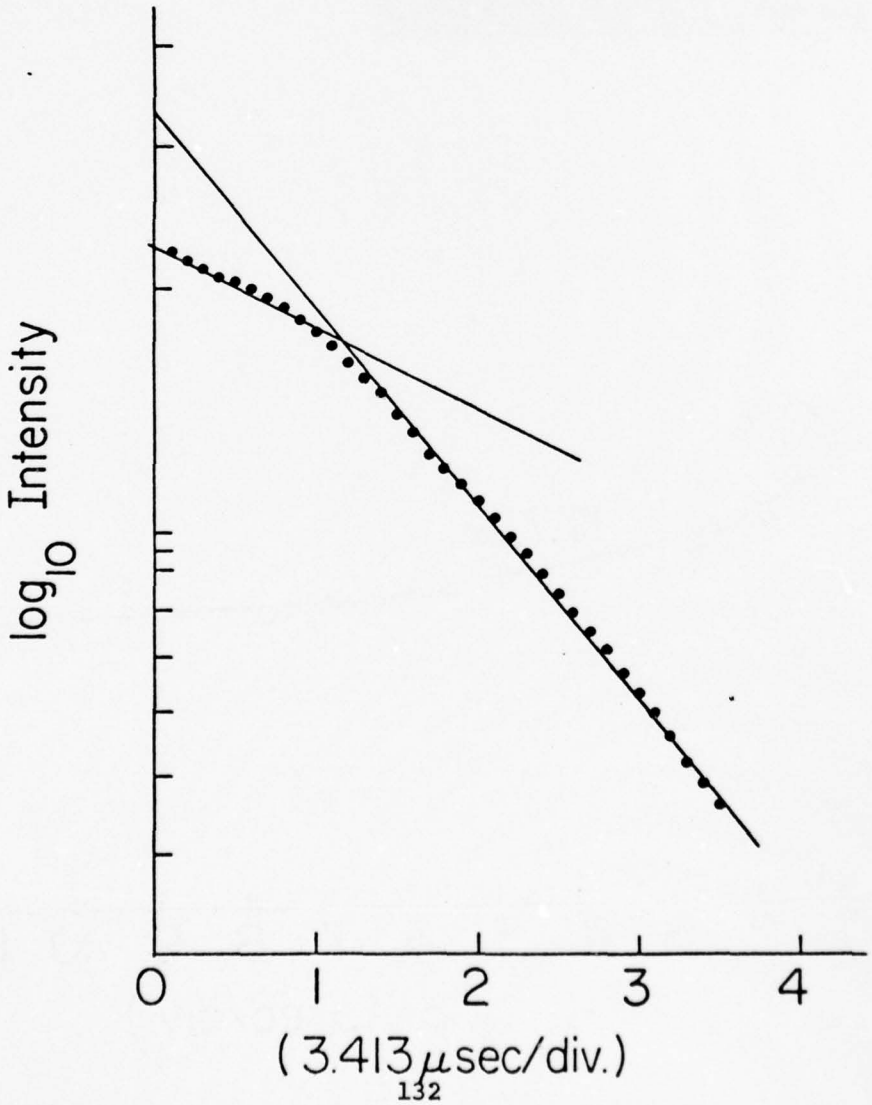

8.6μ CH_3F (ν_6) fluorescence exhibited essentially single exponential rise and decay, the decay being the same as that observed in ν_2, ν_5 curves. The single exponential rise was measured verus CH_3F pressure.

From all the thermal lensing and fluorescence studies to date, the V-V energy transfer mechanism which couples the fundamentals of CH_3F vibrational degrees of freedom has been deduced. After pumping the ν_3 state, the following processes are believed to equilibrate the vibrational modes of CH_3F.

$$CH_3F\ (\nu_3) + CH_3F \underset{k_{-1}}{\overset{k_1}{\rightleftharpoons}} CH_3F\ (\nu_6) + CH_3F\ -133\ cm^{-1} \qquad (1)$$

$$CH_3F\ (\nu_6) + CH_3F \underset{k_{-2}}{\overset{k_2}{\rightleftharpoons}} CH_3F\ (\nu_2, \nu_5) + CH_3F - 280\ cm^{-1} \qquad (2)$$

$$CH_3F\ (\nu_2,\nu_5) + CH_3F\ (\nu_2\nu_5) \rightleftharpoons CH_3F\ (2\nu_2,2\nu_5) + CH_3F + 100cm^{-1} \qquad (3)$$

$$CH_3F\ (2\nu_2,2\nu_5) + CH_3F \rightleftharpoons CH_3F\ (\nu_1,\nu_4) + CH_3F - 150\ cm^{-1} \qquad (4)$$

$$CH_3F\ (\nu_3) + CH_3F\ (\nu_3) \rightleftharpoons CH_3F\ (2\nu_3) + CH_3F + 18\ cm^{-1} \qquad (5)$$

Because of the relatively low power of the Q-switch excitation, the vibrational temperature does not change greatly from ambient. Therefore, Boltzmann statistics at the translational temperature may be employed to obtain vibrational population densities with good accuracy. Since 99% of the excited state population resides in the lowest four states, ν_3,ν_6, and ν_2,ν_5, the contribution of other states to the CH_3F rate matrix can be neglected when solving the

CH_3F 3-level system.

Up-the-ladder processes such as (5) are known to be fast compared to the coupling between vibrational modes of molecules. Therefore, the $2\nu_3$ fluorescence intensity can be expected to rise on the timescale of the up-the-ladder rate, peak as $2\nu_3$ comes into equilibrium with ν_3, and then <u>reflect</u> the population loss of ν_3 as the rest of the vibrational modes begin to come into equilibrium with ν_3. Experiment has shown this to be the case. The $2\nu_3$ fluorescence rises extremely rapidly (5 gas kinetic collisions) and decays in three steps, the slowest being the V-T/R rate. The fast decays simply correspond to the intermode energy transfer processes (1) and (2) which rob ν_3 of its excess population. These have been measured to be 600 $msec^{-1}$ $torr^{-1}$ and 190 $msec^{-1}$ $torr^{-1}$ respectively.

Fig. 42 shows ν_2,ν_5 and $\nu_1\nu_4$ fluorescence curves under identical experimental conditions except for interference filters. The almost perfect match-up indicates that the rate limiting step in the filling of $\nu_1\nu_4$ does not occur after ν_2,ν_5, but that it is the same, being the combination of processes (1) and (2).

In conclusion, a complete vibrational energy flow map has been identified (with the exception of the filling of ν_1,ν_4 which is inferred) for the molecule CH_3F. Two internal v-v rate constants have also been measured. A simple technique has been found (partial rapid decay of fluorescence from the overtone of the pumped state) for monitoring the outflow of excess energy from the pumped state of a polyatomic molecule into the remaining vibrational degrees of freedom of the molecule.

Figure 42

COMPARISON OF FLUORESCENCE FROM ν_1, ν_4 AND ν_2, ν_5 STATES

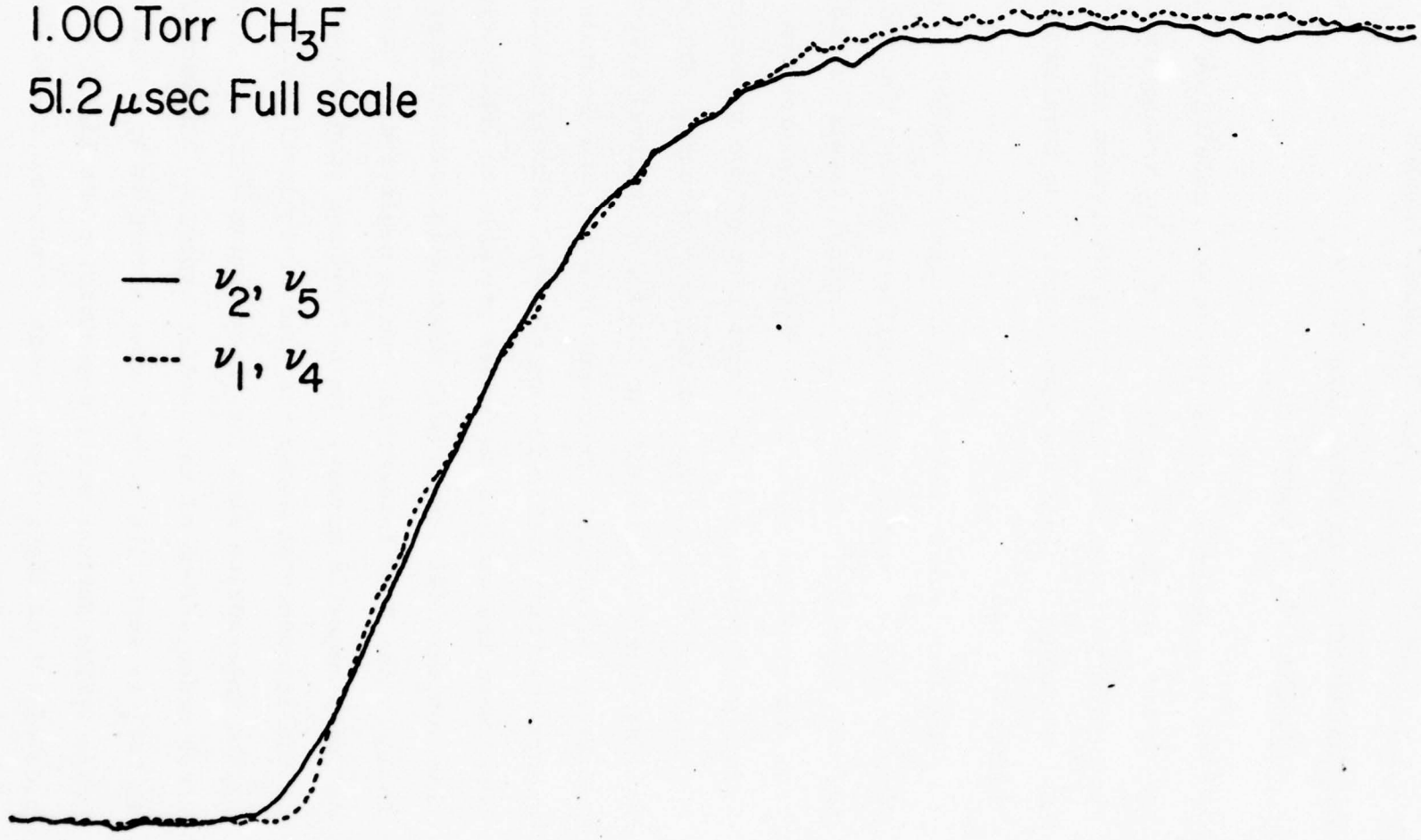

IV. RESONANCE PHYSICS

A. PHOTON ECHOES IN RARE EARTH IONS *

(Y. Chen, S. R. Hartmann)

We have observed strong photon echo modulation effects in Pr^{3+} : LaF_3 for the $^3H_4 \rightarrow {}^3P_o$ and $^3H_4 \rightarrow {}^1D_2$ transitions. Experiments were performed at fixed pulse separation and variable applied magnetic field and visa versa. Our results are shown in Figures 43 - 46.

The modulation effects are interpreted as being due to interference effects within the transitions between the two multilevel systems. For Pr^{3+} in LaF_3, the terminal levels of the echo transition are mixed and split by the hyperfine interaction, the nuclear Zeman interaction, and the interaction of the praseodymium ion with the neighbor fluorine nuclear magnetic moments. Photon echoes arising from these coherently excited multilevel systems exhibit modulation effects,the frequency of which are determined by the energy splitting within the multiplets. Strong modulation effects occur when the excitation pulses are able to coherently couple more than two terminal levels with comparable transition probability. In LaF_3, the Pr-F interaction can be neglected[1] because Pr^{3+} has zero magnetic moment. We believe the echo modulation is due to the interference among the electronic levels split and mixed by the interaction with the praseodymium nucleus. Although the first order effect of the nuclear hyperfine interaction of Pr^{3+} in LaF_3 is zero, the second order effect is appreciable.[2,3] The praseodymium nuclear state degeneracies are lifted by the combination effect of the nuclear Zeeman effect and the second order hyperfine interaction. The second order hyperfine interaction has the general form $\sum_{i=x.y.z} P_i I_i^2$ where P_i's are dependent on both the direction and the

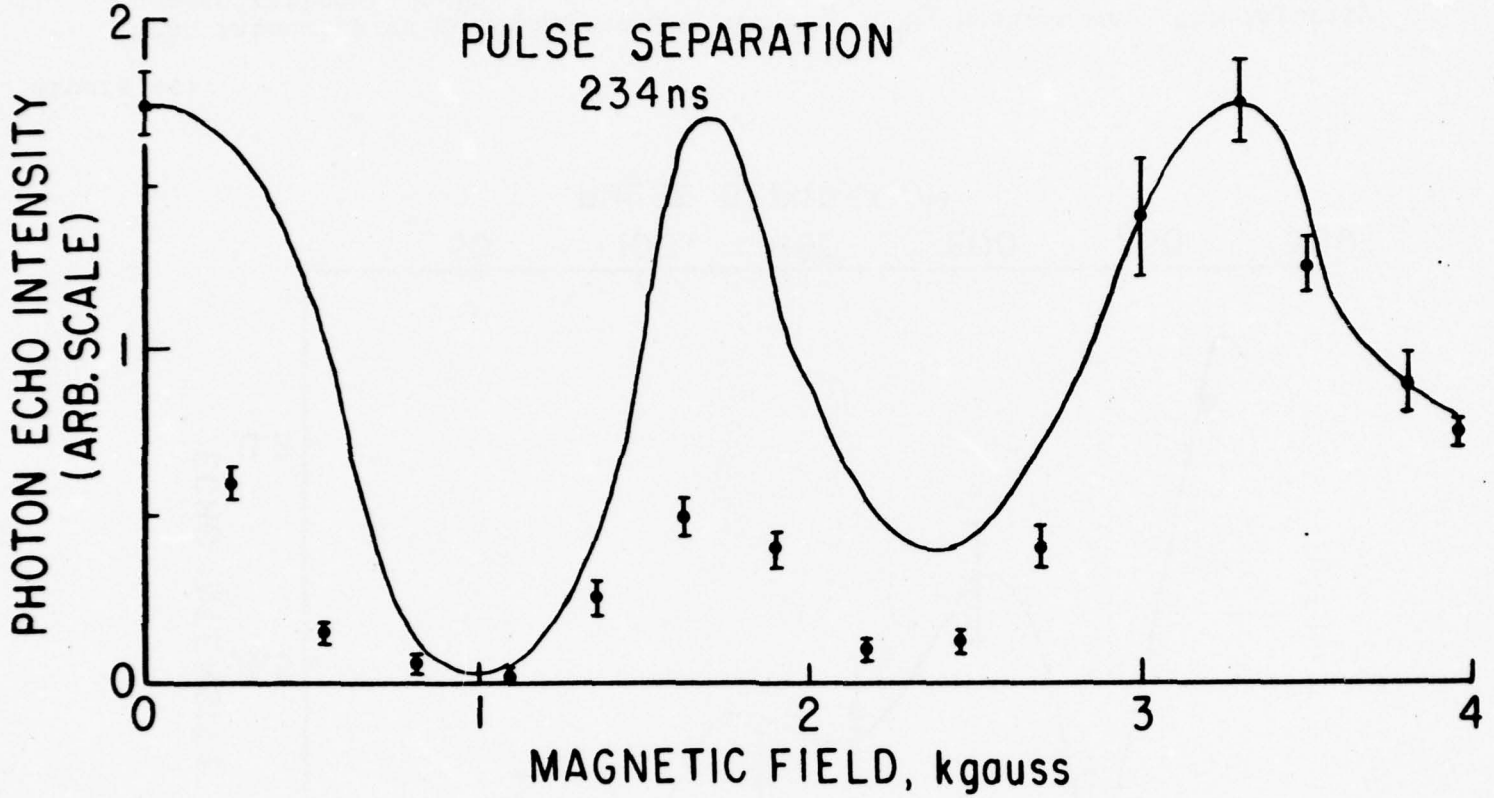

137

Figure 43:

Echo intensity vs magnetic field in $^3H_4 \leftrightarrow {}^3P_0$ transition. The magnetic field is applied along the crystal C axis and perpendicular to the propagation direction of the excitation pulses. The impurity concentration is 0.1%. The solid curve is the calculation based on the hamiltonian Eq. (7) and Eq. (8)

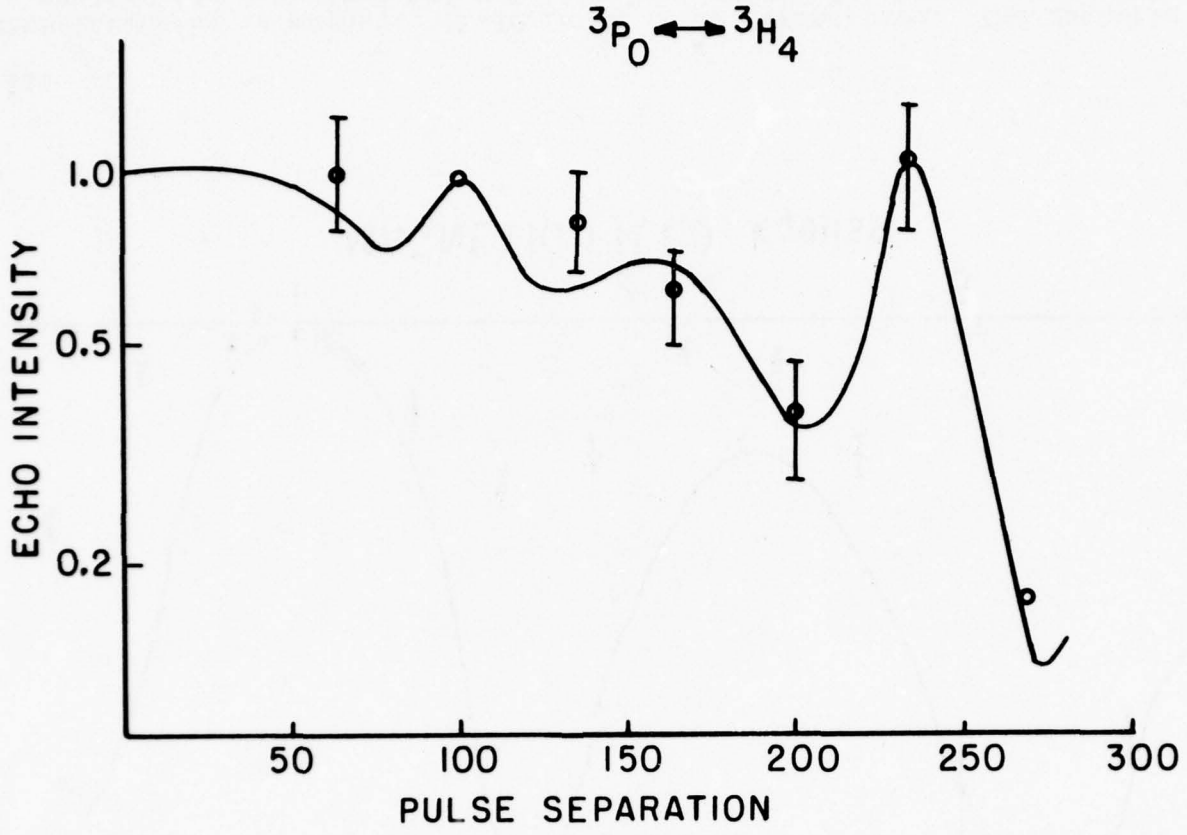

Figure 44:

Echo intensity vs pulse separation for $^3P_o \leftrightarrow {}^3H_4$ transition. The impurity concentration is o.1%.

Figure 45:

Echo intensity vs magnetic field in $^3H_4 \leftrightarrow {}^1D_2$ transition. The magnetic field is applied perpendicular to the crystal C-axis and the propagation direction of the excitation pulses. The impurity concentration is 1%.

Figure 45

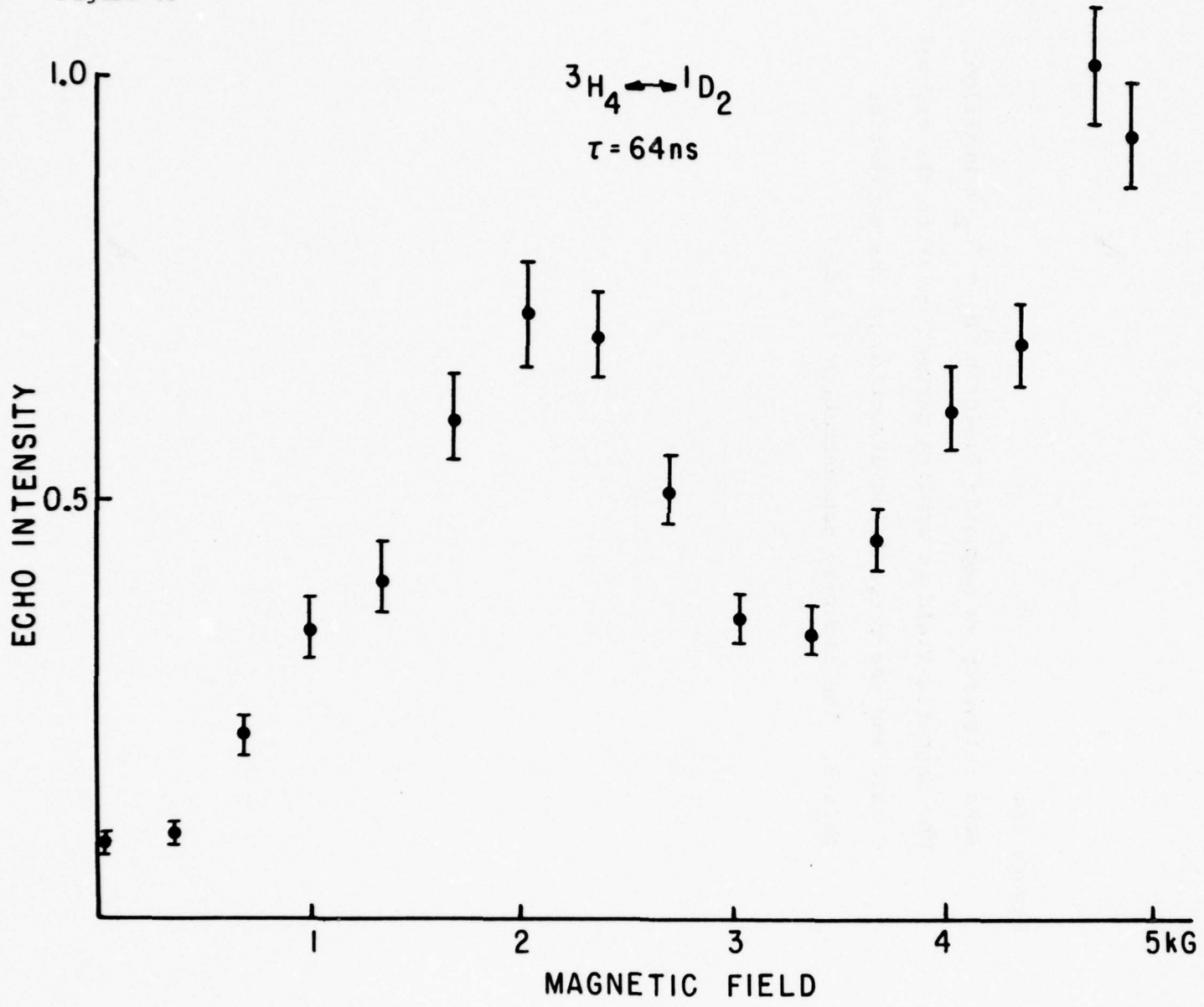
$^3H_4 \leftrightarrow {}^1D_2$
$\tau = 64ns$
1.0
0.5
ECHO INTENSITY
1
2
3
4
5kG
MAGNETIC FIELD

Figure 46:

Photon echo intensity vs pulse separation in $^3H_4 \leftrightarrow {}^1D_2$ transition. The echo intensity at 115ns is taken as a reference point. And echo intensity at all other pulse separations are compared with the reference intensity while keeping the 2nd pulse intensity the same. The impurity concentration is 1%.

Figure 46

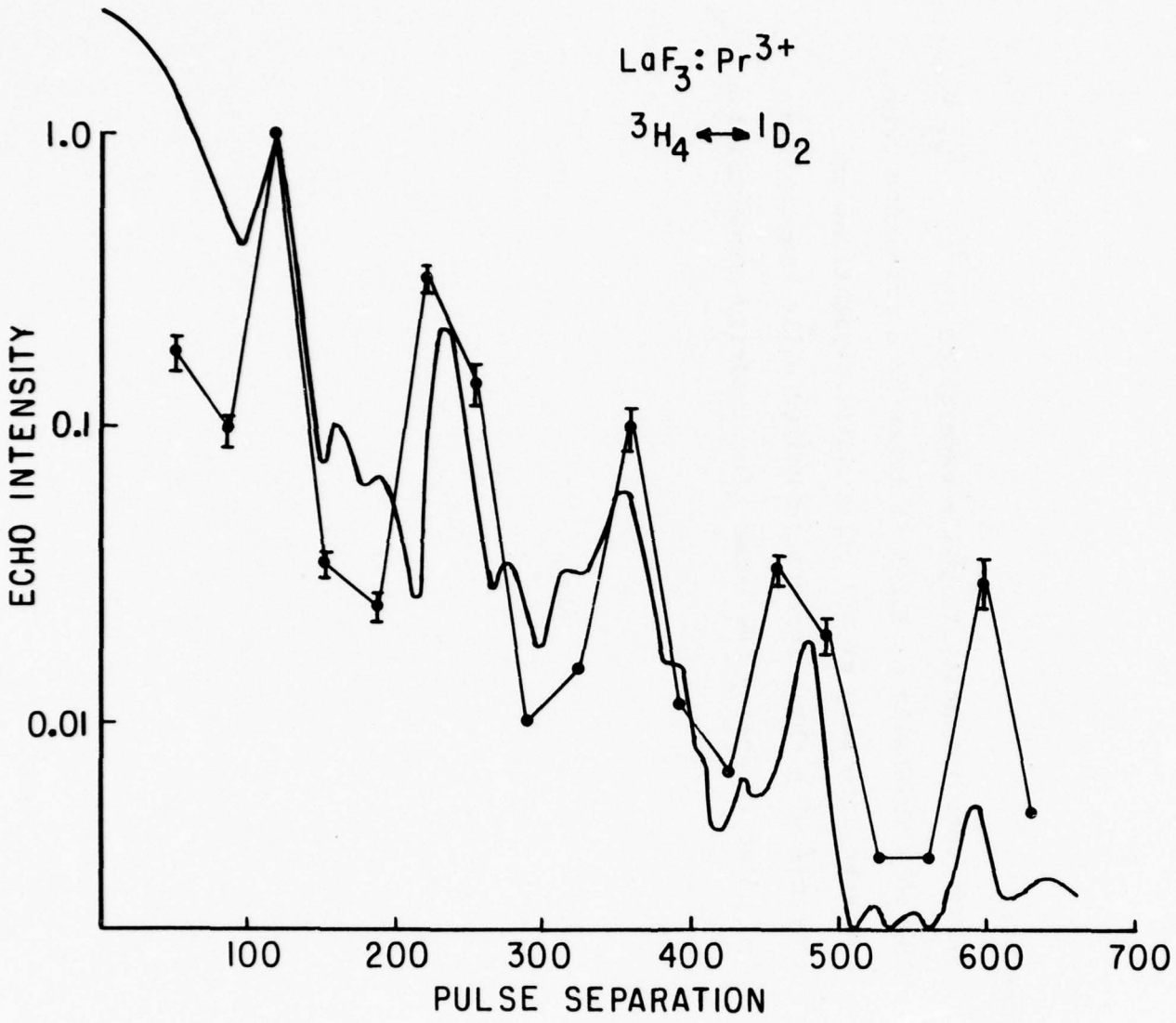
$LaF_3: Pr^{3+}$
$^3H_4 \leftrightarrow {}^1D_2$
1.0
0.1
0.01
ECHO INTENSITY
100
200
300
400
500
600
700
PULSE SEPARATION

hyperfine interaction constant.[3] According to this scheme, [6] the nuclear levels of Pr^{3+} (spin 5/2) are split by the 2nd order hyperfine interaction into three levels, each doubly degenerate. The ratio of the energy differences between them is 2:1. Last year we were able to obtain a reasonable fit for the $^3H_4 - {}^3P_o$ echo transition data taken as a function of magnetic field. On the basis of that analysis we inferred ground electronic state nuclear level splittings of 5 MHz and 10MHz. The recent work of Erickson[4,5] has basically confirmed our prediction. The ground state nuclear splittings are found to be 8.47 MHz and 16.7 MHz. The ratio between them is almost 2:1. The ground state hamiltonian can now be written as

$$H = P\left[(I_z^2 - I(I+1)) + \frac{\eta}{6}(I_+^2 + I_-^2) \right] + \gamma H_z(1+K_z)I_z$$

where P = 4.18MHz . η = 0.105 , γ = 1.13 kHz/ Gauss K_z = 0.7. [7]

The ^3P_o excited state hamiltonian must have a similar hamiltonian with an interaction parameter P much smaller than that in the ground state. The reason is that the level mixing due to quadropole interaction is smaller in the ^3P_o state. The magnitude of the interaction parameter is assumed to be one tenth of that in the ground state since the nearest excited state from ^3P_o is 500 cm^{-1} away while the nearest excited state from $^3H_4$ ground state is 50 cm^{-1} away. The hamiltonian for the ^3P_o state is

$$\mathcal{H} = P I_x^2 + \gamma H_z I_z$$

where P is 0.4 MHz. (8)

If we use Eq. 7 for the ground state and Eq. 8 for the ^3P_o state, the calculation for the echo intensity [6] yields the solid curve in Fig.43. The fit is better than last year. The maxima are now

accurately located. However, the depth of modulation is still not accounted for. It may be that there is an assymetry parameter associated with the excited state and that the magnetic field direction was not accurately directed along crystal C-axis.

In Fig. 44, photon echo intensity vs pulse separation is shown for the $^3H_4$ - ^3P_o transition. The data was taken at zero field. The recovery of the echo intensity at 234 ns implies a modulation frequency 4.20MHz which is roughly one half of the splitting in the ground state. It is possible that a local maximum of echo intensity at 100ns or 130ns was not resolved. A calculation using the same hamiltonian as used for Fig.43 yields the sold curve in Fig. 44. Since the optical delay line is not coated for the excitation pulse frequency 4777$\mathring{A}$, data points for pulse separation longer than 300ns are not avilable. We predict that there must be local maxima at 350ns, 460ns, ... etc.

In Fig. 45, echo intensity vs magnetic field is shown for $^1D_2 \leftrightarrow {}^3H_4$ transition. The dipole moment of the transition is 10 times smaller than the $^3H_4$ - ^3P_o transition. Hence a more concentrated sample (1%) was used. The magnetic field is applied perpendicular to the crystal C-axis. In this case, the impurity Pr^{3+} ions are distributed at three difference sites. The explanation of the data involves knowing energy splittings in the ground states and the excited states, the magnetic enhancement factors along the two axis perpendicular to the C-axis, and the angle between the magnetic field and the crystal a-axis. In principle, all these parameters can be obtained by varying the parameters to get the best fit for the data.

In Fig.46 we present data showing the pulse separation depen-

dence of the photon echo in zero field. The echo intensity oscillates with a regular period of 120ns. This corresponds to the frequency of the ground state nuclear level splittings. The absence of higher frequency in echo modulation seems to imply that the energy splittings in the $^1D_2$ state are abnormally small. This is surprising because the $^1D_2$ state nuclear level splittings are expected to be larger due to larger electronic level mixing. A rough calculation using Erickson's ground state hamiltonian, a similar hamiltonian with P = 1 MHz for the $^1D_2$ state and an echo relaxation time T_2 = 95ns reported by Brewer et al [7] yields the sold curve in Fig. 46. The fitting is preliminary. This is a difficult experiment. The trick is to keep the excitation pulse divergence and pulse shape the same when varying the pulse separation. Hence the distance between the mirrors of the optical delay line (white cell) should be adjusted to be exactly equal to twice the focal length of the mirrors. Also, in order to compare the echo intensities at difference pulse separations, the 2nd pulse intensity must be kept the same for all pulse separations. Hence, the intensity of the 2nd pulse at shorter pulse separation must be attenuated to compensate for the loss of the intensity at longer pulse separations. This can be done by putting a pockel cell and a pair of crossed polarizers in the path of the 2nd pulse. Then we can attenuate the 2nd pulse intensity at shorter pulse separation without deflecting the beam. The drifting of the nitrogen laser intensity may cause large scattering of the data points. The drifting of the laser intensity comes from the motion of the end mirrors which are attached to the nitrogen laser cavity through O-rings. In order to stabilize the nitrogen laser, the feedback mirror was mounted independently so that the change in pressure and temperature in the

nitrogen laser cavity will not influence the mirror. Now the nitrogen laser and dye laser power are steady for longer than 20 minutes.

Echo modulation data contain information about both the ground state and the excited state nuclear splittings. In order to determine the splittings accurately more detailed experimental data is needed. The present optical delay line prevents us getting detailed data because pulse separation can be varied only by discreet steps of 34ns multiples. Also in order to determine small energy splittings, e.g. the splitting in $^1D_2$ states and ^3P_o state, a pulse separation as long as 1 μs will be necessary. At large pulse separations, the beam divergence becomes hard to control. To solve these problems, it may be necessary to build two nitrogen laser pumped dye lasers so that one will fire at a setable time after the other with well defined pulse divergence. Then we should be able to determine the excited state quadropole splittings either by two pulse echo technique or the PENDR technique.

*This research was also supported by The National Science Foundation under Grant NSF-DMR73-07600 A03.

(1) Y. C. Chen and S. R. Hartmann, Phys. Lett., 58A 3, 202 (1976).

(2) B. Bleaney, J. Appl. Phys., 34, 1024 (1963).

(3) B. Bleaney, Physica 69, 317 (1973).

(4) L. E. Erickson, Opt. Commun. (to be published).

(5) L. E. Erickson, Opt. Commun. 15, 246 (1975).

(6) D. Grischkowsky and S. R. Hartmann, Phys. Rev., B2, 60 (1970).

(7) H. Z. Genack, R. M. Macfarlane and G. Brewer, Phys. Rev. Lett., 37, 1078 (1976).

B. PHOTON ECHOES IN RUBY*

(S. Meth, S. R. Hartmann).

The major part of this year was taken up by one of us (S.M.) writing his doctoral thesis. The experiment was then plagued by difficulties with the ruby laser rod coatings and the laser dewar. A new laser dewar had, in fact, to be constructed by our machine shop. We have just completed all repairs and have resumed our investigations. We have concentrated our research on photon echo modulation. We have improved the fit to last year's modulation measurement from 2 to 5 microseconds pulse separation by changing the value of the azimuthal angle of the optic axis and the applied field. (Fig. 47) Since we do not know the orientation of the crystal in the plane perpendicular to the optic axis, we have adjusted this angle in the theoretical calculations to give the best fit to the experimental data. Since the crystal was removed and replaced between the experiment in the 2 to 5 μsec region and that in the .25 to 3 μsec region, we may independently adjust the azimuthal angle for the two experiments. We point out however, that the calculations are relatively insensitive to the azimuthal angle, especially for short pulse separations. Optimization of this parameter results in only a slight improvement of the fit.

*This research was also supported by The National Science Foundation under Grant NSF-DMR73-07600 A03.

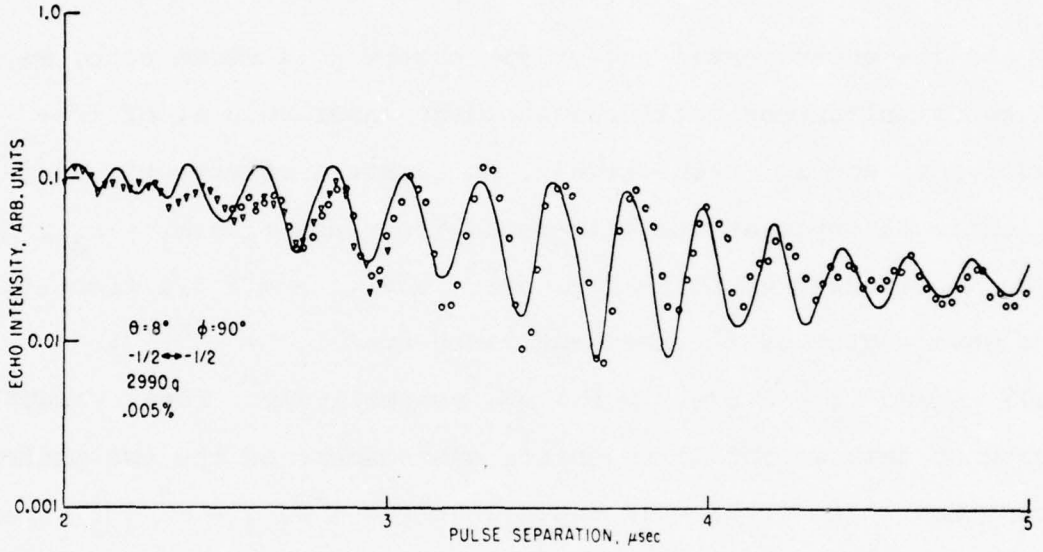

Figure 47:

Photon echo modulation from 2 to 5 μsec. The circles and triangles consist of overlapping experimental runs taken about 15 minutes apart.

C. RAMAN ECHOES

(T. Mossberg, A. Flusberg, S. R. Hartmann).

We have pursued two different research avenues in the past year: (1) Magnetically induced three-wave mixing, and (2) Dicke superradiance. The initial version of each type of experiment was a natural outcome of our interest in observing a Raman echo[1] on the $6^2P_{1/2} - 6^2P_{3/2}$ transition in atomic thallium vapor.[2]

In the experimental set-up for observing a Raman echo, we use two simultaneous collinear incident laser pulses, of frequencies ω_1 and ω_2, respectively, to create a macroscopic excitation in Tl vapor at the difference frequency $\omega_3 = \omega_1 - \omega_2$, which is resonant with the 7793-cm^{-1} $6^2P_{1/2} - 6^2P_{3/2}$ transition. (The wavelengths of the incident laser are $\lambda_1 = 2\pi c/\omega_1 \cong 377$ nm and $\lambda_2 = 2\pi c/\omega_2 \cong 535$ nm, respectively. Their values are chosen so that we obtain resonance enhancement of the two-photon transition.[2]) It is well known that the $6^2P_{1/2} - 6^2P_{3/2}$ superposition cannot radiate via an electric dipole (E1) transition (because of parity conservation). However, this superposition can radiate via either a magnetic dipole (M1) or electric quadrupole (E2) transition. Why should one not expect to see a coherent 7793-cm^{-1} burst of M1 or E2 burst of radiation during the two-laser excitation? This would be an example of three-wave mixing in an atomic vapor.

A simple analysis of this situation reveals that one should <u>not</u> expect any coherent radiation. Consider first the phase-matching condition which the three waves must satisfy. It implies that the generated third wave (at ω_3) be collinear with the

incident collinear waves. Alternatively, this condition may be viewed as that for momentum conservation between the three types of interacting photons; the atoms' linear momentum does not change in the wave-mixing process, since the atom must wind up in the state it started out in. Now consider the restriction imposed by conservation of angular momentum among the photons. Quantizing along the common direction of propagation, we see that the two incident photons impart either 0 or $\pm$ 2 units of angular momentum to an atom; thus, if angular momentum is to be conserved, the generated 7793-cm^{-1} photon must carry 0 or $\pm$ 2 units of angular momentum along its direction of propagation $\hat{z}$. It is well known, however, that a photon may carry only $\mp$1 units of angular momentum along its direction of propagation. Thus three-wave mixing in an atomic vapor is strictly forbidden in the case of collinear propagation.[3] In our experimental attempt to observe this forbidden effect, we discovered a new phenomenon: magnetically induced three-wave mixing.[4] If a DC magnetic field H is applied transverse to the common direction of propagation of the incident laser beams a wave of frequency ω_3 (7793 cm^{-1}) is produced, and its intensity is found to vary as H^2 for $0 < H < 100G$.

This effect cannot be due to the "lifting" of parity conservation; in fact, an external magnetic field, unlike an external electric field, does not remove the requirement that parity be a good quantum number. Some thought reveals that the conservation "law" which is broken by the presence of the external magnetic field is that of angular momentum. Any atomic angular momentum temporarily transferred to an atom during the two-photon excitation will tend to precess about the external magnetic field. Thus the

atom will not necessarily end up in the same Zeeman or hyperfine level in which it started out. Since some of this angular momentum may be transferred to the generated photon, there will be a probability amplitude that it has $\pm$ 1 units of angular momentum along $\hat{z}$. Thus E2 or M1 collinear three-wave mixing is allowed in the presence of a transverse magnetic field.

The experimental observations we have made on the 7793-cm^{-1} difference-frequency (DFG) pulse generated in Tl vapor are summarized in Figs. 48-49. Fig. 48 shows the atomic-density-squared dependence of the DFG intensity; this dependence is characteristic of all wave-mixing processes. The H^2 - dependence of the DFG intensity is shown in Fig. 49. The polarization dependence of the DFG is consistent with that expected for an M1 transition.

We note that if the atomic thallium density is high enough then an incident laser pulse of frequency ω_1 produces stimulated Raman scattering of frequency ω_2. As a result, even with no ω_2-pulse incident, a 7793-cm^{-1} pulse is emitted by what may be considered parametric down-conversion, the emitted pulse at ω_2 acting as the idler wave.

From our explanation of magnetically induced DFG it is clear that magnetically induced sum-frequency generation (SFG) should be observable as well. We have detected this effect on the $3^2S_{1/2}$ - 4^2D transition in atomic sodium vapor.[5] For this case the generation arises from an E2 moment. Since E2 SFG had already been observed on this transition in the case of phase-matched noncollinear incident beams,[6] we decided to perform an experiment which would exhibit interference between the noncollinear effect and the magnetically

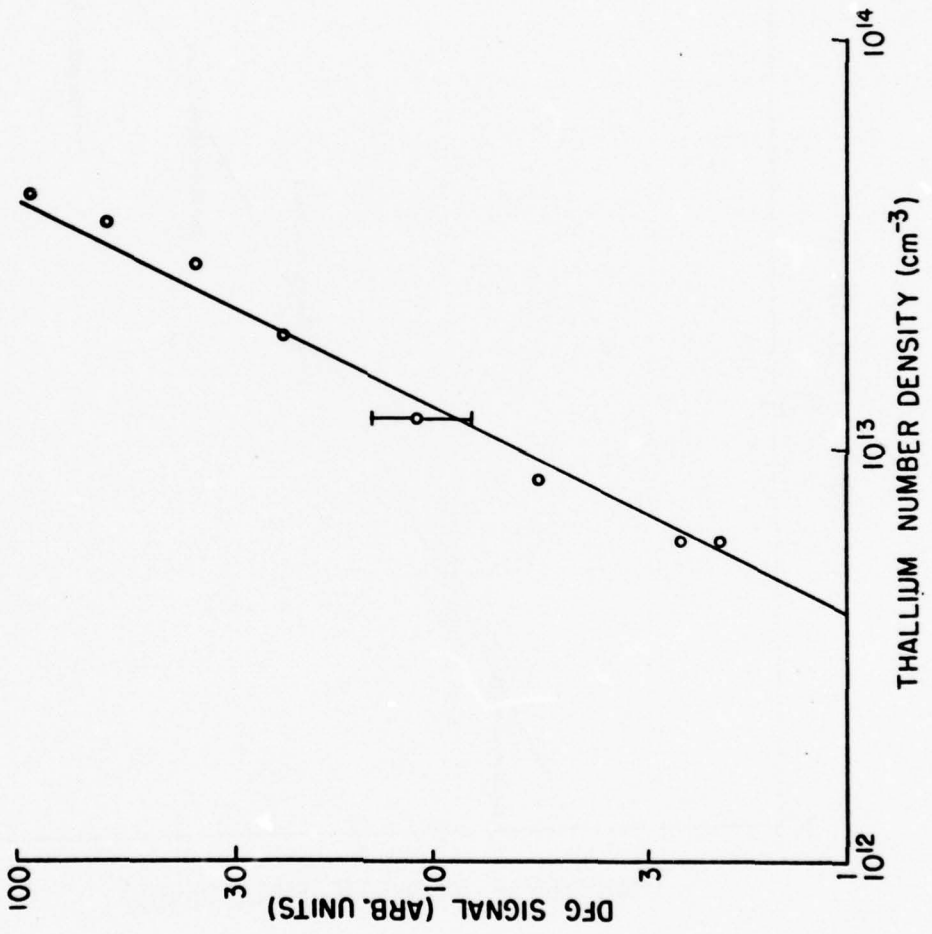
DFG SIGNAL (ARB. UNITS)
100
30
10
3
1
10^{12}
10^{13}
10^{14}
THALLIUM NUMBER DENSITY (cm^{-3})

Figure 48

Figure 49

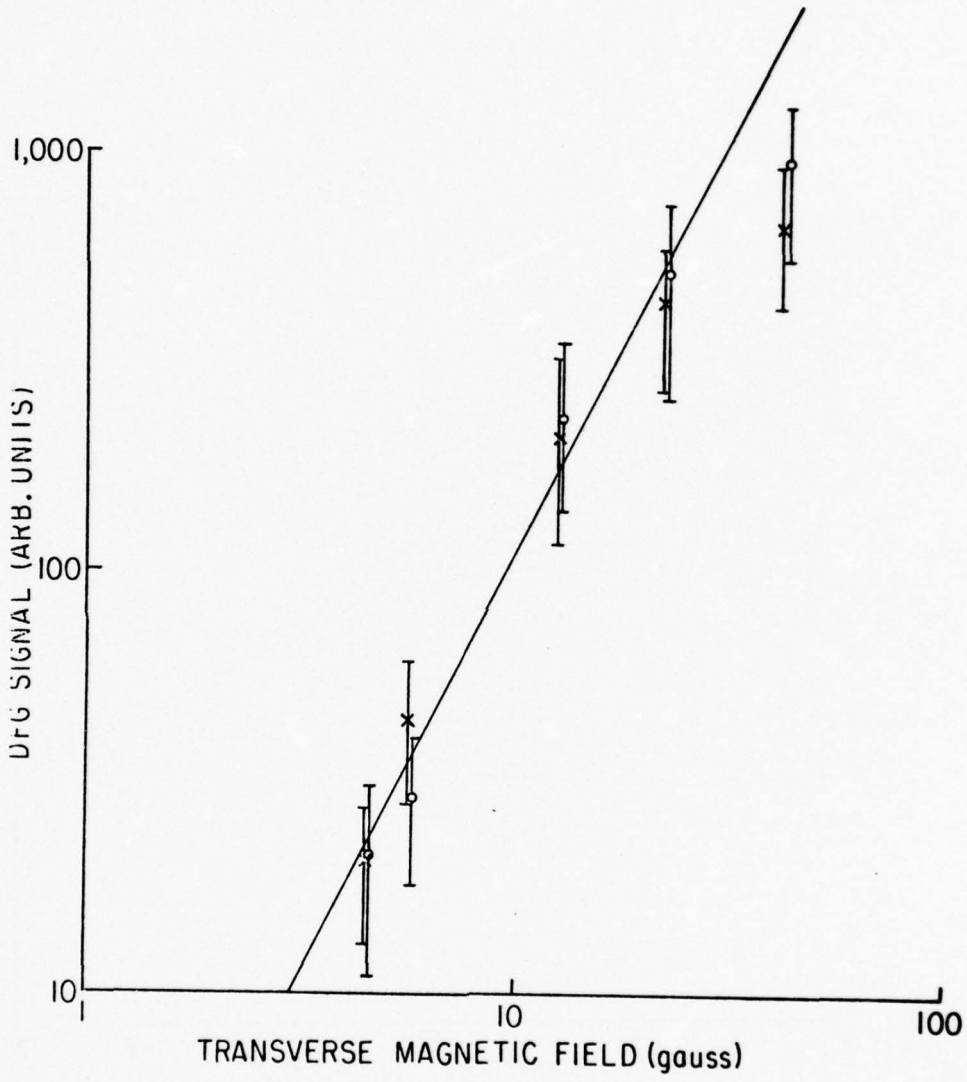
1,000
100
10
DrG SIGNAL (ARB. UNITS)
10
100
TRANSVERSE MAGNETIC FIELD (gauss)

induced effect. The results of such an experiment are shown in Fig. 50, which depicts the SFG intensity as a function of the transversely applied magnetic field. The only difference between the two plots is a reversal of the magnetic-field direction. It will be seen that for H ≅ 30 G a reversal of H changes the SFG intensity by an order of magnitude !

This most unusual effect has a straightforward explanation, whose essential points follow.

Denote the electric vector of the noncollinearly and magnetically produced SFG wave by $\vec{E}_{nc}$ and $\vec{E}_H$, respectively. From symmetry considerations, it may be shown that $\vec{E}_H$ can be written

$$\vec{E}_H = \mu_1 \hat{z} \ (\vec{E}_1 \times \vec{E}_2) \times \vec{H} + \mu_2 \ [\ (\vec{E}_2 \times \vec{H}) \cdot \hat{z} \ \vec{E}_1 + (\vec{E}_1 \times \vec{H}) \cdot \hat{z} \ \vec{E}_2 \ ] \qquad (1)$$

where $\vec{E}_{1,2}$ represents the electric vector of incident wave 1 and 2, respectively. Thus $\vec{E}_H$ reverses sign with respect to E_{nc} when $\vec{H}$ is reversed, and the total intensity I, proportional to $|\vec{E}_{nc} + \vec{E}_H|^2$, changes accordingly. According to this explanation, I (H) may be written as $I_o + BH + VH^2$. As a check, we have used the data of Fig. 50 to plot $I_+ = I(H) + I(-H) - 2I_o$ and $I_- = I(H) - I(-H)$ against H (Fig. 51) As expected $I_+ \propto H^2$, while $I_- \propto H$.

The second avenue of research which has been opened up to us as a result of our study of the coherent excitation of the Tl $6^2P_{1/2} - 6^2P_{3/2}$ transition is Dicke superradiance, a coherent atomic effect in which an initially inverted ensemble of atoms emit a burst of coherent radiation at a characteristic delay time after the inversion is created. Dicke superradiance was first observed by Shribanowitz et. al., in HF gas.[7] More recently it was observed

Figure 50

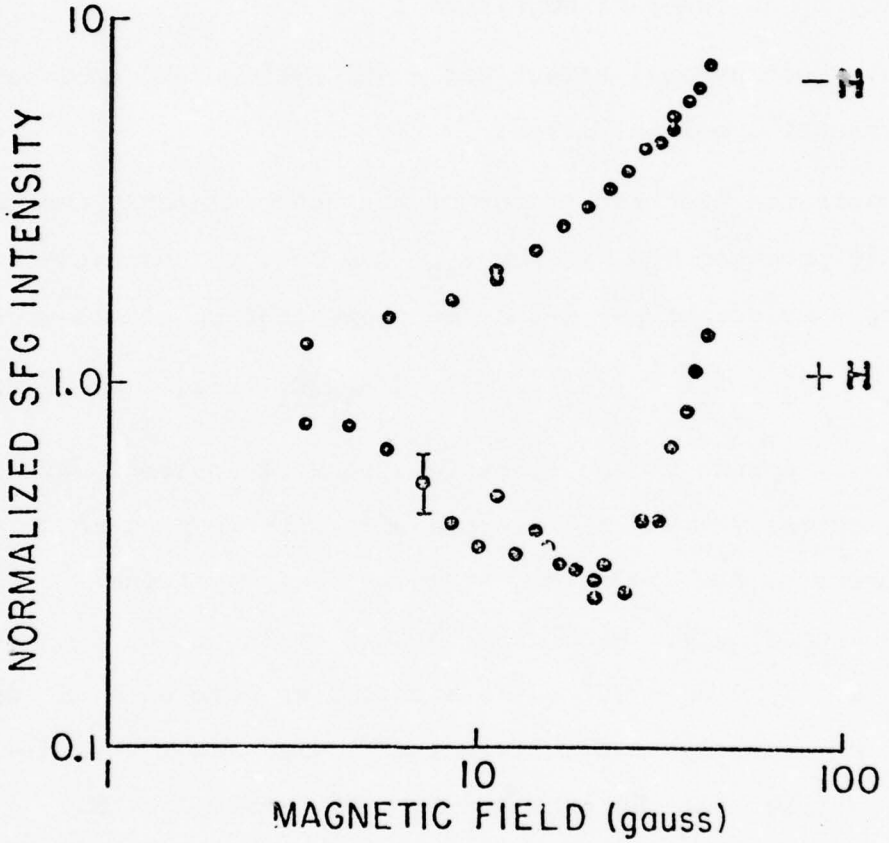
10
1.0
0.1
NORMALIZED SFG INTENSITY
-H
+H
10
100
MAGNETIC FIELD (gauss)

Figure 51

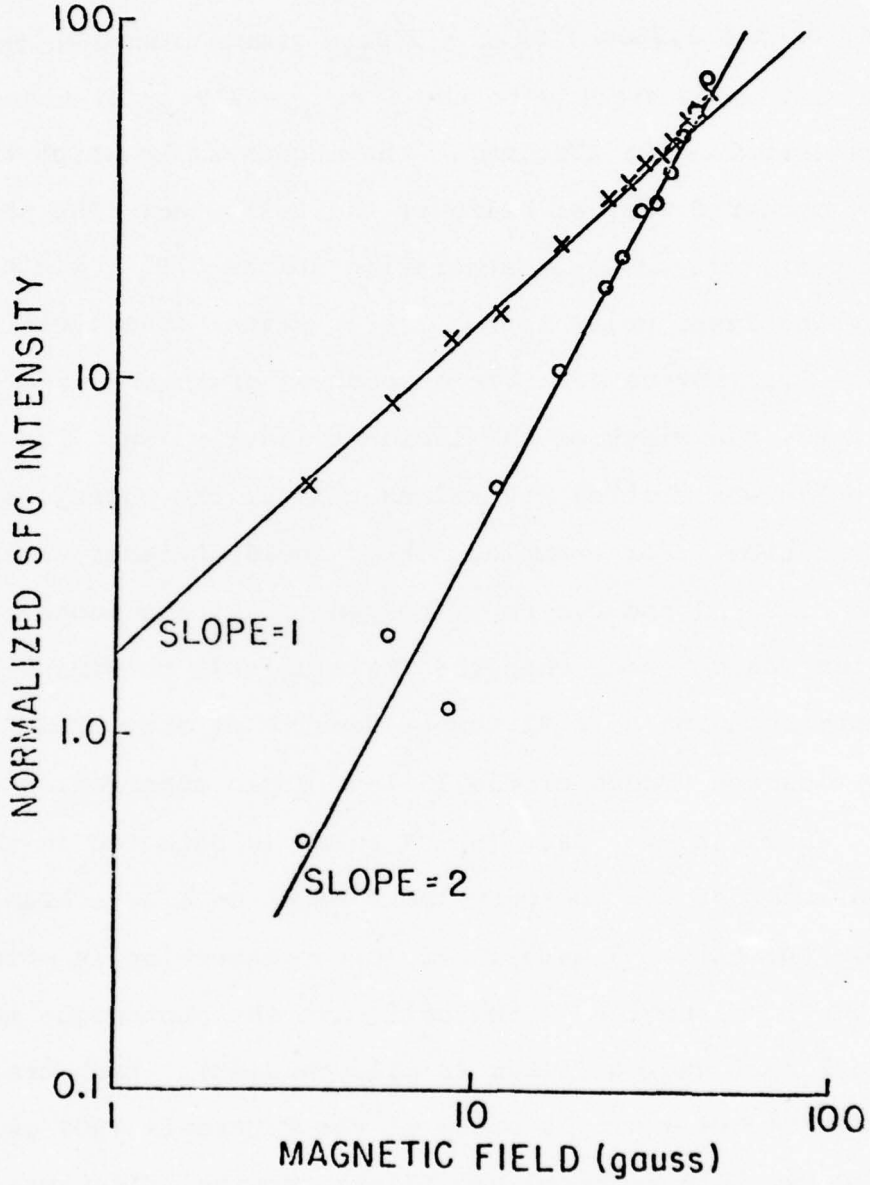
100
10
1.0
0.1
NORMALIZED SFG INTENSITY
SLOPE=1
SLOPE=2
1
10
100
MAGNETIC FIELD (gauss)

by Gross et. al. in atomic Na Vapor.[8] We first observed this effect during our parametric down-conversion study in atomic Tl. A careful investigation[9] showed that the superradiance was occurring on the 1.30μm $7^2S_{1/2}$ - $7^2P_{1/2}$ transition when the laser frequency was tuned exactly to the $6^2P_{3/2}$ - $7^2P_{1/2}$ E2-transition frequency (wavelength: 379.1nm). The mechanism by which the inversion occurred was, we believe, the following: The population created by stimulated Raman scattering in the $6^2P_{3/2}$ state was transferred by the laser pulse to the $7^2P_{1/2}$ state, thus creating a $7^2S_{1/2}$ - $7^2P_{1/2}$ inversion. The excitation of this inversion lasted about 6 nsec, the width of the incident laser pulse. The superradiant pulse was emitted several nsec after the passage of the laser excitation. For example, for an incident laser energy and linewidth of 25 μJ and 0.3 cm^{-1}, respectively, the supperradiant pulse delay was 4-9 nsec when the thallium cell temperature was 770°C (corresponding to a Tl number density of about $2x10^{15}$ cm^{-3}).

Oscilloscope traces of the 1301-nm Dicke superradiance (DS) pulse are shown in Fig. 52. The DS pulse is detected in the forward direction (that of the incident laser beam) on a Ge avalanche photodiode (risetime 1 nsec). Efficient detection is obtained by imaging the focal region in the cell onto the photodiode surface through a 1.2-μm cut-on filter (a silicon disc). Each trace of Fig. 52 represents a single sweep of the Tektronix 7904 oscilloscope using two 7A19 vertical-amplifiers (nominal risetime: 0.7 nsec) to simultaneously display the Ge detector signal as well as a cable-delayed signal from a Si photodiode (Monsanto MD-2) which detects the incident laser pulse. In each trace the laser pulse (the second

Figure 52

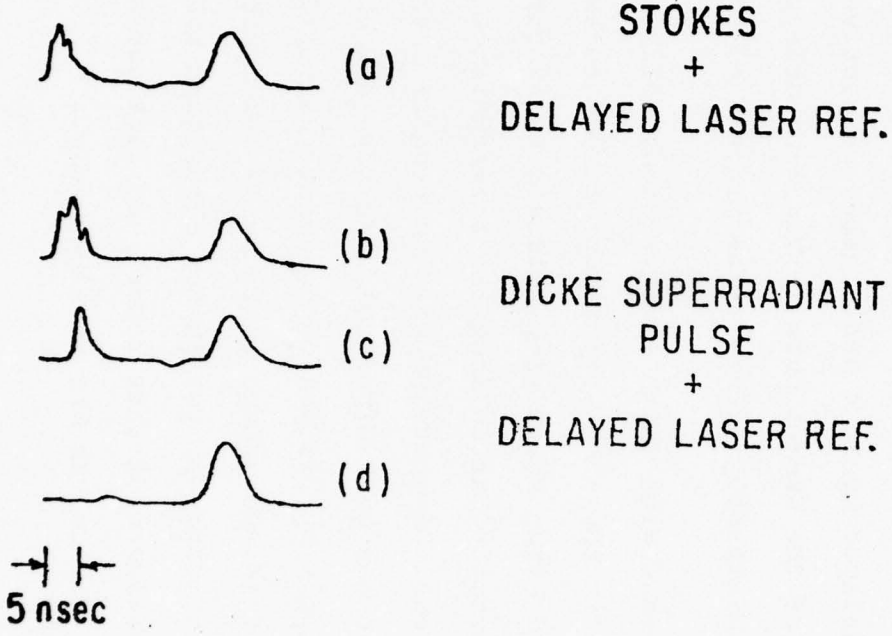
(a)
STOKES
+
DELAYED LASER REF.
(b)
(c)
DICKE SUPERRADIANT
PULSE
+
DELAYED LASER REF.
(d)
5 nsec

peak) serves as a reference-time marker. For Fig. 52a the silicon filter has been replaced by several neutral-density filters and a 535-nm interference filter, so that the first pulse represents the Stokes radiation (at 538 nm) detected by the Ge photodiode. The jitter of the appearance of the Stokes pulse is found to be less than 1 nsec. In Figs. 52b, 52c, and 52d, the infrared pulse appears delayed by 3, 4 and 9 nsec, respectively, with respect to the peak of the Stokes pulse. The long delays and short pulse-widths unmistakably identify the process as Dicke superradiance.

The ease with which an inversion, followed by DS, may be obtained -- in the above experiment it occurs as the result of stimulated Raman scattering followed by electric-quadrupole absorption -- prompted us to look for superradiance in other systems in which an excited state population results from a weak absorption. Our search was quite fruitful. We have now obtained DS in several atomic vapors by the following additional optical-pumping schemes: directly from the ground state by E2 absorption; by stimulated Raman scattering; by two-photon absorption and by E1 absorption. In the remainder of this report, we list our experimental observations for Tl, Cs, Rb and Na separately.

Thallium - We have observed DS when using laser-pump two-photon absorption from the ground state to create inversions on the $7^2S_{1/2} - 7^2P_{1/2}$ and $7^2S_{1/2} - 7^2P_{3/2}$ transitions (Fig. 53). Note in particular that in this experiment the laser frequency is $\sim 8000\ cm^{-1}$ off resonance from the nearest ground-intermediate state splitting! This experiment truly demonstrates how easy it

Figure 53

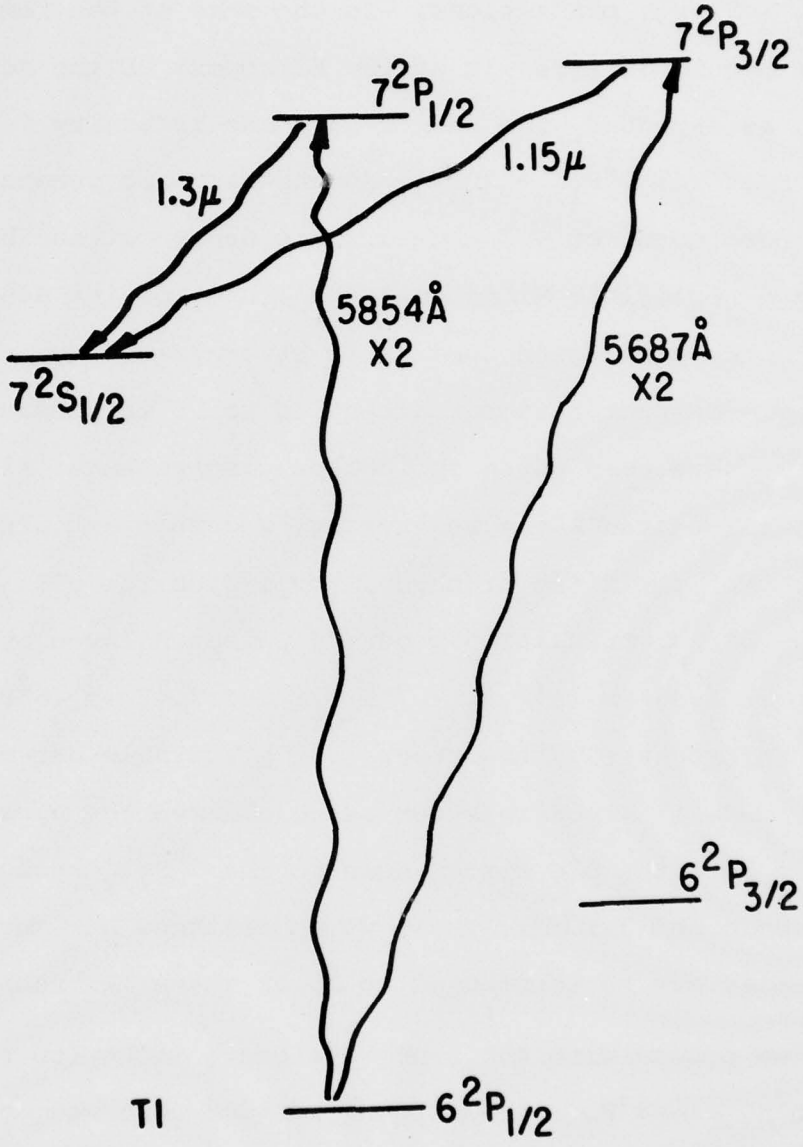

is to obtain a rapid inversion in an atomic system. Interestingly, three-wave mixing is again demonstrated in this experiment: we observe second-harmonic generation on both the $6^2P_{1/2} - 7^2P_{3/2}$ and $6^2P_{1/2} - 7^2P_{1/2}$ transitions. In the case of the former, the generation occurs as a result of the E2 moment of the superposition, and, as expected, the second-harmonic intensity is proportional to H^2. The $6^2P_{1/2} - 7^2P_{1/2}$ second-harmonic generation is, however, independent of H. Indeed, this superposition has no E2 moment and a negligible M1 moment; the source of its associated second-harmonic generation remains to be explained.

Cesium - We next turn our attention to DS in atomic cesium, for which we have used three optical-pumping schemes: E2 absorption (Fig. 54), stimulated Raman scattering, and resonant absorption (Fig. 55). For the first of these, pumping on the $6^2S_{1/2} - 6^2D_{3/2}$ or $6^2S_{1/2} - 6^2F_{5/2}$ transition produced pulses delayed by as much as 10 nsec at 1.36 μm ($6^2P_{1/2} - 7^2S_{1/2}$) and 1.47 μm ($6^2P_{3/2} - 7^2S_{1/2}$). Unfortunately, the absence of a suitable detector in our laboratory made it impossible for us to observe the upper legs of the cascade from the 6^2D states down to the $7^2S_{1/2}$ state (wavelengths: 16 μm and 3.1 μm). Thus, we do not know how much of the observed delay may be attributed to DS at these IR transitions.

When we pumped with 455.5-nm-wavelength light (on resonance with the $6^2S_{1/2} - 7^2P_{3/2}$ transition) we also observed delayed bursts at the various transition wavelengths between 1.34 and 1.47 μm indicated in Fig. 55. The presence of a collimated, coherent burst of light at 5393.5Å, corresponding to the forbidden $6^2S_{1/2} - 7^2S_{1/2}$ transition, is another example of a three-wave

Figure 54

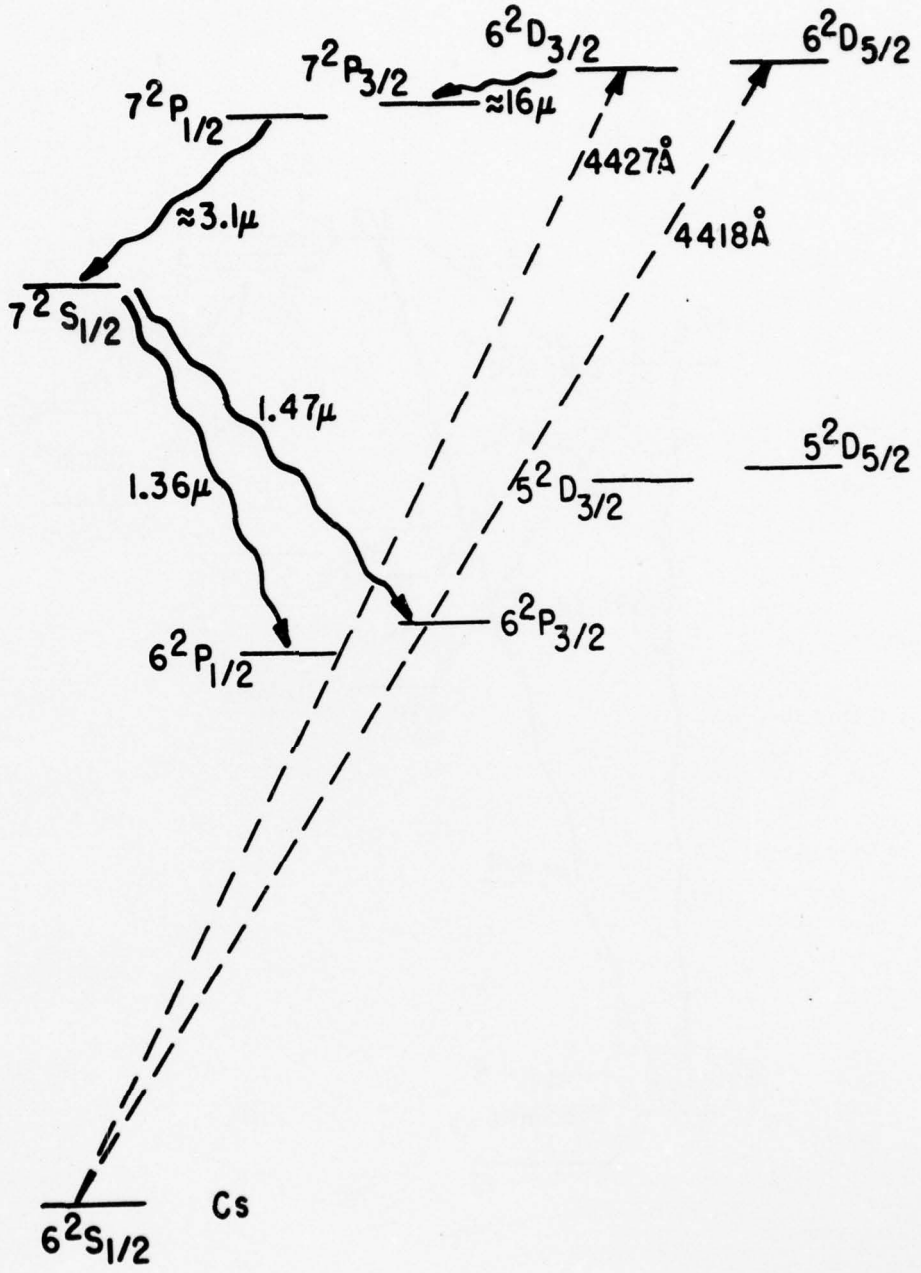
$6^2D_{3/2}$
$6^2D_{5/2}$
$7^2P_{3/2}$
$7^2P_{1/2}$
≈16μ
4427Å
4418Å
≈3.1μ
$7^2S_{1/2}$
1.47μ
1.36μ
$5^2D_{5/2}$
$5^2D_{3/2}$
$6^2P_{3/2}$
$6^2P_{1/2}$
Cs
$6^2S_{1/2}$

Figure 55

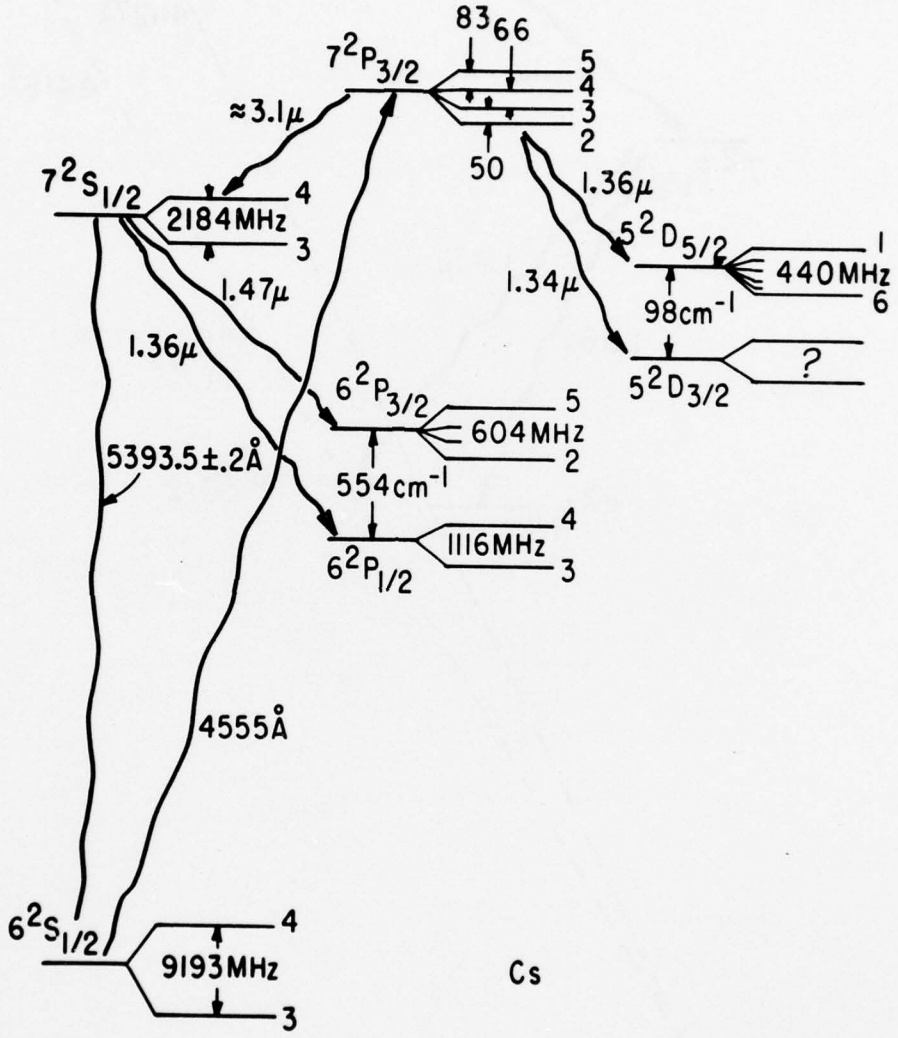
$8^3S_{6\,6}$
$7^2P_{3/2}$
5
4
3
2
50
≈3.1μ
$7^2S_{1/2}$
4
2184MHz
3
1.47μ
1.36μ
1.36μ
$5^2D_{5/2}$
1
440MHz
6
98cm⁻¹
$5^2D_{3/2}$
?
$6^2P_{3/2}$
5
604MHz
2
554cm⁻¹
4
1116MHz
3
$6^2P_{1/2}$
5393.5±.2Å
4555Å
$6^2S_{1/2}$
4
9193MHz
3
Cs

mixing process. As in the case of the $6^2P_{1/2} - 7^2P_{1/2}$ radiation observed in Tl, the 5393.5Å light was emitted in the absence of a magnetic field. We have not yet clarified the mechanism of this radiation.

Fig. 56 shows some examples of DS pulse-shapes in Cs at a Cs vapor pressure of about 10^{-2} torr and using a laser pump at 4555Å. The 1.36 μm pulse associated with the $7^2P_{3/2}$-$5^2D_{5/2}$ transition is delayed by ≅10 nsec from the peak of the exciting laser pulse. Evidently there is some ringing in the DS pulse, but it would be premature to consider it true Dicke superradiant ringing in view of the many possible hyperfine-level beats in the $7^2P_{3/2} - 5^2D_{5/2}$ transition (Fig. 55).

Rubidium - In rubidium (Rb^{87}, 125°C, ≃ 10^{-3} torr vapor pressure) we have used E2-absorption pumping (5166Å vacuum wavelength) to produce an inversion between the 4^2D and $5^2P_{1/2,\ 3/2}$ states. We observe DS on these transitions (1.48, 1.53 μm). The relevant energy levels of these atomic systems are depicted in Fig. 57. Again, we have explicitly labelled the hyperfine levels. The observed DS pulses are delayed from the exciting pulses by as much as 12-15 nsec. Modulation is observed on either of the $4^2D \rightarrow 5^2P_{1/2}$ transitions. (For this experiment an intra-cavity etalon narrowed the dye-laser linewidth to about 700 MHz; thus only one of the 4^2D states was populated by the 5166Å absorption.) The modulation frequency of about 900 MHz is suggestive of the hyperfine splitting of 818 MHz in the $5^2P_{1/2}$ state. It may thus be an example of a quantum-beat effect, rather than superradiant ringing.

Figure 56

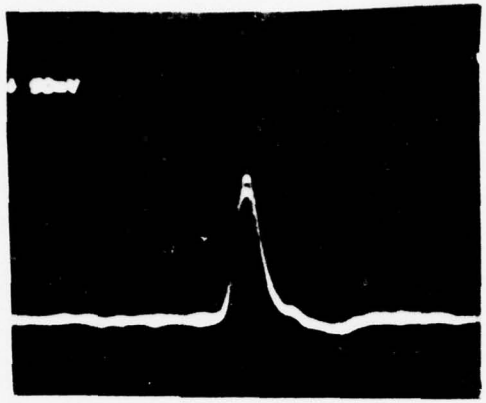

(a)

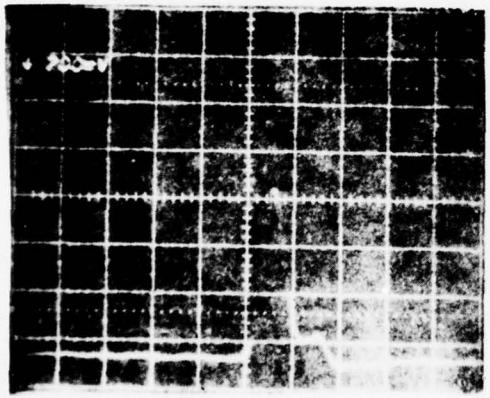

(b)

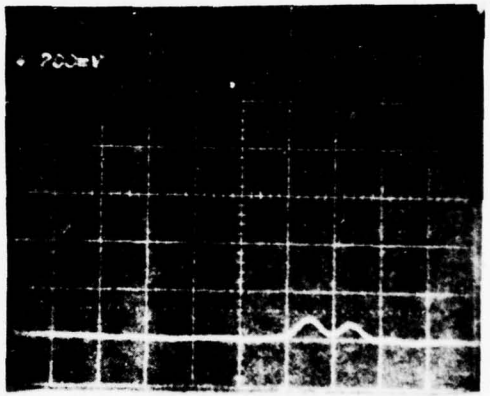

(c)

Figure 57

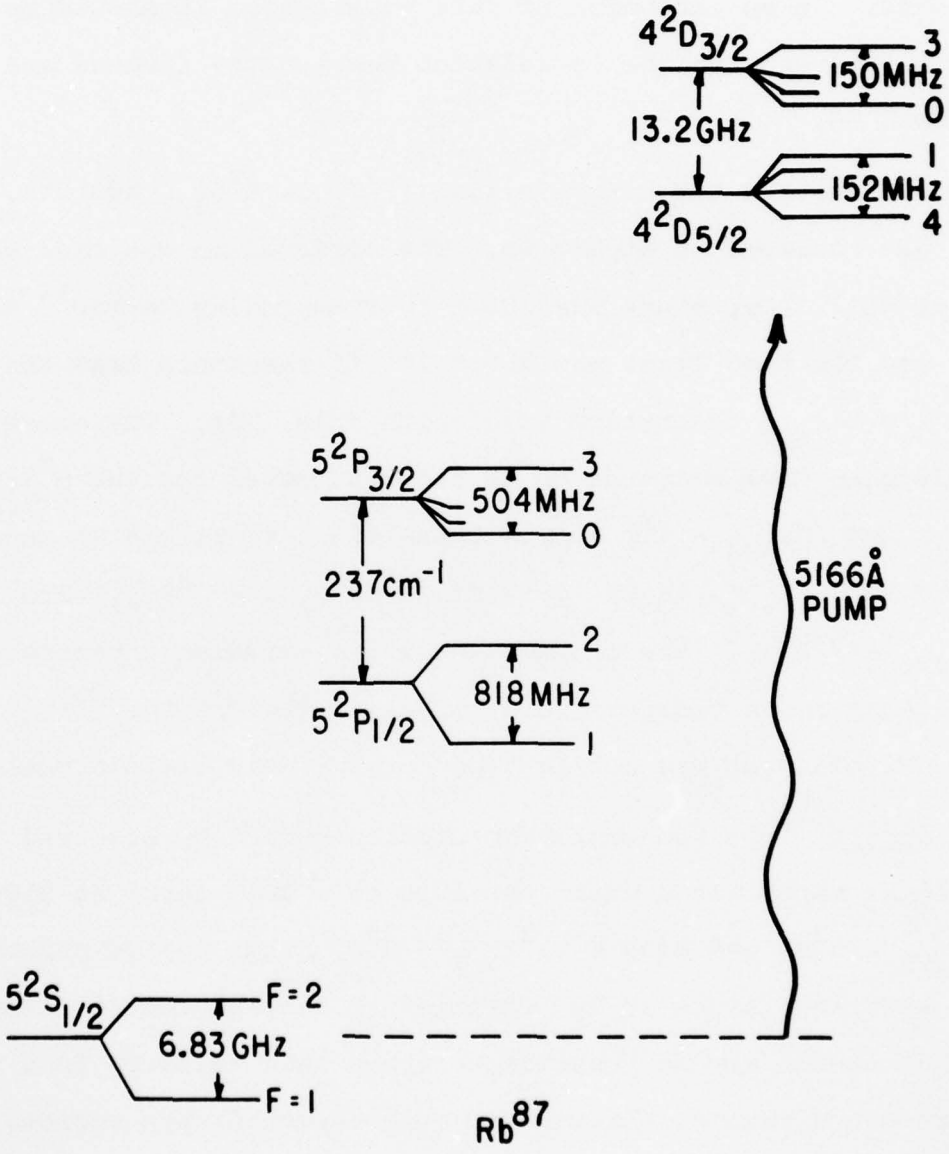
$4^2D_{3/2}$
3
150MHz
0
13.2GHz
1
152MHz
4
$4^2D_{5/2}$
$5^2P_{3/2}$
3
504MHz
0
237cm^{-1}
2
818MHz
1
$5^2P_{1/2}$
5166Å
PUMP
$5^2S_{1/2}$
F=2
6.83GHz
F=1
Rb^{87}

As shown in Fig. 58, the rubidium experiment was set up in a way that allowed the simultaneous observation of both forward and backward-emitted DS on the same detector. Our preliminary observations indicated that the essential features of both were the same. In an extension of this experiment, it should be possible to examine the correlation between the forward and backward DS.

SRS-induced three-wave mixing ($5^2S_{1/2}$- $6^2S_{1/2}$ and $5^2S_{1/2}$ - 4^2D) was observed in atomic Rb. The observation was made when the Rb cell temperature was 300°C (corresponding to $\simeq 10^{16}$ atoms/cm^3) and the pump laser was about 1Å off resonance from the $5^2S_{1/2}$ - $6^2P_{3/2}$ absorption wavelength (Fig. 59). The emission wavelengths were measured to be those expected for the $5^2S_{1/2}$ - $6^2S_{1/2}$ and $5^2S_{1/2}$ - 4^2D atomic transitions to within an uncertainty of about 0.5Å. As in the case of Cs ($6^2S_{1/2}$ - $7^2S_{1/2}$) and Tl ($6^2P_{1/2}$ - $7^2P_{1/2}$), the collimated 4966-Å emission intensities were found to be independent of magnetic field. The 5166-Å radiation (E2 allowed) was not checked for magnetic field dependence.

Sodium - The two-photon-absorption-pumped DS observed in atomic Na vapor (at a vapor pressure of $\simeq 10^{-4}$ torr) at 8183Å ($3^2P_{1/2}$ - 3^2D) and 8195 Å ($3^2P_{3/2}$ - 3^2D) (Fig. 60) is perhaps the most exciting, since it is "visible" to many photomultiplier tubes. Thus it should now be possible to study this emission from the fluorescence regime, through the weak-superradiance regime, all the way to the regime of strong superradiance regime, all the way to the regime of strong superradiance. The short wavelength of this transition implies a proportionally shorter value of T_2*,

Figure 58

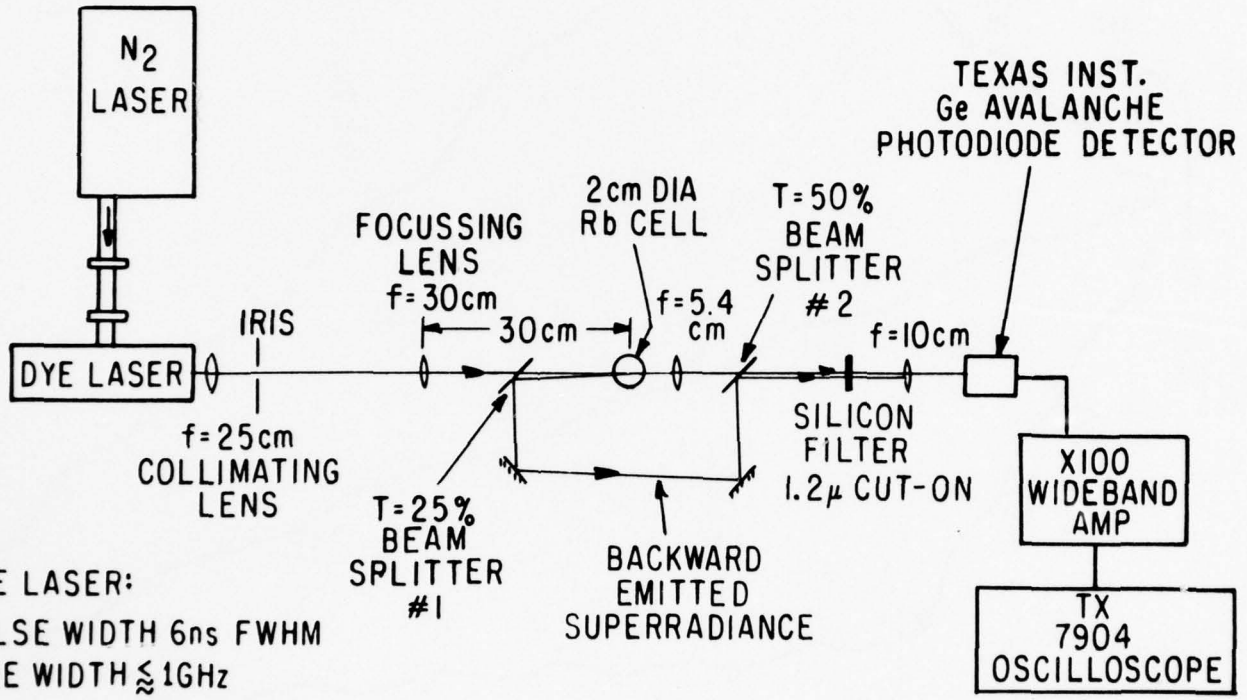
N_2 LASER
DYE LASER
IRIS
f=25cm COLLIMATING LENS
FOCUSSING LENS f=30cm
30cm
2cm DIA Rb CELL
f=5.4 cm
T=25% BEAM SPLITTER #1
BACKWARD EMITTED SUPERRADIANCE
T=50% BEAM SPLITTER #2
SILICON FILTER 1.2μ CUT-ON
f=10cm
TEXAS INST. Ge AVALANCHE PHOTODIODE DETECTOR
X100 WIDEBAND AMP
TX 7904 OSCILLOSCOPE
DYE LASER:
PULSE WIDTH 6ns FWHM
LINE WIDTH ≲ 1GHz

Figure 59

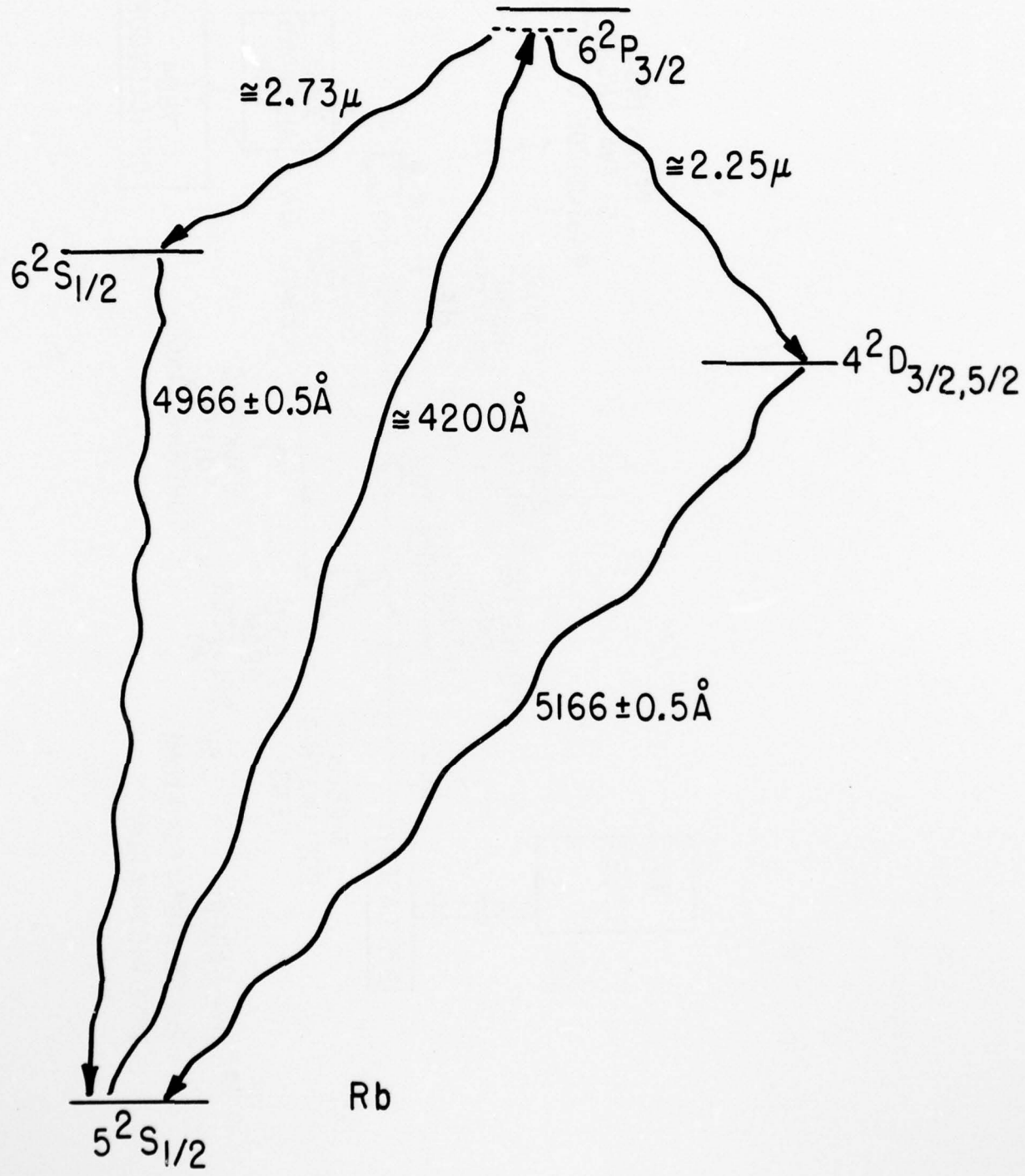
$6^2P_{3/2}$
≅2.73μ
≅2.25μ
$6^2S_{1/2}$
$4^2D_{3/2,5/2}$
4966±0.5Å
≅4200Å
5166±0.5Å
Rb
$5^2S_{1/2}$

Figure 60

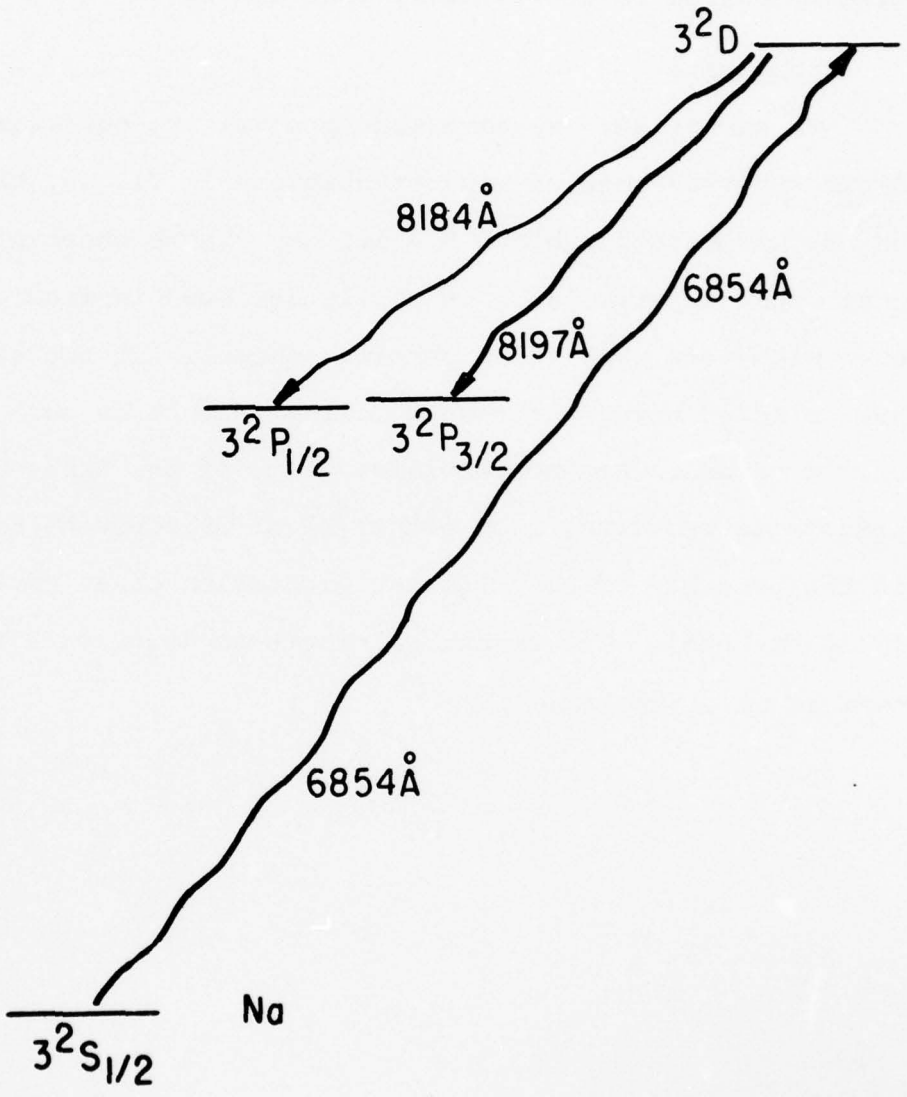

the Doppler dephasing time. Thus one expects a somewhat shorter delay until the onset of superradiance, and indeed the largest delay observed was about 5 nsec. A study of this transition would clearly be more valuable if the laser pump pulse were much shorter than about 5 nsec or if the laser linewidth were sufficiently narrow to artificially increase T_2^*.

SUMMARY -

To summarize: We have made preliminary observations of Dicke superradiance on many transitions in Tl, Cs, Rb, and Na in the wavelength range 0.8 - 1.5 μm. These observations confirm that Dicke superradiance is easily achieved in atomic vapors, even with very weak laser pumping schemes. At the same time, we have studied novel three-wave mixing effects in each of these atomic vapors. We have explained some of the three-wave mixing effects as resulting from either M1 or E2 coherent radiation in the presence of noncollinear excitation or an external magnetic field(or both). The mechanism of others (e.g. Tl $7^2P_{1/2}$) remains to be explained.

(1) S. R. Hartmann, IEEE Journ. Quant. Electron., QE-4, 802 (1968).

(2) Last year's progress report, p. 74.

(3) T. Hänsch and P. Toschek, Z. Phys., 236, 373 (1970).

(4) A. Flusberg, T. Mossberg, and S. R. Hartmann, Phys. Rev. Lett., 38, 59 (1977).

(5) A. Flusberg, T. Mossberg, and S. R. Hartmann, Phys. Rev. Lett., 38, 694 (1977).

(6) D. S. Bethune, R. W. Smith, and Y. R. Shen, Phys. Rev. Lett., 37,431 (1977).

(7) N. Skribanowitz, I. P. Herman, J. C. MacGillivray, and M. S. Feld, Phys. Rev. Lett., 30, 309 (1973).

(8) M. Gross, C. Fabre, P. Pillet, and S. Haroche, Phys. Rev. Lett., 36, 1035 (1976).

(9) A. Flusberg, T. Mossberg, and S. R. Hartmann, Phys. Lett., 58A, 373 (1976).

D. COHERENCE EFFECTS IN TWO-PHOTON ABSORPTION.

(P. F. Leung, A. Flusberg, and S. R. Hartmann).

We have constructed a nitrogen laser which produces a 200-300 KW peak-power pulse having a width of about 10 nsec. A transversely pumped dye laser has also been constructed. A computer program which we will use to make calculations on extended superradiant systems is being written.

E. SPECTRAL DIFFUSION*

(P. Fu, S. R. Hartmann)

Last year, we reported that our electron spin echo results, associated with the Mn^{+2} resonance in $CaWO_4$ doped with Mn^{+2} and Er^{+3}, could be understood qualitatively by using the sudden jump model of spectral diffusion[1] and the mechanism of instantaneous diffusion proposed by Klauder and Anderson.[2] Instantaneous diffusion results from the abrupt change in local field caused by spin reorientation during second excitation pulse, therefore, the echo decay time due to instantaneous diffusion is dependent on the second excitation pulse condition.

This year, we tested for the effect of instantaneous diffusion by varying the excitation pulse amplitude. Our result, shown in Figure 61, proves that instantaneous diffusion plays no role in the echo decay mechanism.

We also found a serious nonlinearity in our detector response which strongly affected our previous results. After correcting for the nonlinearity, we made two-pulse echo measurements at several different temperatures (Fig. 62, Fig. 63, Fig. 64). Our results at temperatures above 3°K (Fig. 62, Fig. 63) can be fitted quite well by using the sudden jump model of spectral diffusion with a single value of inhomogeneous linewidth, $\Delta\omega_{1/2}$, at the Mr^{+2} ions due to Er^{+3} ions, and another parameter W, the Er^{+3} spin flip rate, which varies with temperature. The values of W needed to obtain agreement with experiment are tabulated in Table V. As the temperature is increased the value of W

Figure 61

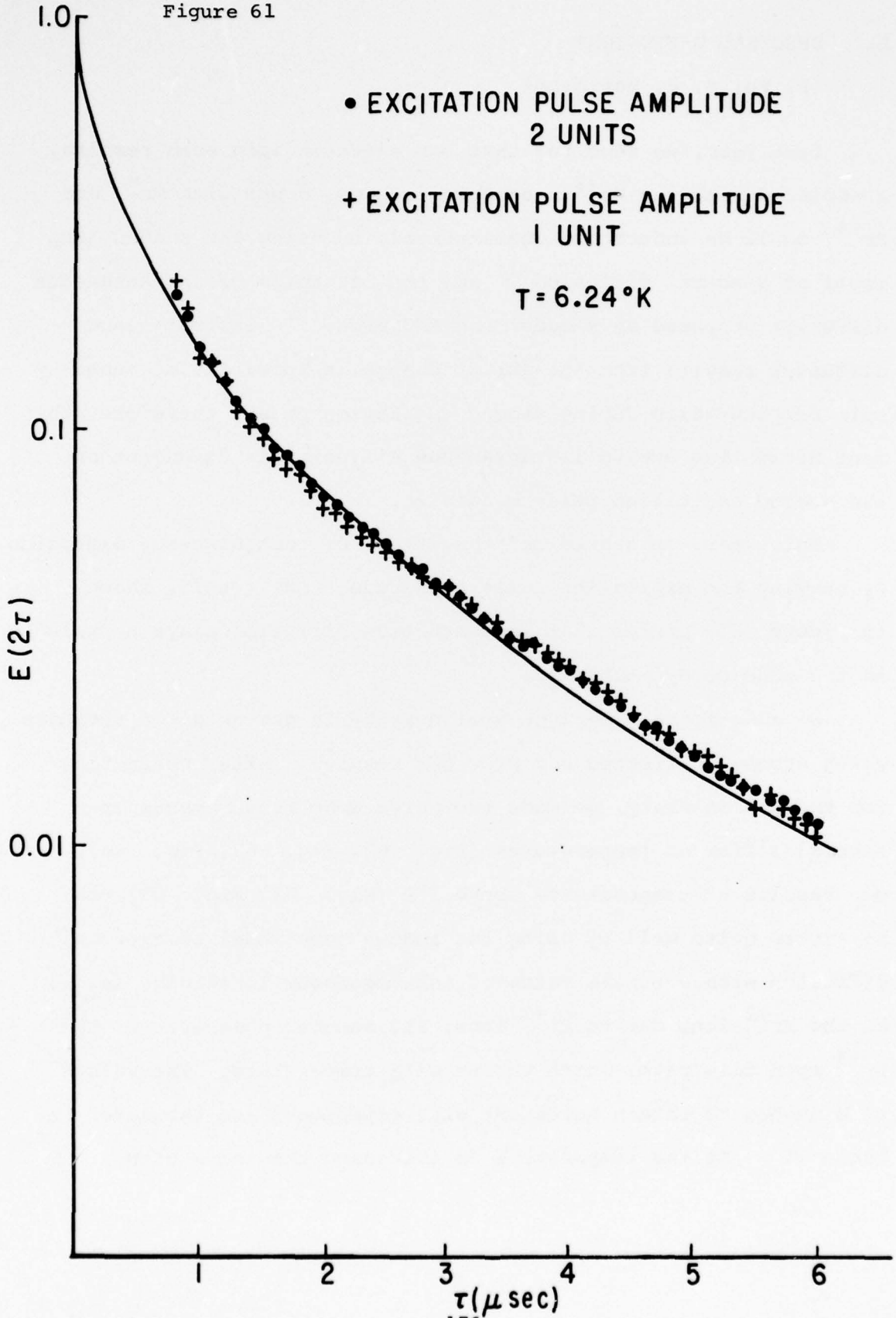
1.0
0.1
0.01
E(2τ)
• EXCITATION PULSE AMPLITUDE
2 UNITS
+ EXCITATION PULSE AMPLITUDE
1 UNIT
T = 6.24°K
1
2
3
4
5
6
τ(μ sec)

Figure 62

TWO PULSE ECHO

$-E(2\tau) = \exp[-2\Delta\omega_{1/2}\tau K(2W\tau)]$

$\Delta\omega_{1/2} = 5 \times 10^6 \text{sec}^{-1}$

Temp.	W
6.24°K	$9.0 \times 10^6 \text{sec}^{-1}$
5.58°K	$5.6 \times 10^6 \text{sec}^{-1}$

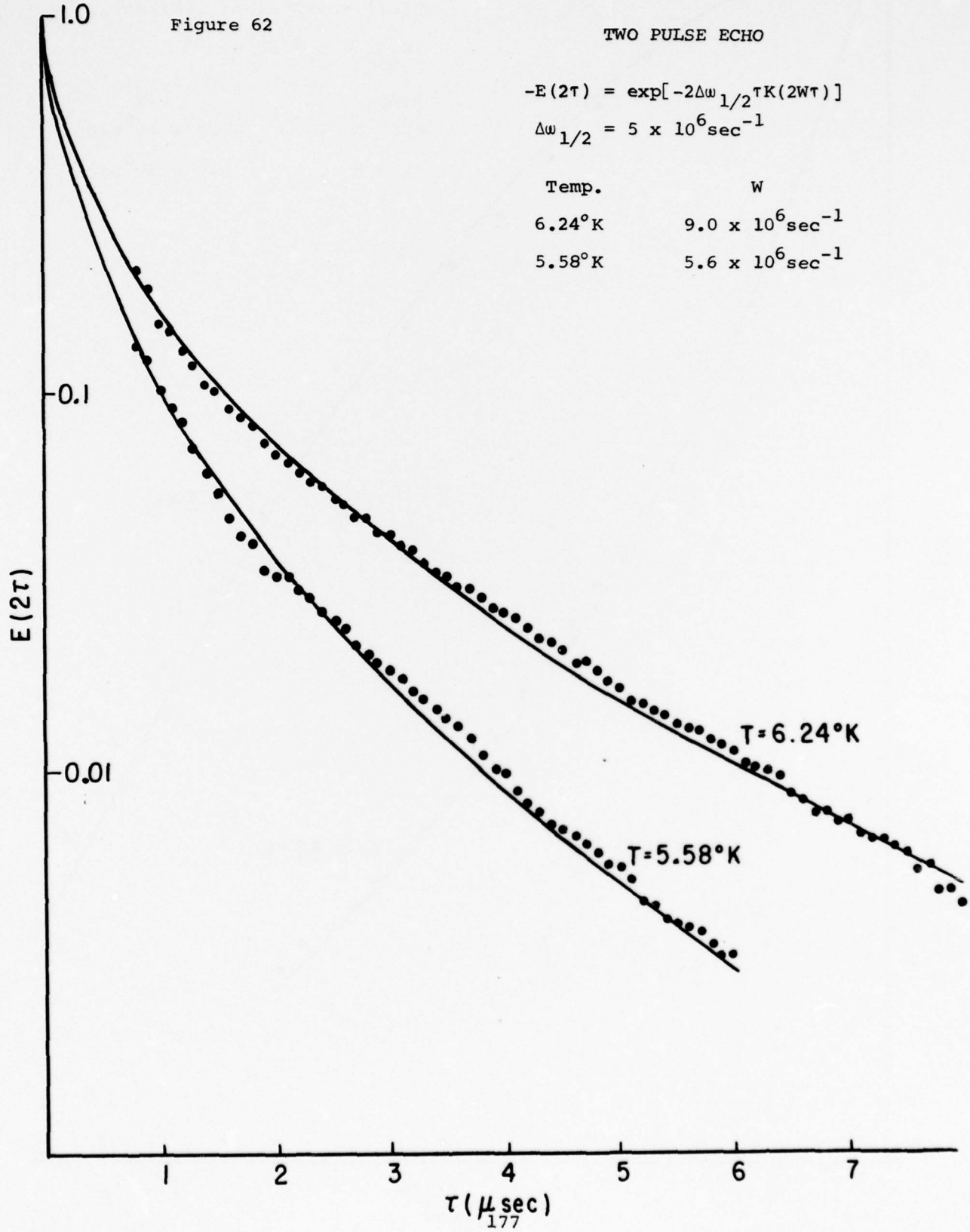

Figure 63

TWO PULSE ECHO

$-E(2\tau) = \exp[-2\Delta\omega_{1/2}\tau K(2W\tau)]$

$\Delta\omega_{1/2} = 5 \times 10^{6}\,\text{sec}^{-1}$

Temp.	W
4.57°K	$2.0 \times 10^{6}\,\text{sec}^{-1}$
3.39°K	$6.0 \times 10^{4}\,\text{sec}^{-1}$

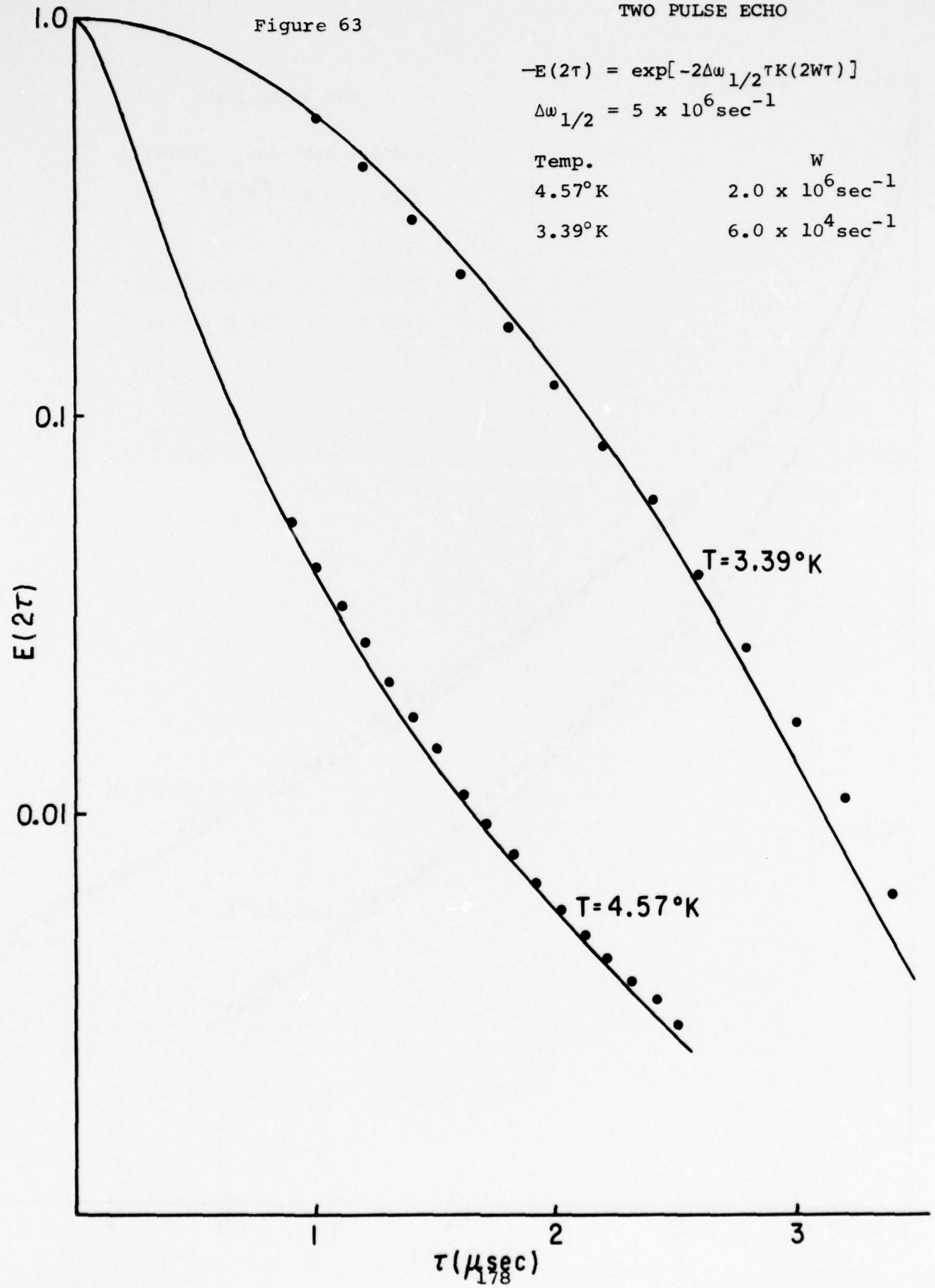

Figure 64

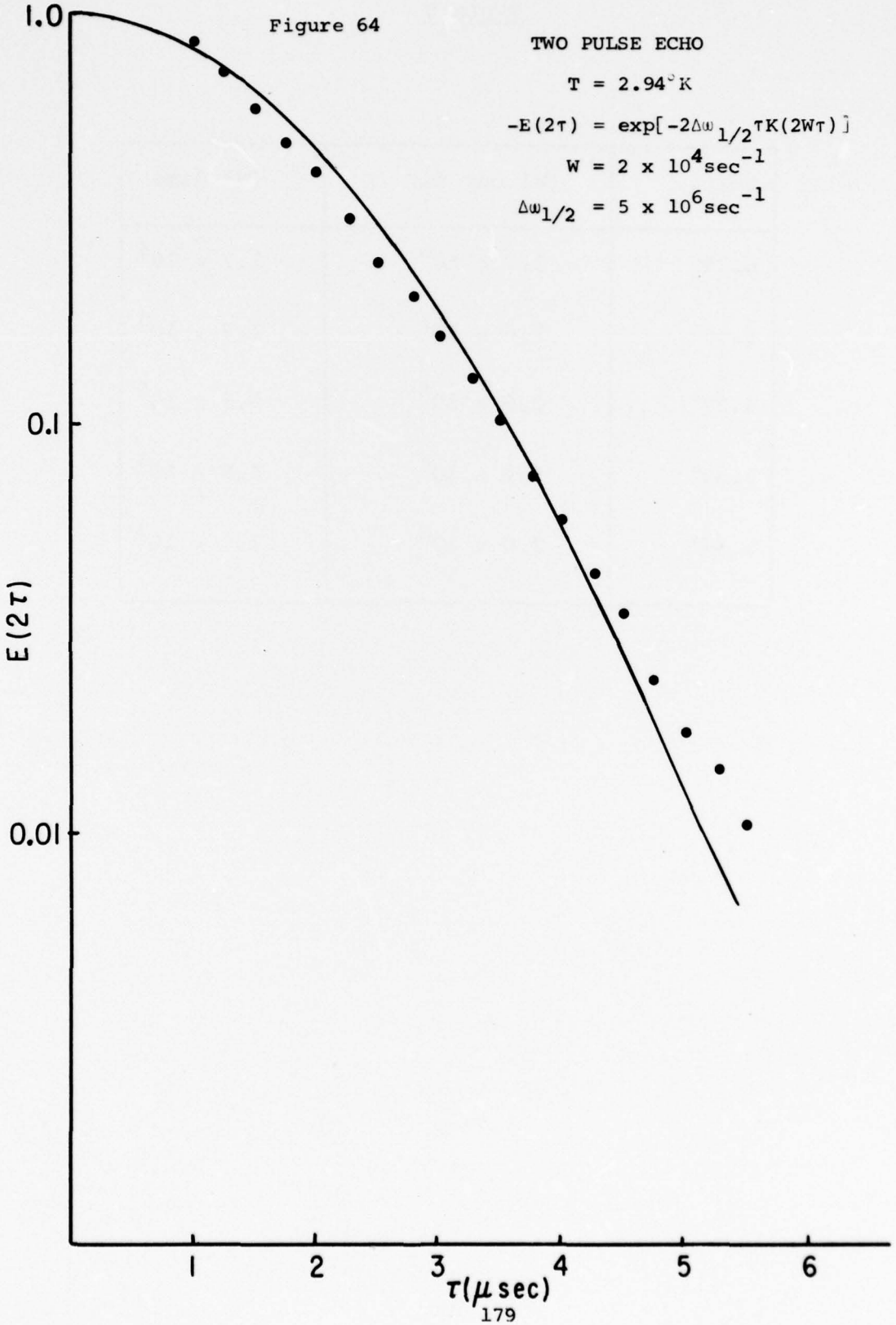
TWO PULSE ECHO
T = 2.94°K
$-E(2\tau) = \exp[-2\Delta\omega_{1/2}\tau K(2W\tau)]$
$W = 2 \times 10^4 sec^{-1}$
$\Delta\omega_{1/2} = 5 \times 10^6 sec^{-1}$
1.0
0.1
0.01
E(2τ)
1
2
3
4
5
6
τ(μsec)

TABLE V

Temp.	(W) our fit	(W) Mims
6.24°	9.0×10^6	3.7×10^5
5.58°	5.6×10^6	1.7×10^5
4.57°	2.0×10^6	0.5×10^5
3.39°	6.0×10^4	5.5×10^3
2.94°	2.0×10^4	1.5×10^3

obtained by fitting also increases as is expected. However, as indicated by Table V, our values of W are an order of magnitude larger than those measured independently by Mims.[3] A similar discrepancy occurs in the magnitude of $\Delta\omega_{1/2}$ where a calculation based on the formula[1]

$$\Delta\omega_{1/2} = [16\ \pi^2/9\sqrt{3}\ ]\ n_{Er}\mu_{Mn}\mu_{Er}\hbar^{-1}$$

yields a value of 0.159×10^6 sec^{-1} when the measured concentration n[4] of Er^{+3} ions

$$[Er^{+3}] = 3.2 \times 10^{17}\ cm^{-3}$$

is used. The factor of twenty discrepancy is presently not understood.

Three pulse echo experiments at 2.94°K have recently been performed. At this temperature, both the two- and three-pulse echo experiments (Fig. 64, Fig. 65) were performed on the same sample, therefore, the same values of $\Delta\omega_{1/2}$ and W have to be used in fitting the data. Considering that we had to impose this restriction the fit is not too bad.

At temperature 2.94°K (Fig. 64), the agreement between experiment and theory is not good. We have not been able to fit results of two-pulse echo decay at temperatures below 2.94°K. One possible reason is the following. The theory of the sudden jump model of spectral diffusion proposed by P. Hu and S. R.

Figure 65

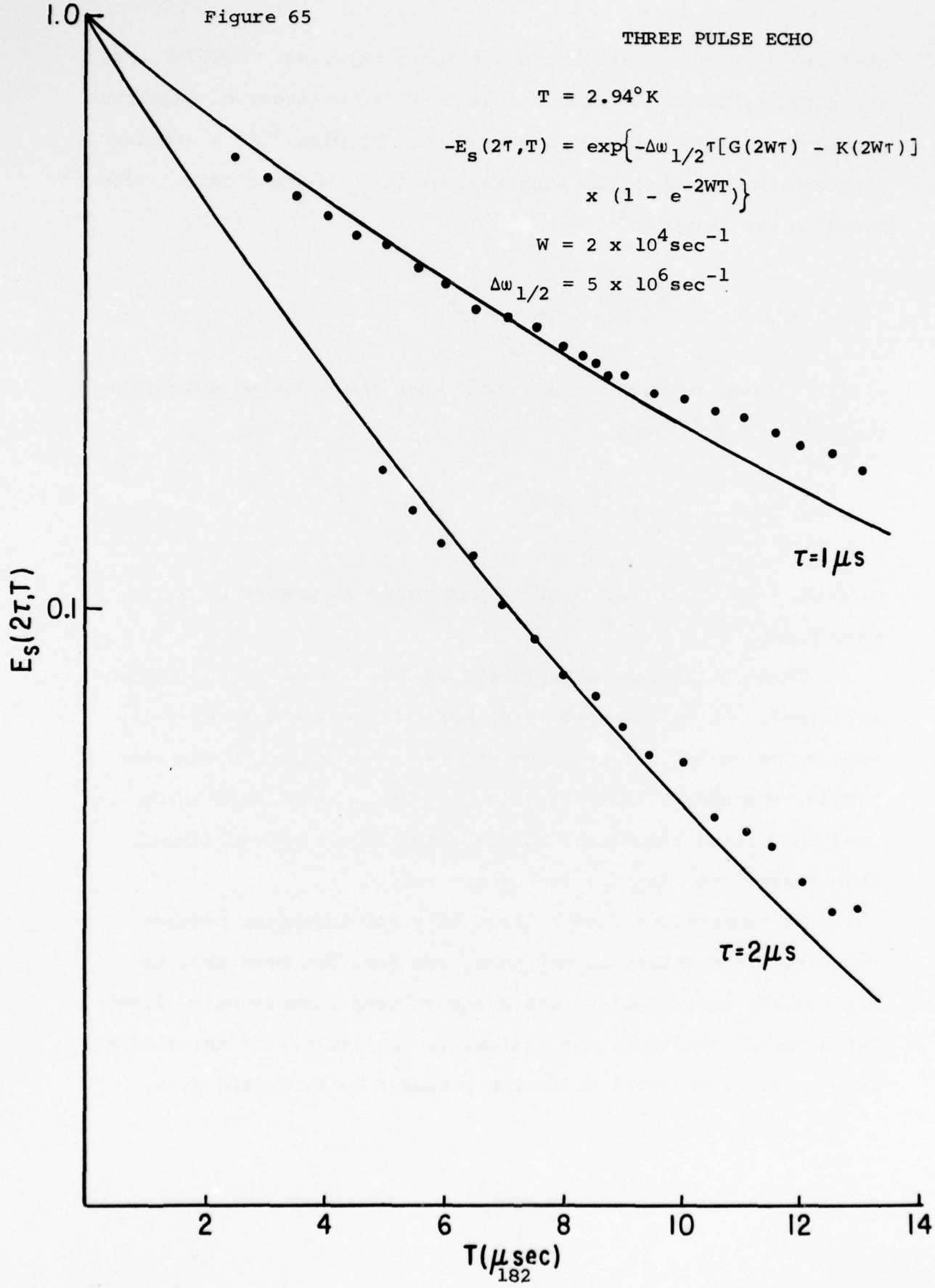
THREE PULSE ECHO
T = 2.94°K
$-E_s(2\tau,T) = \exp\{-\Delta\omega_{1/2}\tau[G(2W\tau) - K(2W\tau)] \times (1 - e^{-2WT})\}$
$W = 2 \times 10^4 sec^{-1}$
$\Delta\omega_{1/2} = 5 \times 10^6 sec^{-1}$
1.0
0.1
$E_s(2\tau,T)$
$\tau=1\mu s$
$\tau=2\mu s$
2
4
6
8
10
12
14
$T(\mu sec)$

Hartmann [1] assumes that the A spins (whose signal we monitor) is relaxed by B spins which flip between two quantum states at an average rate W. This assumption is only valid in the high temperature limit. Actually, the ratio between $W_{\downarrow}$, flipping rate from excited state to ground state, and $W_{\uparrow}$, flipping rate from ground state to excited state is

$$W_{\downarrow}/W_{\uparrow} = \exp(g\beta H/KT).$$

Considering the case at temperature 2.5°K, by using the values

$$g_{H(Er)} = 8.3$$

$$H \simeq 2.5K \text{ Gauss},$$

we get

$$W_{\downarrow}/W_{\uparrow} \simeq 1.75 .$$

In an effort to better understand the low temperature data we have begun to analyze the case for which the up and down spin-flip rates are different. For $W_{\uparrow} \neq W_{\downarrow}$ the theoretical analysis is an order of magnitude more difficult than for the case when $W_{\uparrow} = W_{\downarrow}$. We find that the free decay signal is given by

$$F(\tau) = \exp\{-\Delta\omega_{1/2} G^{(h)}(\tau)\}$$

where

$$G^{(h)}(\tau) = G^{(h\uparrow)}_{odd} + G^{(h\uparrow)}_{even} + G^{(h\downarrow)}_{odd} + G^{(h\downarrow)}_{even}$$

rather than $G^{(h)}(\tau) = G^{(h)}_{odd} + G^{(h)}_{even}$ as obtained in Ref. (1). The notation follows that of Ref. (1) except that now

$$G^{(h)}_{odd} = G^{(h\uparrow)}_{odd} + G^{(h\downarrow)}_{odd}$$

and

$$G^{(h)}_{even} = G^{(h\uparrow)}_{even} + G^{(h\downarrow)}_{even}$$

The terms with arrow heads are new and depend on the initial orientation of the A spin. In Ref. (1) we found

$$G^{(h)}_{even} = e^{-W\tau}\, \tau I_o(W\tau)$$

and

$$G^{(h)}_{odd} = e^{-W\tau}\, \tau I_1(W\tau)$$

where $I_n(W\tau)$ is the modified Bessel function. We now find

$$G^{(h_\downarrow)}_{odd} = e^{-W\tau}\, \frac{W_\uparrow}{\sqrt{W_\uparrow W_\downarrow}}\, \tau \sum_{n=o}^{\infty} \left(\frac{2W_-^2}{\sqrt{W_\uparrow W_\downarrow}}\, \tau\right)^n \frac{n!}{(2n)!}\, I_{n+1}(\sqrt{W_\uparrow W_\downarrow}\, \tau)$$

and a similar but more complicated expression for $G^{(h)}_{even}$. We are now in the process of analyzing these formulas. We also are in the process of deriving the formulas for the two- and three-pulse echo case. With these results in hand we would hope to be able to understand our experimental results.

This project has been terminated June 30, 1977. It will continue with NSF funding alone.

*This research was also supported by the National Science Foundation under Grant NSF-DMR73-07600 A03.

(1) P. Hu and S. R. Hartmann, Phys. Rev. B 9, 1 (1974).

(2) L. R. Klauder and P. W. Anderson, Phys. Rev. 125, 912 (1962).

(3) W. B. Mims, Phys. Rev. 168, 370 (1967).

(4) Schwarzkoph Microanalytical Laboratory Report.

V. PHYSICS OF MOLECULES

A. MICROWAVE SPECTROSCOPY OF IONS*

(W. Nagourney, P. Thaddeus)

We have completed construction of a glow discharge microwave spectrometer and are now using it to measure the spectroscopic constants of a number of interesting molecular ions. We have also begun construction of a fast flow Stark modulated free radical spectrometer and hope to employ it in the near future in the study of some short lived free radicals.

The glow discharge spectrometer has been described previously.[1] Our spectrometer differs from others principally in the use of a rather effective source modulation scheme to suppress signals (baseline) arising from systemic variations in the RF source amplitude with frequency. The scheme is implemented by applying a spectrally pure wideband frequency modulation to a microwave source at a modulation frequency that is greater than the absorption linebreadth. The desired absorption signal is obtained by synchronously detecting the output of the microwave detector at the n^{th} harmonic of the modulation frequency. It can be shown that the system behaves like a high pass filter of order n which discriminates against baseline features that vary slowly with frequency. Equivalently, the system produces a signal proportional to the n^{th} derivative with respect to frequency of the baseline. By virtue of the high modulation frequency and wideband modulation, the signal due to a molecular absorption is not significantly attenuated by the system; it can be shown that, when n=7, the absorption signal is about half that of an equivalent Stark modulated device.

We have found two drawbacks in using the system. The first is the fact that the baseline is not completely suppressed. More importantly, the system cannot distinguish between a molecular absorption and the small but sharp baseline features that appear to originate in the microwave source. We have tested the spectrometer on the J=7 to 8 transition (at 91.052 GHz) of $O^{18}C^{13}S^{32}$ and have obtained a signal to noise of about 5 to 1 with a one second integration time. This corresponds to a minimum detectable signal (with a 1 second integration time) of about 10^{-8} cm^{-1}. The principal features of the noise in the above test appear to have come from the incompletely suppressed baseline features mentioned above. In general, however, the system appears to be quite effective; if the klystron amplitude changed by 20% over the sweep (a typical value), the system has suppressed this variation by a factor of almost 10^5.

The second drawback is the fact that the system considerably distorts the molecular lineshape. Thus, a molecular line having structure can not be easily interpreted; elaborate curve fitting is necessary to measure the molecular parameters. While this is not too great a disadvantage in cases where the number of components and their approximate positions are known, the method will not work at all in other situations. We have tested the curve fitting on the J=0 to 1 triplett of HCN and have measured the splitting with an accuracy of .3%. The problem of a completely unknown line can only be handled by deconvolving (using a computer) the instrumental line; we are currently at work on several promising deconvolution schemes.

We have successfully observed the known molecular ion lines due to the lowest rotational transitions of CO^+, HCO^+, and HN_2^+. In all cases, we have obtained a signal to noise of from 10 to 20 to 1. with a 1 second integration time. The baseline features were generally smaller than or comparable to the random noise. We are currently attempting to measure the quadrupole hyperfine splitting due to the inner nitrogen in HN_2^+; this quantity has so far been obtained only from radioastronomical observations.[2]

We have attempted to measure the lowest rotational frequency of NO^+ using the optical measurements[3] as the starting values in our search. We have been unsuccessful so far using a discharge in NO; various other production strategies are currently under consideration. We plan to measure the J=1 to 2 transition of HCS^+ and are awaiting the calculation of reasonably accurate frequencies by colleagues at the Goddard Insitute for Space Studies.

A fast flowing Stark modulated free radical spectrometer is currently under construction. Our devise is similar to that used by Saito,[4] except for the use of a throttled down diffusion pump instead of a large mechanical pump. We hope to measure the transition frequencies of such radicals as C_2H and C_3N using this system.

*This research was also supported by the National Aeronautics and Space Administration under Grant NGR-33-008-191, Scope T.

(1) CRL Progress Report, June 30, 1976, p. 50.

(2) Thaddeus, P., Turner, B. E., Ap. J. (Letters), 201, L25.

(3) F. Alberti, A. E. Douglas, Can. J. of Phys., 53, 1179 (1975).

(4) Saito, S. and Amano, T., J. Mol. Spect., 34, 383 (1970).

VI. MACROSCOPIC QUANTUM PHYSICS

A. QUANTIZED ROTATION AND VISCOSITY OF SUPERFLUID HELIUM*

(R. Biskeborn and R. Guernsey).

Our apparatus [1] for studying the viscosity temperature dependence with great precision along the Lambda line is now operational. By the end of the current period, it should have provided the first measurements of the viscosity critical exponents as a function of pressure. This may be an important step in understanding the superfluid transition. Sometime earlier,[2] we obtained viscosity exponents at saturated vapor pressure, and these have recently [3] been found to fit a new model of the transition.

Our torsion pendulum can operate at frequencies from 300 to 6000 Hz. The sample pressure is regulated by controlling the temperature of a room temperature ballast tank to $\pm$ 1μK. Temperature resolution at the sample should be 0.1μK, and temperature control to within 1 μK is expected. We have developed a unique bridge circuit that allows the pendulum to run in feedback mode (self resonance) and may increase the damping resolution by two orders of magnitude to .0001%.

At the highest frequency, we will have the viscous penetration depth less than the superfluid "healing length" for $T\lambda - T < 7\mu K$. Our viscosity measurements, then, will be the first direct probe of the boundary layer between a wall and the <u>bulk</u> liquid.

*JSEP support for this project has been phased out during this interval as directed.

(1) CRL Proj. Report #26, P. 118 (1976).

(2) R. Biskeborn and R. W. Guernsey, Jr.,Phys. Rev. Lett., 34, 455 (1975).

(3) D. L. Goodstein, Phys. Rev., 16, #1 (1977).

B. OCCUPATION OF THE HeII SUPERFLUID STATE.

(J. Kaplan, R. Guernsey).

This project was phased out early in the current period. It culminated in the Ph.D. thesis of Jeremy M. Kaplan[1] whose abstract follows.

This thesis is in two parts. In part one we present results of a high precision driven torsion pendulum measurement of the average superfluid fraction in a restricted geometry within 1 milli-Kelvin of T_λ. Our precision is 3×10^{-5} in superfluid fraction, and 2 micro-Kelvin in temperature.

From the difference between the bulk value of superfluid fraction (as measured in second sound experiments) and our restricted geometry value at temperatures below T_λ - 100 micro-Kelvin we infer a healing length consistent with that predicted by the theory of Ginzburg and Pitaevskii as modified by Mamladze. The openness of our sample (49,500Å typical pore size) enables us to extend healing length measurements closer to T_λ than has been done before. The data within 100 micro-Kelvin of T_λ show evidence of the increased entrainment of the superfluid by the porous filler as the healing length increases.

In part two we present a thermal modulation experiment designed to measure the circulation states of the superfluid.

The helium II is contained in an annulus that is fixed to the bob of a high Q torsion pendulum. As the temperature of the sample is modulated at the resonant frequency of the pendulum, momentum exchange between the superfluid and the bob drives the pendulum. The amplitude of the pendulum response is proportional

to the angular velocity of the superfluid with respect to the container walls. The system noise is low enough to permit resolution of single circulation quanta of the anticipated size.

When the experiment was first attempted, an additional, large, unstable signal, equivalent in magnitude to 61,000 circulation quanta, completely masked the effect. Subsequent work has reduced this unwanted signal to the equivalent of a few hundred circulation quanta.

Data on high ($n = \pm 18$ and ± 36) circulation states of the superfluid in the presence of this additional signal show strong, but not conclusive, evidence of the existence of this effect. Instability in the unwanted signal prevents resolution to better than a few quanta.

(1) J. M. Kaplan, "Superfluid Fraction and Healing Length in a Confirmed Geometry Near T_λ; Attempts to Observe the Superfluid Quantization Circulation States." Ph.D. Thesis, Columbia University, 1976.

C. EXPERIMENTS ON THE NEW PHASES OF LIQUID ^{3}He.

(R. Guernsey)

JSEP support for the project was discontinued as of July 1, 1976. It has continued with NSF support.

PERSONNEL

FACULTY

H. C. Card, Associate Professor of Electrical Engineering

A. Flusberg, Assistant Professor of Physics

G. W. Flynn, Professor of Chemistry

R. W. Guernsey, Assistant Professor of Physics

R. Gupta, Assistant Professor of Physics

W. Happer, Professor of Physics, Director

S. R. Hartmann, Professor of Physics

J. M. Luttinger, Professor of Physics

I. I. Rabi, University Professor Emeritus

A. M. Sachs, Professor of Physics

M. C. Teich, Professor of Engineering Science

P. Thaddeus, Adjunct Professor of Physics

C. S. Wu, Pupin Professor of Physics

RESEARCH ASSOCIATES AND PHYSICISTS

Mr. M. J. Bernstein

Dr. K. Casleton

Dr. J. K. McVey

Dr. G. Moe

Dr. W. Nagourney

Dr. A. Tam

Dr. G. R. Tomasevich

GRADUATE RESEARCH ASSISTANTS

R. Biskeborn

Y. Chen

G. Chin

R. Cohen

H. Cong

P. M. Fu

A. Glassman

K. Leung

J. Lyden

S. Meth

T. Mossberg

I. Shamah

R. Sheorey

M. Steinback

TECHNICAL RESEARCH ASSISTANTS

Mr. I. Beller Mr. J. Gorham

PHYSICS DEPARTMENT ELECTRONICS ENGINEERING AND CONSTRUCTION SHOP

Mr. V. Guiragossian

PHYSICS DEPARTMENT MACHINE SHOP

Mr. E. Jauch

The facilities are available for the Columbia Radiation Laboratory.

ADMINISTRATION

Mrs. H. M. Ghobadi

Mrs. P. A. Pohlman Mrs. M. L. Pulliam

JOINT SERVICES DISTRIBUTION

Dr. M. E. Lasser
Chief Scientist
DAMA-ARZ-A
Washington, D. C. 20310

Dr. R. Lundegard
Act. Chief Scientist
ONR
800 N. Quincy St.
Arlington, Va. 22217

Dr. W. L. Lehmann, Dir.
AF Office of Scientific Res.
Bolling AFB
Washington, D. C. 20332

Dr. J. Allen, Dept. Dir.
Res. & Adv. Technology
DDR & E
Washington, D. C. 20310

Mr. L. R. Weisberg, Asst. Dir.
Elet. & Phys. Sci.
DDR & E
Washinton, D. C. 20310

Mr. N. L. Klein
Asst. Dept. of Sci. & Tech.
DRCDMD-ST
Alexandria, Va. 22333

Dr. L. C. Kravitz
AF TAC/JSEP Member
AFOSR, Bolling AFB,
Washington, D. C. 20332

Dr. J. Dimmock
Navy TAC/JSEP Member Code 427,
ONR, 800 N. Quincy St.
Arlington, Va. 22217

Dr. Hermann R. Robl, Tech. Dir.
U.S. Army Research Office
P. O. Box 12211
Research Triangle Park, NC 27709

Dr. J. R. Suttle
Army TAC/JSEP Member
ARO, P. O. Box 12211
RTP, N.C. 27709

Mrs. Ruby Jacobs
Executive Secty., TAC/JSEP
ARO, P. O. Box 12211
RTP, N. C. 27709

Dr. R. S. Wiseman, Dir.
RDE/L, ECOM, DRSEL-RD
Ft. Monmouth, N. J. 07703

Commander
U. S. Army Satellite Comm. Agcy.
Ft. Monmouth, N. J. 07703

Commander
Atmospheric Sciences Lab.
White Sands Missile Range
N. M. 88002

Commander
Avionics Laboratory
U. S. Army Electronics Command
Ft. Monmouth, N. J. 07703

Commander
Combat Surveillance and Target
Acquisition Laboratory
ECOM
Ft. Monmouth, N. J. 07703

Commander
Communications/Automatic Data
Processing Lab., ECOM,
Ft. Monmouth, N. J. 07703

Commander
U.S. Army Computer Systems Command
Ft. Belvoir, Va. 22060

Commander
White Sands Missile Range
WSMR
N. M. 88002

Dr. Richard Duncan, Tech. Dir.
White Sands Missile Range,
N. M. 88002

Dr. R. J. Eichelberger, Tech. Dir.
BRL, Aberdeen Proving Ground
Md. 21005

Dr. J. L. McDaniel, Dir.
Missile Res., Devl. & Eng. Lab
U. S. Army Missile Command
Redstone Arsenal
Alabama 35809

Dr. W. C. Carter, Tech. Dir.
Harry Diamond Laboratories
2800 Powder Mill Rd.
Adelphi, Md. 20783

Dr. T. G. Kirkland, Tech. Dir.
U. S. Army Mobility Eqp. Rsch.
and Devl. Command
Ft. Belvoir, Va. 22060

Mr. E. Sheehan, Dir.
Night Vision Laboratory
Ft. Belvoir, Va. 22060

Mr. C. Hardin, Dir.
Electronic Warfare Laboratories
ECOM
Ft. Monmouth, N. J. 07703

Dr. Al Gilbert
White Sands Missile Range
Attn: STEWS-ID-SR, WSMR
N. M. 88002

Dr. Keat Pullen
Ballistic Research Laboratories
Aberdeen Proving Ground
MD. 21005

ARMY TRC MEMBERS:

Dr. R. G. Buser, Chief
Electro-optics Tech. Area,
Combat Surveillance and Target
Acquisition Lab, ECOM
Ft. Monmouth, N. J. 07703

Dr. Jack A. Kohn, Chief
Electronic Materials Res. Tech.
Area, ETDL, ECOM
Ft. Monmouth, N. J. 07703

Dr. Edward Lieblein, Chief,
Computer Software Tech. Area
COMM/ADP, ECOM,
Ft. Monmouth, N. J. 07703

Dr. Douglas C. Pearce,
Computer Appl. & Systems Tech.
Area, COMM/ADP,
Ft. Monmouth, N. J. 07703

Dr. Felix K. Schwering, Leader
Antennas Team COMM/ADP, ECOM
Ft. Monmouth, N. J. 07703

Dr. J. R. Suttle, Dir.
Electronics Div.
U.S. Army Research Office
P. O. Box 12211
Research Triangle Park, N.C.
27709

Dr. H. R. Wittman, Assoc. Dir.,
U.S. Army Research Office
P. O. Box 12211
Research Triangle Park, N.C.
27709

Dr. Clare G. Thornton, Chief
Semiconductor Devices &
Integrated Elect. Tech. Area
ETDL, ECOM
Ft. Monmouth, N. J. 07703

JSEP LABORATORY DIRECTORS:

Prof. D. J. Angelakos, Dir.
Electronics Research Laboratory
Univ. of California
Berkely, Ca. 94720

Prof. N. Bloembergen, Dir.
Div. of Engineering & Applied
Physics, Pierce Hall
Harvard University
Cambridge, Ma. 02138

Prof. R. T. Chien, Dir.
Coordinated Science Lab
University of Illinois
Urbana, Il. 61801

Prof. M. Chodorow, Dir.
Microwave Laboratory
Stanford University
Stanford, Ca. 94305

Prof. A. A. Dougal, Dir.
Electronics Research Center
Engineering-Science Bldg. 110,
University of Texas at Austin
Austin, Texas 78712

Prof. W. Happer, Dir.
Columbia Radiation Laboratory
Columbia University
538 West 120th Street
New York, New York 10027

Prof. Z. A. Kaprielian, Dir.
Electronic Sciences Lab.
Univ. of Southern California
Los Angeles, Ca.90007

Prof. J. D. Meindl, Dir.
Stanford Electronics Lab.
Stanford University
Stanford, Ca. 94305

Prof. A. A. Oliner, Dir.
Microwave Research Institute
Polytechnic Institute of New York
333 Jay Street,
Brooklyn, New York 11201

Prof. P. A. Wolff, Dir.
Research Laboratory of Electronics
Massachusetts Institute of Tech.
Cambridge, Ma. 02139